

# The effect of telomeric repeats on double-strand break processing and repair

Inauguraldissertation

zur

Erlangung der Würde eines Doktors der Philosophie

vorgelegt der

Philosophisch-Naturwissenschaftlichen Fakultät

der Universität Basel

von

**Isabella Marcomini**

aus Italien

Basel, 2018

Originaldokument gespeichert auf dem Dokumentenserver der  
Universität Basel [edoc.unibas.ch](http://edoc.unibas.ch)

Genehmigt von der Philosophisch-Naturwissenschaftlichen Fakultät  
auf Antrag von

Prof. Dr. Susan M. Gasser  
Prof. Dr. Joachim Lingner

Basel, den 27. März 2018

Prof. Dr. Martin Spiess  
Dekan

# Table of Contents

Thesis overview:.....	5
<b>Chapter 1: An Introduction to DNA end-processing: telomeres versus double-strand breaks.....</b>	<b>7</b>
The double strand break response.....	9
The nature of telomeres .....	11
Double strand break repair proteins with telomeric functions .....	12
Regulation of telomerase .....	14
Control of DNA end resection .....	16
The processing of TG-flanked DSBs .....	19
Persistent DSBs and telomeres share common nuclear subcompartments .....	20
Nuclear organization of telomeres .....	20
Nuclear organization in DSB processing.....	23
Aim of the thesis.....	26
References.....	27
<b>Chapter 2: Processing of DSBs at the nuclear periphery .....</b>	<b>35</b>
SWR1 and INO80 chromatin remodelers contribute to DNA double-strand break perinuclear anchorage site choice.....	35
PolySUMOylation by Siz2 and Mms21 triggers relocation of DNA breaks to nuclear pores through the Slx5/Slx8 STUbL.....	65
<b>Chapter 3: Telomeric repeats near an internal double-strand break prevent MRX recruitment and allow DNA end separation to favor ectopic recombination.....</b>	<b>101</b>
<b>Chapter 4: Conclusions and future perspectives.....</b>	<b>133</b>
Processing of a persistent DSB.....	134
A different approach to investigate repair at the nuclear periphery.....	134
The nucleo- to cytoskeleton connection.....	135
Processing of TG-flanked DSBs.....	137
The resection block imposed by TG repeats.....	138
Control of chromosome length by SMC proteins.....	139
A possible role of transcription in nuclear organization of DNA damage.....	142
The role of end separation in repair pathway choice.....	143
Relevant modifications to the TG-HO system.....	145
A model system for the study of translocations.....	147
References.....	148
Appendices .....	153
List of abbreviations.....	153
Curriculum vitae .....	155
Acknowledgments .....	159



## Thesis overview

This PhD thesis is based on the following publications:

- Horigome C, et al. (2014). SWR1 and INO80 chromatin remodelers contribute to DNA double-strand break perinuclear anchorage site choice. *Molecular Cell* 55(4): 626-39
- Horigome C, et al. (2016). PolySUMOylation by Siz2 and Mms21 triggers relocation of DNA breaks to nuclear pores through the Slx5/Slx8 STUbL. *Genes & Development* 30(8): 931-45
- Marcomini I, Gasser SM (2015). Nuclear organization in DNA end processing: Telomeres vs double-strand breaks. *DNA Repair* 32: 134-40
- Marcomini I, et al. (2018). Asymmetric processing of DNA ends at a double-strand break leads to unconstrained dynamics and ectopic translocation. *Cell reports* 24: 2614-28

This thesis consists of 4 chapters. Chapter 1 is an introduction, based on a published review (Marcomini I, Gasser SM, 2015). Chapter 2 presents the published papers on DSB processing relative to the nuclear periphery in *S. cerevisiae*, to which I contributed. Chapter 3 is the published article about the effect on telomeric repeats on DSB processing.

Chapter 1 gives an overview of the field of end processing in the double-strand break response as well as at telomeres. It is based on a review (Marcomini and Gasser, 2015), but is rearranged, updated and modified in order to avoid redundancy and provide clarity. Additional relevant sections and citations were added that were not adequately discussed in the review or outdated since its publication.

Chapter 2 is an experimental chapter that reports previous works on the role of the nuclear periphery in DSB processing. These studies provided a foundation to develop my own project, and they are some of the first works showing a role for the nuclear periphery in the DNA damage response. While the first one (2014) dissects the requirements for a persistent DSB to interact with the nuclear envelope, the second one focuses on the role and extent of SUMOylation in such interactions, providing functional data for their biological relevance. I participated in both papers (Horigome C et al., 2014 and 2016), which were lead by Dr Horigome.

Chapter 3 presents the paper as published on *Cell reports*. This work stems from the basic question of what determines the identity of a DNA end as a telomere. It isolates telomeric repeats in an internal chromosomal position next to a DSB end, and analyzes their effects on the processing, nuclear localization and repair of the DSB.

Finally, Chapter 4 discusses the significance of these studies in the context of DNA repair and telomere biology, highlights open questions and provides future perspectives.



# CHAPTER 1. AN INTRODUCTION TO DNA END PROCESSING: TELOMERES VERSUS DOUBLE-STRAND BREAKS

---

Based on:

Marcomini I and Gasser S.M.

*DNA Repair* 32:134-40, 2015

## SUMMARY

DNA double strand breaks (DSBs) can arise in eukaryotic cells due to exogenous (radiation, chemicals) or endogenous (oxidative stress, replication fork collapse) processes. DSBs constitute a threat for genome integrity and need to be repaired to avoid loss of genetic material and allow cell cycle progression. Telomeres are the ends of eukaryotic chromosome and, like DSBs, expose a free 3'-OH. What differentiates telomeres from DSBs has been a long-standing question in the field of cell biology: indeed, recognition of telomeres as DSBs would cause chromosome fusions and genomic instability. Unlike DSBs, telomeres are protected from the DNA damage response machinery by a dedicated protein complex, the telosome, as well as by their association in clusters at the nuclear periphery. Interestingly, some components of the telosome have fundamental but different functions in DSB processing. Furthermore, some nuclear envelope binding sites are common to telomeres and the processing of DSBs. This introduction highlights common pathways as well as specific features of these two different kinds of DNA ends.





# Introduction

## The double-strand break response

DNA double-strand breaks (DSBs) are among the most deleterious types of DNA damage in the nucleus, particularly if an intact template is not immediately available for repair (Jackson and Bartek 2009). To ensure cell survival, DSBs trigger a conserved cascade of events called the DNA damage checkpoint, that arrests the cell cycle and stimulates repair (Tsabar and Haber 2013). The Ser/Thr PI3-like kinases ATM (Tel1 in the budding yeast, *S. cerevisiae*) and ATR (Mec1 in *S. cerevisiae*) initiate the checkpoint signaling by phosphorylating other effector kinases, thereby promoting the recruitment of the repair machinery, the stalling of cell cycle progression, and changes in gene expression (Finn et al. 2011; Smeenk and van Attikum 2013; Adam and Polo 2014).

DSBs are repaired through two main pathways in eukaryotic cells. Non-homologous end joining (NHEJ) is active throughout the cell cycle and involves the direct religation of the broken ends, as long as a 3'-OH and a 5' phosphate group are available for religation. If not, then base removal or limited end resection occurs, allowing single-strand annealing, processing and imprecise religation, that leads to short deletions. NHEJ is mediated by a dedicated ligase, ligase IV (Lieber 2010). In S- and G2-phases of the cell cycle, 5' to 3' resection at breaks is more efficient, yielding a long 3' single-strand tail on both sides of the break. DSB repair is then preferentially mediated by homologous recombination (HR), during which single stranded (ss) overhangs anneal with an intact, homologous double stranded DNA (dsDNA) template. The ssDNA overhang mediates both strand invasion and activation of the DNA damage checkpoint kinase ATR-ATRIP (Mec1-Ddc2 in yeast) to arrest the cell cycle.

DSBs are initially sensed by the Mre11-Rad50-Nbs1 (MRN) complex (Mre11-Rad50-Xrs2 or MRX in yeast), which rapidly localizes to DNA ends and, in a process called short range end resection, starts trimming the 5' end, thereby exposing a short protruding 3' end of ssDNA. MRX activity is dependent on phosphorylation of CtIP (Sae2 in yeast) by cyclin-dependent kinases (CDK), which contributes to the observed cell-cycle bias for resection (Cannavo and Cejka 2014). DNA ends are also bound by the Ku70/80 heterodimer: in G1 phase, the Ku complex limits both ssDNA formation and the activity of resection proteins, promoting repair via the NHEJ pathway (Mimitou and Symington 2010). In S- or G2-phase cells, Ku binds the break ends, but homologous recombination in these phases of the cell cycle is by far the preferential repair pathway in yeast. It was assumed that Ku competes with MRX for end binding, but how repair pathway choice

becomes biased towards HR, and how Ku is dealt with at S- and G2-phase DSBs, was rather unclear. Recent data suggest that Ku promotes the initial cleavage catalyzed by Mre11 together with phosphorylated Sae2, thereby favoring resection and HR when Sae2 is modified (Reginato et al. 2018; Wang et al. 2018). It also seems indeed that Ku has a much higher DNA binding affinity for blunt dsDNA ends than for short overhangs (Foster et al. 2011). In mammalian cells repair pathway choice is largely dictated by competition between BRCA1 and 53BP1 at DSBs (Chiba et al. 2008; Xia et al. 2013). While Ku binding to BRCA1 was initially thought to promote end-joining, it now appears that 53BP1 is loaded onto chromatin and through its interacting factors Rif1 and PTIP promotes NHEJ by inhibiting the end resection that is necessary for HR (Zimmermann and de Lange 2013).

The ssDNA stretches created by MRX/Sae2 are coated by Replication Protein A (RPA). RPA promotes long-range resection by recruiting Exo1 endonuclease and/or a complex of Dna2-Sgs1 (DNA2-BLM in mammalian cells) (Myung et al. 2001; Gravel et al. 2008; Symington and Gautier 2011). The resected ssDNA filament bound by RPA recruits the ATR/ATRIP (Mec1/Ddc2 in yeast) kinase, which is further stimulated by the 9-1-1 complex. 9-1-1 binds the ss-dsDNA junction at resected breaks, acting through the BRCT-domain protein, TOPBP1 (or Dbp11 in yeast) (Kumagai et al. 2006; Delacroix et al. 2007). RPA is later replaced by Rad51, facilitated by mediator proteins including BRCA2 (in yeast by Rad52). Rad51 forms a protein-ssDNA filament which is essential for homology search and invasion into the double-stranded template DNA.

The C-terminus of Nbs1 (Xrs2 in yeast) recruits ATM/Tel1 to DSBs (Falck et al. 2005). Once ATM/Tel1 is activated, it phosphorylates itself and the C-terminal tail of histone H2AX ( $\gamma$ H2AX or phosphorylated Ser129 in yeast histone H2A).  $\gamma$ H2AX has the unique propensity to spread from the site of damage, providing a platform for the binding of many other DNA repair enzymes (Bekker-Jensen et al. 2006). Whereas in mammals ATM is specifically activated by DSBs, ATR responds also to replication stress and other lesions that cause ssDNA formation (Gobbini et al. 2013; Hustedt et al. 2013). It seems that in budding yeast, the ATR homolog Mec1 plays a much more central role in DSB processing than Tel1 (the ATM homolog), perhaps because resection and ssDNA formation are more efficient in this organism (Clerici et al. 2008). Indeed, as its name indicates, Tel1 is largely specialized for functions at telomeres; its loss leads to constitutively short TG repeats at chromosome ends (Greenwell et al. 1995). At telomeres, even if short, resection is suppressed and Tel1 activity leads to the recruitment of telomerase, as discussed below.

## The nature of telomeres

The natural ends of eukaryotic chromosomes, or telomeres, expose a short protruding 3' end, just like resected DSBs. However, telomeres contain repetitions of a TG-rich sequence, specifically  $(TG_{1-3})_n$  in budding yeast, and TTAGGG in most vertebrates. The length of this repetitive region varies from 300-400 bp in yeast to ~15 kb in humans, and up to 100 kb in certain species of mice. The TG cap has two main functions: one is to ensure complete replication of chromosomes, the second is to protect the ends from both degradation and from activating the DNA damage checkpoint, which would block cell cycle progression. Replication by polymerase  $\alpha$  proceeds only 5' to 3' and acts in a discontinuous manner on the lagging strand. It makes use of RNA primers, which are removed at the end of the polymerization process(Blackburn 1991). Therefore, on leading strands this mechanism leads to a small loss of the terminal sequence each cell cycle, which would eventually erode unique chromosomal DNA. To compensate for this, a specialized replicative polymerase called telomerase acts at telomeres(Shampay et al. 1984). Telomerase is a protein-RNA complex whose RNA moiety serves as an internal primer that templates DNA synthesis at chromosomal ends. It is generally in very low abundance and its recruitment is highly regulated. On average, fewer than one telomere in 10 is elongated by telomerase each cell cycle(Teixeira et al. 2004), with shorter telomeres being favored, suggesting that there may be a switch from an inaccessible to an accessible structure prior to elongation. Nonetheless, telomerase is not only bound at short telomeres, but also at low frequency at DSBs(Oza et al. 2009).

A second crucial function of the telomere is to suppress the DNA damage response (DDR) and block the action of the repair machinery that would normally act on the terminal 3' ssDNA telomeric overhang as a repair substrate. If DSB repair takes place at telomeres, cells undergo potentially lethal telomere fusions and chromosomal translocations, which result in genomic instability(Burgess 2013). This is normally prevented by a set of proteins that have evolved to specifically recognize telomeric DNA, forming the telosome. The telosome is composed of a ssDNA binding component and a sequence-specific dsDNA repeat-binding component. In budding yeast, the former is the Cdc13-Stn1-Ten1 (CST) complex, while dsDNA repeats are bound by Rap1. Rap1 binds the Rap1-interacting factors, Rif1 and Rif2, as well as Sir3 and Sir4, two yeast-specific nucleosome-binding factors involved in gene silencing. Higher eukaryotes possess a telosome complex called Shelterin that integrates both ss- and ds-DNA binding activities.

In addition, mammalian telomeres form a secondary structure called t-loop, generated by a folding back of the 3' ssDNA overhang, such that it anneals with upstream telomeric repeats to displace the TG-rich strand of the repeats DNA(Griffith et al. 1999). This may

physically sequester the chromosome end from the DSB signaling machinery, at least until replicative polymerases pass through. The human TTAGGG-binding factor TRF2 is required for the formation of such structures even in vitro(Stansel et al. 2001).

Interestingly, telomere repeat-binding proteins in different organisms share very high structural similarity, despite significant sequence divergence(Bilaud et al. 1996; Pitt et al. 2007): their DNA-binding domain is a Myb-like domain of about 60 aa in a helix-turn-helix conformation in their C-terminus, and it is called the telobox. Budding yeast has only one telomeric DNA binding protein, Rap1, that has a dimeric binding site with two teloboxes(Konig et al. 1996). In humans, TRF1 and TRF2 both bind DNA directly, and have one telobox each(König et al. 1998; Court et al. 2004). A similar Myb-like binding domain is also a feature of Tbf1, an essential yeast protein discovered for its ability to bind the mammalian telomeric sequence TTAGGG(Brigati et al. 1993). This sequence is located at yeast subtelomeres as well as in other regions of the yeast genome, where it blocks silent chromatin propagation(Fourel et al. 1999).

In most species, telomeric repeat binding factors also nucleate domains of repressed chromatin that spread inwards from the chromosomal end. In yeast, Rap1 binds the dsTG repeats roughly every 18 bp in a sequence-specific manner, and recruits Sir4 to nucleate SIR-mediated gene repression(Gilson et al. 1993; Kueng et al. 2013). This requires at least 20 Rap1 binding sites, due to competition between Rif1/2 and Sir3/4 for binding the Rap1 C-terminus(Aksenova et al. 2013). This subtelomeric heterochromatin may help distinguish telomeres from breaks, as heterochromatin tends to self-associate in nuclear subcompartments, either adjacent to the nuclear envelope or around the nucleolus(Taddei and Gasser 2012). Cdc13, which binds the ssDNA at telomeres in a sequence-specific manner, further distinguishes breaks from chromosomal ends, as it binds resected TG ssDNA 40-fold more efficiently than random ssDNA (McGee et al. 2010). Cdc13 is phosphorylated in S phase, and its phosphorylation promotes telomere elongation through interaction with Est1 of the telomerase complex(Wu and Zakian 2011; Wu et al. 2012), whereas RPA, a similar trimeric complex that binds ssDNA with little sequence specificity, stabilizes the resected end and activates the Mec1/ATR checkpoint kinase.

### **Double-strand break repair proteins with telomeric functions**

Interestingly, despite the presence of the telosome and its suppression of the DDR, a number of DNA repair proteins have a functional role at telomeres. For example, the MRN/MRX complex is involved in telomere maintenance in both higher eukaryotes and yeast(Lamarche et al. 2010). During the DSB response, Mre11 is one of the earliest

sensors of damage, recruiting ATM/Tel1 as well as helping to activate ATR/Mec1, by initiating resection to form a ssDNA overhang. At telomeres, on the other hand, MRX preferentially binds short telomeres(McGee et al. 2010), although at telomeres it was proposed to inhibit resection: in a *cdc13-1* mutant, where telomeres are uncapped, MRX binding was proposed to hide the ends from other exonuclease activities(Vega et al. 2007) and possibly promote telomerase binding(Foster et al. 2006; Martina et al. 2012). Consistently, mutations in any MRX subunit, like deletion of *tel1* or yeast *Ku* (*yKu*)(Boulton and Jackson 1998), lead to constitutively short telomeres, due to inefficient recruitment of telomerase(Takata et al. 2005).

The roles of MRN at mammalian telomeres may be simpler. It was shown that functional telomeres are indeed recognized as DSBs in late S/G2 in mammalian cells, when they are replicated: at that point, ATM is transiently phosphorylated, although it does not activate effector kinase Chk2 or p53, and cell-cycle progression is not delayed. ATM can be recovered at telomeres with MRN, suggesting that a localized damage response is initiated at telomeres(Verdun et al. 2005), resembling the association of Tel1 at short yeast telomeres bound by MRX(McGee et al. 2010). Finally, an enzymatic assay, based on nucleotide addition by terminal transferase, showed that chromosome ends in S/G2 are accessible, confirming the disruption of the t-loop(Verdun et al. 2005). Thus, disruption of the t-loop coincides with MRN binding, ATM activation and telomerase recruitment.

Ku is another conserved, end-binding protein that has a dual role in DSB repair and in telomere protection. Like MRX, it binds DSBs immediately after break induction and it promotes repair by the NHEJ pathway, by recruiting ligase IV and other enzymes involved in end religation(Boulton and Jackson 1996; Lundblad and Victoria 2003). In budding yeast, *yKu80* mutants display elevated rates of ectopic recombination(Marvin et al. 2009), presumably because NHEJ is compromised. Furthermore, Ku has multiple roles at telomeres, and *yKu* was among the first proteins shown to contribute to telomeric silencing, length maintenance and the spatial organization of telomeres(Boulton and Jackson 1998; Laroche et al. 1998; Mishra and Shore 1999).

In *S. cerevisiae*, telomeres cluster in 6-8 foci at the nuclear periphery(Gotta et al. 1996) in a manner dependent on *yKu80* and Sir4. The targeting of *yKu80* to a randomly localized chromosomal locus was sufficient to shift it to the nuclear periphery(Taddei et al. 2004), in a manner dependent on Mps3 and Est1 in S phase (Schober et al. 2009). The loss of *yKu* leads to a physical release of telomeres from their sequestration by Mps3, a SUN domain protein of the inner nuclear membrane(Schober et al. 2009). In addition, due to its interaction with Sir4, *yKu* also contributes to the nucleation of subtelomeric gene repression(Boulton and Jackson 1998; Laroche et al. 1998; Mishra and Shore 1999), an

activity that can be separated genetically from its anchorage function(Taddei et al. 2004). Finally, genetic screens have identified mutants(Bertuch and Lundblad 2003; Stellwagen et al. 2003) that separate the function of yKu in DSB repair from its roles at telomeres. This genetic approach showed that through binding Tlc1 (the RNA moiety of telomerase) yKu helps recruit telomerase and suppress recombination. This latter function may be aided by an S-phase sequestration of telomeres(Schober et al. 2009). Yku-Tlc1 interaction is also important for telomerase accumulation in the nucleus(Gallardo et al. 2008). Thus, both MRN/MRX and the Ku complex moonlight at telomeres with profoundly different roles than they have at DSBs. Besides distinct interaction partners, these roles may in part be determined by posttranslational modification of Ku; both yKu70 and yKu80 are SUMOylated in vivo, and this modification plays a key role in their ability to shift chromatin to the nuclear envelope protein Mps3(Ferreira et al. 2011).

Intriguingly, although yeast Cdc13 has a strong preference for TG-rich sequences(Lin and Zakian 1996), it can also bind ssDNA at resected DSBs, and both Cdc13 and Est2 can be detected by chromatin immunoprecipitation (ChIP) at HO-induced DSBs at internal loci (e.g. *MAT*(Oza et al. 2009)), albeit at low levels. Given this observation, it became relevant to examine mechanisms that actively prevent *de novo* telomere addition at non-TG ends, an event called telomere healing. Recent work showed that Mec1-Ddc2 phosphorylates Cdc13 at these DSBs, inhibiting telomere addition in a manner regulated by the PP4 phosphatase Pph3(Zhang and Durocher 2010). A further deterrent of telomere addition at breaks is the Pif1 helicase, a conserved and potent unwinder of G-quadruplex structures, that is able to evict telomerase from its substrate(Schulz and Zakian 1994). Consistently, telomere addition at breaks increases 200-fold in cells lacking nuclear Pif1(Schulz and Zakian 1994). In addition, the yeast ATR kinase, Mec1, phosphorylates Pif1 at specific sites, promoting Pif1-mediated eviction of telomerase. On the other hand, this does not affect Pif1 function at telomeres, suggesting that a selective mechanism inhibits telomerase activity at sites of damage(Makovets and Blackburn 2009). As described above, this acts in parallel through the DSB-induced phosphorylation of Cdc13 and Pif1.

Given that DSBs and telomeres share key ligands, it appears that the crucial determinants of telomere identity are the inhibition of resection and recruitment of telomerase.

### **Regulation of telomerase**

Several recent studies have shed light on how telomerase recruitment occurs and how telomere addition is prevented at internal breaks. At short telomeres the amount of Rap1-Rif2 complex drops, which leads to the association of MRX and Tel1, and phosphorylation

of Cdc13 and Rif1(McGee et al. 2010; Wu and Zakian 2011). Phosphorylated Cdc13 associates directly with Est1, which is in complex with Est3, Est4 and Est2, the catalytic subunit of telomerase that triggers telomere elongation. Coincidentally, the phosphorylation of Rif1 appears to reduce its telomerase-inhibiting activity(McGee et al. 2010). yKu70/80 is also essential for telomerase recruitment. Tlc1 (the RNA moiety of telomerase), is exported to the cytoplasm and needs to be imported back in the nucleus in early S phase. Ku mutants fail to accumulate TLC1 in the nucleus(Gallardo et al. 2008; Pfingsten et al. 2012). YKu has also been proposed to bind the TLC1-Est2 complex in subtelomeric domains in G1 phase of the cell cycle(Schober et al. 2009).

At mammalian telomeres, telomerase recruitment is achieved by interaction of the Shelterin component TPP1 with the transcriptase (TERT) subunit of telomerase(Nandakumar et al. 2012; Zhong et al. 2012; Schmidt et al. 2014). It was recently shown that mammalian telomerase probes each telomere hundreds of time in each S phase, establishing short-lived, unstable interactions with TPP1. Stable engagement of telomerase for elongation, by its interaction with the DNA end, is instead a slow and rare event whose mechanics are not entirely clear(Schmidt et al. 2016).

Whereas the *de novo* addition of telomeric repeats at a DSB is disfavored in all species due to the risk of losing the genetic information distal to the break, there can be instances in which telomere healing is needed. For instance, telomere addition may be favored when repair pathways are compromised, when replication forks collapse in difficult-to-replicate zones, or during fork collapse in subtelomeric regions, where the risk of crucial gene loss following telomere addition is low. Indeed, telomere healing was shown to be far more frequent at breaks in subtelomeric zones. Furthermore, in the yeast double mutant *sgs1Δexo1Δ*, subtelomeric breaks showed reduced resection and a 60% increase in survival due to telomere healing(Maringele and Lydall 2002), suggesting that telomere healing may be linked to reduced levels of resection. These data suggest that resection may well disfavor telomerase recruitment and activation. In fact, Mec1 activation leads to a modulation of Cdc13 or Pif1 activities to disfavor telomerase activation(Dewar and Lydall 2010). This is in apparent contradiction with the fact that MRX, that is able to initiate resection, is required for efficient recruitment of telomerase. The mechanism of MRX function at telomeres is not entirely clear, however it is notable that the nuclease activity of Mre11 is not required for the telomerase-promoting activity of the MRX complex(Tsukamoto et al. 2001), although MRX mutants have a modest delay in telomeric resection. A plausible model for MRX role in telomeric repeat addition is that the binding of MRX to short telomeres promotes recruitment of Tel1 through Xrs2. Phosphorylation of unidentified targets by Tel1 stabilizes telomerase association to the ends, thereby

promoting telomere lengthening. MRX at short telomeres might also favor nucleolytic activities that extend the 3' ss overhang, offering a better substrate to telomerase(Gao et al. 2010; Churikov et al. 2013). It is clear, however, that how resection is coordinated by MRX is a central problem in telomerase biology.

### **Control of DNA end resection**

Resection is a tightly controlled process. In mammals this is particularly the case, because mammalian cells use end joining much more than yeast. This can be rationalized by the fact that the mammalian genome comprises up to 70% repeat sequences, in the form of mini- and micro-satellites, and DNA and RNA transposons. This means that HR must be strongly down-regulated to prevent homeologous and deleterious recombination. The competition between BRCA1 and 53BP1 largely determines repair pathway choice in mammals. P53 binding protein 1 (53BP1) binds in the vicinity of DNA lesions, recruited by methylated histone H4K20 and ubiquitylated K15 on histone H2A(Fradet-Turcotte et al. 2013). In G1, 53BP1 blocks resection by limiting the accumulation of BRCA1, a protein that binds CtIP and MRN(Chen et al. 2008). 53BP1 also prevents resection at deprotected telomeres, when TRF2 is depleted(Lange et al. 2013). The resection block by 53BP1 in all contexts requires intact S/TQ phosphorylation sites in its N terminus: these sites are not necessary for its recruitment at DSBs(Bothmer et al. 2011), but rather for the recruitment of its effectors Rif1 and PTIP. How the block to resection is exactly executed is not known. PTIP and Rif1 both lack an enzymatic domain directly involved in repair, but Rif1 binds a phosphatase that may be implicated in downregulating resection. The downstream effector of PTIP is the nuclease Artemis: Artemis is thought to interact with PTIP at DSBs in an ATM-dependent manner and trim DNA ends to promote end joining, thereby making them inaccessible to the resection machinery. One downstream effector of Rif1 is MAD2L2: it operates at both telomeres and DSBs(Jacobs et al. 2015). Another player in resection inhibition at DSBs is Rap80: it binds SUMO and ubiquitin chains at break sites, protecting them from deubiquitinating enzymes(Kakaroukas et al. 2013). It is recruited together with BRCA1, however it does not promote BRCA1 activity in resection, instead Rap80 sequesters BRCA1 away from interaction with CtIP, that would foster resection. Inhibition of end resection at telomeres has multiple levels, but is fundamentally achieved by Shelterin, that acts at the level of DNA damage signalling: inhibition of CtIP-MRN mediated resection, that would lead to ATM activation, is ensured by TRF2 and its ability to promote the formation of a t-loop(Doksani et al. 2013). Inhibition of ATR is ensured by POT1-TPP1. In both pathways the block to resection is mediated by 53BP1 and Rif1 epistatically. A specific role in actively promoting end joining at telomeres was uncovered



for 53BP1: it increases the movement of deprotected telomeres, favoring telomere fusions(Dimitrova et al. 2008). None of the known 53BP1 effectors share this activity. New mechanisms are starting to emerge on how resection is controlled once it started. DNA helicase B (HELB) was recently discovered to control resection through its 5'-3' translocase activity. HELB is recruited by RPA at DSBs and inhibits EXO1 and BLM-DNA2 nucleases. Its nuclear levels increase gradually until entry in S phase. Phosphorylation by CDK drives the gradual export of HELB from the nucleus, thereby relieving the block to long-range resection. The effect of HELB on resection, however, does not influence repair pathway choice(Tkac et al. 2016).

In budding yeast, beside Ku70/80, several other factors have emerged as key resection regulators. One of these is Rif1: in yeast it has been long known for its role at telomeres as part of the Rap1-Rif1-Rif2 complex. At telomeres, it inhibits the recruitment of telomerase(Mattarocci et al. 2017) and thus should act as an antagonist to MRX. Rif1 was recently identified at DSBs also in yeast(Ira and Nussenzweig 2014; Martina et al. 2014). It binds 16 bp of a DNA end in a head-to-tail dimer, thereby preventing access of the end to other processing factors, in a way similar to the Ku70/80 heterodimer. This end protection results in slight inhibition of resection, which favors repair by end joining(Mattarocci et al. 2017). In apparent contrast with this study, a different study implicated Rif1 in promoting resection, with a role particularly apparent in G1(Martina et al. 2014). The 2 studies use different detection method for ssDNA: while Martina et al. rely on Southern blot, Mattarocci et al. use a much more quantitative PCR approach. Repair by NHEJ is very quick and it might reduce the amount of ssDNA detected by Southern blot, thereby mimicking a defect in resection. Moreover, Martina et al. do not inquire the outcome of possible increased resection in *rif1* $\Delta$ : they detect only a slight increase in resection in *rif1* $\Delta$  and it cannot be assumed that this leads to increased HR repair. In fact, resection assays are performed on the entire population of cells, most of which are destined to die: in the system used in both papers (HO-induce DSB at *MAT*), imprecise NHEJ is anyway a rare event involving 0.1-0.3% of the cells, so that variation in its frequency cannot be easily detected without a specific NHEJ assay. However, it cannot be excluded that both conclusions of these studies are valid, and that Rif1 has a dual role: in G1 it could contribute to minimal resection at DSBs, in order to ensure appropriate timing of extensive resection in the following S phase, whereas in S, possibly upon modifications and/or conformational changes, it could bind DNA in a conformation that encases the ends, attenuating end resection.

Mec1 itself controls resection at yeast DSBs, albeit indirectly: it promotes phosphorylation of H2A and DSB sites, and phosphorylated H2A (YH2A) recruits Rad9(Hammet et al. 2007; di Cicco et al. 2017). Rad9 is often considered to be the yeast ortholog of 53BP1, which is a resection inhibitor. However, the yeast Rad9 is a main actor of checkpoint activation in all phases of the cell cycle, a function that is not shared with 53BP1. Moreover, distinct from 53BP1, there is no apparent role of Rad9 at telomeres, probably because subtelomeric chromatin does not have much H3K79me, a histone mark that provides a binding site for Rad9(Takahashi et al. 2011).

Chromatin structure indeed plays also an important role in coordinating resection. Chromatin remodeling occurs at breaks in order to allow coordinated access to processing and repair components. For example, in yeast the initiation of resection by MRX is controlled by the SWI/SNF ATP-dependent nucleosome remodeler (although SWI/SNF does not affect MRX-related functions in end joining)(Wiest et al. 2017). Fun30 counteracts the action of Rad9 at DSBs, where Fun30 promotes long-range resection by facilitating access both to Exo1 and Sgs1/Dna2 nucleases(Chen et al. 2012). Fun30 recruitment at breaks is dependent on its interaction with Dpb11 and with the 9-1-1 complex. The interaction Fun30-Dpb11 is CDK-dependent, thereby restricting long range resection to S phase(Bantele et al. 2017). In humans, the homolog of Fun 30 is SMARCAD1. SMARCAD1 is also involved in promoting resection: the complex BRCA1-BARD1 acts as E3 ubiquitin ligase and modifies histone H2A. Ubiquitinated histone H2A is bound by SMARCAD1, that by sliding nucleosomes promotes repositioning of 53BP1 to the periphery of IR-induced foci(Neely et al. 2016).

When NHEJ is compromised, or resection is initiated but does not progress efficiently, another highly mutagenic repair mechanism called alternative end joining (A-EJ) comes into play. A-EJ is independent of Dnl4 as well as yKu70/80. High mobility group protein 1 (Hmo1) is a DNA-binding factor that prevents this end joining mechanism by limiting resection and channeling break repair towards classical NHEJ. Hmo1 is not evenly distributed in the genome: its occupancy and effect is highest at ribosomal protein genes and nucleosome-free regions. The effect of Hmo1 on resection is due to its ability to stabilize chromatin by slowing chromatin remodeling(Panday et al. 2017).

Recently the role of short ncRNA transcribed and acting in *cis* at sites of DSBs is starting to emerge in several organisms: in higher eukaryotes, these damage-induced RNAs were proposed to favor recruitment of remodelers and other processing enzymes. In *S. cerevisiae*, it was demonstrated that short RNAs can promote repair of a DSB by acting directly as donors in homologous recombination(Storici et al. 2014). In *S. pombe* the mechanism of action of this short RNA was elucidated: the initial resection by MRN

promotes recruitment of PolII and transcription, with the nascent short RNAs annealing directly at their strand DNA template: in this way, they stabilize the ssDNA at the break site and inhibit RPA binding. Although a direct contribution of these RNAs to inhibiting resection was not tested, it was apparent that the length of RPA-bound ssDNA at a DSB was significantly increased in presence of RNase H1(Ohle et al. 2016).

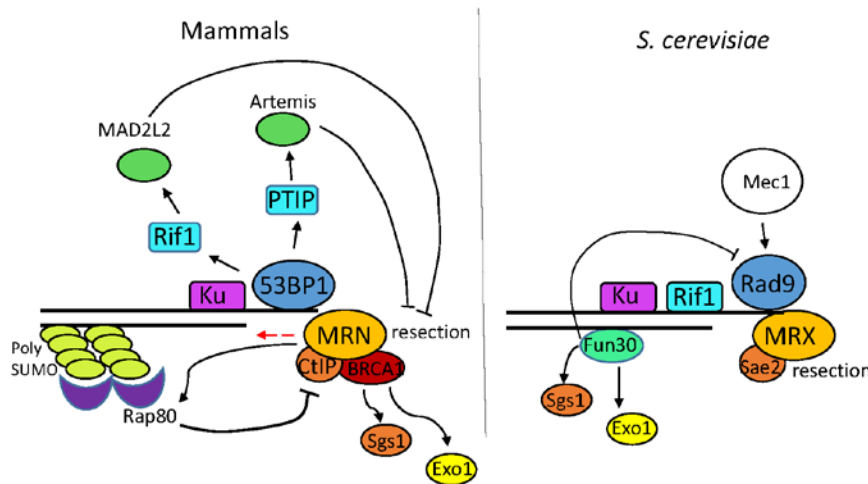


**Fig.1. The main players in early resection control in mammals versus *S. cerevisiae*.** Coordinated colors indicate homologs.

### The processing of TG-flanked DSBs

To study the specific effects of sequence composition at DSBs, an internal HO cleavage site was flanked by TG repeats at the budding yeast *MAT* locus(Diede and Gottschling 2000). Initial studies on this system placed 80bp of TG sequence at the cut site, which was shown to be sufficient to serve as a seed for telomerase in S/G2 phase cells, although no elongation was detected when cells were arrested in G1(Diede and Gottschling 2000). Indeed, replicative polymerases were also necessary for telomere addition. In this context, the MRX complex appeared to be crucial for determining the repair outcome of the break: at normal DSBs, it initiated resection and promoted Mec1 recruitment. At telomeres and TG80-flanked HO breaks, MRX recruited Tel1, although the binding of Cdc13 inhibited MRX nuclease activity(Hirano and Sugimoto 2007). This in turn reduced Mec1 recruitment and activation.

Another study compared the checkpoint response stemming from a DSB flanked by 80bp or 250bp of TG repeats. Whereas the TG80 break bound RPA, showed resection and partial activation of the DNA damage checkpoint, the TG250 break did not bind DSB signaling proteins (Mec1, RPA, or Cdc13), nor did it induce a checkpoint response(Negrini et al. 2007). This suggests that 250bp of exposed TG repeats are recognized as a *bona fide*

telomere in cells, blocking both resection and checkpoint activation. DSBs flanked by short yeast telomeric and human-like telomeric repeats arrays, on the other hand, represent an intermediate state: although they are uncapped and bind DSB signaling proteins upon cleavage, they do not undergo repair, but serve as a template for telomerase elongation(Ribaud et al. 2012). Similar effects were seen at telomeres in human cell lines undergoing senescence: although telomere dysfunction-induced foci (TIFs) reflect DNA damage signaling, no fusion events were detected(Cesare et al. 2009; Kaul et al. 2011), suggesting that DSB repair was suppressed.

In summary, the presence of telomeric DNA sequences flanking a DSB is sufficient to affect its processing. This is also influenced by the chromosomal context of the break, the length of the repeat sequence and other determinants that are currently unknown. One potential factor in this response may be the spatial organization of damage processing, as discussed below.

## **Persistent DSBs and telomeres share common nuclear subcompartments**

### **Nuclear organization of telomeres**

Although there is extensive genetic and biochemical data about telomeric DNA processing, less is known about the spatial organization of these events and their relation to the nuclear architecture of chromosomal domains or sites of DSB repair. In budding yeast, fission yeast and *C. elegans*, telomeres tend to cluster adjacent to the nuclear envelope, bound by redundant interaction pathways(Funabiki et al. 1993; Gotta et al. 1996; Hediger et al. 2002b; Ferreira et al. 2013). In budding yeast S-phase cells, peripheral anchorage is dependent on the Ku complex (yKu70-yKu80) and on the silent information regulatory complex that consists of Sir4, Sir2 and Sir3(Hediger et al. 2002b; Taddei and Gasser 2004; Kueng et al. 2013). Sir4 binds Esc1, an acidic protein of the inner nuclear membrane, as well as yKu80 and a putative anchor called cohibin(Chan et al. 2011). Deletion of the two genes encoding Esc1 and yKu80 is sufficient to release yeast telomeres from the nuclear periphery, while deletion of only one, or of *SIR4*, leads to partial release(Taddei et al. 2004). Indeed, yKu-mediated anchorage of telomeres in S-phase cells depends on yKu interaction with the SUN domain protein Mps3, which Ku binds indirectly but in a manner independent of Sir4. YKu80 in S phase also binds Tlc1, the telomerase RNA, which is also bound by Est1, which in turn binds the N-terminal nucleoplasmic domain of Mps3(Antoniacci et al. 2007; Bupp et al. 2007; Schober et al. 2009). Also in G1-phase cells multiple pathways of telomere anchoring (Sir4- and yKu-mediated) were detected, although the membrane partner for yKu in G1 phase is unknown. Nuclear pores seem not to be directly involved in undamaged telomere

anchorage, although the nuclear basket proteins Mlp1/Mlp2 affect telomere length on a pathway that is epistatic with Tel1(Hediger et al. 2002a).

Intriguingly, short telomeres, and especially those that are dependent on recombination for length maintenance (e.g. in telomerase deficient strains), show a different distribution. First, a critically short telomere in a newly formed yeast zygote was shown to shift away from the nuclear envelope during the first round of elongation by telomerase(Ferreira et al. 2011). Moreover, in absence of telomerase, a single eroded telomere that activates the DSB response was shown to bind recombination factors and colocalize with the nuclear pore, although this might be a transient interaction(Khadaroo et al. 2009). Consistent with the notion that the normal S-phase sequestration of telomeres at Mps3 reduces recombination, an N-terminal deletion of Mps3 causes elevated recombination between telomeres(Schober et al. 2009). In another study, the 3D position of fluorescently labeled telomere XI-L with respect to the nuclear periphery was tracked: the peripheral location of this telomere was found to be disrupted in mutants of the Nup84 complex. In such mutants Sir3 was partially dispersed, causing a silencing defect of subtelomeric genes(Therizols et al. 2006). A further link of nuclear pores to telomere function came from the study of Nup170. This nucleoporin impacts gene silencing in subtelomeric domains, possibly by regulating nucleosome positioning. Sir4 and Nup170 were shown to co-immunoprecipitate, primarily in M phase, and to favor each other's interaction with subtelomeric DNA. Finally, *nup170Δ* mutants influenced the peripheral localization of telomeres in G1-, but not in S-phase cells(Van de Vosse et al. 2013).

Recently, Lapetina and colleagues proposed that although Esc1 can interact with pores, and Nup170 is a NPC component, their interaction with Sir4 and Siz2 occurs outside of the holo-NPC, in a separate complex called Snup, that regulates telomere silencing and localization(Lapetina et al. 2017).

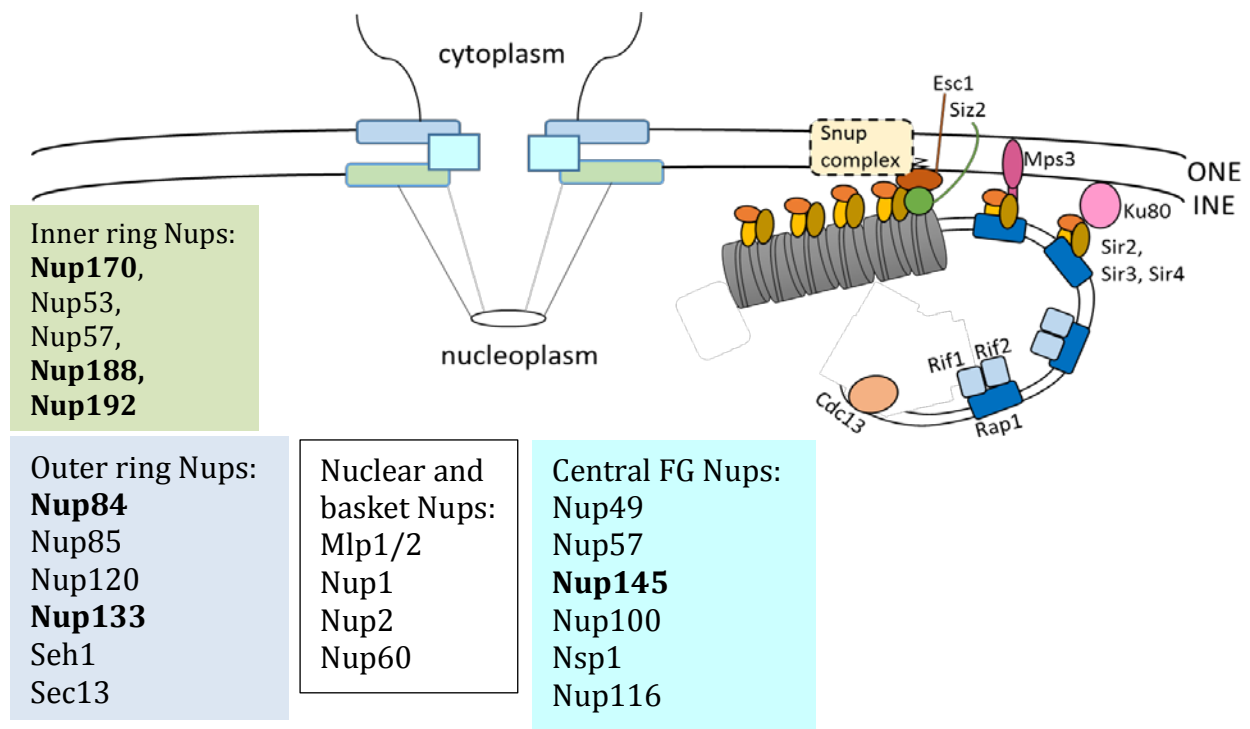


**Fig. 2. Anchorage of telomeric heterochromatin at the nuclear periphery in *S. cerevisiae*.**

Sir4 interacts with Rap1 and nucleates subtelomeric heterochromatin. Telomeres are located at the nuclear periphery through interactions of Sir4 with Ku80 and with the inner nuclear membrane protein Esc1. In S phase, anchorage of telomeres also depends on the interaction of Ku80 with the SUN domain protein Mps3, which is mediated by the telomerase subunit Est1 (not shown). While nuclear pores are not directly involved in anchorage of steady state telomeres, several nucleoporins were shown to play a role in subtelomeric silencing and organization. Recently it was proposed that a Snup complex, composed of Nup170, Sir4, Esc1, Siz2 and other nucleoporins, assembles outside of the holo-nuclear pore complex and regulates telomeric nuclear organization (Lapetina et al. 2017). Tested components of the Snup complex are highlighted in bold. ONE = outer nuclear envelope. INE = inner nuclear envelope.

organisms as well: *C. elegans* telomeres in somatic cells are not clustered but they localize at the nuclear envelope through a direct interaction between the Shelterin component POT-1 and the Mps3 homolog SUN-1 (Ferreira et al. 2013). In most eukaryotes, telomeres cluster in meiosis at the nuclear envelope through the SUN and KASH domain nuclear membrane proteins, in a so-called bouquet arrangement that favors recombination between homologous chromosomes. These proteins interact to link the cytoskeleton to the nuclear structural proteins, connecting telomeres with the cytoskeleton (Ding et al. 2007) and potentially also to the extracellular matrix in complex tissues. In contrast to yeast, eroded mammalian telomeres in cells lacking telomerase do not shift to nuclear pores, but are recruited to Promyelocytic Leukemia (PML) bodies together with the recombination factors that are needed to maintain telomere length. Telomere length in these cells is maintained through a recombination-mediated ALT pathway. In so-called ALT cells, the SUMO-targeted Ubiquitin ligase (STUbL) RNF4 and the SMC5/6 complex promote colocalization of telomeres with PML bodies, where the E3 SUMO ligase Mms21 leads to the modification of TRF1 and TRF2. Extensive SUMOylation appears to be required for telomeric recombination. Intriguingly, nuclear pores in yeast are the binding sites of the RNF4 homologue, Slx5/Slx8, and the major site of SUMO metabolism.

Furthermore, in yeast Slx5/8 was shown to be necessary for formation of type II survivors at telomeres, the recombination-mediated process of telomere maintenance analogous to mammalian ALT (Azam et al. 2006). Therefore, the functional role of eroded telomere relocation to sites of high SUMOylation (nuclear pores in yeast, PML bodies in mammals) in absence of telomerase may be conserved (Potts and Yu 2007).

### **Nuclear organization in DSB processing**

In mammalian cells, PML bodies are not general sites of DNA repair, because not all proteins related to repair behave the same in relation to these foci: some accumulate upon damage while others are released, and yet others translocate only late after induction of damage (Bernardi and Pandolfi 2007). Nonetheless, PML bodies increase in number and size upon genotoxic stress in an ATM- and ATR-dependent manner, accumulate some checkpoint and repair proteins, as well as ssDNA and SUMOylated proteins (Bischof et al. 2001; Dellaire et al. 2006). PML bodies sequester irreparable or hard-to-repair DNA damage and harbor sumoylating enzymes and substrates (Saitoh et al. 2006), much like the nuclear periphery in budding yeast, as described below.

Consistently, the processing of DSBs in *S. cerevisiae* in the absence of a donor for HR appears to occur at nuclear pores. Conversely, DSBs that can be rapidly repaired by NHEJ or by the classic HR in which sister chromatids provide the sequence template, remain randomly distributed in the nucleoplasm, away from the nuclear envelope, as scored by the distribution of Rad52 foci (Bystricky et al. 2008). Nuclear pores are not the only perinuclear sites that bind damage. The only SUN domain protein in yeast, Mps3, was also shown by CHIP to interact specifically with irreparable DSBs, through its N-terminal domain, which also recognizes the histone variant Htz1 (Kalocsay et al. 2009; Gardner et al. 2011). Htz1 is rapidly incorporated at DSBs in yeast, by the SWR1 nucleosome remodeler, and its SUMOylation is required for DSB relocation to the nuclear envelope (Kalocsay et al. 2009). Interestingly, Htz1 seems to have also a chromatin-independent role in targeting Mps3 to the inner nuclear membrane by interacting with its N terminal soluble domain (Gardner et al. 2011). Moreover, breaks in rDNA relocate transiently outside of the nucleolus in a manner that requires SUMOylation of Rad52 by the SMC5/6 complex (Torres-Rosell et al. 2007). However, when both sister chromatids are cleaved, or a replication fork collapses prior to producing a template, these DSBs are shifted to nuclear pores within 40 minutes (Nagai et al. 2008).

Expanded CAG repeats, in yeast as in mammals, are fragile sites prone to replication stress. These repeats were shown to relocate to nuclear pores, but not to Mps3, in a Slx5/8 dependent manner. It was proposed that Slx5/8 promotes removal of SUMOylated Rad52

to limit HR-driven repeats instability and favor replication fork restart(Su et al. 2015). By using a reporter assay for gene conversion, it was seen that tethering a locus to the nuclear envelope by *lexA* fusions enhances the frequency of recombination. These results started to uncover the role of SUMOylation in DSB repair and led to the hypothesis that an alternative repair pathway takes place at nuclear pores: a SUMOylated protein may accumulate at DSB sites and require ubiquitination and proteasomal degradation to allow repair.

This scenario finds genetic support in the epistatic relationship (E-MAP) between the SUMO-targeted ubiquitin ligases (STUbLs) *SLX5*, *SLX8*, genes encoding the Nup84 complex, and mutants in components of recombinational repair(Nagai et al. 2008). These mutations also led to a sensitivity to conditions of replication fork collapse and in telomerase-deficient cells, this pathway appears to promote type II survivors(Burgess et al. 2007). The relevant target(s) of these STUbLs at DSBs are still unknown and their identification is complicated by the extensive and promiscuous SUMOylation of proteins at DSBs(Cremona et al. 2012).

Current studies have been focusing on whether these subnuclear compartments in DNA repair have distinct functions. The loss of the Slx5/8 complex, which is partially located at nuclear pores, reduces break-induced replication (BIR) and other imprecise exchange pathways of repair, while loss of Mps3 increases telomeric exchange(Schober et al. 2009). Thus, it appears that the functions of these two peripheral binding sites are quite distinct, although it cannot be excluded that they hand-off damage from one to the other. Moreover, in yeast there are other putative STUbLs that are involved in DNA repair: the Swi2/Snf2 family of ATPases Irc2 and Uls1(Alvaro et al. 2007; Cal-Bakowska et al. 2011; Miura et al. 2012). A possible role of these STUbLs in DSB processing or repair, has not yet been explored.

Relocation of damage to specialized domains is not unique to yeast. In *Drosophila*, a DSB in a heterochromatic region is preferentially repaired by HR: it forms  $\gamma$ H2AX foci in heterochromatin and is resected but then moves to the periphery of a heterochromatic domain to form Rad51 foci and be further processed by recombination proteins(Chiolo et al. 2011). Also in mice, induction of a DSB in the chromocenter induces a similar phenomenon: breaks are seen to move outside the chromocenter and its heterochromatin domain(Jakob et al. 2011).

However, relocation may not be common to all organisms, nor to all kinds of heterochromatin. In a recent study in mammalian cells, breaks in lamina-associated domains, but not breaks that occur elsewhere in the nucleus, were not relocated outside of heterochromatin for repair, instead they were shown to repair with delayed kinetics



and preferentially by microhomology mediated end joining(Lemaitre et al. 2014). In mice, HR proteins are assumed to be unable to access the dense lamina-associated heterochromatin, indicating that chromatin context and subnuclear location can affect repair pathway choice. Thus, although DSB interactions with the nuclear envelope are not common in mammalian cells, the spatial segregation of DSB processing pathways into subdomains of the nucleus is something that is found across many eukaryotic species. In addition, an indirect role for nucleoporins in coordinating DSB repair seems to be conserved in mammalian cells: Nup153, a nucleoporin belonging to the pore basket, plays two roles in 53BP1 function: it mediates 53BP1 nuclear import(Moudry et al. 2011) and promotes NHEJ by intranuclear targeting of 53BP1 to sites of DNA damage(Lemaitre et al. 2014; Mackay et al. 2017). In the latter function, Nup153 is assisted by another nucleoporin: Nup50, which is dispensable for 53BP1 import(Ullman et al. 2017). Although no direct interaction of these NPC components with DSBs was detected, Nup153 interacts directly with SUMO proteases SENP1 and SENP2(Dasso and Mary 2002; Chow et al. 2012) which may regulate 53BP1 SUMOylation at DSB sites. Modification of 53BP1 by SUMO-1 E3 ligase is required for efficient accumulation of 53BP1 at DSBs and efficient repair by NHEJ(Duheron et al. 2017). These studies are reminiscent of a very similar SUMO-dependent effect of nucleoporins Nup60 and Nup84 on DSB repair in budding yeast: they modulate Ulp1 SUMO protease levels at pores and the SUMOylation levels of several DSB processing factors, among which is yKu70(Palancade et al. 2007).

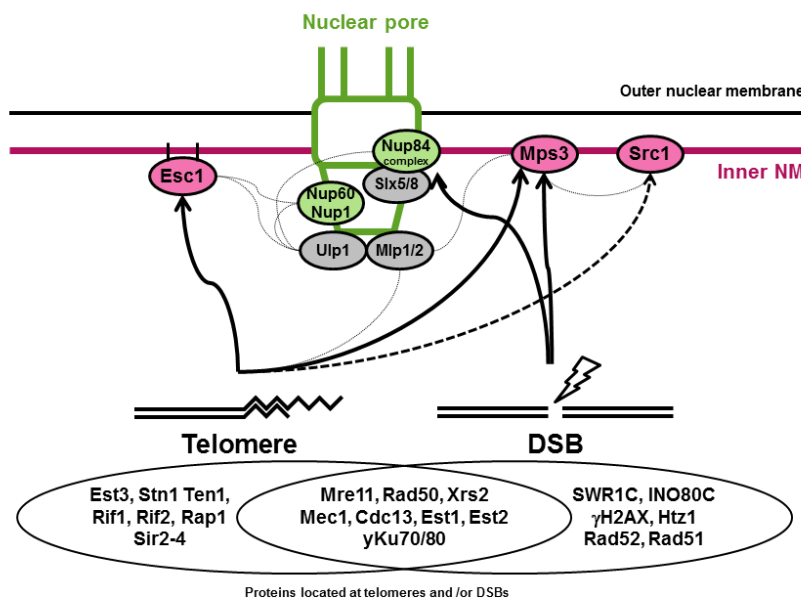


### **Fig. 3. Proteins and binding sites shared by telomeres and DSBs in budding yeast.**

Yeast telomeres and DSBs share both ligands relevant for repair and checkpoint activation, as well as sites of perinuclear anchorage. Shown schematically are two types of “exposed” chromosomal ends found in living cells. Telomeres and DSBs share some ligands (see middle, bottom) while others are unique. Breaks and telomeres are both found at specific binding sites on the inner nuclear membrane. Heavy black lines show direct interactions, while lighter lines show synthetic interactions consistent with occasional contact. See text for details.

## **Aim of the thesis**

Already in 1938, with the studies of Müller on the effects of X-rays on *Drosophila* chromosomes, it became apparent that natural chromosomal ends have special protective features that prevent them from being recognized as DSBs in the cellular environment. Since then, the features that specify telomere identity have been a major field of research in cell biology. The features that confer a distinct identity on telomeres with respect to DNA repair have been identified, and they include both a specific set of telomeric DNA repeat-binding proteins (the telosome), and mechanisms that sequester the telomere in heterochromatic foci, which in yeast are located at the inner nuclear membrane. However, as highlighted in this introduction, it is now clear that many telomeric proteins are shared with DSBs, yet have a different function in the two situations. Moreover, the nuclear envelope has emerged as a site of DSB end processing and break repair, as well as a zone that sequesters telomeres.

My project stems from the apparently contradictory observation that telomeres and DSBs share common proteins and subnuclear locations yet must ultimately have opposite fates: DSBs need to be repaired to maintain genome integrity and cell proliferation, whereas telomeres need to be protected from unwanted repair events that can cause chromosome fusions and a different sort of genomic instability. I tackled this apparent contradiction addressing two questions:

1. Two common anchorage sites of DSBs and telomeres are known at the nuclear envelope: Mps3 and the nuclear pore. It is conceivable that they might determine break or telomere identity by favoring one or more end processing events that are common to breaks and telomeres. I shed light on this hypothesis by contributing the definition of requirements for a DSB to move to the NE, and by testing the efficiency of specific repair pathways with reporter assays in NE mutants. These results are published in the two Horigome et al. papers (chapter 2).
2. Chromosome ends differ from break ends by a repetitive DNA sequence in all eukaryotes. I hypothesized that suppression of repair at telomeres is entirely

specified by this DNA sequence. I tested this hypothesis by inserting a telomeric sequence, flanked by an inducible DSB, in the middle of a chromosome arm, far from the telomeric environment. I analyzed the effects of the telomeric repeats on DSB processing and repair, also in relation to its nuclear location. These results are leading to the paper whose manuscript is included in chapter 3.

## References

- Adam S, Polo SE. 2014. Blurring the line between the DNA damage response and transcription: the importance of chromatin dynamics. *Experimental cell research* **329**: 148-153.
- Aksenova AY, Greenwell PW, Dominska M, Shishkin AA, Kim JC, Petes TD, Mirkin SM. 2013. Genome rearrangements caused by interstitial telomeric sequences in yeast. *Proceedings of the National Academy of Sciences of the United States of America* **110**: 19866-19871.
- Alvaro D, Lisby M, Rothstein R. 2007. Genome-Wide Analysis of Rad52 Foci Reveals Diverse Mechanisms Impacting Recombination. *PLoS genetics* **3**.
- Antoniacci LM, Kenna MA, Skibbens RV. 2007. The nuclear envelope and spindle pole body-associated Mps3 protein bind telomere regulators and function in telomere clustering. *Cell cycle (Georgetown, Tex)* **6**: 75-79.
- Azam M, Lee JY, Abraham V, Chanoux R, Schoenly KA, Johnson FB. 2006. Evidence that the *S.cerevisiae* Sgs1 protein facilitates recombinational repair of telomeres during senescence. *Nucleic acids research* **34**: 506-516.
- Bantele SC, Ferreira P, Gritenaite D, Boos D, Pfander B. 2017. Targeting of the Fun30 nucleosome remodeller by the Dpb11 scaffold facilitates cell cycle-regulated DNA end resection. *Elife* **6**.
- Bekker-Jensen S, Lukas C, Kitagawa R, Melander F, Kastan MB, Bartek J, Lukas J. 2006. Spatial organization of the mammalian genome surveillance machinery in response to DNA strand breaks. *The Journal of cell biology* **173**: 195-206.
- Bernardi R, Pandolfi PP. 2007. Structure, dynamics and functions of promyelocytic leukaemia nuclear bodies. *Nature reviews Molecular cell biology* **8**: 1006-1016.
- Bertuch AA, Lundblad V. 2003. The Ku Heterodimer Performs Separable Activities at Double-Strand Breaks and Chromosome Termini. in *Molecular and cellular biology*, pp. 8202-8215.
- Bilaud T, Koering CE, Binet-Brasselet E, Ancelin K, Pollice A, Gasser SM, Gilson E. 1996. The telobox, a Myb-related telomeric DNA binding motif found in proteins from yeast, plants and human. *Nucleic acids research* **24**: 1294-1303.
- Bischof O, Kim SH, Irving J, Beresten S, Ellis NA, Campisi J. 2001. Regulation and localization of the Bloom syndrome protein in response to DNA damage. *The Journal of cell biology* **153**: 367-380.
- Blackburn EH. 1991. Structure and function of telomeres. *Nature* **350**: 569-573.
- Bothmer A, Robbiani DF, Di Virgilio M, Bunting SF, Klein IA, Feldhahn N, Barlow J, Chen HT, Bosque D, Callen E et al. 2011. Regulation of DNA end joining, resection, and immunoglobulin class switch recombination by 53BP1. *Molecular cell* **42**: 319-329.
- Boulton SJ, Jackson SP. 1996. Identification of a *Saccharomyces cerevisiae* Ku80 homologue: roles in DNA double strand break rejoining and in telomeric maintenance. *Nucleic acids research* **24**: 4639-4648.
- . 1998. Components of the Ku-dependent non-homologous end-joining pathway are involved in telomeric length maintenance and telomeric silencing. *The EMBO journal* **17**: 1819-1828.
- Brigati C, Kurtz S, Balderes D, Vidali G, Shore D. 1993. An essential yeast gene encoding a TTAGGG repeat-binding protein. *Molecular and cellular biology* **13**: 1306-1314.
- Bupp JM, Martin AE, Stensrud ES, Jaspersen SL. 2007. Telomere anchoring at the nuclear periphery requires the budding yeast Sad1-UNC-84 domain protein Mps3. *The Journal of cell biology* **179**: 845-854.
- Burgess DJ. 2013. Genome stability: Specialist responses at telomeres. *Nature reviews Genetics* **14**: 597.

- Burgess RC, Rahman S, Lisby M, Rothstein R, Zhao X. 2007. The Slx5-Slx8 complex affects sumoylation of DNA repair proteins and negatively regulates recombination. *Molecular and cellular biology* **27**: 6153-6162.
- Bystricky K, Van Attikum H, Montiel MD, Dion V, Gehlen L, Gasser SM. 2008. Regulation of nuclear positioning and dynamics of the silent mating type loci by the yeast Ku70/Ku80 complex. *Molecular and cellular biology* **29**: 835-848.
- Cal-Bakowska M, Litwin I, Bocer T, Wysocki R, Dziadkowiec D. 2011. The Swi2-Snf2-like protein Uls1 is involved in replication stress response. *Nucleic acids research* **39**: 8765-8777.
- Cannavo E, Cejka P. 2014. Sae2 promotes dsDNA endonuclease activity within Mre11-Rad50-Xrs2 to resect DNA breaks. *Nature* **514**: 122-125.
- Cesare AJ, Kaul Z, Cohen SB, Napier CE, Pickett HA, Neumann AA, Reddel RR. 2009. Spontaneous occurrence of telomeric DNA damage response in the absence of chromosome fusions. *Nature structural & molecular biology* **16**: 1244-1251.
- Chan JN, Poon BP, Salvi J, Olsen JB, Emili A, Mekhail K. 2011. Perinuclear cohibin complexes maintain replicative life span via roles at distinct silent chromatin domains. *Developmental cell* **20**: 867-879.
- Chen L, Nievera CJ, Lee AY, Wu X. 2008. Cell cycle-dependent complex formation of BRCA1.CtIP.MRN is important for DNA double-strand break repair. *The Journal of biological chemistry* **283**: 7713-7720.
- Chen X, Cui D, Papusha A, Zhang X, Chu CD, Tang J, Chen K, Pan X, Ira G. 2012. The Fun30 nucleosome remodeller promotes resection of DNA double-strand break ends. *Nature* **489**: 576-580.
- Chiba LW, Li L, Zehui H, Akira Y, Chikashi I, Natsuko. 2008. Rapid Recruitment of BRCA1 to DNA Double-Strand Breaks Is Dependent on Its Association with Ku80.
- Chiolo I, Minoda A, Colmenares SU, Polyzos A, Costes SV, Karpen GH. 2011. Double-strand breaks in heterochromatin move outside of a dynamic HP1a domain to complete recombinational repair. *Cell* **144**: 732-744.
- Chow KH, Elgort S, Dasso M, Ullman KS. 2012. Two distinct sites in Nup153 mediate interaction with the SUMO proteases SENP1 and SENP2. *Nucleus (Austin, Tex)* **3**: 349-358.
- Churikov D, Corda Y, Luciano P, Geli V. 2013. Cdc13 at a crossroads of telomerase action. *Frontiers in oncology* **3**: 39.
- Clerici M, Mantiero D, Guerini I, Lucchini G, Longhese MP. 2008. The Yku70-Yku80 complex contributes to regulate double-strand break processing and checkpoint activation during the cell cycle. *EMBO reports* **9**: 810-818.
- Court R, Chapman L, Fairall L, Rhodes D. 2004. How the human telomeric proteins TRF1 and TRF2 recognize telomeric DNA: a view from high-resolution crystal structures. *EMBO reports* **6**: 39-45.
- Cremona CA, Sarangi P, Yang Y, Hang LE, Rahman S, Zhao X. 2012. Extensive DNA damage-induced sumoylation contributes to replication and repair and acts in addition to the mec1 checkpoint. *Molecular cell* **45**: 422-432.
- Dasso JH, Mary. 2002. Association of the Human SUMO-1 Protease SENP2 with the Nuclear Pore.
- Delacroix S, Wagner JM, Kobayashi M, Yamamoto K, Karnitz LM. 2007. The Rad9-Hus1-Rad1 (9-1-1) clamp activates checkpoint signaling via TopBP1. *Genes & development* **21**: 1472-1477.
- Dellaire G, Ching RW, Dehghani H, Ren Y, Bazett-Jones DP. 2006. The number of PML nuclear bodies increases in early S phase by a fission mechanism. *Journal of cell science* **119**: 1026-1033.
- Dewar JM, Lydall D. 2010. Pif1- and Exo1-dependent nucleases coordinate checkpoint activation following telomere uncapping. *The EMBO journal* **29**: 4020-4034.
- di Cicco G, Bantele SCS, Reuswig KU, Pfander B. 2017. A cell cycle-independent mode of the Rad9-Dpb11 interaction is induced by DNA damage. *Scientific reports* **7**: 11650.
- Diede SJ, Gottschling DE. 2000. Telomerase-mediated telomere addition in vivo requires DNA primase and DNA polymerases alpha and delta. *Cell* **99**: 723-733.
- Dimitrova N, Chen YC, Spector DL, de Lange T. 2008. 53BP1 promotes non-homologous end joining of telomeres by increasing chromatin mobility. *Nature* **456**: 524-528.
- Ding X, Xu R, Yu J, Xu T, Zhuang Y, Han M. 2007. SUN1 is required for telomere attachment to nuclear envelope and gametogenesis in mice. *Developmental cell* **12**: 863-872.
- Doksani Y, Wu JY, de Lange T, Zhuang X. 2013. Super-resolution fluorescence imaging of telomeres reveals TRF2-dependent T-loop formation. *Cell* **155**: 345-356.

- Duheron V, Nilles N, Pecenko S, Martinelli V, Fahrenkrog B. 2017. Localisation of Nup153 and SENP1 to nuclear pore complexes is required for 53BP1-mediated DNA double-strand break repair. *Journal of cell science* **130**: 2306-2316.
- Falck J, Coates J, Jackson SP. 2005. Conserved modes of recruitment of ATM, ATR and DNA-PKcs to sites of DNA damage. *Nature* **434**: 605-611.
- Ferreira HC, Luke B, Schober H, Kalck V, Lingner J, Gasser SM. 2011. The PIAS homologue Siz2 regulates perinuclear telomere position and telomerase activity in budding yeast. *Nature cell biology* **13**: 867-874.
- Ferreira HC, Towbin BD, Jegou T, Gasser SM. 2013. The shelterin protein POT-1 anchors *Caenorhabditis elegans* telomeres through SUN-1 at the nuclear periphery. *The Journal of cell biology* **203**: 727-735.
- Finn K, Lowndes NF, Grenon M. 2011. Eukaryotic DNA damage checkpoint activation in response to double-strand breaks. *Cellular and molecular life sciences : CMLS* **69**: 1447-1473.
- Foster SS, Balestrini A, Petrini JH. 2011. Functional interplay of the Mre11 nuclease and Ku in the response to replication-associated DNA damage. *Molecular and cellular biology* **31**: 4379-4389.
- Foster SS, Zubko MK, Guillard S, Lydall D. 2006. MRX protects telomeric DNA at uncapped telomeres of budding yeast *cdc13-1* mutants. *DNA repair* **5**: 840-851.
- Fourel G, Revardel E, Koering CE, Gilson E. 1999. Cohabitation of insulators and silencing elements in yeast subtelomeric regions. *The EMBO journal* **18**: 2522-2537.
- Fradet-Turcotte A, Canny MD, Escribano-Diaz C, Orthwein A, Leung CC, Huang H, Landry MC, Kitevski-LeBlanc J, Noordermeer SM, Sicheri F et al. 2013. 53BP1 is a reader of the DNA-damage-induced H2A Lys 15 ubiquitin mark. *Nature* **499**: 50-54.
- Funabiki H, Hagan I, Uzawa S, Yanagida M. 1993. Cell cycle-dependent specific positioning and clustering of centromeres and telomeres in fission yeast. *The Journal of cell biology* **121**: 961-976.
- Gallardo F, Olivier C, Dandjinou AT, Wellinger RJ, Chartrand P. 2008. TLC1 RNA nucleocytoplasmic trafficking links telomerase biogenesis to its recruitment to telomeres. *The EMBO journal* **27**: 748-757.
- Gao H, Toro TB, Paschini M, Braunstein-Ballew B, Cervantes RB, Lundblad V. 2010. Telomerase recruitment in *Saccharomyces cerevisiae* is not dependent on Tel1-mediated phosphorylation of Cdc13. *Genetics* **186**: 1147-1159.
- Gardner JM, Smoyer CJ, Stensrud ES, Alexander R, Gogol M, Wiegraebe W, Jaspersen SL. 2011. Targeting of the SUN protein Mps3 to the inner nuclear membrane by the histone variant H2A.Z. *The Journal of cell biology* **193**: 489-507.
- Gilson E, Roberge M, Giraldo R, Rhodes D, Gasser SM. 1993. Distortion of the DNA double helix by RAP1 at silencers and multiple telomeric binding sites. *Journal of molecular biology* **231**: 293-310.
- Gobbini E, Cesena D, Galbiati A, Lockhart A, Longhese MP. 2013. Interplays between ATM/Tel1 and ATR/Mec1 in sensing and signaling DNA double-strand breaks. *DNA repair* **12**: 791-799.
- Gotta M, Laroche T, Formenton A, Maillet L, Scherthan H, Gasser SM. 1996. The clustering of telomeres and colocalization with Rap1, Sir3, and Sir4 proteins in wild-type *Saccharomyces cerevisiae*. *The Journal of cell biology* **134**: 1349-1363.
- Gravel S, Chapman JR, Magill C, Jackson SP. 2008. DNA helicases Sgs1 and BLM promote DNA double-strand break resection. *Genes & development* **22**: 2767-2772.
- Greenwell PW, Kronmal SL, Porter SE, Gassenhuber J, Obermaier B, Petes TD. 1995. TEL1, a gene involved in controlling telomere length in *S. cerevisiae*, is homologous to the human ataxia telangiectasia gene. *Cell* **82**: 823-829.
- Griffith JD, Comeau L, Rosenfield S, Stansel RM, Bianchi A, Moss H, de Lange T. 1999. Mammalian telomeres end in a large duplex loop. *Cell* **97**: 503-514.
- Hammet A, Magill C, Heierhorst J, Jackson SP. 2007. Rad9 BRCT domain interaction with phosphorylated H2AX regulates the G1 checkpoint in budding yeast. *EMBO reports* **8**: 851-857.
- Hediger F, Dubrana K, Gasser SM. 2002a. Myosin-like proteins 1 and 2 are not required for silencing or telomere anchoring, but act in the Tel1 pathway of telomere length control. *Journal of structural biology* **140**: 79-91.

- Hediger F, Neumann FR, Van Houwe G, Dubrana K, Gasser SM. 2002b. Live imaging of telomeres: yKu and Sir proteins define redundant telomere-anchoring pathways in yeast. *Current biology : CB* **12**: 2076-2089.
- Hirano Y, Sugimoto K. 2007. Cdc13 telomere capping decreases Mec1 association but does not affect Tel1 association with DNA ends. *Molecular biology of the cell* **18**: 2026-2036.
- Hustedt N, Gasser SM, Shimada K. 2013. Replication checkpoint: tuning and coordination of replication forks in s phase. *Genes* **4**: 388-434.
- Ira G, Nussenzweig A. 2014. A new Riff: Rif1 eats its cake and has it too. *EMBO reports* **15**: 622-624.
- Jackson SP, Bartek J. 2009. The DNA-damage response in human biology and disease. *Nature* **461**: 1071-1078.
- Jacobs VB, Nathalie M, Sandra S-B, Marieke HP, Jaco van der T, Brigitte AW, Alexandre O, Daniel D, Jacqueline JL. 2015. MAD2L2 controls DNA repair at telomeres and DNA breaks by inhibiting 5[prime] end resection. *Nature* **521**: 537-540.
- Jakob B, Splinter J, Conrad S, Voss KO, Zink D, Durante M, Lohrich M, Taucher-Scholz G. 2011. DNA double-strand breaks in heterochromatin elicit fast repair protein recruitment, histone H2AX phosphorylation and relocation to euchromatin. *Nucleic acids research* **39**: 6489-6499.
- Kakarougkas A, Ismail A, Katsuki Y, Freire R, Shibata A, Jeggo PA. 2013. Co-operation of BRCA1 and POH1 relieves the barriers posed by 53BP1 and RAP80 to resection. *Nucleic acids research* **41**: 10298-10311.
- Kalocsay M, Hiller NJ, Jentsch S. 2009. Chromosome-wide Rad51 spreading and SUMO-H2A.Z-dependent chromosome fixation in response to a persistent DNA double-strand break. *Molecular cell* **33**: 335-343.
- Kaul Z, Cesare AJ, Huschtscha LI, Neumann AA, Reddel RR. 2011. Five dysfunctional telomeres predict onset of senescence in human cells. *EMBO reports* **13**: 52-59.
- Khadaroo B, Teixeira MT, Luciano P, Eckert-Boulet N, Germann SM, Simon MN, Gallina I, Abdallah P, Gilson E, Geli V et al. 2009. The DNA damage response at eroded telomeres and tethering to the nuclear pore complex. *Nature cell biology* **11**: 980-987.
- König P, Fairall L, Rhodes D. 1998. Sequence-specific DNA recognition by the myb-like domain of the human telomere binding protein TRF1: a model for the protein-DNA complex. *Nucleic acids research* **26**: 1731-1740.
- Konig P, Giraldo R, Chapman L, Rhodes D. 1996. The crystal structure of the DNA-binding domain of yeast RAP1 in complex with telomeric DNA. *Cell* **85**: 125-136.
- Kueng S, Oppikofer M, Gasser SM. 2013. SIR proteins and the assembly of silent chromatin in budding yeast. *Annual review of genetics* **47**: 275-306.
- Kumagai A, Lee J, Yoo HY, Dunphy WG. 2006. TopBP1 activates the ATR-ATRIP complex. *Cell* **124**: 943-955.
- Lamarche BJ, Orazio NI, Weitzman MD. 2010. The MRN complex in double-strand break repair and telomere maintenance. *FEBS letters* **584**: 3682-3695.
- Lange FL, Anne B, Davide FR, Michel CN, Titia d. 2013. Role of 53BP1 oligomerization in regulating double-strand break repair.
- Lapetina DL, Ptak C, Roesner UK, Wozniak RW. 2017. Yeast silencing factor Sir4 and a subset of nucleoporins form a complex distinct from nuclear pore complexes. *The Journal of cell biology*.
- Laroche T, Martin SG, Gotta M, Gorham HC, Pryde FE, Louis EJ, Gasser SM. 1998. Mutation of yeast Ku genes disrupts the subnuclear organization of telomeres. *Current biology : CB* **8**: 653-656.
- Lemaitre C, Grabarz A, Tsouroula K, Andronov L, Furst A, Pankotai T, Heyer V, Rogier M, Attwood KM, Kessler P et al. 2014. Nuclear position dictates DNA repair pathway choice. *Genes & development* **28**: 2450-2463.
- Lieber MR. 2010. The mechanism of double-strand DNA break repair by the nonhomologous DNA end-joining pathway. *Annual review of biochemistry* **79**: 181-211.
- Lin JJ, Zakian VA. 1996. The *Saccharomyces* CDC13 protein is a single-strand TG1-3 telomeric DNA-binding protein in vitro that affects telomere behavior in vivo. *Proceedings of the National Academy of Sciences of the United States of America* **93**: 13760-13765.
- Lundblad AAB, Victoria. 2003. Which end: dissecting Ku's function at telomeres and double-strand breaks.

- Mackay DR, Howa AC, Werner TL, Ullman KS. 2017. Nup153 and Nup50 promote recruitment of 53BP1 to DNA repair foci by antagonizing BRCA1-dependent events. *Journal of cell science* **130**: 3347-3359.
- Makovets S, Blackburn EH. 2009. DNA damage signalling prevents deleterious telomere addition at DNA breaks. *Nature cell biology* **11**: 1383-1386.
- Maringele L, Lydall D. 2002. EXO1-dependent single-stranded DNA at telomeres activates subsets of DNA damage and spindle checkpoint pathways in budding yeast yku70Delta mutants. *Genes & development* **16**: 1919-1933.
- Martina M, Bonetti D, Villa M, Lucchini G, Longhese MP. 2014. Saccharomyces cerevisiae Rif1 cooperates with MRX - Sae2 in promoting DNA - end resection.
- Martina M, Clerici M, Baldo V, Bonetti D, Lucchini G, Longhese MP. 2012. A balance between Tel1 and Rif2 activities regulates nucleolytic processing and elongation at telomeres. *Molecular and cellular biology* **32**: 1604-1617.
- Marvin ME, Becker MM, Noel P, Hardy S, Bertuch AA, Louis EJ. 2009. The association of yKu with subtelomeric core X sequences prevents recombination involving telomeric sequences. *Genetics* **183**: 453-467, 451si-413si.
- Mattarocci S, Reinert JK, Bunker RD, Fontana GA, Shi T, Klein D, Cavadini S, Faty M, Shyian M, Hafner L et al. 2017. Rif1 maintains telomeres and mediates DNA repair by encasing DNA ends. *Nature structural & molecular biology* **24**: 588-595.
- McGee JS, Phillips JA, Chan A, Sabourin M, Paeschke K, Zakian VA. 2010. Reduced Rif2 and lack of Mec1 target short telomeres for elongation rather than double-strand break repair. *Nature structural & molecular biology* **17**: 1438-1445.
- Mimitou EP, Symington LS. 2010. Ku prevents Exo1 and Sgs1-dependent resection of DNA ends in the absence of a functional MRX complex or Sae2. *The EMBO journal* **29**: 3358-3369.
- Mishra K, Shore D. 1999. Yeast Ku protein plays a direct role in telomeric silencing and counteracts inhibition by rif proteins. *Current biology : CB* **9**: 1123-1126.
- Miura T, Yamana Y, Usui T, Ogawa HI, Yamamoto MT, Kusano K. 2012. Homologous Recombination via Synthesis-Dependent Strand Annealing in Yeast Requires the Irc20 and Srs2 DNA Helicases. in *Genetics*, pp. 65-78.
- Moudry P, Lukas C, Macurek L, Neumann B, Heriche JK, Pepperkok R, Ellenberg J, Hodny Z, Lukas J, Bartek J. 2011. Nucleoporin NUP153 guards genome integrity by promoting nuclear import of 53BP1. *Cell death and differentiation* **19**: 798-807.
- Myung K, Datta A, Chen C, Kolodner RD. 2001. SGS1, the Saccharomyces cerevisiae homologue of BLM and WRN, suppresses genome instability and homeologous recombination. *Nature genetics* **27**: 113-116.
- Nagai S, Dubrana K, Tsai-Pflugfelder M, Davidson MB, Roberts TM, Brown GW, Varela E, Hediger F, Gasser SM, Krogan NJ. 2008. Functional targeting of DNA damage to a nuclear pore-associated SUMO-dependent ubiquitin ligase. *Science (New York, NY)* **322**: 597-602.
- Nandakumar J, Bell CF, Weidenfeld I, Zaugg AJ, Leinwand LA, Cech TR. 2012. The TEL patch of telomere protein TPP1 mediates telomerase recruitment and processivity. *Nature* **492**: 285-289.
- Neely, Nicholas HK, Felicity ZW, Joanna R Morris RMD, Alexander JG, Helen RS, Joanna S, Robert AB, Manuel D-M, Alice F et al. 2016. Human BRCA1-BARD1 ubiquitin ligase activity counteracts chromatin barriers to DNA resection. *Nature structural & molecular biology* **23**: 647.
- Negrini S, Ribaud V, Bianchi A, Shore D. 2007. DNA breaks are masked by multiple Rap1 binding in yeast: implications for telomere capping and telomerase regulation. *Genes & development* **21**: 292-302.
- Ohle C, Tesorero R, Schermann G, Dobrev N, Sinning I, Fischer T. 2016. Transient RNA-DNA Hybrids Are Required for Efficient Double-Strand Break Repair. *Cell* **167**: 1001-1013.e1007.
- Oza P, Jaspersen SL, Miele A, Dekker J, Peterson CL. 2009. Mechanisms that regulate localization of a DNA double-strand break to the nuclear periphery. *Genes & development* **23**: 912-927.
- Palancade B, Liu X, Garcia-Rubio M, Aguilera A, Zhao X, Doye V. 2007. Nucleoporins Prevent DNA Damage Accumulation by Modulating Ulp1-dependent Sumoylation Processes. *Molecular biology of the cell* **18**: 2912-2923.
- Panday A, Xiao L, Gupta A, Grove A. 2017. Control of DNA end resection by yeast Hmo1p affects efficiency of DNA end-joining. *DNA repair* **53**: 15-23.

- Pfingsten JS, Goodrich KJ, Taabazuing C, Ouenzar F, Chartrand P, Cech TR. 2012. Mutually exclusive binding of telomerase RNA and DNA by Ku alters telomerase recruitment model. *Cell* **148**: 922-932.
- Pitt CW, Valente LP, Rhodes D, Simonsson T. 2007. Identification and characterization of an essential telomeric repeat binding factor in fission yeast. *The Journal of biological chemistry* **283**: 2693-2701.
- Potts PR, Yu H. 2007. The SMC5/6 complex maintains telomere length in ALT cancer cells through SUMOylation of telomere-binding proteins. *Nature structural & molecular biology* **14**: 581-590.
- Reginato G, Cannavo E, Cejka P. 2018. Physiological protein blocks direct the Mre11-Rad50-Xrs2 and Sae2 nuclease complex to initiate DNA end resection. *Genes & development* **31**: 2325-2330.
- Ribaud V, Ribeyre C, Damay P, Shore D. 2012. DNA-end capping by the budding yeast transcription factor and subtelomeric binding protein Tbf1. *The EMBO journal* **31**: 138-149.
- Saitoh N, Uchimura Y, Tachibana T, Sugahara S, Saitoh H, Nakao M. 2006. In situ SUMOylation analysis reveals a modulatory role of RanBP2 in the nuclear rim and PML bodies. *Experimental cell research* **312**: 1418-1430.
- Schmidt JC, Dalby AB, Cech TR. 2014. Identification of human TERT elements necessary for telomerase recruitment to telomeres. *Elife* **3**.
- Schmidt JC, Zaug AJ, Cech TR. 2016. Live Cell Imaging Reveals the Dynamics of Telomerase Recruitment to Telomeres. *Cell* **166**: 1188-1197.e1189.
- Schober H, Ferreira H, Kalck V, Gehlen LR, Gasser SM. 2009. Yeast telomerase and the SUN domain protein Mps3 anchor telomeres and repress subtelomeric recombination. *Genes & development* **23**: 928-938.
- Schulz VP, Zakian VA. 1994. The saccharomyces PIF1 DNA helicase inhibits telomere elongation and de novo telomere formation. *Cell* **76**: 145-155.
- Shampay J, Szostak JW, Blackburn EH. 1984. DNA sequences of telomeres maintained in yeast. *Nature* **310**: 154-157.
- Smeenk G, van Attikum H. 2013. The chromatin response to DNA breaks: leaving a mark on genome integrity. *Annual review of biochemistry* **82**: 55-80.
- Stansel RM, de Lange T, Griffith JD. 2001. T-loop assembly in vitro involves binding of TRF2 near the 3' telomeric overhang. *The EMBO journal* **20**: 5532-5540.
- Stellwagen AE, Haimberger ZW, Veatch JR, Gottschling DE. 2003. Ku interacts with telomerase RNA to promote telomere addition at native and broken chromosome ends. *Genes & development* **17**: 2384-2395.
- Storici HK, Ying S, Fei H, Mikir P, Taehwan Y, Katie A, Alexander VM, Francesca. 2014. Transcript-RNA-templated DNA recombination and repair. *Nature* **515**: 436-439.
- Su XA, Dion V, Gasser SM, Freudenreich CH. 2015. Regulation of recombination at yeast nuclear pores controls repair and triplet repeat stability. *Genes & development* **29**: 1006-1017.
- Symington LS, Gautier J. 2011. Double-strand break end resection and repair pathway choice. *Annual review of genetics* **45**: 247-271.
- Taddei A, Gasser SM. 2004. Multiple pathways for telomere tethering: functional implications of subnuclear position for heterochromatin formation. *Biochimica et biophysica acta* **1677**: 120-128.
- . 2012. Structure and function in the budding yeast nucleus. *Genetics* **192**: 107-129.
- Taddei A, Hediger F, Neumann FR, Bauer C, Gasser SM. 2004. Separation of silencing from perinuclear anchoring functions in yeast Ku80, Sir4 and Esc1 proteins. *The EMBO journal* **23**: 1301-1312.
- Takahashi YH, Schulze JM, Jackson J, Hentrich T, Seidel C, Jaspersen SL, Kobor MS, Shilatifard A. 2011. Dot1 and histone H3K79 methylation in natural telomeric and HM silencing. *Molecular cell* **42**: 118-126.
- Takata H, Tanaka Y, Matsuura A. 2005. Late S phase-specific recruitment of Mre11 complex triggers hierarchical assembly of telomere replication proteins in *Saccharomyces cerevisiae*. *Molecular cell* **17**: 573-583.
- Teixeira MT, Arneric M, Sperisen P, Lingner J. 2004. Telomere length homeostasis is achieved via a switch between telomerase- extendible and -nonextendible states. *Cell* **117**: 323-335.



- Therizols P, Fairhead C, Cabal GG, Genovesio A, Olivo-Marin JC, Dujon B, Fabre E. 2006. Telomere tethering at the nuclear periphery is essential for efficient DNA double strand break repair in subtelomeric region. *The Journal of cell biology* **172**: 189-199.
- Tkac J, Xu G, Adhikary H, Young JTF, Gallo D, Escribano-Diaz C, Krietsch J, Orthwein A, Munro M, Sol W et al. 2016. HELB Is a Feedback Inhibitor of DNA End Resection. *Molecular cell* **61**: 405-418.
- Torres-Rosell J, Sunjevaric I, De Piccoli G, Sacher M, Eckert-Boulet N, Reid R, Jentsch S, Rothstein R, Aragon L, Lisby M. 2007. The Smc5-Smc6 complex and SUMO modification of Rad52 regulates recombinational repair at the ribosomal gene locus. *Nature cell biology* **9**: 923-931.
- Tsabar M, Haber JE. 2013. Chromatin modifications and chromatin remodeling during DNA repair in budding yeast. *Current opinion in genetics & development* **23**: 166-173.
- Tsukamoto Y, Taggart AK, Zakian VA. 2001. The role of the Mre11-Rad50-Xrs2 complex in telomerase-mediated lengthening of *Saccharomyces cerevisiae* telomeres. *Current biology : CB* **11**: 1328-1335.
- Ullman DRM, Amanda CH, Theresa LW, Katharine S. 2017. Nup153 and Nup50 promote recruitment of 53BP1 to DNA repair foci by antagonizing BRCA1-dependent events.
- Van de Vosse DW, Wan Y, Lapetina DL, Chen WM, Chiang JH, Aitchison JD, Wozniak RW. 2013. A role for the nucleoporin Nup170p in chromatin structure and gene silencing. *Cell* **152**: 969-983.
- Vega LR, Phillips JA, Thornton BR, Benanti JA, Onigbanjo MT, Toczyski DP, Zakian VA. 2007. Sensitivity of yeast strains with long G-tails to levels of telomere-bound telomerase. *PLoS genetics* **3**: e105.
- Verdun RE, Crabbe L, Haggblom C, Karlseder J. 2005. Functional human telomeres are recognized as DNA damage in G2 of the cell cycle. *Molecular cell* **20**: 551-561.
- Wang W, Daley JM, Kwon Y, Krasner DS, Sung P. 2018. Plasticity of the Mre11-Rad50-Xrs2-Sae2 nuclease ensemble in the processing of DNA-bound obstacles. *Genes & development* **31**: 2331-2336.
- Wiest NE, Houghtaling S, Sanchez JC, Tomkinson AE, Osley MA. 2017. The SWI/SNF ATP-dependent nucleosome remodeler promotes resection initiation at a DNA double-strand break in yeast. *Nucleic acids research* **45**: 5887-5900.
- Wu Y, DiMaggio PA, Jr., Perlman DH, Zakian VA, Garcia BA. 2012. Novel phosphorylation sites in the *S. cerevisiae* Cdc13 protein reveal new targets for telomere length regulation. *Journal of proteome research* **12**: 316-327.
- Wu Y, Zakian VA. 2011. The telomeric Cdc13 protein interacts directly with the telomerase subunit Est1 to bring it to telomeric DNA ends in vitro. *Proceedings of the National Academy of Sciences of the United States of America* **108**: 20362-20369.
- Xia GJ, Isabelle P, Tong W, Mohammad R, Ju Hwan C, Eddy Y, Bernard SL, Fen. 2013. BRCA1-Ku80 Protein Interaction Enhances End-joining Fidelity of Chromosomal Double-strand Breaks in the G1 Phase of the Cell Cycle.
- Zhang W, Durocher D. 2010. De novo telomere formation is suppressed by the Mec1-dependent inhibition of Cdc13 accumulation at DNA breaks. *Genes & development* **24**: 502-515.
- Zhong FL, Batista LF, Freund A, Pech MF, Venteicher AS, Artandi SE. 2012. TPP1 OB-fold domain controls telomere maintenance by recruiting telomerase to chromosome ends. *Cell* **150**: 481-494.
- Zimmermann M, de Lange T. 2013. 53BP1: pro choice in DNA repair. *Trends in cell biology* **24**: 108-117.



# CHAPTER 2. PROCESSING OF DSBs AT THE NUCLEAR PERIPHERY

---

## SWR1 and INO80 chromatin remodelers contribute to DNA double-strand break perinuclear anchorage site choice

Chihiro Horigome<sup>1, 5#</sup>, Yukako Oma<sup>2#</sup>, Tatsunori Konishi<sup>2</sup>, Roger Schmid<sup>3</sup>, Isabella Marcomini<sup>1,4</sup>, Michael H. Hauer<sup>1,4</sup>, Vincent Dion<sup>1,6</sup>, Masahiko Harata<sup>2</sup>, and Susan M. Gasser<sup>1,4\*</sup>

<sup>1</sup> Friedrich Miescher Institute for Biomedical Research, Maulbeerstrasse 66, CH-4058 Basel, Switzerland

<sup>2</sup> Laboratory of Molecular Biology, Tohoku University, Tsutsumidori-Amamiyamachi 1-1, Aoba-ku, Sendai 981-8555, Japan

<sup>3</sup> Institute of Plant Biology, University of Zurich, Zollikerstrasse 107, 8008 Zurich, Switzerland

<sup>4</sup> University of Basel, Faculty of Natural Sciences, CH-4056 Basel, Switzerland

<sup>5</sup> Present address: Institute of Molecular and Cellular Biosciences; The University of Tokyo; 1-1-1, Yayoi, Bunkyo-ku, Tokyo, 113-0032, Japan

<sup>6</sup> Present address: Center for Integrative Genomics, University of Lausanne, 1015 Lausanne, Switzerland

# equal contribution

*Published in Mol Cell, 2014, 55(4), 626-39*

This paper investigates for the first time requirements for a persistent double strand break (DSB) to move to two sites at the nuclear envelope: pores and Mps3. More specifically, it shows that DSB binding to Mps3 can only be detected in S/G2 phases, and this interaction is Rad51- and Ino80-dependent. On the other hand, interaction with pores occurs throughout the cell cycle. Swr1 complex controls relocation of a DSB to either site. In particular, in this work I contributed to show that mobility increase of the break site and relocation of it to the NE are events with different genetic requirements: *lexA*-mediated targeting of Arp6 (SwrC subunit) or Htz1 to an undamaged locus was not sufficient to increase its mobility, but promoted NE recruitment of the locus. The opposite effect was observed by tethering *lexA*-Ino80 or *lexA*-Rad51 to the undamaged locus (Figures 3c, 4c, f).



# SWR1 and INO80 Chromatin Remodelers Contribute to DNA Double-Strand Break Perinuclear Anchorage Site Choice

Chihiro Horigome,<sup>1</sup> Yukako Oma,<sup>2</sup> Tatsunori Konishi,<sup>2</sup> Roger Schmid,<sup>1,3</sup> Isabella Marcomini,<sup>1,4</sup> Michael H. Hauer,<sup>1,4</sup> Vincent Dion,<sup>1,5</sup> Masahiko Harata,<sup>2</sup> and Susan M. Gasser<sup>1,4,\*</sup>

<sup>1</sup>Friedrich Miescher Institute for Biomedical Research, Maulbeerstrasse 66, 4058 Basel, Switzerland

<sup>2</sup>Laboratory of Molecular Biology, Tohoku University, Tsutsumidori-Amamiyamachi 1-1, Aoba-ku, Sendai 981-8555, Japan

<sup>3</sup>Institute of Plant Biology, University of Zurich, Zollikerstrasse 107, 8008 Zurich, Switzerland

<sup>4</sup>University of Basel, Faculty of Natural Sciences, 4056 Basel, Switzerland

<sup>5</sup>Present address: Center for Integrative Genomics, University of Lausanne, 1015 Lausanne, Switzerland

\*Correspondence: [susan.gasser@fmi.ch](mailto:susan.gasser@fmi.ch)

<http://dx.doi.org/10.1016/j.molcel.2014.06.027>

## SUMMARY

Persistent DNA double-strand breaks (DSBs) are recruited to the nuclear periphery in budding yeast. Both the Nup84 pore subcomplex and Mps3, an inner nuclear membrane (INM) SUN domain protein, have been implicated in DSB binding. It was unclear what, if anything, distinguishes the two potential sites of repair. Here, we characterize and distinguish the two binding sites. First, DSB-pore interaction occurs independently of cell-cycle phase and requires neither the chromatin remodeler INO80 nor recombinase Rad51 activity. In contrast, Mps3 binding is S and G2 phase specific and requires both factors. SWR1-dependent incorporation of Htz1 (H2A.Z) is necessary for break relocation to either site in both G1- and S-phase cells. Importantly, functional assays indicate that mutations in the two sites have additive repair defects, arguing that the two perinuclear anchorage sites define distinct survival pathways.

## INTRODUCTION

Improperly repaired DNA double-strand breaks (DSBs) can lead to genomic rearrangements and loss of genetic information (Jackson and Bartek, 2009), making them one of the most hazardous forms of genomic damage. DSBs arise both from exogenous agents, such as  $\gamma$  irradiation or chemical insult, and from endogenous events, such as replication fork collapse (Pfeiffer et al., 2000).

DSB repair is generally achieved by two conserved mechanisms: nonhomologous end-joining (NHEJ) or homologous recombination (HR) (Chapman et al., 2012). In haploid yeast, NHEJ is prominent only in G1 phase, whereas, in mammals, it dominates throughout the cell cycle (Smeenk and van Attikum, 2013). Repair by HR requires a homologous donor that serves as a template for DNA synthesis, being most commonly provided

by the replicated sister chromatid. The choice of repair by HR over NHEJ is dictated in part by 5' to 3' end resection at the break, which requires the activity of the S-phase cyclin-dependent kinase (Ira et al., 2004). The resulting single-stranded DNA (ssDNA) overhang is coated by replication protein A (RPA) and later by the Rad51 recombinase. This ssDNA-Rad51 nucleoprotein filament mediates homology search and strand invasion, enabling error-free, recombination-mediated repair. Other less-precise, recombination-based events can also occur, including break-induced replication or template switching, particularly at damaged replication forks (Aguilera and García-Muse, 2013).

Recent work has highlighted the importance of ATP-dependent chromatin remodelers in DSB repair. In yeast, the remodeler complexes RSC and INO80 and the SWR1 complex (SWR-C) are sequentially recruited to breaks, whereas, in mammalian cells, the SWI/SNF homolog as well as INO80 and SRCAP are implicated in repair pathway choice and outcome (reviewed in Peterson and Almouzni, 2013; Price and D'Andrea, 2013; Seeber et al., 2013b; Smeenk and van Attikum, 2013). The budding yeast complexes INO80 and SWR-C accumulate at breaks at much higher levels in S and G2 than G1, coincident with end resection and Rad51 binding (Bennett et al., 2013). Indeed, the recruitment of INO80 facilitates short-range resection at DSBs and Rad51 binding, possibly because of the preferential eviction of H2A.Z-containing nucleosomes (Papamichos-Chronakis et al., 2011; Tsukuda et al., 2005; van Attikum et al., 2004, 2007). More recent work implicates the FUN30 remodeler in long-range end resection (Chen et al., 2012; Costelloe et al., 2012). In contrast, SWR-C exchanges H2A-H2B dimers for Htz1-H2B at promoters, telomeres, centromeres, and, in some cases, DSBs, but its loss does not impair end resection (Kobor et al., 2004; Krogan et al., 2003; Luk et al., 2010; Mizuguchi et al., 2004; Papamichos-Chronakis et al., 2006; van Attikum et al., 2007; Wu et al., 2005). Instead, SWR-C appears to promote the association of yeast Ku to broken ends, facilitating error-free NHEJ (van Attikum et al., 2007). INO80, on the other hand, was shown to facilitate replication fork restart after stalling or collapse of replication forks (Papamichos-Chronakis and Peterson, 2008; Shimada et al., 2008).

Another intriguing effect of chromatin remodeler recruitment to DSBs is the enhanced subdiffusive movement scored for

fluorescently tagged DSBs in yeast (Dion et al., 2012; Miné-Hat-tab and Rothstein, 2012; Neumann et al., 2012). Not only the site of damage, but other tagged loci throughout the genome showed a general increase in mobility after DSB induction in a manner dependent on checkpoint response and the INO80 remodeler (Neumann et al., 2012; Seeber et al., 2013a). Other studies established that DSBs, which lack a functional donor for HR shift at least transiently to the nuclear periphery, where they appear to bind either the Nup84 nuclear pore subcomplex or an essential inner nuclear membrane Sad1-Unc-84-related (SUN) domain protein Mps3 (Kalocsay et al., 2009; Nagai et al., 2008; Oza et al., 2009; Oza and Peterson, 2010). Fluorescence microscopy confirmed that critically short telomeres and collapsed replication forks associate with nuclear pores (Khadaroo et al., 2009; Nagai et al., 2008), yet it has remained unclear whether Mps3 and pores constitute independent or interdependent sites of DSB interaction. Moreover, it was unresolved what relationship, if any, exists between the enhanced subdiffusive movement that stems from damage and the localization of DSBs to the inner nuclear membrane (INM).

Previous work from our laboratory has shown that Mps3 and nuclear pores distribute independently around the nuclear rim in vegetatively growing cells (Horigome et al., 2011). Unlike Mps3, nuclear pores harbor the SUMO protease Ulp1 and the heterodimeric SUMO-dependent ubiquitin ligase Slx5–Slx8 (Nagai et al., 2008; Zhao et al., 2004; Palancade et al., 2007), which is implicated in alternative recombination-mediated pathways of repair (Khadaroo et al., 2009; Nagai et al., 2008). In contrast, Mps3 was shown to sequester DSBs from promiscuous interactions with chromatin and suppress telomere-telomere recombination in mutant strains (Oza et al., 2009; Schober et al., 2009). These results provide indirect arguments that these DSB binding sites have different functions, yet it is unclear what differentiates one binding site from the other.

Here, we combine chromatin immunoprecipitation (ChIP) and fluorescence imaging approaches in appropriate mutant backgrounds in order to distinguish and characterize the two DSB binding sites at the nuclear envelope. We find cell-cycle-dependent binding site selection with differential dependence on the INO80 chromatin remodeler. On the other hand, the related SWR-C and its deposition of Htz1 were required for relocation to both sites. By studying factors that affect DSB mobility, we also distinguish perinuclear binding site choice from DNA-damage-response-enhanced mobility. Finally, we confirm that mutants that ablate one or the other binding site have distinct outcomes on repair, arguing that the spatial segregation of damage participates selectively in pathways of repair.

## RESULTS

### SWR-C-Dependent H2A.Z Incorporation Is Required to Shift a DSB to the Nuclear Periphery

To study the relocation of damaged DNA to the nuclear periphery, we used a strain in which a unique DSB can be induced at the mating type locus (*MAT*) by galactose-controlled expression of the homothallic (HO) endonuclease. The donor sequences at *HML* and *HMR* are deleted in order to prevent intrachromosomal

repair by gene conversion (Figure 1A). To determine the subnuclear localization of the DSB, we inserted an array of *lacO* sites at 4.4 kb from *MAT* and expressed a GFP-LacI fusion and either a GFP- or cyan fluorescent protein (CFP)-tagged pore protein (Figures 1A and 1B). In wild-type (WT) cells exposed to galactose for 2 hr, the induced DSB shifts efficiently to the nuclear periphery, and 59% of the cleavage sites mapped to the outermost rim (zone 1; 52% in WT CFP-Nup49-expressing strains;  $p < 1.0 \times 10^{-30}$  or  $p = 1.2 \times 10^{-11}$  versus random; Figures 1C and 1E; Table S3 available online). On the other hand, the uncleaved *MAT* locus has a random subnuclear localization (Figure 1C) (Nagai et al., 2008).

Histone variant Htz1 is deposited at DSBs, and its loss was shown to abolish the association of the break with Mps3 in S or G2-phase cells (Kalocsay et al., 2009). Although Htz1 physically interacts with Mps3 in vitro, recent work showed that Htz1 also serves as an essential chaperone for the insertion of Mps3 into the INM (Gardner et al., 2011). Thus, the negative effect of *htz1* deletion on DSB localization could stem from a failure to integrate Mps3 into the INM and not an absence of Htz1 at the break. To resolve this issue, we made use of a mutant called *htz1ΔM6* (Wu et al., 2005), which ensures proper INM localization of Mps3 but fails to bind SWR-C. Therefore, the mutant histone *htz1ΔM6* is not incorporated into chromatin by SWR-C (Gardner et al., 2011; Wu et al., 2005). We confirmed that the cleaved *MAT* locus failed to shift to the nuclear periphery in the *htz1Δ* strain and that relocation could be faithfully restored by expression of WT Htz1 (Figure 1D). However, the mutant histone *htz1ΔM6* failed to support break relocation to the nuclear rim (Figure 1D). This, along with the fact that either loss of Swr1 or the SWR-C component Arp6 completely eliminated DSB relocation to the nuclear periphery (Figure 1E), argued strongly that the deposition of Htz1 at damage by SWR-C is indeed crucial for DSB relocation. Consistently, complementation of the *swr1Δ* background with a WT *SWR1* gene (+*SWR1*; Figure 1F), but not the catalytic site mutation (+*swr1K727G*; Figure 1F), restored relocation of the DSB to the nuclear periphery, demonstrating dependence on both SWR-C and Htz1 deposition.

Although SWR-C is implicated in Htz1 incorporation, INO80 has been proposed to remove this histone variant at both damage and other sites (Kobor et al., 2004; Krogan et al., 2003; Luk et al., 2010; Mizuguchi et al., 2004; Papamichos-Chronakis et al., 2006; van Attikum et al., 2007; Wu et al., 2005). To see whether the importance of Htz1 deposition by SWR-C is to recruit INO80 to breaks, we examined whether ablation of the INO80 chromatin remodelling complex would affect DSB relocation. Because *ino80Δ* itself is lethal in our yeast background, we instead tested the effects of *arp5Δ* or *arp8Δ* mutants, which compromise INO80-remodelling activity and reduce INO80 recruitment to breaks (Shen et al., 2000; van Attikum et al., 2004). Surprisingly, there was no effect of *arp5* or *arp8* deletion on DSB relocation (Figure 1E).

INO80 has been implicated in the removal of nucleosomes to favor resection at DSBs, whereas *swr1* mutants showed no defect in resection (van Attikum et al., 2007; Chen et al., 2012). Although resection is not sufficient for relocation, it leads to the binding of Rad51, which, along with Rad52, was shown to be necessary for the detection of damaged DNA at Mps3 by ChIP

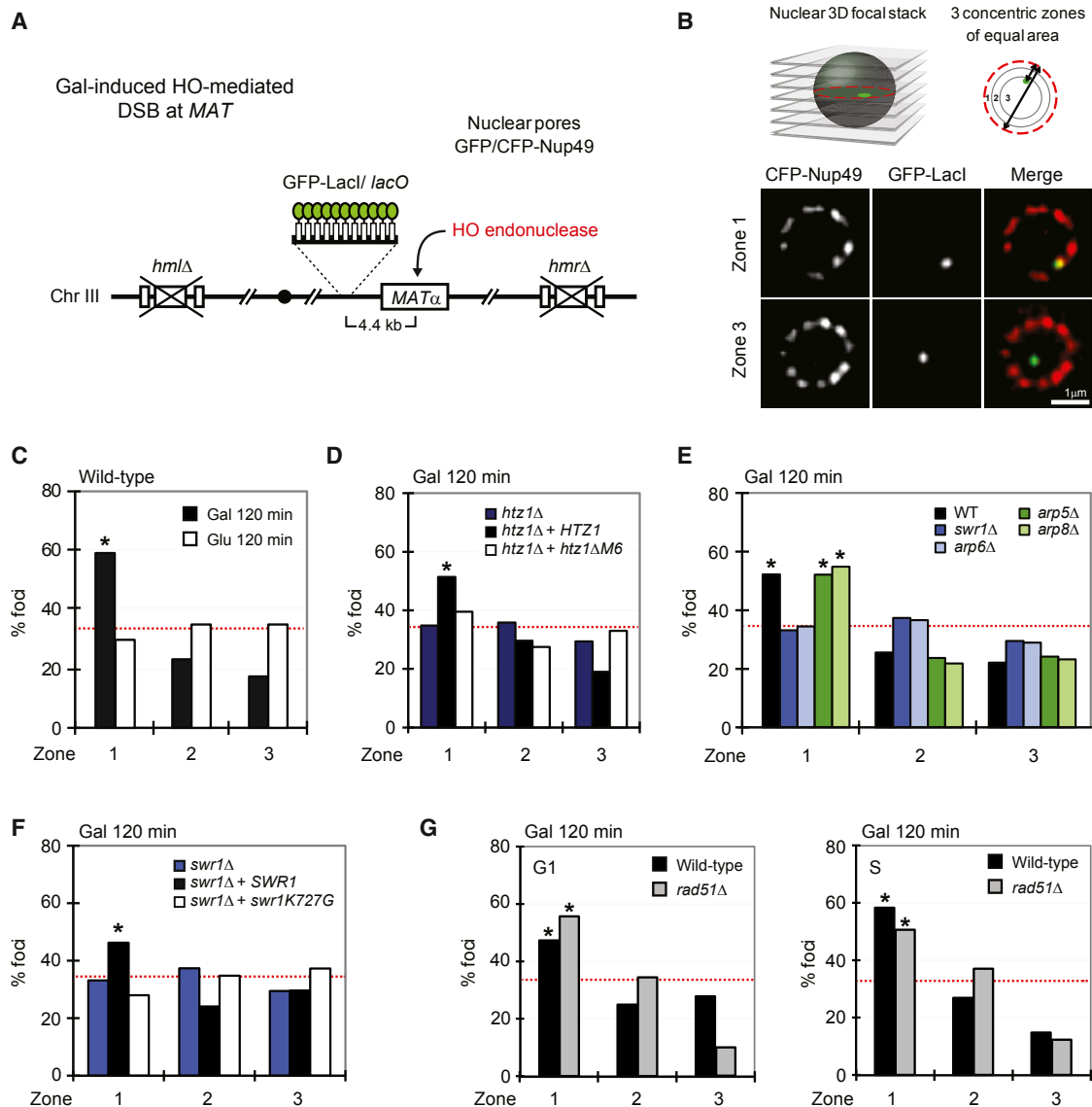


### Figure 1. SWR1-Dependent H2A.Z Incorporation Is Required to Shift DSBs to the Nuclear Periphery

(A) Shown is Chr III in strains GA-1496 and GA-6844 bearing deleted homologous donor loci (*hmlΔ/hmrΔ*) and a *lacO* array 4.4 kb from the HO cut site at *MAT*, which allows visualization by GFP-LacI. Pores are visualized by GFP-Nup49 (GA-1496) or CFP-Nup49 (GA-6844).

(B) Locus position is scored relative to the nuclear diameter in its plane of focus, as described in the Supplemental Information. Distance over diameter ratios are binned into three equal zones. 33% distribution = random.

(C) *MAT* position in GA-1496 (WT) after 120 min on galactose (Gal) or glucose (Glu). \* = significantly nonrandom distribution on the basis of cell number and confidence values from a proportional test between random and experimental distribution (see Table S3).

(D) In strain GA-7095 expressing *HTZ1* or *htz1ΔM6* from the *HTZ1* promoter at *URA3*, *MAT* position was scored at 120 min on galactose as in C. Strains: *htz1Δ* (GA-7095), *htz1Δ + HTZ1* (GA-8110), and *htz1Δ + htz1ΔM6* (GA-8111).

(E) *MAT* position relative to CFP-Nup49 in WT (GA-6844), *swr1Δ* (GA-7003), *arp6Δ* (GA-7094), *arp5Δ* (GA-8069), and *arp8Δ* (GA-7103) as in (C) and (D).

(F) In *swr1Δ* (GA-7003) strain or same expressing *SWR1* or *swr1K727G* from a *TEF* promoter, *MAT* position was scored as in (C) and (D). *swr1Δ* (GA-7003), *swr1Δ + SWR1* (GA-8667), and *swr1Δ + swr1K727G* (GA-8668).

(G) *MAT* position scored in WT (GA-6844) and *rad51Δ* (GA-7099) cells as in (C) and (D) but binned into G1 (unbudded) and S (budded) cells.

See also Figure S1.

(Kalocsay et al., 2009; Oza et al., 2009). Using our quantitative positioning assay, we tested whether Rad51 or Rad52 was necessary for the perinuclear relocation of the DSB. Surprisingly, and in contrast to Mps3-ChIP results (Kalocsay et al., 2009), we

scored a significant enrichment of the DSB at the nuclear periphery in both *rad51Δ* and *rad52Δ* mutants (Figures 1G and S1). Altogether, these results led us to propose that in addition to Mps3, a Rad51-independent DSB binding site, should exist at

the nuclear periphery. The obvious candidate for this would be the Nup84 subcomplex of the nuclear pore, which was shown by ChIP and fluorescence microscopy to interact with irreparable DSBs in an asynchronous population of cells (Nagai et al., 2008).

Although Kalocsay et al. (2009) claimed that they could not distinguish between pore and Mps3 binding by ChIP, the two INM complexes are indeed distinct by high-resolution fluorescence microscopy (Horigome et al., 2011). In WT cells, endogenously tagged Mps3 (EGFP-Mps3; Figure 2A) shows a bright focus at the spindle pole body (SPB; Figure 2A, arrow) and a weak perinuclear ring. To see whether the weak Mps3 rim staining was pore dependent, we induced the clustering of nuclear pores by deleting a portion of the N-terminal domain of Nup133 ( $\Delta$  amino acids [aa] 44–236) (Doye et al., 1994). In this mutant, pores cluster without loss of function. However, the EGFP-tagged Mps3 retained its rim staining (Figure 2A, red = pore, green = Mps3), even though the bright SPB was often adjacent to a pore cluster. The independence of the non-SPB Mps3 signals from pores reinforced the hypothesis that the Rad51-independent perinuclear localization of DSBs might reflect their association with pores.

To correlate nuclear pore and/or Mps3 binding with the effects of the mutations described in Figure 1, we performed ChIP assays with Mab414 (antinuclear pore) and anti-HA (recognizing 3HA-Mps3) in WT and mutant yeast strains (Figure 2B). Consistent with previous work, an induced DSB could be recovered in immunoprecipitates for either nuclear pore or Mps3 in WT cells (Figure 2B). The level of association increased rapidly for 120 min after cut induction before reaching a plateau. In *swr1 $\Delta$*  strains, break association with either pores or Mps3 was reduced to a background level, which existed prior to HO induction. Thus, ChIP confirms that the SWR-C is required for DSB relocation.

In contrast, in the INO80-deficient *arp8 $\Delta$*  strain, DSB association with the nuclear pore occurred at WT levels, whereas break binding to Mps3 was lost (Figure 2B). Thus, the binding of DSBs to Mps3, but not pores, requires INO80 activity. The fact the breaks bind pores in the absence of INO80 is consistent with the INM-localization of the DSB in *arp5 $\Delta$*  and *arp8 $\Delta$*  strains, as presented in Figure 1. Given that break association with either the pore or Mps3 required SWR-C, the action of INO80 appears to distinguish damage that is destined for Mps3 from damage that is targeted to pores. This could reflect either the direct binding of INO80 or an alteration of the DSB that is INO80-dependent and renders the DSB able to bind Mps3.

#### Microscopic Confirmation that INO80 Contributes Only to DSB-Mps3 Association

We sought to confirm this finding with an assay that does not depend on protein-DNA crosslinking, given that formaldehyde crosslinking efficiency varies significantly from protein to protein. To achieve this, we scored for colocalization of a GFP-LacI-tagged DSB and CFP-tagged nuclear pores with high-resolution spinning disk confocal microscopy. To enhance the accuracy of scoring colocalization by microscopy, we used a *nup133 $\Delta$*  background, in which pores form a large, single cluster (Doye et al., 1994). The deletion of the Nup133 N terminus does not affect macromolecular import or export and does not confer

sensitivity to DNA-damaging agents, unlike complete loss of Nup133 or Nup84 subcomplex components (Doye et al., 1994; Loeillet et al., 2005). We scored three degrees of colocalization with the pore cluster: fully overlapping, partially overlapping, and juxtaposition (“touching”; Figure 2C). All three degrees of colocalization are consistent with molecular interaction of the break with the pore cluster, given the relative signal sizes of the *lacO* array and the clustered pore (Schober et al., 2009).

The background level of colocalization was determined with a strain that lacks the gene for the HO endonuclease (*ho $\Delta$* ). In this strain, we found *MAT* juxtaposed to a pore cluster in 20% of the cells, and this value did not change over time. This background is higher than the computed likelihood of a *lacO* focus coinciding with the pore cluster (9%) (see Schober et al., 2009). Nonetheless, we use this empirically determined value as the background above which colocalization of the DSB and pore is considered significant (Figures 2C–2E, *ho $\Delta$* ).

In a WT yeast strains, DSB colocalization with pores showed a rapid increase upon induction of cleavage, which was then reduced to a plateau of 30% (Figure 2C). This could indicate that DSB binding at pores is transient for a subpopulation of breaks or else that extensive resection at the break eliminates the *lacO* signal at later time points (Figure S2). Nonetheless, there was significant colocalization of DSBs with the pore cluster in both G1- and S-phase cells (Figure 2D). Importantly, DSB-pore interaction was diminished in *swr1 $\Delta$* , but not *arp8 $\Delta$* , strains, providing independent confirmation that pore association of a DSB requires SWR-C but not a functional INO80 complex. The slight delay in DSB accumulation at pores in the *arp8 $\Delta$*  strain correlates with both reduced chromatin mobility and reduced resection rate at the break in that mutant (Neumann et al., 2012; van Attikum et al., 2007). In conclusion, quantitative microscopy confirms a differential requirement for SWR-C and INO80 in the association of DSBs with pores.

Another variable in break relocation is the stage of the cell cycle at which position is measured. In previous ChIP studies, the Mps3-DSB interaction was detected in asynchronous cultures, yet it was lost when cells were arrested in G1 (Kalocsay et al., 2009). Cell-cycle effects were not examined in the context of DSB association with pores. Taking advantage of the ease with which one can determine cell-cycle stage by yeast cell morphology, we binned the cells scored by microscopy into unbudded (G1 phase) and budded cells, counting only those in which the nuclei were still round (early to mid S phase) (Figure 2D). We conclude from this that DSB-pore interaction occurs in both G1- and S-phase cells, reaching 36% and 43% colocalization with pores, respectively. In both sets of cells, pore association depends on SWR-C (Figure 2D) and cleavage (Figure 2E, *ho $\Delta$*  background, ~20%). However, in S phase, DSB association with the pore was independent of INO80 function, and even increased in the absence of Arp8 (Figure 2D). Moreover, whereas Mps3 binding was reported to be sensitive to loss of Rad51 (Kalocsay et al., 2009; Oza et al., 2009), we found that DSB-pore association was intact in the *rad51 $\Delta$*  mutant (Figure 2D). Thus pore-DSB interaction occurs in G1- and S-phase cells and is dependent on SWR-C but independent of Rad51 and INO80. On the other hand, DSB recruitment to Mps3 requires Rad51 and INO80 and is restricted to S phase.



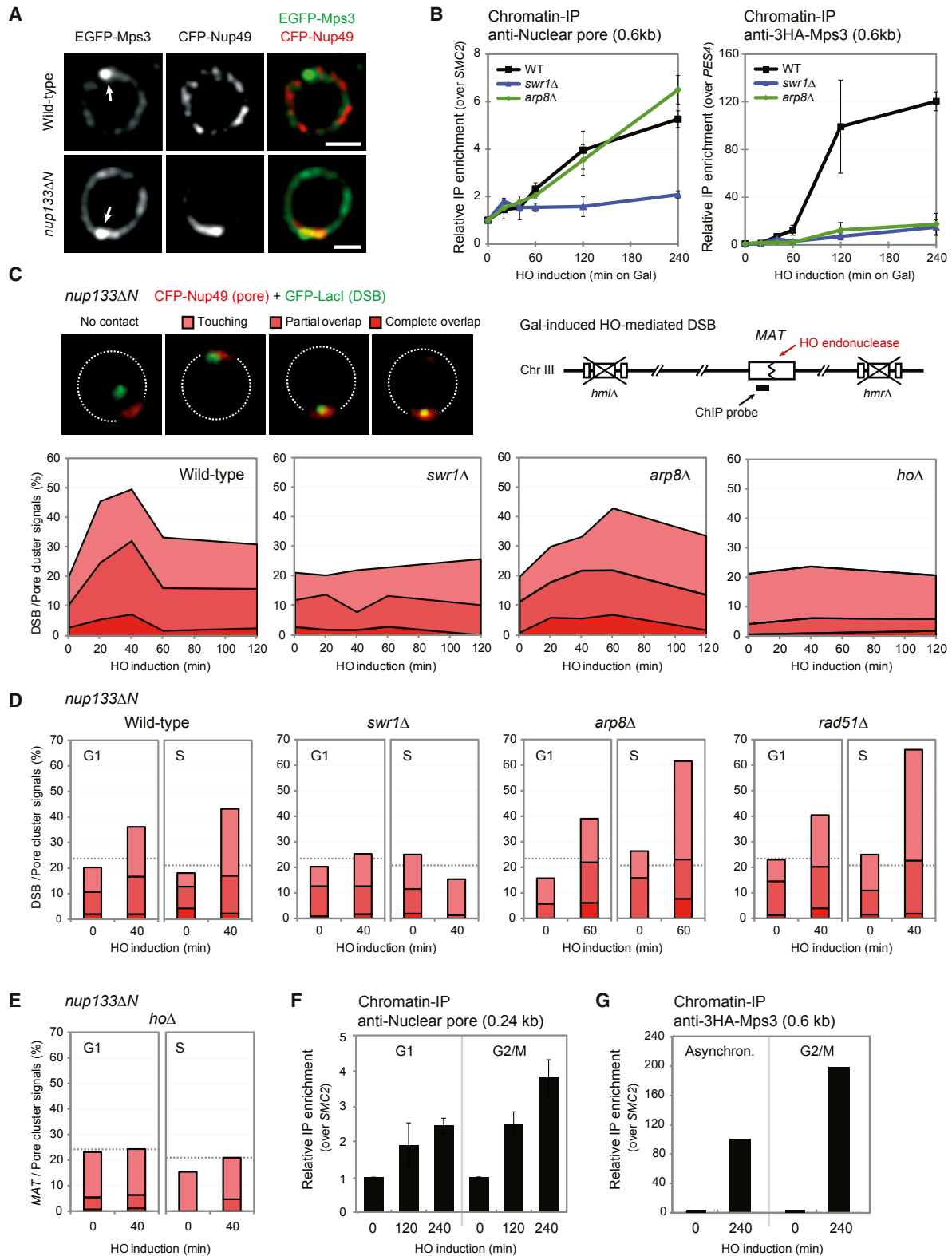


**Figure 2. SWR-C Is Required for DSB Binding at Both Nuclear Pores and Mps3, and INO80 Is Only Required for Mps3 Interaction**

(A) EGFP-Mps3 and CFP-Nup49 localization in WT (GA-6647) and in pore-clustering cells (*nup133ΔN*, GA-6650). Images are reproduced from (Horigome et al., 2011) with permission. Arrow = spindle pole body; white bars = 1  $\mu$ m.

(legend continued on next page)

To make sure that these cell-cycle conclusions were not artifacts of the *nup133ΔN* strain, we confirmed them with ChIP assays for nuclear pore proteins (Mab414, see the [Experimental Procedures](#)) and HA-tagged Mps3 in synchronized *NUP133<sup>+</sup>* cells. Cells arrested in G1 showed a cleavage-dependent increase in association with nuclear pores but not Mps3 (Figures 2F and 2G) (Kalocsay et al., 2009; Oza et al., 2009). Both types of association increased in G2- and M-phase cells (Figures 2F and 2G). This contrasts with the fluorescence colocalization analysis, where we scored a drop in DSB-pore interaction in both WT and *arp8Δ* cells at 120 min after cut induction (Figure S2A). Given that this correlates with a reduced number of bright *Lacl/lacO* foci (<1 per cell), we suggest that the drop in colocalization stems from resection through the *lacO* repeat sequence at 120 min postcleavage (Figures 2A and 2B). Intriguingly, in both *rad51Δ* and *arp8Δ* cells, DSBs bind more efficiently to pores in S-phase than WT cells, even though the Mps3 interaction drops in these mutants. This is consistent with the two binding sites being competitive, rather than sequential binding sites.

### Htz1 Is Able to Mediate Direct Interaction with Mps3 but Not Nuclear Pores

The loss of perinuclear interactions in remodeler deletion strains does not necessarily mean that the remodeler itself mediates interaction with pores or Mps3. Rather, the effects could be achieved indirectly by the action of the complex on the substrate; i.e., modification of chromatin or processing of the DSB. However, in the case of Htz1, it was proposed that this histone variant interacts directly either with nuclear pores (Dilworth et al., 2005; Light et al., 2010) or Mps3 (Gardner et al., 2011). To test whether Htz1 incorporation is sufficient to shift chromatin to either nuclear pores, Mps3, or both, we made use of a gain-of-function assay in which LexA fusion proteins are targeted to four double LexA operators inserted near a fluorescently labeled locus (ARS607). Then, subnuclear position of ARS607 was monitored in the absence of DNA damage. This locus has a random subnuclear localization even when *Lacl/lacO* is near it, and, consistent with previous work, the binding of LexA does not alter its random distribution (Taddei et al., 2004) (open bars, Figures 3A–3C). On the other hand, the binding of LexA fused to a protein that has affinity for an INM protein shifts ARS607 in a statistically significant manner to zone 1, which is the case for LexA-Htz1 in both WT and *swr1Δ* cells (Figures 3B and 3C). Moreover, LexA-htz1ΔM6, which cannot bind SWR-C, worked as efficiently as LexA-Htz1 itself in translocation (Figure 3B). Not surprisingly, these interactions were cell-cycle independent.

Next, we asked whether the Htz1-mediated interaction with the nuclear periphery reflects binding to nuclear pore complexes, as had been previously shown for LexA-Arp6 (Yoshida et al., 2010). To score this, we targeted LexA-htz1ΔM6 to the LexA/*lacO*-tagged *LYS2* in a *nup133ΔN* background expressing CFP-Nup49 and scored colocalization of *LYS2* with the pore cluster. LexA-htz1ΔM6 was unable to enhance interaction with the nuclear pores above background levels (20%), whereas the targeting of LexA-Swr1 could (Figure 3D). Finally, to see whether Htz1 functions by binding Mps3, we overexpressed the nucleoplasmic N-terminal domain of Mps3, which distributes throughout the nucleoplasm (Schober et al., 2009), along with LexA-htz1ΔM6. In this case, LexA-htz1ΔM6 no longer shifted ARS607 to zone 1 in either WT or *swr1Δ* cells (Figure 3E), suggesting that the soluble Mps3N competes for Htz1-Mps3 interaction at the INM. Unfortunately, we were unable to test an *mps3ΔN* mutant in this assay, given that the cells show severely impaired growth (data not shown). In conclusion, the targeting of a LexA-Htz1 fusion is sufficient to shift chromatin to the INM in the absence of damage, probably because of its affinity for Mps3N. Previous work showed that LexA-Arp6 can shift an internal LexA-tagged locus to the nuclear pore cluster (Yoshida et al., 2010) as we show here for LexA-Swr1 (Figure 3D). The significance of this Swr1 interaction for DSB relocation is unclear, given that we showed above that point mutants that eliminate the ATPase activity of SWR-C blocked DSB relocation (Figure 1F). In summary, we suggest that SWR-C functions in DSB relocation in multiple interdependent ways: by depositing Htz1, by serving as a bridge for pore interaction, and possibly by enhancing the subdiffusive mobility of chromatin in response to breaks (Dion et al., 2012; Miné-Hattab and Rothstein, 2012).

### Testing the Role of Remodeler-Enhanced DSB Mobility in DSB Relocalization

Previous work demonstrated a role for INO80 remodeling activity in chromatin movement both at a DSB and when targeted to undamaged sites (Neumann et al., 2012), whereas the role of SWR-C or Htz1 deposition had not been tested. To examine this, we scored the mobility of a *lacO*-tagged induced DSB at the *ZWF1* locus in the middle of the long left arm of chromosome XIV in *swr1-* and *htz1-*deficient strains (Figure 4A). The deletion of *swr1* did not affect in the mobility of the locus in the absence of damage (Figure 4B); however, after I-SceI-induced cleavage, the dramatic increase in DSB movement that occurs in WT cells was compromised in *swr1-* and *htz1-*deficient strains (Figure 4C). The effect was similar in the absence of other SWR-C subunits,

(B) Top: ChIP against nuclear pores (Mab414) and 3HA-Mps3 (anti-HA) at the indicated times on galactose. Enrichment of *MAT* (0.6 kb from the cut site) over uncut *SMC2* or *PES4* was quantified with quantitative PCR in WT (GA-7002), *swr1Δ* (GA-7004), and *arp8Δ* (GA-7161) cells. Bottom: ChrIII in strains used.

(C) Scoring of *MAT* colocalization with the pore cluster in *nup133ΔN* (GA-7314) after cut induction as shown in WT (GA-7314), *swr1Δ* (GA-8142), *arp8Δ* (GA-8143), and *hoΔ* (GA-8669) cells. Scored at indicated times on galactose. Pink/red shaded region = colocalization; *hoΔ* values = background.

(D and E) Experiments performed as in (C) with data binned into G1- or S-phase cells. Strains are the same as in (C) plus *rad51Δ* (GA-8072) with *nup133ΔN*. Dotted line = background (see *hoΔ*).

(F) ChIP analysis performed as in (B) on galactose with Mab414 in WT (GA-8627) cells. Cells were synchronized in G1 phase by  $\alpha$  factor and in G2 and M phase by nocodazole. PCR primers for *MATa* are 0.24 kb from cut site. Enrichment over an uncut *SMC2* locus was calculated and normalized to 0 min Gal and cut efficiency.

(G) ChIP analysis at 0 or 240 min on galactose for 3HA-Mps3 and at *MATa* in WT (GA-7002) cells as in (B). Cells are asynchronous or synchronized in G2 and M phase by nocodazole. Enrichment was calculated as in (F), and data from multiple experiments are represented as mean  $\pm$  SEM.

See also Figure S2.

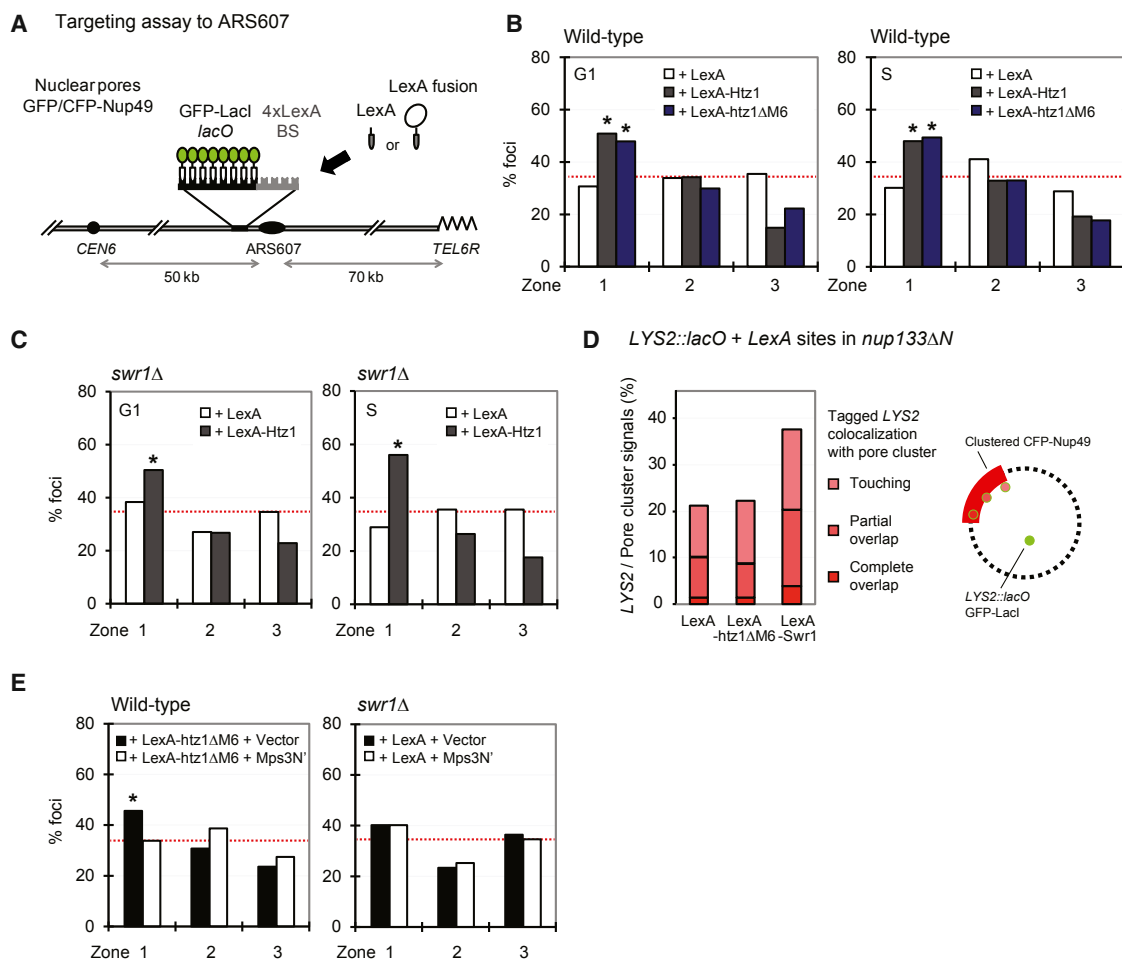


**Figure 3. Htz1 Is Sufficient to Shift an Internal Locus to the Nuclear Periphery**

(A) The position of *lacO*/LexA-tagged ARS607 was visualized by GFP-LacI and scored as in Figure 1B. Cells are binned into G1 or S phase as in Figure 1G. Strains carry either GFP-Nup49 (GA-1461) or CFP-Nup49 (GA-1993). LexA fusion proteins are expressed from plasmids.

(B) WT strain (GA-1993) expresses indicated LexA fusion constructs. ARS607 position was scored as in (A).

(C) Experiments were performed as in (B) with strain bearing *swr1Δ* (GA-7898).

(D) Pore cluster colocalization for LexA-tagged *LYS2* in a strain bearing *nup133ΔN* (GA-4584) transformed with LexA fusions. Colocalization (pink to red) is presented as in Figure 2C.

(E) In a WT strain (GA-1993) expressing LexA-htz1ΔM6 and Mps3N', ARS607 position was scored as in (B). Right, same experiments performed with *swr1Δ* (GA-7898) bearing LexA and either an empty vector or the Mps3N' construct.

Swc2 and Swc5 (Figure S3), which are necessary for remodeler function (Wu et al., 2005). The reduction in mobility was as strong as, if not stronger than, the reduced mobility of the same DSB in *arp8Δ* or *rad51Δ* mutants (Figure 4D) (results from Dion et al., 2012; Neumann et al., 2012). However, in *arp8Δ* or *rad51Δ* strains, we still score the shift of DSBs to the INM (Figures 1 and 2), ruling out an absolute requirement of enhanced mobility for relocation to pores.

Having demonstrated that the LexA-mediated targeting of Swr1, Arp6, and Htz1 can mediate relocation to the nuclear periphery, we tested whether they also affect the mobility of the undamaged locus to which they are bound. We find that the expression of LexA-Arp6, LexA-Htz1, or LexA-htz1ΔM6 confers no significant increase in ARS607 mobility (Figures 4E and 4F), yet they can still shift the locus to the INM (Figure 3).

Indeed, the targeting of LexA-Arp6, which can bring an internal locus to pores (Yoshida et al., 2010), reduces ARS607 mobility (Figure 4E). Given that LexA-Arp5, LexA-Arp8, or LexA-Ino80 bound to various undamaged sites enhance locus mobility (Neumann et al., 2012) and do not lead to perinuclear enrichment (Figure S4), we conclude that enhanced random movement is neither sufficient nor necessary for shifting a DSB to the INM.

### Crosstalk between Anchorage at Pores and Mps3 Reveals Additive Phenotypes

We have distinguished the two INM binding sites for DSBs with respect to INO80 and cell-cycle dependence, yet it remained possible that the two sites influence each other in some way. For example, pore binding might precede binding to Mps3 or

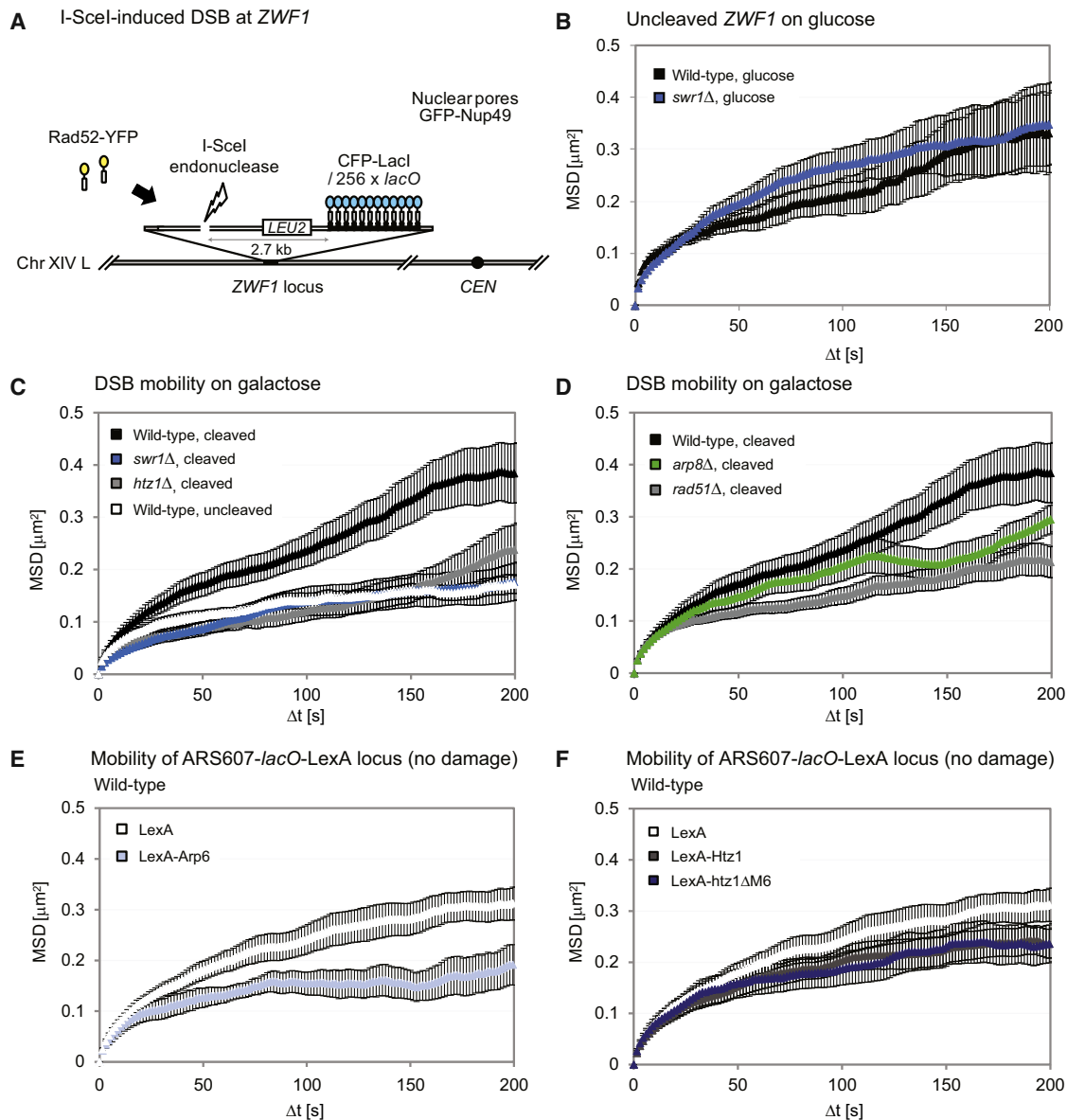


**Figure 4. Enhanced DSB Mobility Depends on SWR-C and H2A.Z but Is Not Required for Relocalization**

(A) Schematic representations of the I-SceI cut site and a *lacO* array inserted at *ZWF1* on chromosome 14L (GA-6208). Strains express CFP-LacI and galactose-induced I-SceI from a 2  $\mu$ m plasmid.

(B) MSD plots (see the [Experimental Procedures](#)) of the *ZWF1* locus in WT and *swr1* $\Delta$  cells during S phase in glucose medium show no mobility change for undamaged chromatin in *swr1* $\Delta$ .

(C) MSD plots of I-SceI-induced Rad52-YFP foci in WT (GA-6208), *swr1* $\Delta$  (GA-6335), *htz1* $\Delta$  (GA-6637) strains, and CFP-LacI at uncut site (GA-6215) during S phase. Only the cut WT sample increases mobility.

(D) MSD plots of I-SceI-induced Rad52-YFP foci in WT (GA-6208), *arp8* $\Delta$  (GA-6317), and *rad51* $\Delta$  (GA-6225) strains during S phase reproduced with permission (Dion et al., 2012; Neumann et al., 2012).

(E and F) MSD plots of the undamaged *lacO*/LexA-tagged ARS607 tracked after binding LexA or the indicated LexA fusion during G1 phase. The reduction in mobility due to Arp6 binding is significant. MSD data are represented as mean  $\pm$  SEM.

See also [Figures S3](#) and [S4](#).

vice versa. This was tested directly by monitoring DSB relocation in mutants lacking one or the other site.

Consistent with earlier findings (Oza et al., 2009), we show through both microscopic analysis and ChIP that DSBs fail to relocate to the nuclear periphery in the *mps3* $\Delta$ 65-145 strain

([Figures 5A–5C](#)). Interestingly, the relocation defect in the *mps3* $\Delta$ 65-145 strain was observed in both G1- and S-phase cells, even though DSB binding to Mps3 is only detected in G1 (Kalocsay et al., 2009). Using the colocalization assay, we confirmed that a GFP-tagged DSB failed to bind the CFP-labeled

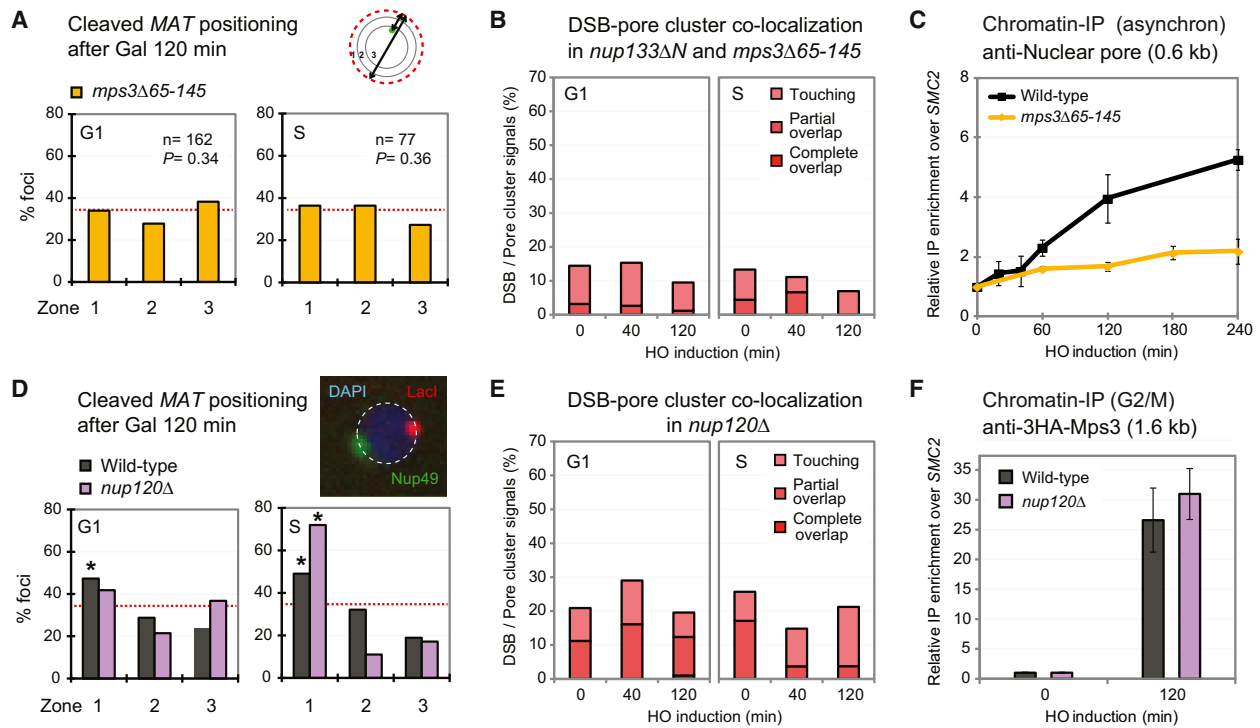


**Figure 5. Nonreciprocal Effects of the Loss of Mps3N or of Nup120 on DSB Positioning**

(A) Position of cleaved MAT loci in *mps3Δ65-145* (GA-7096) scored at 120 min after HO induction as in Figure 1G.

(B) Colocalization of the nuclear pore cluster and the MAT scored for G1 or S phase in *mps3Δ65-145* cells with *nup133ΔN* (GA-7897). Quantified as in Figure 2D.

(C) ChIP for nuclear pores (Mab414) after the indicated time on galactose in WT (GA-7002) and *mps3Δ65-145* cells (GA-7096). Quantitation and enrichment over SMC2 was normalized as in Figure 2B. Data from multiple experiments are represented as mean  $\pm$  SEM.

(D) GFP-tagged MAT position was determined in WT (GA-6844) and *nup120Δ* (GA-8141) relative to the nuclear periphery determined from DAPI staining as in Figure 1G. An S-phase *nup120Δ* cell nucleus is shown.

(E) MAT colocalization with nuclear pores scored in G1- or S-phase *nup120Δ* cells (GA-8141) as in (B).

(F) ChIP for 3HA-Mps3 monitors MAT locus after 120 min on galactose in WT (GA-8306) and *nup120Δ* (GA-8308) cells synchronized in G2 and M phase by nocodazole. Enrichment by quantitative PCR as in Figure 2B but with a probe that recognizes both mating-type alleles (1.6 kb from cut site). ChIP data are mean  $\pm$  SEM.

See also Figure S5.

pore cluster in *nup133ΔN* in the absence of the Mps3 N terminus in both G1- and S-phase cells (Figure 5B). This did not reflect obvious pore misdistribution (Figure S5). The effects were confirmed by nuclear pore ChIP on the cleaved MAT locus: loss of Mps3N reduces break-induced association with pores from 5- to 2-fold (Figure 5C).

To test whether this crosstalk was reciprocal or not, we scored for the effect of deleting a component of the Nup84 subcomplex on DSB relocation to Mps3. The short arms of the Nup84 Y-shaped complex mediate key contacts with components of the nuclear pore complex, and these are lost upon deletion of any Nup84 subcomplex component (Fernandez-Martinez et al., 2012). Therefore, we used a strain lacking Nup120, which disrupts DSB interaction with the pore (Nagai et al., 2008). Importantly, in this mutant, we found that DSB relocation to the nuclear periphery is lost in G1- phase, but not S-phase, cells (Figure 5D). We could prove that this mutant disrupts interaction with the nuclear pore by scoring colocalization of the tagged DSB with the CFP-labeled pore cluster in *nup120Δ* cells. As expected, cleavage-induced association with the nuclear pore

cluster was lost upon ablation of Nup120 in both G1- and S-phase cells (Figure 5E). On the other hand, Mps3 ChIP showed WT levels of DSB association with 3HA-Mps3 in the absence of Nup120 (Figure 5F). Thus, Mps3 influences DSB binding to pores but not vice versa.

#### Repair Defects in *mps3* or Pore Mutants Are Additive

To test whether interactions at the two binding sites are functionally epistatic or additive for repair, we constructed double mutants that compromise the Nup84 subcomplex (*nup120Δ*) and the Mps3 nuclear anchorage domain (*mps3Δ65-145*). Single and double mutants were challenged with DNA damage. In a simple drop assay that monitors sensitivity to 0.03% methyl methanesulfonate (MMS), we found that the effects of *nup120Δ* and *mps3Δ65-145* on cell viability after plating on MMS were indeed additive (Figure 6A). This suggests that the two anchorage sites mediate different functions under conditions of S phase damage.

To extend this to a more precise pathway of repair, we scored for DSB repair by unequal sister chromatid recombination

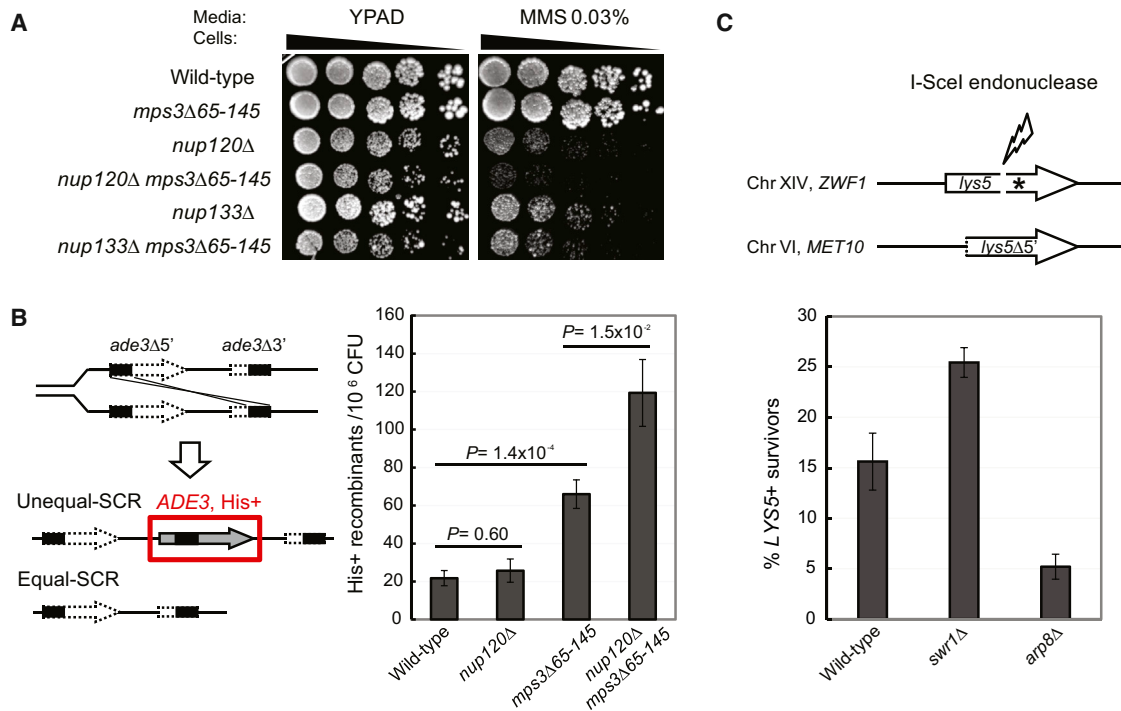


**Figure 6. Additive Effects of *nup120* and *mps3* on Unequal Sister Chromatid Exchange**

(A) Serial dilutions of isogenic strains bearing indicated mutations (*nup120Δ* or *nup133Δ* and *mps3Δ65-145*) were spotted onto the YPAD ± 0.03% MMS. Plates shown are after 3 days of growth.

(B) The uSCR frequencies of WT (SCRMTL2), *nup120Δ* (YH1301), *mps3Δ65-145* (YH1302), and *nup120Δ mps3Δ65-145* (YH1303) cells were determined by plating on YPAD or SC-His medium. Recombination frequency = number of His<sup>+</sup> recombinants per 10<sup>6</sup> colony forming units (CFUs) from eight experiments. Error bars indicate SD.

(C) An I-SceI cut site was placed within the *lys5* gene bearing a frameshift mutation on Chr XIV in a strain with a galactose-inducible I-SceI. An induced DSB repaired by gene conversion with the truncated *lys5* template at *MET10* (Chr VI) allows survival on galactose-Lys plates. Survivors over total plated cells yields the rate of gene conversion. Tested were eight independent colonies of *swr1Δ* (GA-6386), six colonies of *arp8Δ* (GA-6382), and 14 colonies of WT (GA-6217). An *rsc2Δ* strain yielded same as *arp8Δ* (data not shown). Significance was determined by a Student's t test ( $p = 0.0209$ ; WT versus *swr1Δ*,  $p = 0.0306$ ; WT versus *arp8Δ*). Error bars indicate SD.

(uSCR) (González-Barrera et al., 2003; Kadyk and Hartwell, 1992, 1993). It has been proposed that uSCR occurs when the replication fork bypasses lesions that normally obstruct its passage. The frequency of uSCR in the absence of Nup120 did not increase significantly over WT frequencies (Figure 6B). However, in the *mps3Δ65-145* mutant, we scored a strong increase in uSCR recombination (Figure 6B). Again, the double mutant showed additive effects, arguing that unequal sister chromatid exchange is indeed repressed by binding to Mps3 (Figure 6B), whereas an alternative pathway of repair appears to be lost by *nup120* deletion. If pore and Mps3 anchorage worked on the same pathway to repress recombination, then the two mutations would have shown epistatic effects on uSCR efficiency.

Finally, we scored for rates of homologous recombination with an ectopic donor at an induced DSB (Figure 6C). We found that loss of SWR-C increases HR with an exact ectopic donor, again confirming that sequestration of a DSB at the INM probably disfavors either homology search or the recombination event (Dion et al., 2012; Oza et al., 2009). As expected, the loss of Arp8 had the opposite effect (Figure 6C), confirming earlier results that scored reduced rates of resection and chromatin mobility in this mutant (van Attikum et al., 2007; Neumann et al., 2012).

## DISCUSSION

Many nuclear events have been shown to be localized to nuclear subcompartments, although it has remained unclear what establishes the localization of damage and whether different positions impact repair pathways differentially. Here, we exploited both quantitative microscopy and ChIP studies in order to examine the relocation of DSBs to the nuclear envelope in budding yeast. Although each assay has inherent weaknesses, the combination allows us to show conclusively that the two proposed binding sites for DNA damage, the SUN domain protein Mps3, and the Nup84 subcomplex of the nuclear pore, are distinct DSB binding sites. We resolve apparent contradictions in the literature by showing that DSBs bind pores in both G1 and S-phase cells, whereas they associate with Mps3 only in S and G2. A differential requirement for INO80 and SWR-C remodelers for translocation to Mps3 and pores reinforces the argument that the binding sites are distinct. Furthermore, disruption of the two anchors has differential effects on DSB repair: anchor site loss has additive, and not epistatic, impact on the survival of alkylating damage and for uSCR (Figure 6). Finally, we identified a nonreciprocal crosstalk between the Mps3 N terminus and

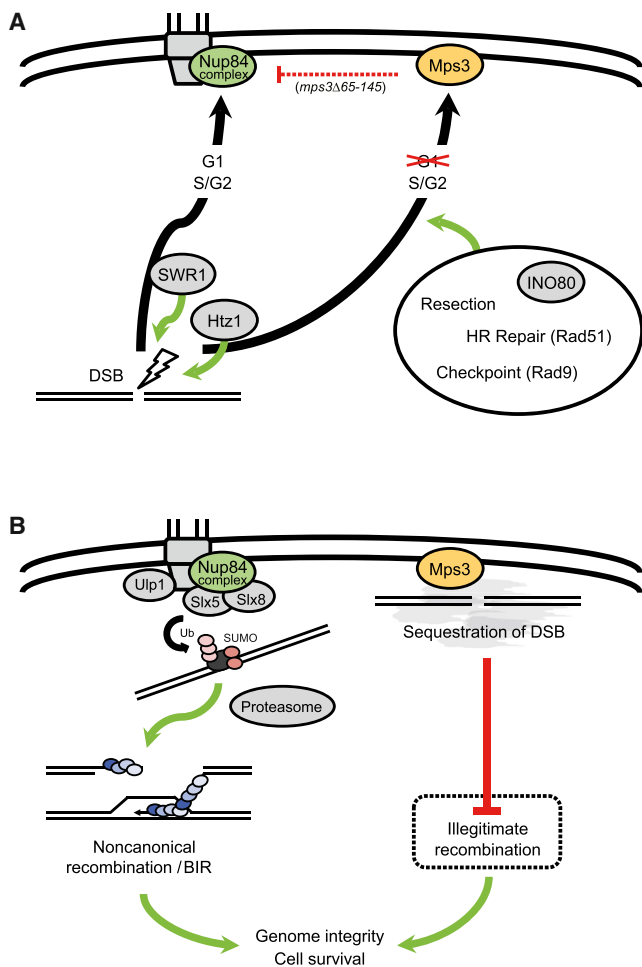


**Figure 7. Model of the DSB Relocation and the Outcome**

(A) SWR-C and INO80 influence DSB relocation to either Mps3 or pores, as described in the Results. SWR-C incorporated Htz1 (H2A.Z) is essential throughout the cell cycle. Outside of G1, DSBs can bind Mps3 in an INO80- and Rad51-dependent manner independent of pore integrity.

(B) DSB binding to nuclear pores and Mps3 suppresses uSCR, a hallmark of the illegitimate recombination.

nuclear pores with the use of three independent assays. Collectively, they show that the loss of Mps3 affects damage binding at pores, but the loss of pore binding does not impair association with Mps3. This means that either Mps3 acts on pore organization in a subtle manner that ablates the DSB interaction site or there is a necessary, but very transient, interaction of irreparable breaks with Mps3 prior to binding the pore. This latter is unlikely, given that the remodeler INO80 is selectively required for break association with Mps3 and not nuclear pores. Indeed, our final insight into DSB position stems from the relationship of chromatin remodelers to the subnuclear positioning of damage, as depicted in the model in Figure 7.

DSB recruitment to nuclear pores in G1 phase depends on SWR-C activity. Because there is neither resection nor available homology from the replicated sister in G1-phase cells, the preferred pathway of repair in G1 phase is NHEJ. Consistently,

previous work has shown that SWR-C is required both for efficient Ku80 recruitment to an induced DSB and for optimal error-free NHEJ (van Attikum et al., 2007). DSB-pore interactions may be stabilized by the affinity of yKu for the pore basket components Mlp1 and Mlp2 (Galy et al., 2000). On the other hand, Arp6 binding to pores is independent of Mlp1 and Mlp2 in G1 phase and is dependent on them in S phase (Yoshida et al., 2010). This may suggest that there is more than one anchorage site for DSBs at pores in G1-phase cells. Pore binding was also implicated in NHEJ-dependent repair of subtelomeric DSBs (Therizols et al., 2006). Finally, and in contrast to *swr1Δ*, the INO80-deficient mutant *arp8Δ* did not affect break recruitment to pores in G1, nor did it alter rates of error-free NHEJ (van Attikum et al., 2007).

In S-phase cells, on the other hand, sister chromatid recombination (SCR) becomes the preferred mechanism of DSB repair (González-Barrera et al., 2003; Kadyk and Hartwell, 1992). Although equal SCR is difficult to monitor, unequal exchange (uSCR) can be readily scored. Spontaneous uSCR rates were unaffected in the *nup120Δ* mutant, whereas rates increased in *mps3Δ65-145* (Figure 6). Given that DSB-Mps3 binding is intact in the *nup120Δ* mutant, Mps3 most likely serves as a repressor of uSCR. This is consistent with previous reports of enhanced recombination between telomeres in *mps3ΔN* mutants (Schober et al., 2009). Whether Mps3 acts simply by sequestration of the free end or by helping to load Mre11 (González-Barrera et al., 2003) and/or cohesin (Cortés-Ledesma and Aguilera, 2006) is unknown. Consistent with our findings, previous work showed the SWR-C-deficient *arp6* mutant has an increased level of spontaneous uSCR in this same assay (Kawashima et al., 2007).

In an assay for ectopic HR, we found that loss of INO80 function (*arp8Δ*) decreased efficiency, whereas *swr1* deletion increased the rate of DSB-induced HR (Figure 6). Collectively, these results argue for a recombination-repressive role for Mps3, which is consistent with previous observations on telomere-telomere exchange and the likelihood of DNA-DNA interactions detected in a chromosome conformation capture technology (Oza et al., 2009; Schober et al., 2009). Given that we score a delayed but intact DSB-pore interaction in INO80-deficient strains (Figure 2), we propose that nuclear pore association normally does not repress recombination. However, if Mps3 binding is ablated, then S-phase association with nuclear pores may compensate, as supported by the additive effects of the double *nup120 mps3Δ65-145* mutant on uSCR. Consistent with this, spontaneous Rad52 foci were found to be more mobile in *arp8* and in *swr1* mutants, which might favor ectopic repair over SCR (data not shown; Dion et al., 2013). We speculate that the role of the nuclear pore in S-phase DSB repair may reflect SUMO- and/or ubiquitin metabolism because of the nuclear pore-associated SUMO protease Ulp1 and the SUMO-dependent ubiquitin ligase Slx5-Slx8 (Nagai et al., 2008; Zhao et al., 2004). Strains mutant for the Nup84 complex (Nup84, Nup120, and Nup133) are hypersensitive to DNA-damaging agents, synthetic lethal with mutations that impair HR, and accumulate spontaneous damage foci containing Rad52 (Nagai et al., 2008; Palancade et al., 2007).

How do remodelers affect DSB binding site choice? The catalytic effects of the INO80 complex under conditions of DNA

damage are well documented and include nucleosome eviction, enhanced resection, and enhanced subdiffusive mobility (reviewed in Seeber et al., 2013b). It is likely that INO80 acts on the substrate itself, generating 3' overhang without remaining bound to tether the break to Mps3, given that Ino80, Arp5, or Arp8, when fused to LexA, could not shift a tagged locus to the nuclear periphery (Figure S4). The contribution of SWR-C and Htz1 to DSB relocation and repair may instead reflect their binding at the break site. A role for SWR-C and Htz1 in DSB repair appears to be conserved in mammals, given that the Swr1 homolog p400 ATPase and H2A.Z play critical roles in Rad51-mediated repair (Courilleau et al., 2012; Xu et al., 2012). The striking deposition of H2A.Z at laser-induced damage in mammalian cells correlates with an open conformation of chromatin at DSBs and the loading of the Brca1 complex (Xu et al., 2012). Additionally, H2A.Z exchange appears to restrict formation of ssDNA and favor loading of the Ku70/Ku80 complex. We propose that, in yeast, the equivalent phenomenon is break sequestration by Mps3, which is indeed Htz1 dependent. Intriguingly, SWR-C favors Ku loading in yeast (van Attikum et al., 2007), just as its homolog, SRCAP, does in mammalian cells (Xu et al., 2012), which may suppress recombination by sequestration and thus favor NHEJ. Given that remodelers show conserved functions in surviving DNA damage, it is most likely that a spatial segregation of repair functions, such as that shown here, is a conserved aspect of the cell's arsenal of defense against genomic insult.

## EXPERIMENTAL PROCEDURES

### Plasmids, Yeast Strains, and Yeast Techniques

Yeast strains used in this study are described in Table S1. Conditions for DSB induction and relocalization were previously described (Nagai et al., 2008), and cell culture and synchronization conditions are described in the Supplemental Information.

### Microscopy and Movie Analysis

Fluorescence microscopy and quantification was performed according to Meister et al. (2010). For specific details, see the Supplemental Information. Movie analysis and other parameters are available in Table S2.

### Statistical Analyses and Cutting Efficiency

To determine zone enrichment, we applied a  $\chi^2$  test comparing zone 1 to a random distribution (degree of freedom = 2, confidence limit = 95%). p values are listed in Table S3. To compare the perinuclear enrichment of two different strains, we used a proportional analysis with a confidence limit of 95%. The error bars of all mean squared displacement (MSD) plots and ChIP experiments represent the SEM. The uSCR results were compared with a Student's t test. The efficiency of DSB induction was determined by quantitative PCR with TaqMan probes as previously described (van Attikum et al., 2007). The cutting efficiencies are available in Table S3.

### Chromatin Immunoprecipitation

ChIP was carried out as previously described (Yoshida et al., 2010) with modifications described in the Supplemental Information.

### Assay for Spontaneous Unequal SCR

uSCR was previously described (Ui et al., 2007) with the generation of functional ADE3 by reciprocal recombination or gene conversion. Ade3 participates in histidine prototrophy, and thus recombination frequency was monitored by scoring viable colonies on SC-His. After growth at 30°C overnight, cells were collected by centrifugation, washed once, counted, and appropriately diluted onto either yeast extract, bactopectone, adenine, dextrose

(YPAD; 10<sup>3</sup> cells) in order to determine cell viability or SC-His (10<sup>6</sup> cells). Colonies were scored after 3–4 days at 30°C.

## SUPPLEMENTAL INFORMATION

Supplemental Information includes Supplemental Experimental Procedures, five figures, and three tables and can be found with this article online at <http://dx.doi.org/10.1016/j.molcel.2014.06.027>.

## ACKNOWLEDGMENTS

We thank Y. Orihara for help in ChIP experiments, J.E. Haber and M. Seki for yeast strains, S.L. Jaspersen, C. Wu, and K. Mizuta for plasmids, and the Friedrich Miescher Institute Microscopy Facility for technical help. C.H. thanks the Marie Curie International program and JSPS Research Abroad program for fellowships. S.M.G. thanks the Novartis Research Foundation, the Swiss National Science Foundation Sinergia grant, NCCR Frontiers in Genetics, and the Human Frontier Science Program (RGP0017) for support, and M.H. is supported by the Grant-in-Aid for Scientific Research on Innovative Areas.

Received: January 22, 2014

Revised: May 5, 2014

Accepted: June 17, 2014

Published: July 24, 2014

## REFERENCES

- Aguilera, A., and Garcia-Muse, T. (2013). Causes of genome instability. *Annu. Rev. Genet.* 47, 1–32.
- Bennett, G., Papamichos-Chronakis, M., and Peterson, C.L. (2013). DNA repair choice defines a common pathway for recruitment of chromatin regulators. *Nat Commun* 4, 2084–2092.
- Chapman, J.R., Taylor, M.R., and Boulton, S.J. (2012). Playing the end game: DNA double-strand break repair pathway choice. *Mol. Cell* 47, 497–510.
- Chen, X., Cui, D., Papusha, A., Zhang, X., Chu, C.D., Tang, J., Chen, K., Pan, X., and Ira, G. (2012). The Fun30 nucleosome remodeler promotes resection of DNA double-strand break ends. *Nature* 489, 576–580.
- Cortés-Ledesma, F., and Aguilera, A. (2006). Double-strand breaks arising by replication through a nick are repaired by cohesin-dependent sister-chromatid exchange. *EMBO Rep.* 7, 919–926.
- Costelloe, T., Louge, R., Tomimatsu, N., Mukherjee, B., Martini, E., Khadaroo, B., Dubois, K., Wiegant, W.W., Thierry, A., Burma, S., et al. (2012). The yeast Fun30 and human SMARCAD1 chromatin remodellers promote DNA end resection. *Nature* 489, 581–584.
- Courilleau, C., Chailleux, C., Jauneau, A., Grimal, F., Briois, S., Boutet-Robinet, E., Boudsocq, F., Trouche, D., and Canitrot, Y. (2012). The chromatin remodeler p400 ATPase facilitates Rad51-mediated repair of DNA double-strand breaks. *J. Cell Biol.* 199, 1067–1081.
- Dilworth, D.J., Tackett, A.J., Rogers, R.S., Yi, E.C., Christmas, R.H., Smith, J.J., Siegel, A.F., Chait, B.T., Wozniak, R.W., and Aitchison, J.D. (2005). The mobile nucleoporin Nup2p and chromatin-bound Prp20p function in endogenous NPC-mediated transcriptional control. *J. Cell Biol.* 171, 955–965.
- Dion, V., Kalck, V., Horigome, C., Towbin, B.D., and Gasser, S.M. (2012). Increased mobility of double-strand breaks requires Mec1, Rad9 and the homologous recombination machinery. *Nat. Cell Biol.* 14, 502–509.
- Dion, V., Kalck, V., Seeber, A., Schleker, T., and Gasser, S.M. (2013). Cohesin and the nucleolus constrain the mobility of spontaneous repair foci. *EMBO Rep.* 14, 984–991.
- Doye, V., Wepf, R., and Hurt, E.C. (1994). A novel nuclear pore protein Nup133p with distinct roles in poly(A)<sup>+</sup> RNA transport and nuclear pore distribution. *EMBO J.* 13, 6062–6075.
- Fernandez-Martinez, J., Phillips, J., Sekedat, M.D., Diaz-Avalos, R., Velazquez-Muriel, J., Franke, J.D., Williams, R., Stokes, D.L., Chait, B.T.,



- Sali, A., and Rout, M.P. (2012). Structure-function mapping of a heptameric module in the nuclear pore complex. *J. Cell Biol.* *196*, 419–434.
- Galy, V., Olivo-Marín, J.C., Scherthan, H., Doye, V., Rascalou, N., and Nehrbass, U. (2000). Nuclear pore complexes in the organization of silent telomeric chromatin. *Nature* *403*, 108–112.
- Gardner, J.M., Smoyer, C.J., Stensrud, E.S., Alexander, R., Gogol, M., Wiegraebe, W., and Jaspersen, S.L. (2011). Targeting of the SUN protein Mps3 to the inner nuclear membrane by the histone variant H2A.Z. *J. Cell Biol.* *193*, 489–507.
- González-Barrera, S., Cortés-Ledesma, F., Wellinger, R.E., and Aguilera, A. (2003). Equal sister chromatid exchange is a major mechanism of double-strand break repair in yeast. *Mol. Cell* *11*, 1661–1671.
- Horigome, C., Okada, T., Shimazu, K., Gasser, S.M., and Mizuta, K. (2011). Ribosome biogenesis factors bind a nuclear envelope SUN domain protein to cluster yeast telomeres. *EMBO J.* *30*, 3799–3811.
- Ira, G., Pelliccioli, A., Balijja, A., Wang, X., Fiorani, S., Carotenuto, W., Liberi, G., Bressan, D., Wan, L., Hollingsworth, N.M., et al. (2004). DNA end resection, homologous recombination and DNA damage checkpoint activation require CDK1. *Nature* *431*, 1011–1017.
- Jackson, S.P., and Bartek, J. (2009). The DNA-damage response in human biology and disease. *Nature* *461*, 1071–1078.
- Kadyk, L.C., and Hartwell, L.H. (1992). Sister chromatids are preferred over homologs as substrates for recombinational repair in *Saccharomyces cerevisiae*. *Genetics* *132*, 387–402.
- Kadyk, L.C., and Hartwell, L.H. (1993). Replication-dependent sister chromatid recombination in rad1 mutants of *Saccharomyces cerevisiae*. *Genetics* *133*, 469–487.
- Kalocsay, M., Hiller, N.J., and Jentsch, S. (2009). Chromosome-wide Rad51 spreading and SUMO-H2A.Z-dependent chromosome fixation in response to a persistent DNA double-strand break. *Mol. Cell* *33*, 335–343.
- Kawashima, S., Ogiwara, H., Tada, S., Harata, M., Wintersberger, U., Enomoto, T., and Seki, M. (2007). The INO80 complex is required for damage-induced recombination. *Biochem. Biophys. Res. Commun.* *355*, 835–841.
- Khadaroo, B., Teixeira, M.T., Luciano, P., Eckert-Boulet, N., Germann, S.M., Simon, M.N., Gallina, I., Abdallah, P., Gilson, E., Géli, V., and Lisby, M. (2009). The DNA damage response at eroded telomeres and tethering to the nuclear pore complex. *Nat. Cell Biol.* *11*, 980–987.
- Kobor, M.S., Venkatasubrahmanyam, S., Meneghini, M.D., Gin, J.W., Jennings, J.L., Link, A.J., Madhani, H.D., and Rine, J. (2004). A protein complex containing the conserved Swi2/Snf2-related ATPase Swr1p deposits histone variant H2A.Z into euchromatin. *PLoS Biol.* *2*, E131.
- Krogan, N.J., Keogh, M.C., Datta, N., Sawa, C., Ryan, O.W., Ding, H., Haw, R.A., Pootoolal, J., Tong, A., Canadien, V., et al. (2003). A Snf2 family ATPase complex required for recruitment of the histone H2A variant Htz1. *Mol. Cell* *12*, 1565–1576.
- Light, W.H., Brickner, D.G., Brand, V.R., and Brickner, J.H. (2010). Interaction of a DNA zip code with the nuclear pore complex promotes H2A.Z incorporation and INO1 transcriptional memory. *Mol. Cell* *40*, 112–125.
- Loeillet, S., Palancade, B., Cartron, M., Thierry, A., Richard, G.F., Dujon, B., Doye, V., and Nicolas, A. (2005). Genetic network interactions among replication, repair and nuclear pore deficiencies in yeast. *DNA Repair (Amst.)* *4*, 459–468.
- Luk, E., Ranjan, A., Fitzgerald, P.C., Mizuguchi, G., Huang, Y., Wei, D., and Wu, C. (2010). Stepwise histone replacement by SWR1 requires dual activation with histone H2A.Z and canonical nucleosome. *Cell* *143*, 725–736.
- Meister, P., Gehlen, L.R., Varela, E., Kalck, V., and Gasser, S.M. (2010). Visualizing yeast chromosomes and nuclear architecture. *Methods Enzymol.* *470*, 535–567.
- Miné-Hattab, J., and Rothstein, R. (2012). Increased chromosome mobility facilitates homology search during recombination. *Nat. Cell Biol.* *14*, 510–517.
- Mizuguchi, G., Shen, X., Landry, J., Wu, W.H., Sen, S., and Wu, C. (2004). ATP-driven exchange of histone H2AZ variant catalyzed by SWR1 chromatin remodeling complex. *Science* *303*, 343–348.
- Nagai, S., Dubrana, K., Tsai-Pflugfelder, M., Davidson, M.B., Roberts, T.M., Brown, G.W., Varela, E., Hediger, F., Gasser, S.M., and Krogan, N.J. (2008). Functional targeting of DNA damage to a nuclear pore-associated SUMO-dependent ubiquitin ligase. *Science* *322*, 597–602.
- Neumann, F.R., Dion, V., Gehlen, L.R., Tsai-Pflugfelder, M., Schmid, R., Taddei, A., and Gasser, S.M. (2012). Targeted INO80 enhances subnuclear chromatin movement and ectopic homologous recombination. *Genes Dev.* *26*, 369–383.
- Oza, P., and Peterson, C.L. (2010). Opening the DNA repair toolbox: localization of DNA double strand breaks to the nuclear periphery. *Cell Cycle* *9*, 43–49.
- Oza, P., Jaspersen, S.L., Miele, A., Dekker, J., and Peterson, C.L. (2009). Mechanisms that regulate localization of a DNA double-strand break to the nuclear periphery. *Genes Dev.* *23*, 912–927.
- Palancade, B., Liu, X., Garcia-Rubio, M., Aguilera, A., Zhao, X., and Doye, V. (2007). Nucleoporins prevent DNA damage accumulation by modulating Ulp1-dependent sumoylation processes. *Mol. Biol. Cell* *18*, 2912–2923.
- Papamichos-Chronakis, M., and Peterson, C.L. (2008). The Ino80 chromatin-remodeling enzyme regulates replisome function and stability. *Nat. Struct. Mol. Biol.* *15*, 338–345.
- Papamichos-Chronakis, M., Krebs, J.E., and Peterson, C.L. (2006). Interplay between Ino80 and Swr1 chromatin remodeling enzymes regulates cell cycle checkpoint adaptation in response to DNA damage. *Genes Dev.* *20*, 2437–2449.
- Papamichos-Chronakis, M., Watanabe, S., Rando, O.J., and Peterson, C.L. (2011). Global regulation of H2A.Z localization by the INO80 chromatin-remodeling enzyme is essential for genome integrity. *Cell* *144*, 200–213.
- Peterson, C.L., and Almouzni, G. (2013). Nucleosome dynamics as modular systems that integrate DNA damage and repair. *Cold Spring Harb. Perspect. Biol.* *5*, <http://dx.doi.org/10.1101/cshperspect.a012658>.
- Pfeiffer, P., Goedecke, W., and Obe, G. (2000). Mechanisms of DNA double-strand break repair and their potential to induce chromosomal aberrations. *Mutagenesis* *15*, 289–302.
- Price, B.D., and D'Andrea, A.D. (2013). Chromatin remodeling at DNA double-strand breaks. *Cell* *152*, 1344–1354.
- Schober, H., Ferreira, H., Kalck, V., Gehlen, L.R., and Gasser, S.M. (2009). Yeast telomerase and the SUN domain protein Mps3 anchor telomeres and repress subtelomeric recombination. *Genes Dev.* *23*, 928–938.
- Seeber, A., Dion, V., and Gasser, S.M. (2013a). Checkpoint kinases and the INO80 nucleosome remodeling complex enhance global chromatin mobility in response to DNA damage. *Genes Dev.* *27*, 1999–2008.
- Seeber, A., Hauer, M., and Gasser, S.M. (2013b). Nucleosome remodelers in double-strand break repair. *Curr. Opin. Genet. Dev.* *23*, 174–184.
- Shen, X., Mizuguchi, G., Hamiche, A., and Wu, C. (2000). A chromatin remodeling complex involved in transcription and DNA processing. *Nature* *406*, 541–544.
- Shimada, K., Oma, Y., Schleker, T., Kugou, K., Ohta, K., Harata, M., and Gasser, S.M. (2008). Ino80 chromatin remodeling complex promotes recovery of stalled replication forks. *Curr. Biol.* *18*, 566–575.
- Smeenk, G., and van Attikum, H. (2013). The chromatin response to DNA breaks: leaving a mark on genome integrity. *Annu. Rev. Biochem.* *82*, 55–80.
- Taddei, A., Hediger, F., Neumann, F.R., Bauer, C., and Gasser, S.M. (2004). Separation of silencing from perinuclear anchoring functions in yeast Ku80, Sir4 and Esc1 proteins. *EMBO J.* *23*, 1301–1312.
- Therizols, P., Fairhead, C., Cabal, G.G., Genovesio, A., Olivo-Marín, J.C., Dujon, B., and Fabre, E. (2006). Telomere tethering at the nuclear periphery is essential for efficient DNA double strand break repair in subtelomeric region. *J. Cell Biol.* *172*, 189–199.
- Tsukuda, T., Fleming, A.B., Nickoloff, J.A., and Osley, M.A. (2005). Chromatin remodeling at a DNA double-strand break site in *Saccharomyces cerevisiae*. *Nature* *438*, 379–383.

Ui, A., Seki, M., Ogiwara, H., Lai, M.S., Yamamoto, K., Tada, S., and Enomoto, T. (2007). Activation of a novel pathway involving Mms1 and Rad59 in sgs1 cells. *Biochem. Biophys. Res. Commun.* 356, 1031–1037.

van Attikum, H., Fritsch, O., Hohn, B., and Gasser, S.M. (2004). Recruitment of the INO80 complex by H2A phosphorylation links ATP-dependent chromatin remodeling with DNA double-strand break repair. *Cell* 119, 777–788.

van Attikum, H., Fritsch, O., and Gasser, S.M. (2007). Distinct roles for SWR1 and INO80 chromatin remodeling complexes at chromosomal double-strand breaks. *EMBO J.* 26, 4113–4125.

Wu, W.H., Alami, S., Luk, E., Wu, C.H., Sen, S., Mizuguchi, G., Wei, D., and Wu, C. (2005). Swc2 is a widely conserved H2AZ-binding module essential for ATP-dependent histone exchange. *Nat. Struct. Mol. Biol.* 12, 1064–1071.

Xu, Y., Ayrapetov, M.K., Xu, C., Gursoy-Yuzugullu, O., Hu, Y., and Price, B.D. (2012). Histone H2A.Z controls a critical chromatin remodeling step required for DNA double-strand break repair. *Mol. Cell* 48, 723–733.

Yoshida, T., Shimada, K., Oma, Y., Kalck, V., Akimura, K., Taddei, A., Iwahashi, H., Kugou, K., Ohta, K., Gasser, S.M., and Harata, M. (2010). Actin-related protein Arp6 influences H2A.Z-dependent and -independent gene expression and links ribosomal protein genes to nuclear pores. *PLoS Genet.* 6, e1000910.

Zhao, X., Wu, C.Y., and Blobel, G. (2004). Mlp-dependent anchorage and stabilization of a desumoylating enzyme is required to prevent clonal lethality. *J. Cell Biol.* 167, 605–611.

**Molecular Cell, Volume 55**

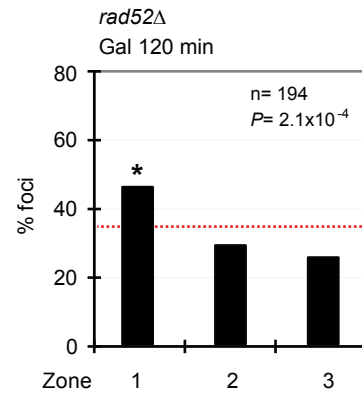
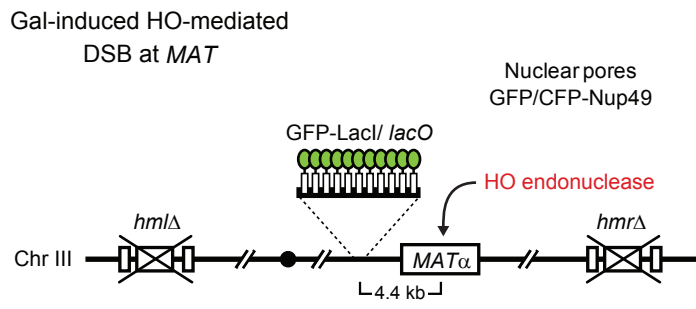
**Supplemental Information**

## **SWR1 and INO80 Chromatin Remodelers**

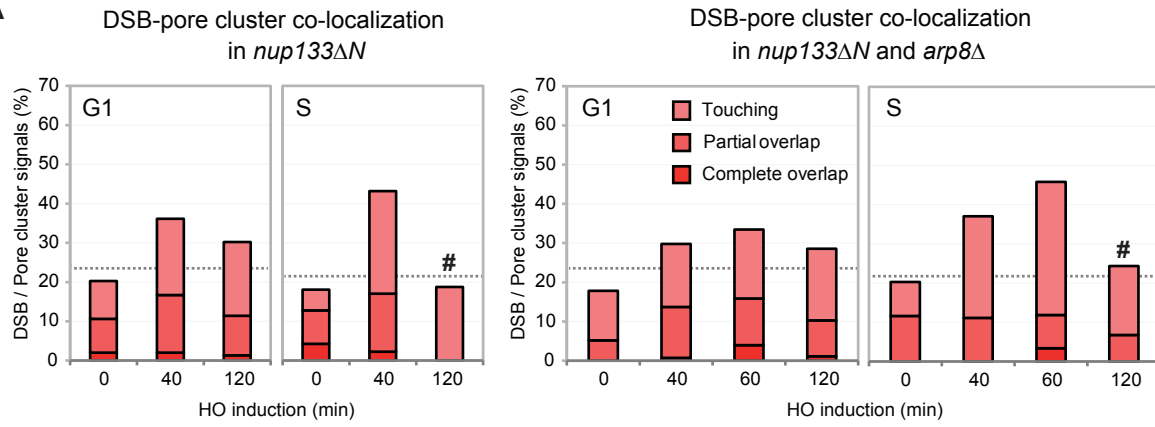
### **Contribute to DNA Double-Strand Break**

#### **Perinuclear Anchorage Site Choice**

**Chihiro Horigome, Yukako Oma, Tatsunori Konishi, Roger Schmid, Isabella Marcomini,  
Michael H. Hauer, Vincent Dion, Masahiko Harata, and Susan M. Gasser**



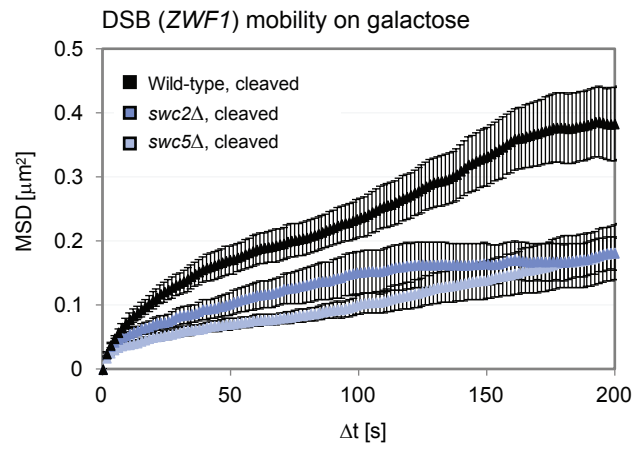
Horigome *et al.*, Figure S1

**A****B**

*nup133ΔN* CFP-Nup49 (pore) + GFP-Lacl (DSB)  
Nuclei with bright foci (%)

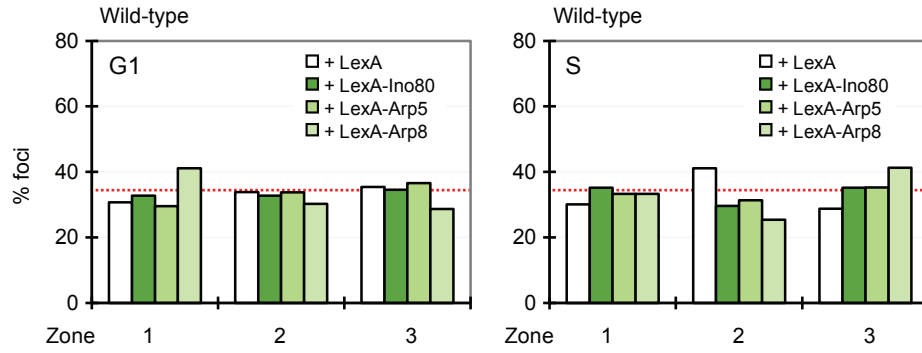
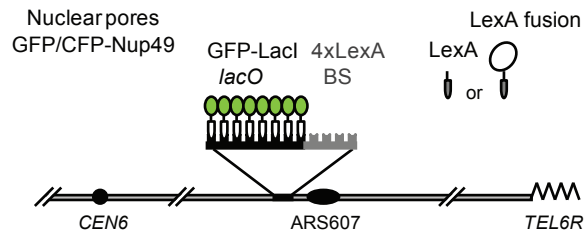
	HO 40 min	HO 120 min
G1	62.8	67.6
S	64.5	33.3 #

Horigome *et al.*, Figure S2

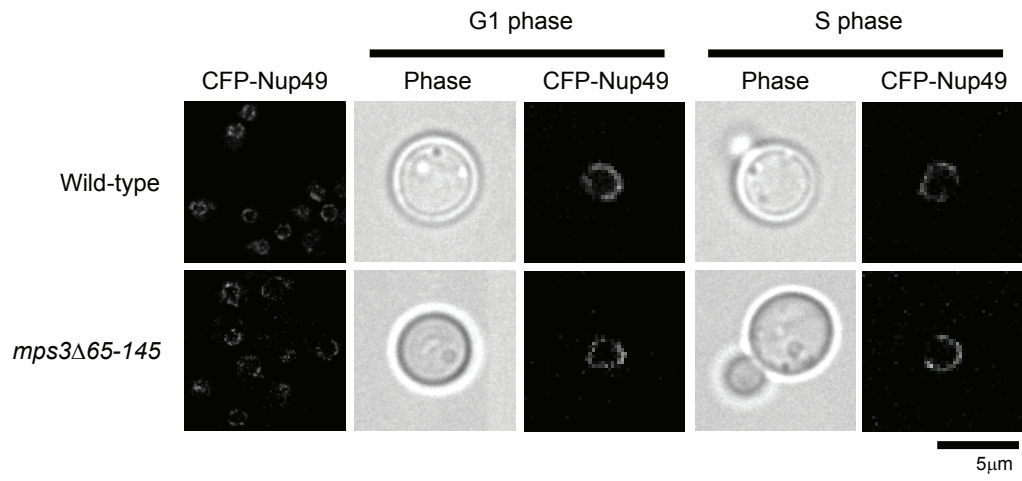


Horigome *et al.*, Figure S3

Targeting assay to ARS607



Horigome *et al.*, Figure S4



Horigome *et al.*, Figure S5



## Supplementary Materials:

**Figures S1 – S5, Legends and Figures**

**Tables S1 – S3 (Table S3 is an excel file)**

**Supplemental materials and methods**

**Supplementary references**

## Supplementary Figure legends

### **Figure S1. Rad52 is not necessary for the DSB relocation, Related to Figure 1**

The position of the *lacO*-tagged *MAT* locus on Chr III in a *rad52* $\Delta$  background (GA-7100) was scored 120 min after HO cut induction on galactose, as in Figure 1C. The asterisk indicates a significantly non-random distribution and the dotted line indicates a random distribution. Number of cells analysed (n) = 194; the *P* value indicates a comparison with a random distribution.

### **Figure S2. DSB-pore co-localization is lost by 120 min after cleavage in S-phase due to resection of the *lacO* repeat, Related to Figure 2**

(A) The co-localization of clustered nuclear pores and the *MAT* locus was scored in G1- or S-phase in both wild-type (GA-7314) and *arp8* $\Delta$  (GA-8143) cells after induction of HO on galactose. Co-localization was determined as in Figure 2D, in a *nup133* $\Delta$ N background expressing CFP-Nup49. Hatch mark indicates reduction to background signals after 120 min. The number of nuclei scored are 222 or 237 for G1 phase after 40 or 120 min on galactose, or 57 and 51 for S phase after 40 or 120 min on galactose. (B) The percentage of cells that still have bright GFP-LacI/ *lacO* foci at *MAT* drops to 33% after 120 min in S phase (GA-7314), probably due to resection and loss of *lacO* repeats.

**Figure S3. Loss of functional SWR-C impairs enhanced DSB mobility, Related Figure 4**

A mobility assay based on time-lapse tracking of a tagged and I-SceI-cleaved *ZWF1* locus is shown. The movement of Rad52-YFP is tracked in multiple movies over time after HO endonuclease induction on galactose, as in Figure 4C,D. MSD plots of the Rad52-YFP foci in wild-type (GA-6208), *swc2* $\Delta$  (GA-6581) and *swc5* $\Delta$  (GA-6673) cells during S phase are shown. Swc2 and Swc5 are components of SWR-C and are essential for its function. The data of MSD are represented as mean +/- SEM.

**Figure S4. INO80 is not sufficient to shift an internal locus to the nuclear periphery, Related to Figure 4**

Relocation of a randomly distributed locus (ARS607) due to the binding of a LexA-fusion protein, is shown for a wild-type strain (GA-1993) that was transformed plasmids expressing LexA alone or LexA-Ino80, LexA-Arp5 or LexA-Arp8 fusion constructs. The position of the ARS607 relative to three concentric zones (see Figure 1B) was scored. The dotted line indicates a random distribution. None of the distributions shown here are non-random.

**Figure S5. Nuclear pore distribution is not affected in *mps3* $\Delta$ 65-145, Related to Figure 5**

CFP-Nup49 was localized in the G1- or S-phase of the living wild-type (GA-6844) and *mps3* $\Delta$ 65-145 (GA-7096) cells by fluorescence confocal microscopy. Corresponding phase images reveal the cell cycle phase. Fluorescence images show little or no difference between mutant and wild-type cells.

**Table S1. Yeast strains used in this study, Related to Figure 1-6, S1, S3**

<b>Name</b>	<b>Genotype</b>	<b>Source</b>
GA-1081	JKM179; <i>MAT<math>\alpha</math></i> , $\Delta$ <i>hml::ADE1 hmr::ADE1 ade3::GALHO ade1-100 leu2-3, 112 lys5 trp1::hisG ura3-52</i>	(Lee et al., 1998)
GA-1496	GA-1081 <i>GFP-NUP49 GFP-LacI:Leu2 MAT::LacO repeats:TRP1</i>	(Nagai et al., 2008)
GA-6844	GA-1081 <i>CFP-NUP49 GFP-LacI:Leu2 MAT::LacO repeats:TRP1</i>	This study
GA-7095	GA-6844 <i>htz1::natMX4</i>	This study
GA-8110	GA-6844 <i>htz1::natMX4 ura3::3HA-HTZ1:URA3</i>	This study
GA-8111	GA-6844 <i>htz1::natMX4 ura3::3HA-htz1<math>\Delta</math>M6:URA3</i>	This study
GA-7003	GA-6844 <i>swr1::natMX4</i>	This study
GA-7094	GA-6844 <i>arp6::natMX4</i>	This study
GA-8069	GA-6844 <i>arp5::natMX4</i>	This study
GA-7103	GA-6844 <i>arp8::natMX4</i>	This study
GA-8667	GA-6844 <i>swr1::natMX4 pRS416-SWR1</i>	This study
GA-8668	GA-6844 <i>swr1::natMX4 pRS416-sw1K727G</i>	This study
GA-7099	GA-6844 <i>rad51::natMX4</i>	This study
GA-6647	W303 <i>MAT<math>\alpha</math></i> , <i>mps3::HIS3 pRS314-EGFP-MPS3 NUP49::CFP-NUP49:URA3</i>	(Horigome et al., 2011)
GA-6650	W303 <i>MAT<math>\alpha</math></i> , <i>nup133::HIS3 pUN100-nup133<math>\Delta</math>N:kanMX6 NUP49::NUP49-CFP:URA3 mps3::HIS3 pRS314-EGFP-MPS3</i>	(Horigome et al., 2011)
GA-7002	GA-6844 <i>3HA-MPS3</i>	This study
GA-7004	GA-6844 <i>3HA-MPS3 swr1::natMX4</i>	This study
GA-7161	GA-6844 <i>3HA-MPS3 arp8::natMX4</i>	This study
GA-7314	GA-6844 <i>nup133::natMX4 pUN100-nup133<math>\Delta</math>N:kanMX6</i>	This study
GA-8142	GA-6844 <i>nup133::natMX4 pUN100-nup133<math>\Delta</math>N:kanMX6 swr1::C.a.URA3</i>	This study
GA-8143	GA-6844 <i>nup133::natMX4 pUN100-nup133<math>\Delta</math>N:kanMX6 arp8::C.a.URA3</i>	This study
GA-8072	GA-6844 <i>nup133::natMX4 pUN100-nup133<math>\Delta</math>N:kanMX6 rad51::C.a.URA3</i>	This study
GA-8669	GA-7314 <i>ho::C.a.URA3</i>	This study
GA-8627	GA-1259 <i>bar1::C.a.URA3</i>	This study
GA-1461	W303 <i>MAT<math>\alpha</math></i> , <i>PES4:4xLexA:lacO array:TRP1 his3-15::GFP-LacI:HIS3 NUP49-GFP</i>	(Heun et al., 2001)
GA-1993	W303 <i>MAT<math>\alpha</math></i> , <i>PES4:4xLexA:lacO array:TRP1 his3-15::GFP-LacI:HIS3 NUP49-CFP</i>	This study
GA-7898	GA-1461 <i>swr1::natMX4</i>	This study
GA-4584	W303 <i>MAT<math>\alpha</math></i> , <i>ade2-1 trp1-1 his3-11 his3-15 ura3-1 leu2-3 leu1-112 can1-100 nup133::HIS3 pUN100-nup133<math>\Delta</math>N:kanMX6 NUP49::CFP-NUP49:URA3 ade2::lacI-GFP:ADE2 lys2::LexALacOPs:TRP</i>	This study
GA-6208	W303 <i>MAT<math>\alpha</math></i> , <i>ade2-1 trp1-1 his3-11 his3-15 ura3-1 leu2-3 leu2-112 RAD52-YFP NUP49-GFP ADE2::TetR-mCherry lys5::LacI-CFP:TRP leu2::LoxP, ZWF1:cutsite (Lmn:lys5:IsceIcs:LEU2:LacO array:Lmn)</i>	(Dion et al., 2012)
GA-6335	GA-6208 <i>swr1::natMX4</i>	This study
GA-6637	GA-6208 <i>htz1::HIS3p-natMX4</i>	This study
GA-6215	W303 <i>MAT<math>\alpha</math></i> , <i>ade2-1 trp1-1 his3-11 his3-15 ura3-1 leu2-3 leu2-112</i>	(Dion et

	<i>RAD52-YFP NUP49-GFP ADE2::TetR-mCherry lys5::LacI-CFP:TRP leu2::LoxP, ZWF1:cutsite (Lmn:lys5:IsceIcs:LEU2:LacO array:Lmn) met10::lmn adaptamers-HIS3-delLys5del-LexAOx4-TetO array</i>	al., 2012)
GA-6317	GA-6208 <i>arp8::natMX4</i>	(Neumann et al.,2012)
GA-6225	GA-6208 <i>rad51::natMX4</i>	(Dion et al., 2012)
GA-7096	GA-6844 <i>mps3Δ65-145</i>	This study
GA-7897	GA-6844 <i>nup133::natMX4 pUN100-nup133ΔN:kanMX6 mps3Δ65-145</i>	This study
GA-8141	GA-6844 <i>nup120::natMX4</i>	This study
GA-1259	JKM139; <i>MATa, Δho hml::ADE1 hmr::ADE1 ade3::GALHO ade1-100 leu2-3, 112 lys5 trp1::hisG ura3-52</i>	(Lee et al., 1998)
GA-8306	GA1259 <i>3HA-MPS3</i>	This study
GA-8308	GA1259 <i>3HA-MPS3 nup120::natMX4</i>	This study
GA-7895	GA-6844 <i>nup120::natMX4 mps3Δ65-145</i>	This study
GA-7106	GA-6844 <i>nup133::natMX4</i>	This study
GA-7896	GA-6844 <i>nup133::natMX4 mps3Δ65-145</i>	This study
SCRMTL2	<i>MATa, ade2 ade3-130 leu2 trp1 ura3 cyh2 SCR::LEU2</i>	(Onoda et al., 2004), <sup>a</sup>
YH1301	SCRMTL2 <i>nup120::natMX4</i>	This study
YH1302	SCRMTL2 <i>mps3Δ65-145</i>	This study
YH1303	SCRMTL2 <i>nup120::natMX4 mps3Δ65-145</i>	This study
GA-6217	W303 <i>MATα, RAD52-YFP, NUP49-GFP, ADE2::TetR-mCherry, lys5:LacI-CFP:TRP, template site (MET10, lmn adaptamers-HIS3-delLys5del-LexAOx4-TetO array), cut site (ZWF1, Lmn:lys5:IsceIcs:LEU2:LacO array:Lmn), leu2::LoxP</i>	This study
GA-6386	GA-6217 <i>swr1::natMX4</i>	This study
GA-6382	GA-6217 <i>arp8::natMX4</i>	This study
GA-7100	GA-6844 <i>rad52::natMX4</i>	This study
GA-6581	GA-6208 <i>swc2::natMX4</i>	This study
GA-6673	GA-6208 <i>swc5::natMX4</i>	This study

<sup>a</sup> Gift from M. Seki (Graduate School of Pharmaceutical Sciences, Tohoku University)

**Table S2. Summary of movement parameters, Related to Figure 4, S3**

Figure	Genotype	Condition	Locus	Cell cycle	$D$ ( $\times 10^{-3}$ $\mu\text{m}^2 \text{s}^{-1}$ )	$R_c$ ( $\mu\text{m}$ )	# of nuclei
Fig 4B	Wild-type	Glucose	<i>ZWF1</i>	S	1.98	0.6056	9
Fig 4B	<i>swr1</i> $\Delta$	Glucose	<i>ZWF1</i>	S	1.67	0.6225	11
Fig 4C, D	Wild-type (Neumann et al., 2012)	DSB (Gal)	<i>ZWF1</i>	S	1.69	0.6958	17
Fig 4C	<i>swr1</i> $\Delta$	DSB (Gal)	<i>ZWF1</i>	S	0.79	0.4071	16
Fig 4C	<i>htz1</i> $\Delta$	DSB (Gal)	<i>ZWF1</i>	S	1.06	0.4488	10
Fig 4C	Wild-type (Dion et al., 2012)	Uncleaved	<i>ZWF1</i>	S	1.18	0.4635	20
Fig 4D	<i>arp8</i> $\Delta$ (Neumann et al., 2012)	DSB (Gal)	<i>ZWF1</i>	S	1.46	0.5305	9
Fig 4D	<i>rad51</i> $\Delta$ (Dion et al., 2012)	DSB (Gal)	<i>ZWF1</i>	S	1.44	0.4823	16
Fig 4E	+ LexA	Targeting	ARS607	G1	1.81	0.6247	19
Fig 4E	+ LexA-Arp6	Targeting	ARS607	G1	1.44	0.4893	6
Fig 4F	+ LexA-Htz1	Targeting	ARS607	G1	1.57	0.552	17
Fig 4F	+ LexA-htz1 $\Delta$ M6	Targeting	ARS607	G1	1.7	0.5485	14
Fig S3	<i>swc2</i> $\Delta$	DSB (Gal)	<i>ZWF1</i>	S	1.06	0.4552	10
Fig S3	<i>swc5</i> $\Delta$	DSB (Gal)	<i>ZWF1</i>	S	0.79	0.4185	13

**Table S3. Summary of localization assay statistics, Related to Figure 1-3, 5, S1-S4 (see separate Excel file)**

## Supplemental Experimental Procedures

### Plasmids, yeast strains and yeast techniques

JKM139 and JKM179 are gifts from J. E. Haber and have been previously described (Lee et al., 1998). Standard methods for genetic modification of yeast were used (Longtine et al., 1998) and verified by PCR and phenotypic analysis. Yeast strains with *3HA-MPS3* and *mps3Δ65-145* are created by using the plasmids pRS306-*3HA-MPS3* and pRS306-*mps3Δ65-145* (gifts from Dr. Mizuta) (Horigome et al., 2011). For the DSB localization assay, yeast cells were grown at 30 °C for 2 days on YPAD plate (or selective SC media if selection is required), then inoculated the cells in synthetic media containing 0.05% glucose, 3% glycerol and 2% lactate (SCLGg) overnight to obtain an exponentially growing cell population with no more than  $5\text{-}7\times 10^6$  cells ml<sup>-1</sup> the next morning. We added 20% galactose (final 2%) to the medium to induce HO. The cells were harvested, fixed with paraformaldehyde (final 4%) and washed three times with PBS. Targeting assay was carried out with cells grown at 30°C in selective SC media to a concentration of  $5\times 10^6$  cells ml<sup>-1</sup>. G1 arrest was achieved using 1 μM α factor in a *bar1Δ* strain. G2/M arrest was achieved using 15 μg ml<sup>-1</sup> nocodazole in 1% DMSO. Arrests were confirmed by visual microscopy, and budding indices. Cell cycle stages were assigned based on the following criteria: cells in G1 have no bud and a round nucleus, cells in S phase have a bud up to 2/3 the size of the mother cells and a round nucleus.

### Microscopy and movie analysis

Images for zoning measurements were captured on a Metamorph-driven Spinning-disk confocal system based on an Olympus IX81 microscope, Yokogawa CSU-X1 scan head, EM-CCD Cascade II (Photometrics) camera and an ASI MS-2000 Z-piezo stage. We used PlanApo ×100, NA 1.45 total internal reflection fluorescence microscope oil objective. LacI-GFP position was determined with a through-focus stack of 16-21 0.2 μm steps and was

measured by ImageJ (NIH, USA) and the plug-in software PointPicker (Meister et al., 2010). The numbers of nuclei scored are available in Table S2. Movie analysis was carried out as described previously (Dion et al., 2012; Heun et al., 2001; Lisby et al., 2004). Briefly, the images obtained Spinning-disk confocal system were deconvolved using Huygens Remote Manager. We further processed the movies of fluorescence-labelled chromatin loci, which are very bright when compared with the nuclear background, by taking the cubic root of the pixel intensities using ImageJ and normalizing the pixel intensities across 2D projections to correct for bleaching using Imaris (Bitplane). This improved definition of the nuclear background and both the alignment and tracking quality, with the plug-in SpotTracker. The movement data were analysed by  $MSD = (x(t+\Delta t) - x(t))^2$  where  $x$  is the position of the spot and  $t$  is time in seconds (Neumann et al., 2012).

### **Statistical analyses and cutting efficiency**

The value was normalized to *SMC2* locus. Primer and probe sequences are available on request.

### **Chromatin immunoprecipitation (ChIP)**

Yeast cells cultured in 45 ml medium were cross-linked at 30 °C for 20 min, and disrupted using a bead beater (TOMY) and Zirconia/Silica beads. The recovered chromatin fraction was subjected to sonication using Bioruptor Plus (Diagenode) to obtain fragmented chromatin < 500 bp in length. An anti-HA antibody (sc-7392, Santa Cruz Biotech, Inc) or an anti-nuclear pore FG-repeat antibody (Mab414, Sigma) combined with anti-mouse IgG magnetic beads (Invitrogen) or Protein G magnetic beads (Invitrogen), respectively, were used for IP. ChIP DNA was purified and was analysed by quantitative PCR using primers adapted to the *MATa* or *MATα* locus (available on request).

## Supplementary references

- Dion, V., Kalck, V., Horigome, C., Towbin, B.D., and Gasser, S.M. (2012). Increased mobility of double-strand breaks requires Mec1, Rad9 and the homologous recombination machinery. *Nature Cell Biol* 14, 502-509.
- Heun, P., Laroche, T., Shimada, K., Furrer, P., and Gasser, S.M. (2001). Chromosome dynamics in the yeast interphase nucleus. *Science* 294, 2181-2186.
- Horigome, C., Okada, T., Shimazu, K., Gasser, S.M., and Mizuta, K. (2011). Ribosome biogenesis factors bind a nuclear envelope SUN domain protein to cluster yeast telomeres. *EMBO J* 30, 3799-3811.
- Lee, S.E., Moore, J.K., Holmes, A., Umezu, K., Kolodner, R.D., and Haber, J.E. (1998). *Saccharomyces* Ku70, mre11/rad50 and RPA proteins regulate adaptation to G2/M arrest after DNA damage. *Cell* 94, 399-409.
- Lisby, M., Barlow, J.H., Burgess, R.C., and Rothstein, R. (2004). Choreography of the DNA damage response: spatiotemporal relationships among checkpoint and repair proteins. *Cell* 118, 699-713.
- Longtine, M.S., McKenzie, A., 3rd, Demarini, D.J., Shah, N.G., Wach, A., Brachat, A., Philippsen, P., and Pringle, J.R. (1998). Additional modules for versatile and economical PCR-based gene deletion and modification in *Saccharomyces cerevisiae*. *Yeast* 14, 953-961.
- Nagai, S., Dubrana, K., Tsai-Pflugfelder, M., Davidson, M.B., Roberts, T.M., Brown, G.W., Varela, E., Hediger, F., Gasser, S.M., and Krogan, N.J. (2008). Functional targeting of DNA damage to a nuclear pore-associated SUMO-dependent ubiquitin ligase. *Science* 322, 597-602.
- Neumann, F.R., Dion, V., Gehlen, L.R., Tsai-Pflugfelder, M., Schmid, R., Taddei, A., and Gasser, S.M. (2012). Targeted INO80 enhances subnuclear chromatin movement and ectopic homologous recombination. *Genes & Dev* 26, 369-383.
- Onoda, F., Seki, M., Wang, W., and Enomoto, T. (2004). The hyper unequal sister chromatid recombination in an *sgs1* mutant of budding yeast requires MSH2. *DNA Repair* 3, 1355-1362.



# PolySUMOylation by Siz2 and Mms21 triggers relocation of DNA breaks to nuclear pores through the Slx5/Slx8 STUbL

Chihiro Horigome<sup>1,4#</sup>, Denise E. Bustard<sup>2#</sup>, Isabella Marcomini<sup>1,3</sup>, Neda Delgoshaie<sup>1</sup>, Monika Tsai-Pflugfelder<sup>1</sup>, Jennifer A. Cobb<sup>2</sup> and Susan M. Gasser<sup>1,3\*</sup>

<sup>1</sup> Friedrich Miescher Institute for Biomedical Research, Maulbeerstrasse 66, CH-4058 Basel, Switzerland

<sup>2</sup> Southern Alberta Cancer Research Institute, Departments of Biochemistry & Molecular Biology and Oncology, Cumming School of Medicine; University of Calgary; 3330 Hospital Drive N.W., Calgary, AB T2N 4N1, Canada ([jcobb@ucalgary.ca](mailto:jcobb@ucalgary.ca))

<sup>3</sup> University of Basel, Faculty of Natural Sciences, CH-4056 Basel, Switzerland

<sup>4</sup> Present address: Institute of Molecular and Cellular Biosciences; The University of Tokyo; 1-1-1, Yayoi, Bunkyo-ku, Tokyo, 113-0032, Japan.

# equal contribution

*Published in Genes Dev., 2016, 30(8):931-45*

This paper explores the role of SUMOylation and SUMOylation-dependent enzymes in the movement of a DSB to the nuclear periphery. It shows that SUMOylation is required for DSB relocation to the NE, but to different extents: In G1, relocation to pores requires Slx5 that recognizes a polySUMOylated target, whereas in S phase binding to Mps3 requires monoSUMOylation mediated by Mms21 SUMO E3 ligase. Interaction with Mps3 depends on SMC5/6 complex but not on Slx5/8. In this study, my main interest was in determining the functionality of the DSB binding sites. My main contribution was in testing a role for pore and STUbL mutants in repair outcome. I could detect a differential role in precise and imprecise end joining: only the latter is significantly affected by the Nup84 complex. Besides, I used a reporter assay to demonstrate an effect of pores on break-induced replication (Figure 6b, c).



# PolySUMOylation by Siz2 and Mms21 triggers relocation of DNA breaks to nuclear pores through the Slx5/Slx8 STUbL

Chihiro Horigome,<sup>1,5,6</sup> Denise E. Bustard,<sup>2,3,6</sup> Isabella Marcomini,<sup>1,4</sup> Neda Delgosaie,<sup>1</sup> Monika Tsai-Pflugfelder,<sup>1</sup> Jennifer A. Cobb,<sup>2,3</sup> and Susan M. Gasser<sup>1,4</sup>

<sup>1</sup>Friedrich Miescher Institute for Biomedical Research, CH-4058 Basel, Switzerland; <sup>2</sup>Department of Biochemistry and Molecular Biology, <sup>3</sup>Department of Oncology, Robson DNA Science Centre, Arnie Charbonneau Cancer Institute, Cumming School of Medicine, University of Calgary, Calgary, Alberta T2N 4N1, Canada; <sup>4</sup>Faculty of Natural Sciences, University of Basel, CH-4056 Basel, Switzerland

**High-resolution imaging shows that persistent DNA damage in budding yeast localizes in distinct perinuclear foci for repair. The signals that trigger DNA double-strand break (DSB) relocation or determine their destination are unknown. We show here that DSB relocation to the nuclear envelope depends on SUMOylation mediated by the E3 ligases Siz2 and Mms21. In G1, a polySUMOylation signal deposited coordinately by Mms21 and Siz2 recruits the SUMO targeted ubiquitin ligase Slx5/Slx8 to persistent breaks. Both Slx5 and Slx8 are necessary for damage relocation to nuclear pores. When targeted to an undamaged locus, however, Slx5 alone can mediate relocation in G1-phase cells, bypassing the requirement for polySUMOylation. In contrast, in S-phase cells, monoSUMOylation mediated by the Rtt107-stabilized SMC5/6–Mms21 E3 complex drives DSBs to the SUN domain protein Mps3 in a manner independent of Slx5. Slx5/Slx8 and binding to pores favor repair by ectopic break-induced replication and imprecise end-joining.**

[*Keywords:* SUMO; Siz2; Mms21; Slx5; DNA damage; nuclear pores; nuclear organization]

Supplemental material is available for this article.

Received January 11, 2016; revised version accepted March 18, 2016.

The accurate repair of DNA double-strand breaks (DSBs) is crucial for genome integrity. Nonhomologous end-joining (NHEJ) and repair by homologous recombination (HR) are common and highly conserved pathways of DSB repair. Breaks that are difficult to repair due to a lack of homologous donor sequences or conditions that impair end-to-end ligation must be repaired by alternative pathways, which include imprecise or microhomology-mediated end-joining or break-induced replication (BIR) (for review, see Ceccaldi et al. 2016). Repair pathway choice is influenced by both the cell cycle (which in turn impacts resection at the break site) and the chromatin context of the damage (Nagai et al. 2010; Geli and Lisby 2015).

Certain types of DNA repair appear to be favored by specific subnuclear compartments. Compartmentation can either stem from the chromatin context of the damage (Therizols et al. 2006; Khadaroo et al. 2009; Agmon et al. 2013) or arise through recruitment of the damage to specific subnuclear sites (for review, see Nagai et al. 2010; Geli and Lisby 2015). For example, DSBs in the re-

petitive ribosomal DNA locus of yeast or in heterochromatic satellite repeats of flies and mammalian cells shift away from the repetitive sequence domain prior to repair by HR (Torres-Rosell et al. 2007; Chiolo et al. 2011; Lemaître et al. 2014). This is thought to avoid unequal crossover events in *cis* and/or chromosomal translocations that arise from strand invasion into other chromosomes. In budding yeast, DSBs that occur in unique sequences also shift their subnuclear position if they lack an intact donor for HR or if repeated cleavage/ligation cycles occur (Nagai et al. 2008). Within 2 h of their induction, such persistent DNA breaks accumulate at the nuclear envelope (NE) (Nagai et al. 2008). Similarly, collapsed replication forks and those stalled at expanded triplet repeats (Su et al. 2015) were shown to shift to nuclear pores, as do uncapped telomeres that arise from telomere erosion in telomerase-deficient cells (for review, see Geli and Lisby 2015). It is noteworthy that the repair of these three types of damage requires mechanisms other than precise end-joining or canonical HR.

<sup>5</sup>Present address: Institute of Molecular and Cellular Biosciences, The University of Tokyo, Yayoi, Bunkyo-ku, Tokyo 113-0032, Japan

<sup>6</sup>These authors contributed equally to this work.

Corresponding author: susan.gasser@fmi.ch

Article published online ahead of print. Article and publication date are online at <http://www.genesdev.org/cgi/doi/10.1101/gad.277665.116>.

© 2016 Horigome et al. This article is distributed exclusively by Cold Spring Harbor Laboratory Press for the first six months after the full-issue publication date (see <http://genesdev.cshlp.org/site/misc/terms.xhtml>). After six months, it is available under a Creative Commons License (Attribution-NonCommercial 4.0 International), as described at <http://creativecommons.org/licenses/by-nc/4.0/>.

The perinuclear sites at which yeast damage accumulates were initially identified as nuclear pores, and, in several instances, sequestration was shown to require the Nup84 complex, which, in budding yeast, includes Nup84, Nup120, Nup133, and the associated Nup60 (Nagai et al. 2008; Khadaroo et al. 2009). Subsequent studies identified a second binding site at the NE, the *Saccharomyces cerevisiae* SUN domain protein Mps3 (Kalocsay et al. 2009; Oza et al. 2009). Mps3 sequesters repair intermediates containing ssDNA complexed with Rad51 and reduces promiscuous recombination events (Kalocsay et al. 2009; Oza et al. 2009; Ferreira et al. 2011). The loss of the Nup84 complex or its associated Slx5/Slx8 SUMO targeted ubiquitin ligase (STUbL), on the other hand, compromised survival after replication fork collapse and enhanced ectopic recombination (Nagai et al. 2008; Oza et al. 2009; Horigome et al. 2014). The two sites of sequestration not only affect repair outcome differentially but have distinct requirements for damage recruitment. Binding to Mps3 appears to be restricted to S and G2 phases of the cell cycle and requires extensive resection at DSBs (Kalocsay et al. 2009; Oza et al. 2009), unlike relocation to nuclear pores, which occurs in G1 without extensive end resection (Horigome et al. 2014). We note that in otherwise unperturbed cells, a transient pore association of triplet repeat stalled replication forks was scored in late S/G2 phase, while they could not be recovered with Mps3 (Su et al. 2015). Intriguingly, ablation of the relevant Nup84 pore subcomplex or of the STUbL subunits Slx5/Slx8 increased the frequency of triplet repeat expansion/contraction events during stalled fork recovery (Su et al. 2015).

Early genetic screens in budding yeast implicated nuclear pore proteins in DNA repair. Screens for survival of ionizing radiation showed that the yeast Nup84 complex contributes to cell survival (Bennett et al. 2001; Loeillet et al. 2005), and loss of Nup84, Nup120, or Nup133 led to pleiotropic DNA damage sensitivities and synthetic lethality with components of the Rad52 pathway of HR (Chang et al. 2002; Loeillet et al. 2005; Nagai et al. 2008). This sensitivity is consistent with the notion that pores mediate repair pathways distinct from canonical HR. Indeed, sites of active HR, visualized as Rad52 foci, are found in the nuclear interior and are specifically excluded from the NE and the nucleolus (Bystricky et al. 2009; Dion et al. 2013). Besides conferring sensitivity to exogenous agents (Bennett et al. 2001), nuclear pore mutants showed impaired replication fork restart (for review, see Bukata et al. 2013; Geli and Lisby 2015) and have recently been implicated in the repair of subtelomeric DSBs by strand invasion events (Chung et al. 2015). In human cells, components in the Nup84 complex were found to suppress elevated levels of H2AX phosphorylation in cells exposed to aphidicolin (Paulsen et al. 2009), and, in flies, the loss of the corresponding complex enhanced the appearance of damage foci provoked by ionizing irradiation (Ryu et al. 2015).

In both yeast and flies, Nup84-linked damage sensitivity and the closely associated nuclear pore basket proteins Nup60 and Mlp1/Mlp2 have been linked to enzymes that

control SUMO metabolism (Zhao et al. 2004; Palancade et al. 2007; Nagai et al. 2008; Ryu et al. 2015). Indeed, DSBs that occur in the ribosomal DNA in budding yeast (Torres-Rosell et al. 2007) and in heterochromatin in flies (Chiolo et al. 2011) were shown to shift away from the domain of repetitive sequences in a manner dependent on the SMC5/6 complex and its associated SUMO ligase, Mms21. Although Rad52 SUMOylation influenced damage relocation from the nucleolus to the nucleoplasm (Torres-Rosell et al. 2007), Rad52 was not needed for the relocation of a euchromatic DSB to pores (Horigome et al. 2014). In flies, the STUbL subunit Dgrn, along with the SMC5/6 complex, was necessary for DSB relocation away from heterochromatin (Chiolo et al. 2011; Ryu et al. 2015). This shift required the STUbL interactor Rad60 (ScEsc2/HsNIP45) and the Nup84 pore complex (Ryu et al. 2015).

The molecular link between pores and STUbL enzymes is less clear. Earlier work showed that the yeast STUbL Slx5/Slx8 can be precipitated with Nup84 from cell extracts (Nagai et al. 2008), yet it was unclear whether Slx5/Slx8 mediates damage relocation or instead processes breaks once they reach the periphery. Moreover, the damage-associated signal that triggers relocation remained unknown. Because STUbLs contain SUMO-interacting motifs (SIMs) (for review, see Sarangi and Zhao 2015) and because repair proteins of many different pathways are SUMOylated (Cremona et al. 2012; Psakhye and Jentsch 2012), it became important to test whether SUMO ligases contribute to the relocation of damage to the NE.

Here we dissect the role of SUMO-mediated events mediated by the E3 ligases Siz2 (PIAS in humans) and the SMC5/6-associated Mms21 in damage recognition by the yeast STUbL Slx5/Slx8 and examine how these components affect DSB relocation to the NE. We used rigorous assays that distinguish pore-binding from Mps3-binding sites and G1-phase from S-phase cells. Both loss-of-function and gain-of-function assays allowed us to correlate different sites of damage sequestration with the binding of Slx5, whose recruitment reflects recognition of a poly-SUMO modification. We found that SUMO chain length helps determine the perinuclear site for damage sequestration. These data likely reflect conserved rules governing damage relocation and appropriate repair pathway choice.

## Results

### *SUMO E3 ligases affect DSB relocation*

In addition to phosphorylation and ubiquitination (Smeenk and van Attikum 2013), many proteins become SUMOylated at sites of DNA damage (Cremona et al. 2012; Psakhye and Jentsch 2012). Targets include proteins implicated in basically every pathway of repair, including Rad52, Rad59, Srs2, RPA, Sae2, yKu, Sgs1, and Mre11. Indeed, the loss of Mre11 actually alters SUMOylation of other repair factors (Cremona et al. 2012). SUMO E3 ligases such as Siz2 and Mms21 themselves are recruited to

damage (Zhao et al. 2004; Zhao and Blobel 2005; De Piccoli et al. 2006; Chung and Zhao 2015) and were shown to cooperate with Slx5/8 to suppress duplication-mediated genome rearrangements (Albuquerque et al. 2013). We therefore reexamined the role of SUMO E3 ligases in DSB relocation to the NE.

In budding yeast, there are four SUMO E3 ligases—namely, Siz1 and Siz2, the yeast PIAS homologs; Mms21, a highly conserved ligase component of the SMC5/6 complex; and Cst9, the meiosis-specific putative E3. Siz1 and Siz2 mediate the vast majority of SUMOylation in vegetatively growing yeast, with Siz1 primarily targeting cytoplasmic proteins, and Siz2 modifying a large number of factors involved in HR and other pathways of repair (Ferreira et al. 2011; Cremona et al. 2012; Psakhye and Jentsch 2012; Chung and Zhao 2015). Because Siz1 tends to compensate for survival of DNA damage in the absence of Siz2 (Cremona et al. 2012), we first monitored DSB relocation in cells lacking both PIAS homologs.

To do this, we used a high-resolution microscopic approach that monitors the subnuclear position of an HO-induced DSB at a GFP-LacI-tagged *MAT* locus in cells lacking both *HM* donor sites (Fig. 1A,B). A focal stack of images through a population of intact cells allowed us to determine the position of the break relative to the Nup49-CFP-tagged NE and score for the cell cycle phase based on bud size and nuclear position. PCR analysis monitored the efficiency DSB induction. This assay allowed us to differentiate G1-phase from S/G2-phase requirements for DSB relocation (Fig. 1B; Nagai et al. 2008; Horigome et al. 2014).

At 120 min after induction of the HO endonuclease, we note that the peripheral relocation of the induced DSB observed in wild-type cells was lost in the *siz1Δ siz2Δ* double mutant in both G1- and S-phase cells (Fig. 1C; Supplemental Table S1). We tested the deletion alleles individually and found that *siz2Δ* compromises perinuclear relocation more efficiently than *siz1Δ* alone, especially at early time points (Supplemental Fig. S1B). This is consistent with recent work showing a dominant role of Siz2 in damage-associated SUMOylation (Chung and Zhao 2015; for review, see Sarangi and Zhao 2015), although Siz1 may compensate over time (Supplemental Fig. S1B).

The SUMO E3 ligase Mms21, like all components of its associated SMC5/6 complex, is essential for yeast viability, although its SUMO ligase activity is not. Mms21 SUMOylation activity, on the other hand, is critical for survival of genotoxic stress and becomes essential in the absence of Siz1 and Siz2 activities (Cremona et al. 2012). We therefore tested the effects of a SUMO ligase-deficient Mms21, *mms21ΔC*, on DSB relocation. Similar to the *siz1Δ siz2Δ* double mutant, cells harboring the *mms21ΔC* allele were completely deficient in break relocation to the NE in both G1- and S-phase cells (Fig. 1C).

To determine which of the two perinuclear anchorage sites, pores or Mps3, was affected by loss of SUMOylation, we used two independent assays. The most rigorous means to score pore association is with a microscopy-based assay that exploits a strain with a small N-terminal

deletion in Nup133 that allows Nup49-CFP-tagged pores to form a single cluster in the NE without compromising the pore's transport function (Fig. 1D). Uncut controls and computer simulations of random distributions let us distinguish colocalization with the pore cluster above the level of stochastic coincidence (stochastic colocalization zone in Fig. 1D, shaded gray; see Horigome et al. 2014, 2015). As above, we can also determine cell cycle stage cell by cell. Colocalization with Mps3 is not possible to do by microscopy because the perinuclear rim staining of Mps3 in mitotic cells is weak (Horigome et al. 2014). Mps3 association is instead monitored by chromatin immunoprecipitation (ChIP). Previous studies showed that the association of resected breaks with Mps3 is S-phase-specific even though Mps3 is expressed throughout the cell cycle (Oza et al. 2009; Horigome et al. 2014).

We found that DSBs are enriched at the nuclear pore cluster for 2 h in G1-phase cells and for at least 40 min in S-phase cells (Fig. 1D). While resection through the *lacO* repeats attenuates the DSB signal in S-phase cells, nuclear pore-ChIP (using a monoclonal antibody against FG repeats) confirmed that DSBs persist at nuclear pores up to 4 h after the cut is induced. In the absence of Siz2, however, the DSB association with nuclear pores is significantly reduced both in G1- and S-phase cells, when monitored by either microscopy or pore ChIP (Fig. 1D,E). Intriguingly, *siz2Δ* did not alter DSB association with Mps3, suggesting that another signal addresses damage to Mps3 (Fig. 1F).

As shown in Figure 1C, we observed that loss of either the Siz2 or Mms21 SUMO ligase led to a loss of peripheral sequestration. One way to explain this double dependence is that the two ligases act sequentially to generate a polySUMOylation signal at damage, which in turn triggers relocation to the pore. Consistent with this model, it was observed that a number of Siz2 targets retain monoSUMOylation but lose polySUMO chains in the absence of Siz2, suggesting that another enzyme, such as Mms21, might deposit the initial SUMO conjugate (Mullen and Brill 2008; Psakhye and Jentsch 2012; D'Ambrosio and Lavoie 2014; Chung and Zhao 2015). Analogously, sequential action of Mms21 and Siz2 has been proposed to regulate sister chromatid segregation in yeast (Mullen and Brill 2008; D'Ambrosio and Lavoie 2014).

To see whether polySUMOylation is important for relocation, we evaluated DSB position in a mutant strain that cannot form SUMO chains due to mutations in three lysine residues of the N-terminal domain of the SUMO-1 homolog Smt3 (K11, K15, and K19) (Tatham et al. 2001; Bylebyl et al. 2003), compromising almost all polySUMOylation. In this *smt3-3KR* allele, DSB relocation is compromised in both G1- and S-phase cells (Fig. 1G), consistent with a requirement for SUMO chain formation. Given that this mutant alters all SUMO chain formation in the cell, affecting transcription as well as chromosome segregation, we cannot exclude that there are indirect effects of *smt3-3KR*. Nonetheless, the observed results are consistent with our hypothesis that Mms21 and Siz2 cooperate to deposit a polySUMOylation signal that might trigger DSB relocation. Intriguingly, *smt3-3KR* is

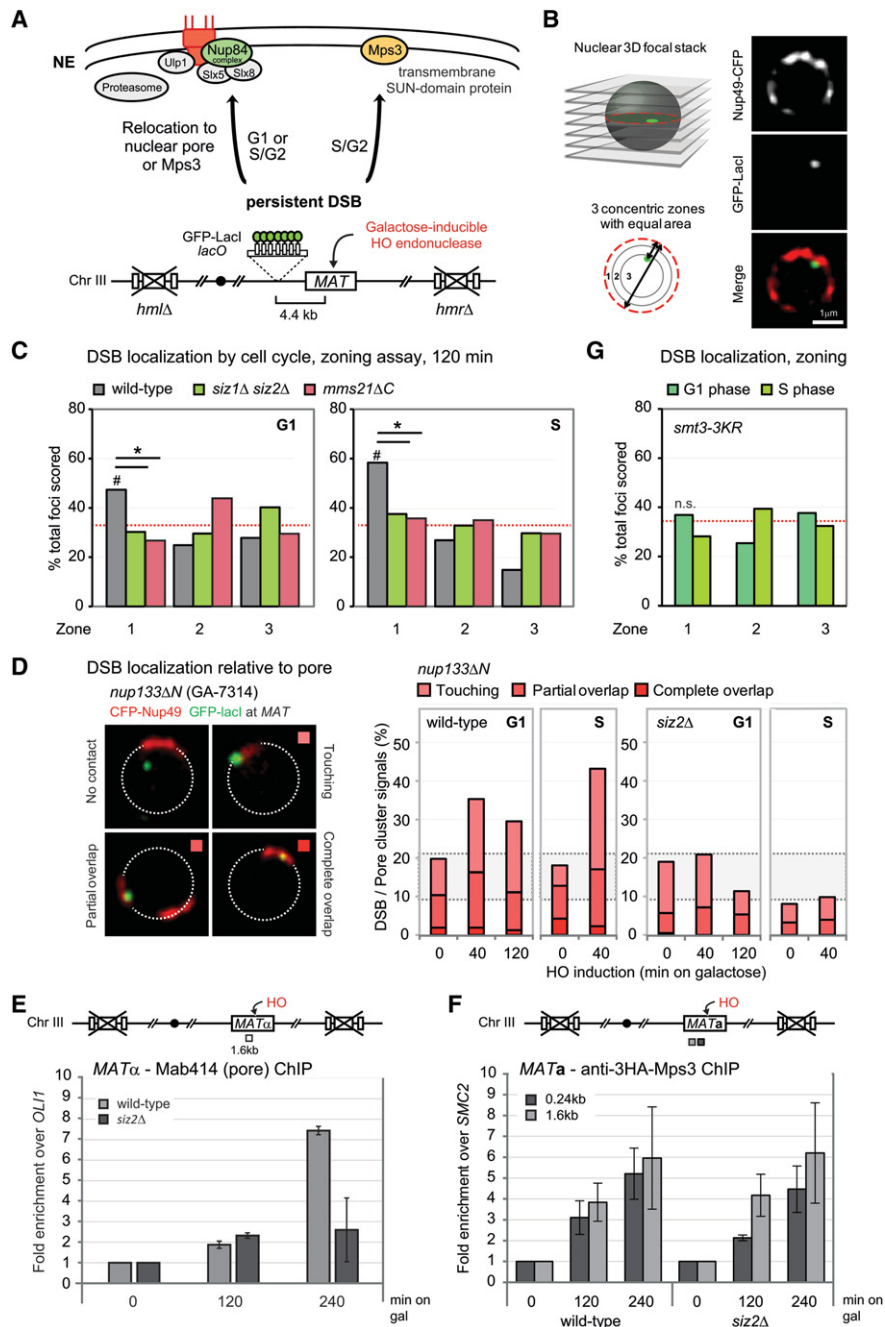


**Figure 1.** SUMO E3 ligases are required for the DSB anchoring to the nuclear periphery. (A) Shown is chromosome III (Chr III) in GA-6844 bearing deleted homologous donor loci (*hmlΔ/hmrΔ*) and a *lacO* array inserted 4.4 kb from the HO cut site at *MAT*. GFP-LacI and CFP-Nup49 label DSB and pores, respectively. Relocation to Mps3 was previously shown to occur in S or G2 phase, coincident with extensive resection. (B) Locus position was scored relative to the nuclear diameter in the locus' plane of focus using a spinning disc confocal image stack. Distance over diameter ratios are binned into three equal zones. (C) Position of cleaved *MAT* position relative to CFP-Nup49 in *siz1Δ siz2Δ* (GA-7968) and *mms21ΔC* (JC3654) after 120 min on galactose. The mutants compromise relocation in both G1- and S-phase cells. (#) Significantly nonrandom based on cell number and confidence values from a proportional test comparing random and experimental distributions; (\*) significantly different distribution between wild type and the mutant; (red dotted line) 33% or random distribution. Cleavage efficiency, nuclei counted, and statistical significance for all imaging experiments are summarized in Supplemental Table S1. (D) Scoring of *MAT* colocalization with the pore cluster in *nup133ΔN* (GA-7314) after cut induction. Scoring criteria are shown at the left, and results comparing wild type (GA-7314) and *siz2Δ* (GA-7970) are at the right. A gray-shaded zone between dotted lines represents empirically (top) and computationally (bottom) determined limits of stochastic colocalization (Horigome et al. 2014, 2015). (E) Pore-ChIP (chromatin immunoprecipitation) was performed with Mab414 monoclonal (Abcam) with wild-type and *siz2Δ* isogenic derivatives of JKM179 (Lee et al. 1998). HO cleavage was induced for the indicated times on galactose. Quantitative PCR (qPCR) at 1.6 kb from the HO cut site was performed in triplicate on two biological replicates. See the Supplemental Material for normalization techniques. (F) Chromosome III in the *MATα* strain was used for ChIP, with the positions of primer/probe sets shown. ChIP of *MAT* colocalization with HA-tagged Mps3 is shown for wild-type (GA-8306) and *siz2Δ* (GA-8541) cells at the indicated times after cut induction. Data from two independent experiments quantified in triplicate are represented as mean  $\pm$  SEM. (G) The position of the cleaved *MAT* relative to CFP-Nup49 in *smt3-3KR* (GA-9072) after 120 min on galactose, as in C. (n.s.) Not significantly different from random.

synthetic lethal with both *sgs1Δ* and *slx5Δ* (Mullen et al. 2011).

*PolySUMOylation is required for Slx5 recruitment and DSB relocation to pores in G1*

Earlier work indicated that Slx5/Slx8 binds the Nup84 complex and showed that its recruitment to DSBs correlates with DSB relocation to pores, although positioning was not shown to depend on Slx5/Slx8 in the case of persistent DSBs (Nagai et al. 2008). Slx5 contains multiple SIMs, which are required for the formation of damage-induced foci of Slx5 in a SUMO-dependent manner (Cook et al. 2009). Moreover, the human homolog RNF4 preferentially binds polySUMO chains. We therefore asked whether Slx5 recruitment to the DSB at *MAT* is affected by the presence or absence of Siz2 or by the non-chain-forming SUMO mutant (*smt3-3KR*). Control ChIP for a fully functional HA-tagged Slx5 at *MAT* after 2 or 4 h of cut induction showed a strong enrichment for Slx5, which dropped to half the wild-type level in a *siz2Δ* strain, consistent with partial compensation by Siz1 (Fig. 2A). In the *smt3-3KR* mutant, on the other hand, Slx5 recruitment was completely eliminated (Fig. 2A; Bylebyl et al.

2003). We note that cleavage efficiency ranged from 75% to 90% in all samples, and ChIP data were normalized to cut efficiency at each time point.

We next asked whether Slx5 or Slx8 binding was necessary for DSB relocation to the NE. We monitored the position of the induced DSB at the GFP-lacI-tagged *MAT* locus in *slx5Δ* and *slx8Δ* strains, distinguishing G1-phase from S-phase cells (Fig. 2B). Loss of either subunit completely compromised DSB relocation to the nuclear periphery in G1-phase cells, but the effect was attenuated in S phase. Indeed, in S-phase cells, zone 1 enrichment of the DSB was still significant in *slx5Δ* and *slx8Δ* S-phase cells (Fig. 2B). From this, we conclude that the Slx5/Slx8 STUbL is essential for DSB-pore association in G1, while it accounts for only part of the shift in S.

We surmised that the partial effect of the STUbL mutants in S phase could reflect the fact that DSBs can bind Mps3 as well as pores in S phase, while Mps3 is not an option in G1. We therefore examined whether the loss of Slx5/Slx8 selectively compromises pore binding. Indeed, in the quantitative pore colocalization assay, the *slx5* deletion strain lost DSB-pore association in both G1- and S-phase cells, while the interaction of the DSB with Mps3, as monitored by ChIP, was unchanged or even

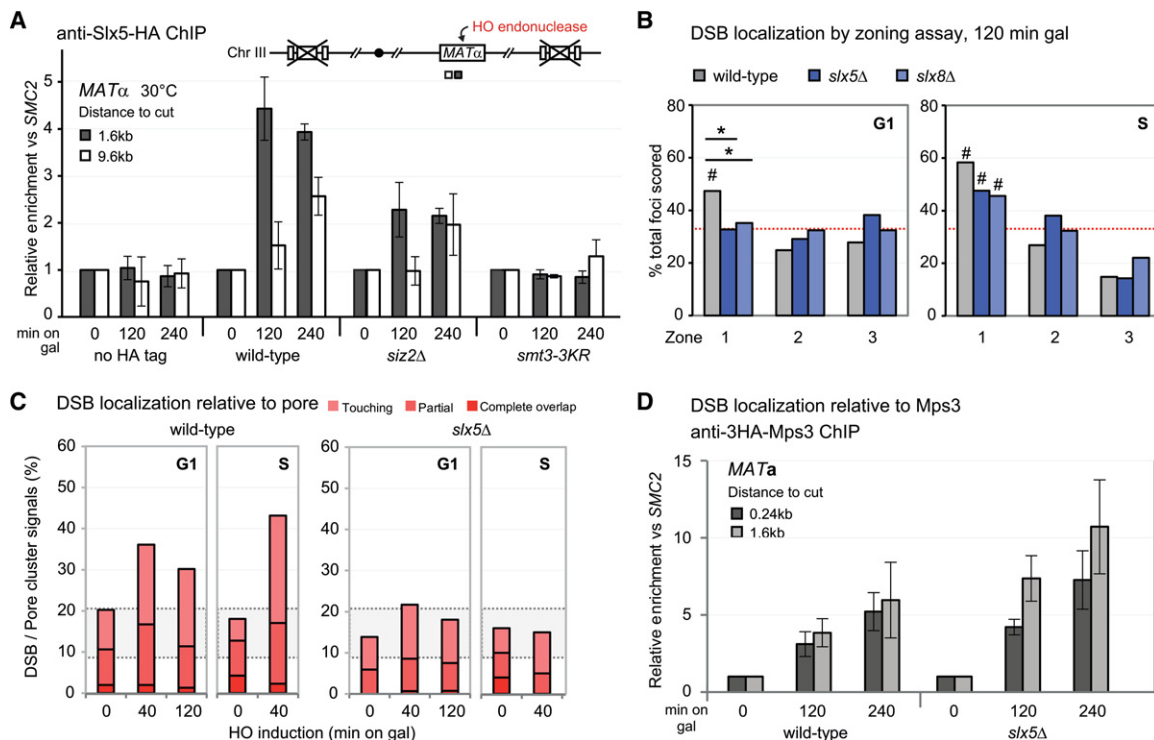


**Figure 2.** The STUbL Slx5/8 promotes DSB relocation to the nuclear pore. (A) ChIP for HA-tagged Slx5 monitored *MAT* locus binding of Slx5 at the indicated time after cut induction on galactose in wild-type (JC3020), *siz2Δ* (JC3668), *smt3-3KR* (JC3214), and a nontagged strain (JC727). Data from three independent experiments are represented as mean  $\pm$  SEM. (B) *MAT* position relative to GFP-Nup49 in wild-type (GA-6844), *slx5Δ* (GA-7097), and *slx8Δ* (GA-7098) after 120 min on galactose. Symbols and scoring are as in Figure 1, C and G. (C) Scoring of *MAT* colocalization with the pore cluster in *nup133ΔN* (GA-7314) after cut induction as in Figure 1D. Strains scored at the indicated times on galactose were wild type (GA-7314) and *slx5Δ* (GA-7969). (Pink/red shaded region) Colocalization. (D) ChIP for HA-tagged Mps3 monitored *MAT* locus association with Mps3 at the indicated times after cut induction in wild-type (GA-8306) and *slx5Δ* (GA-8539) cells. Data from three independent experiments are represented as mean  $\pm$  SEM.

slightly increased (Fig. 2C,D). A similar loss of DSB–pore association was scored in *slx5Δ* and *slx8Δ* cells by pore-ChIP, with the effect being strongest very close to the DSB (Supplemental Fig. S2a). We conclude that the yeast STUbL is required for DSB recruitment selectively to nuclear pores, which can occur in either G1- or S-phase cells, while the S-phase relocation to Mps3 is Slx5/Slx8-independent. This does not mean that Mps3 interaction is SUMO-independent; indeed, the results shown in Figure 1 argue that it is also largely dependent on some form of SUMOylation.

*LexA-polySUMO and LexA-Slx5 can trigger pore binding in the absence of damage and Siz2*

While STUbL recruitment and damage movement to pores both correlate with polySUMOylation, it remained unresolved whether polySUMOylation is a sufficient signal for break relocation and whether it acts specifically by recruiting Slx5. Given the pleiotropic effects of the *smt3-3KR* mutant, we turned to a gain-of-function assay in which we targeted LexA fusion proteins to a GFP-tagged reporter. This allowed us to monitor the sufficiency of Smt3 moieties (SUMO) or specific ligands like Slx5 for relocation activity. We created a LexA-polySUMO fusion

protein by stringing four Smt3s lacking the internal diglycine motifs together with LexA (see the Supplemental Material). This fusion was able to bind an undamaged genomic locus (*PES4*) thanks to a cluster of four LexA-binding sites inserted next to the *lacO* array (Fig. 3A). If we expressed LexA alone, the *PES4* locus distributed randomly in the nucleoplasm (Fig. 3B), as did the locus in the absence of LexA (Taddei et al. 2004). We confirmed by microscopy that there was no change in the abundance of budded versus unbudded cells in cultures expressing LexA or the polySUMO fusion, arguing against any damage or checkpoint induction arising from expression of these constructs. However, the expression of LexA-polySUMO (LexA-4×Smt3) triggered a highly significant relocation of *PES4* to the NE in G1-phase but not S-phase cells (Fig. 3B). Importantly, the LexA-polySUMO chain fusion lost its ability to shift to the NE in cells lacking Slx5 (Fig. 3B), arguing that Slx5 acts downstream from SUMO chain formation for DSB relocation (Fig. 3B). In *siz2Δ* cells, the LexA-polySUMO construct retained at least partial relocation activity, although it was significantly reduced ( $P = 1.8 \times 10^{-4}$  in G1 phase) (Fig. 3B). This reduction in the absence of Siz2 may argue that Siz2 itself is part of the relocation machinery or might simply reflect pleiotropic effects arising from loss of the Siz2 E3 ligase (Fig. 3B).

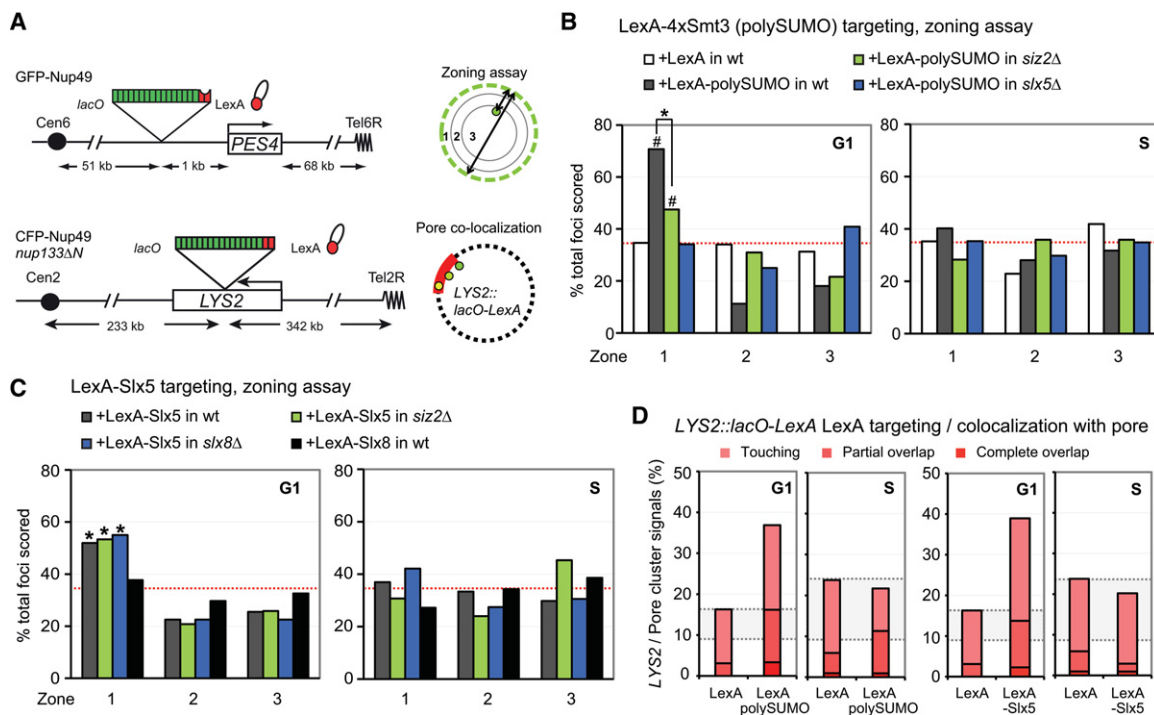


**Figure 3.** Targeted polySUMO and Slx5 promote chromatin relocation to the nuclear pore, bypassing Siz2 and Slx8 activities. (A) Scheme of the LexA fusion protein targeting to *PES4::lacO-LexA* for the zoning assay (GA-1461) and to *LYS2::lacO-LexA* in a strain bearing *nup133ΔN* (GA-8194) for nuclear pore colocalization of the intact targeted locus. (B,C) The position of *lacO/LexA*-tagged *PES4* was visualized by GFP-LacI and scored in cells classified as G1 or S phase. Strains carried GFP-Nup49 (GA-1461) and the indicated LexA fusion proteins (polySUMO = 4×Smt3) (see the Supplemental Material) or LexA alone expressed from pAT4 derivatives. LexA fusion was expressed in wild-type (wt) (GA-1461), *siz2Δ* (GA-4447), *slx5Δ* (GA-4448), or *slx8Δ* (GA-4449) strains. Position was scored as in Figure 1C. (D) Pore cluster colocalization for LexA-tagged *LYS2* in a strain bearing *nup133ΔN* (GA-8194) transformed with the indicated LexA fusion. Colocalization (pink to red) is as described in Figure 1D.



To determine whether the binding of Slx5 itself is sufficient to shift *PES4* to pores, we expressed a LexA-Slx5 fusion in the same reporter strain. Like LexA-polySUMO, LexA-Slx5 was sufficient to shift its target locus to the NE in G1-phase cells, while LexA alone could not (Fig. 3C). Intriguingly, LexA-Slx5 did not relocate *PES4* in S-phase cells, arguing that there may be cell cycle modifications of Slx5 or the Nup84 pore complex to which it binds (Fig. 3C). To see whether Slx5 is the key factor recruited by polySUMO with respect to the relocation event, we examined whether the artificial recruitment of Slx5 is sufficient to trigger relocation in the absence of Siz2. Indeed, LexA-Slx5 is able to shift *PES4* to the periphery in the absence of Siz2 (Fig. 3C), arguing that, with respect to subnuclear targeting, an artificial recruitment of Slx5 (Fig. 3B) bypasses the requirement for Siz2. Furthermore, relocation by LexA-Slx5 was independent of an intact Slx8 (Fig. 3C) even though Slx8 is recruited to breaks with efficiency equal to that of Slx5 (Supplemental Fig. S2b). Consistently, a targeted LexA-Slx8 does not shift *PES4* position to the NE (Fig. 3C). This result was not due to misfolding of the fusion protein, since the LexA-Slx8 fusion complements the impaired growth of a *slx8Δ* strain on HU (Supplemental Fig. S3a). We conclude that Slx8-mediated ubiquitination is not the signal for relocation to nuclear pores, although, in the living cell, when persistent DSBs are scored for their positioning, Slx8 contributes to pore association (Fig. 2, Supplemental Fig. S2a). This may reflect a role for Slx8 in promoting the stable binding of Slx5 at DSBs.

This partial divergence in function between Slx5 and Slx8 has precedents. Although Slx5 and Slx8 form a complex and the null alleles share many phenotypes, epistatic miniarray profiling (EMAP) analysis suggests that loss of Slx5 is more deleterious than loss of Slx8 on damaging agents (Nagai et al. 2008; Hustedt et al. 2015). Indeed, *slx5Δ* populations tend to generate polyploid cells, which is not the case in *slx8* mutants, and Slx5 can form repair foci in the absence of Slx8 (Cook et al. 2009).

To determine whether the Slx5/polySUMO chain-mediated positioning at the NE reflected binding at pores or at Mps3, we coupled a LacI-LexA-tagged internal locus (*LYS2*, chromosome 2) with the *nup133ΔN* mutant in which pores cluster on one side of the nucleus. This allowed us to monitor the position of the reporter relative to a pore cluster. Upon the targeting of LexA-polySUMO to *LYS2*, we observed a strong colocalization with the nuclear pore cluster (Fig. 3D). This result is remarkably consistent with our finding that DSB relocation to pores is Slx5-dependent in G1-phase cells and that relocation to Mps3 is not affected by loss of Slx5 (Fig. 2D). Similarly, LexA-Slx5 was sufficient to shift the tagged *LYS2* locus to the nuclear pore cluster in G1 only, like LexA-polySUMO (Fig. 3B–D). These sufficiency studies lack the complex signals that arise from checkpoint activation and the recruitment of irrelevant DNA repair factors. They allow us to establish a dependency between Slx5- and Siz2-mediated polySUMOylation for locus recruitment to nuclear pores. Indeed, we bypassed the requirement for Siz2-mediated polySUMOylation by targeting

Slx5 to a tagged locus (Fig. 3C). These gain-of-function studies argue that Slx5 binding may be sufficient to shift the break to pores, at least in G1 phase. We hypothesize that S-phase cells incur other modifications that block Slx5's relocation activity or else that additional S-phase constraints impair relocation, provoking a need for factors other than Slx5.

In flies, it was shown that dRad60 (the homolog of Rad60 in fission yeast, Esc2 in budding yeast, and NIP45 in humans) contributes to the shift of DSBs away from heterochromatin in irradiated *Drosophila* cells (Ryu et al. 2015). This class of factors, called RENi, is thought to stimulate the ubiquitination activity of the Slx5/8 STUbL in yeast (Prudden et al. 2007). Therefore, we tested a complete deletion of the *S. cerevisiae* RENi homolog Esc2 to see whether it would phenocopy loss of Slx5/Slx8, which blocks relocation primarily in G1. Indeed, we found that *esc2Δ* cells show a significant drop in relocation of the DSB to the NE only in G1 phase and not in S phase (cf. Fig. 3B and Supplemental Fig. S2b). Unlike Slx5, however, the targeting of a LexA-Esc2 fusion did not trigger a shift to the NE (Supplemental Fig. S3c), arguing that it is not directly involved in pore association. Rather, like Slx8, Esc2 may help stabilize Slx5 binding to polySUMO motifs at damage.

#### *MonoSUMOylation relocates exclusively to Mps3-binding sites in S-phase cells*

In Figure 1, we showed that the loss of SUMO E3 ligases impaired break relocation in S phase as well as in G1, unlike *slx5Δ*, and found strong effects of *mms21ΔC*, which is thought to mediate primarily monoSUMOylation (D'Ambrosio and Lavoie 2014). Given the inability of LexA-polySUMO to relocate damage in S-phase cells, we next examined whether the fusion of a single Smt3 moiety to LexA might promote the positioning of an undamaged site in S phase. We expressed two monoSUMO LexA fusions (i.e., to either a single Smt3 moiety or a *smt3-3KR* moiety) and monitored the position of *PES4* locus tagged with *lacO-LexA* sites. In both cases, the randomly distributed undamaged locus shifted to zone 1 upon expression of the LexA-monoSUMO construct only in S-phase and not in G1-phase cells (Fig. 4A). The LexA-*smt3-3KR* fusion was also expressed in a *siz2Δ* strain, and there was a slightly reduced but still significant Siz2-independent relocation activity (Fig. 4A). We next determined whether the relocated locus showed enrichment at the nuclear pore cluster using the *LYS2::lacO-LexA* strain bearing *nup133ΔN* and Nup49-CFP. In contrast to the LexA-polySUMO construct, the LexA-*smt3-3KR* (monoSUMO) fusion did not colocalize with the pore cluster (Fig. 4B), suggesting that the relocated locus binds Mps3. To address this hypothesis, we overexpressed the soluble Mps3 N-terminal domain, which can displace other nucleoplasmic ligands from interaction with membrane-bound Mps3-binding sites (Ferreira et al. 2011). The soluble Mps3N' domain indeed successfully competed for LexA-*smt3-3KR*'s relocation activity (Fig. 4C). Consistent with the fact that Mps3 functions as a tethering

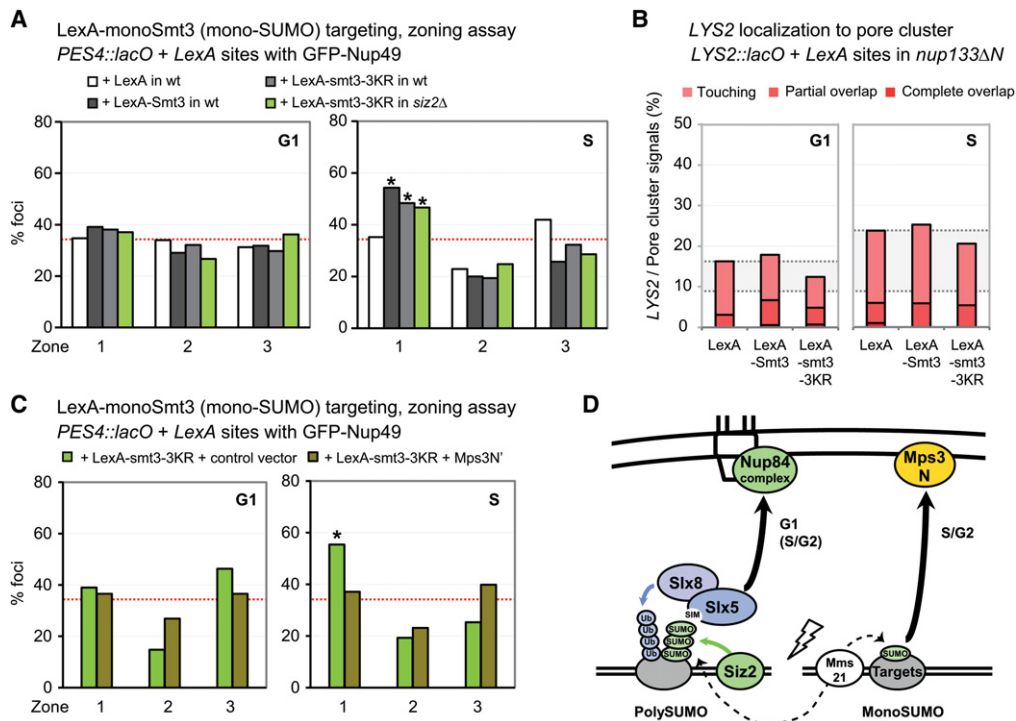


**Figure 4.** The targeted monoSUMO construct shifts chromatin to the nuclear periphery in S phase but not to nuclear pores. (A) The indicated LexA fusion proteins are expressed in the wild-type (wt) strain (GA-1461) and *siz2Δ* (GA-4447). The position of *lacO*/LexA-tagged *ARS607* was visualized by GFP-LacI and scored as in Figure 1C. (B) Pore cluster colocalization for LexA-tagged *LYS2* in a strain bearing *nup133ΔN* (GA-8194) transformed with the indicated LexA fusions. Colocalization (pink to red) was scored as in Figure 1D. (C) In a wild-type strain (GA-1461) expressing LexA-smt3-3KR and either an empty vector or the Mps3N' construct, *PES4* position was scored as in A. (D) Summary of the chromatin positioning roles of monoSUMO and polySUMO chains based on the targeting assays.

site only in S phase, the monoSUMO fusion can only mediate relocation in S-phase cells. Taken together, our data argue that, in S-phase cells, monoSUMOylation events mediate DSB relocation to Mps3, whereas, in G1, relocation to the nuclear pore requires a polySUMO chain that acts through the recruitment of Slx5. Given that LexA-Slx5 can bypass the requirement for Siz2, we suggest that Slx5 does not need to be SUMOylated to interact with Nup84 (see the model in Fig. 4D), although, in S-phase, there may be other factors at play. Nonetheless, we note that not all Slx5 foci that arise from ionizing radiation are associated with nuclear pores (Supplemental Fig. S4); thus, there may be ways to impair Slx5-pore association in S phase. Alternatively, Slx5-pore binding may be transient in nature, allowing some foci to shift away from the NE after processing of the damage.

#### *Slx5* binding to Nse5, part of the SMC5/6 complex, is compromised by the L247A mutation

In addition to being a target of SUMO E3 ligases, and binding SUMO chains, Slx5 and its orthologs have been shown to interact with a component of the SMC5/6 complex (i.e., Nse5), with factors involved in kinetochore function (Ndc10), and with the repair factor family RENi (Rad60, Esc2, and Nip45) (summarized in Cook et al. 2009). The

SMC5/6 complex contains the Nse2/Mms21 E3 SUMO ligase as well as Nse1, an E3 ubiquitin ligase, and the Nse3–6 subunits (Supplemental Fig. S5a; Jeppsson et al. 2014). High-throughput yeast two-hybrid (Y2H) screens suggested that budding yeast Nse5 might bind Slx5 (Hazbun et al. 2003), like its *Schizosaccharomyces pombe* homolog (Prudden et al. 2007). Nse5 contributes to SMC5/6 complex stability and its recruitment to sites of replication stress by binding Nse6 (Cook et al. 2009; Bustard et al. 2012), but Nse5 also binds directly to Smt3 and indirectly to E3 ligases Siz1, Siz2, and Mms21 and the upstream E2 ligase Ubc9 (DE Bustard and JA Cobb, pers. comm.). To see whether Nse5 contributes to the recruitment of Slx5/Slx8, we first characterized the proposed protein–protein interaction between Nse5 and Slx5 by Y2H assays.

With galactose-inducible expression of LexA-Nse5 as the bait and of a Slx5 activation domain (AD) fusion as prey, we scored a  $>10^3$ -fold increase in  $\beta$ -galactosidase activity in cells exposed to galactose. This reflects an efficient interaction between Slx5 and Nse5 (Supplemental Fig. S5b). Given that both Slx5 and Nse5 are reported to interact with SUMO (Hazbun et al. 2003), we asked whether the Y2H interaction might be compromised in strains that fail to efficiently deposit SUMO chains (i.e., either *smt3-3KR*, which blocks SUMO chain formation, or *smt3-331*, which reduces SUMOylation efficiency). The Slx5–

Nse5 binding was reduced, yet there was still interaction that was 350-fold above background (Supplemental Fig. S5b), suggesting that Nse5 and Slx5 may interact independently of SUMO. Consistently, a mutant form of Slx5 in which the two demonstrated SIM elements A and B were mutated (alanine substitutions at amino acids 25–27 and amino acids 93–96) (Xie et al. 2007) did not significantly reduce Nse5–Slx5 interaction (Supplemental Fig. S5b). In all cases, both constructs were efficiently expressed on galactose (Supplemental Fig. S6).

In earlier work, SMC5/6 was shown to facilitate the relocation of DSBs away from the nucleolus (Torres-Rosell et al. 2007) and away from heterochromatin in *Drosophila* cells (Chiolo et al. 2011), yet it was unclear whether it acts solely by delivering the SUMO E3 ligase Mms21 or whether it stabilizes the recruitment or binding of the STUBL complex. In order to be able to test the relevance of the Nse5–Slx5 interaction in relocation assays, we screened previously isolated point mutations in Nse5 for one that would lose interaction with Slx5 without disrupting the stability of SMC5/6 and the SUMO ligase activity of Mms21. The *nse5* L247A mutant protein completely abrogated the Nse5–Smt3 interaction (Supplemental Fig. S5c) but retained wild-type levels of binding to Nse6 (Supplemental Fig. S5c) and, unlike the *mms21-11* mu-

tant, did not induce MMS sensitivity (DE Bustard and JA Cobb, pers. comm.). It did, however, abolish Nse5's interaction with Slx5 as monitored by Y2H (Supplemental Fig. S5c). While this may be partly through a loss of SUMO recognition, the L247A allele appeared to be a useful tool to perturb the Slx5–SMC5/6 complex interaction without interfering with SMC5/6 complex integrity or its SUMOylation activity. In contrast, the temperature-sensitive *smc6-9* allele both disrupts the SMC5/6 complex (Torres-Rosell et al. 2005; De Piccoli et al. 2006; Sollier et al. 2009) and compromises its E3 ligase function (Bermudez-Lopez et al. 2015). A summary of the relevant interactions disrupted by Nse5 L247A is shown in Figure 5A.

Using the temperature-sensitive *smc6-9* allele, we first asked whether the disruption of SMC5/6 would affect DSB relocation to the NE. Not unexpectedly, like the E3 ligase-deficient allele (*mms21Δ*) (Fig. 1C), the *smc6-9* mutant lost perinuclear anchorage in both G1- and S-phase cells (Fig. 5B). SMC5/6 is known to be recruited to DSBs by Rtt107 when phosphorylated by the DNA damage checkpoint kinase Mec1 (De Piccoli et al. 2006; Ohouo et al. 2010; Leung et al. 2011; Ullal et al. 2011). Consistently, the *rtt107Δ* strain also compromised relocation of DSBs to the NE in both stages of the cell cycle (Fig. 5B). In contrast to the effects of *smc6-9* and *mms21Δ*

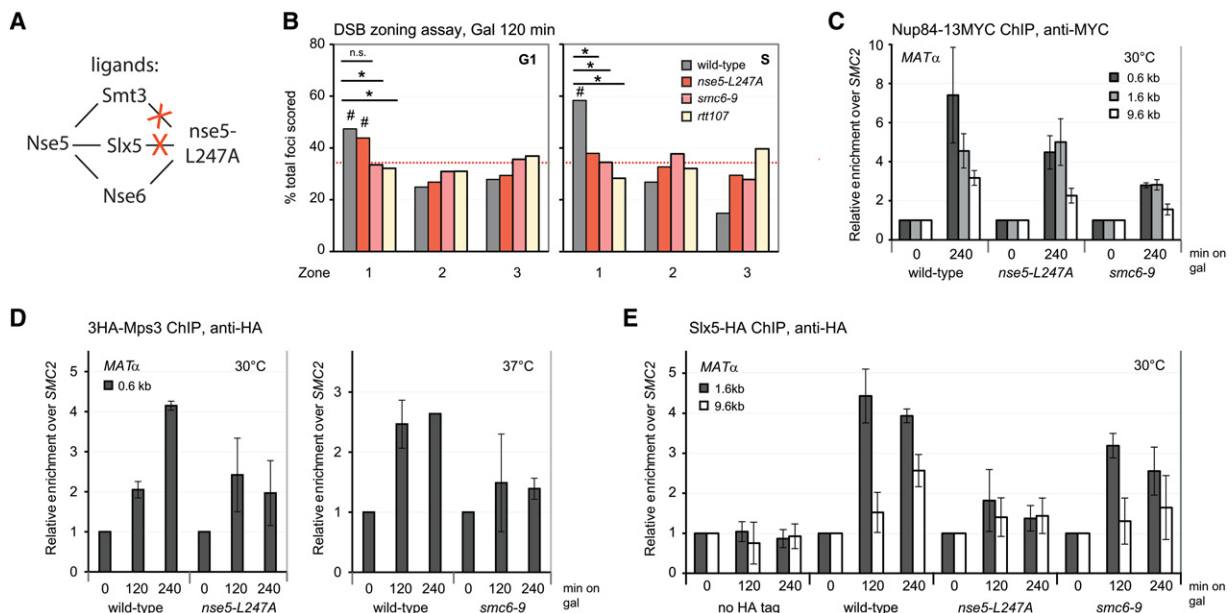


**Figure 5.** The SMC5/6 complex, the recruiter Rtt107, and the efficient interaction of Nse5 with Slx5/Slx8 facilitate DSB anchoring to Mps3. (A) Depiction of Nse5 interactions with SUMO (Smt3), Slx5, and Nse6 and the effects of the *nse5*<sup>L247A</sup> mutation (Supplemental Fig. S5; see the text). (B) The position of the cleaved *MAT* locus relative to CFP-Nup49 in wild-type (GA-6844), *nse5-L247A* (JC3161), *smc6-9* (JC3131), and *rtt107Δ* (GA-7092) cells after 120 min on galactose at 30°C is shown. Binning into G1 and S as well as the symbols are as in Figure 1C. (C) ChIP for Nup84-13MYC monitored the *MAT* locus after 240 min on galactose in wild-type (GA-4133), *nse5-L247A* (JC3154), and *smc6-9* (JC3150) cells grown at 30°C. Data from four experiments are represented as mean ± SEM. PCR probes were at the indicated distances from the HO cut site. (D) ChIP against 3HA-Mps3 (anti-HA) at the indicated times on galactose. Enrichment of *MAT* (0.6 kb from the cut site) over uncut *SMC2* was quantified by qPCR in wild type (JC3167) and *nse5-L247A* (JC3114). For the *smc6-9* temperature-sensitive alleles (JC3115), strains were grown at 25°C and then transferred for 1 h to 37°C to inactivate the *smc6-9* allele before HO induction at 35°C. Data from three independent experiments are represented as mean ± SEM. (E) ChIP for HA-tagged Slx5 monitored *MAT* locus association at the indicated time after cut induction in wild-type (JC3020), *nse5-L247A* (JC3621), *smc6-9* (JC3198), and non-tagged (JC727) cells at 30°C. Data from three independent experiments are represented as mean ± SEM.

mutants, break relocation to the NE in the *nse5*<sup>L247A</sup> allele has a reduced but still significant perinuclear association in G1 (Fig. 5B). This may reflect its ability to sustain functional Mms21 activity in G1-phase cells, which neither *smc6-9* nor *rtt107Δ* does.

This model predicts that the *smc6-9* mutation might affect recruitment to both pores and Mps3, phenocopying the loss of Mms21's SUMOylation activity, while the *nse5*<sup>L247A</sup> allele might only impair S-phase recruitment to Mps3, since the Mms21 SUMOylation activity, necessary for the polySUMO signal in G1, would be intact. We tested this with both pore-ChIP and Mps3-ChIP assays and, whenever possible, elevated the temperature to 37°C to induce the *smc6-9* defect (Fig. 5C,D). Indeed, the *nse5*<sup>L247A</sup> protein allowed DSB association with Nup84 (see the 1.6-kb probe in Fig. 5C), while *smc6-9* did not (both probes in Fig. 5C). Thus, the Nse5 interaction with Slx5 may not be essential for G1-phase relocation to pores. In the case of Mps3, both mutants showed a similar reduction to levels less than twofold above background (Fig. 5D). We asked whether the *nse5*<sup>L247A</sup> allele actually reduces Slx5 binding at the break by performing HA-Slx5 ChIP in the *nse5*<sup>L247A</sup> and *smc6-9* strains (Fig. 5E). Slx5-HA recruitment was indeed compromised by *nse5*<sup>L247A</sup> at the DSB, suggesting that Nse5 at least partially stabilizes Slx5 binding, probably acting in S-phase and not in G1-phase cells, since relocation to the pore was intact in the *nse5*<sup>L247A</sup> mutant. We were unable to test the *smc6-9* allele combined with Slx5-HA at 37°C due to poor growth of this strain on galactose at this temperature. However, at a semipermissive 30°C, we could score a partial reduction in Slx5 recruitment in the *smc6-9* strain, consistent with a loss of Mms21-mediated SUMOylation.

In addition to its effect on Slx5/Slx8 recruitment, we propose that the SMC5/6 complex plays a Slx5/8-independent role in relocation of breaks to Mps3, acting at least in part through Mms21. The *nse5*<sup>L247A</sup> mutant protein may fail to bind an S-phase ligand necessary for efficient relocation to Mps3. This ligand most likely is not Slx5, since LexA-Slx5 was unable to shift *PES4* to either nuclear pores or Mps3 in S-phase cells (Fig. 3C).

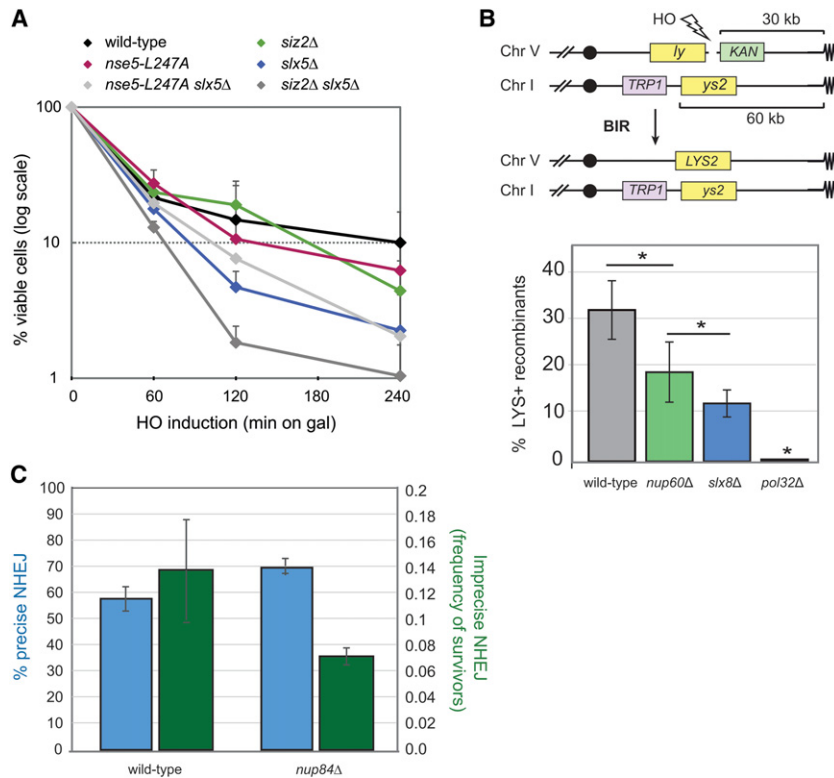
Our results establish a hierarchy of molecular interactions that mediate the relocation of DSBs to distinct perinuclear sites where the relative importance of these pathways varies with the cell cycle. We found that polySUMOylation has a specific role in G1, acting at least in part through Slx5, while monoSUMOylation functions in S phase, acting through an unknown ligand. It is not clear what the relocation-relevant targets of SUMOylation are, although it seems likely that multiple targets could function in this case given that LexA-polySUMO had a fairly efficient relocation activity. Given the conservation of SUMOylation across species, the conservation of STUbL enzymes, and the fact that SMC5/6 and the recruitment factors responsible (Rtt107/Esc4 and Esc2/Rad60) are important for break relocation in flies and yeast, we suggest that SUMO conjugation and STUbL recruitment will be relevant positioning signals in other species.

### *Slx8 and pore proteins facilitate BIR and imprecise end-joining*

To determine whether the functional hierarchy of factors for break relocation translates into a repair function, we scored for cell survival after 1, 2, or 4 h of growth on galactose, during which the HO endonuclease would be induced. After this incubation, cells were plated on glucose-containing plates to score for the efficiency of repair through the number of colony-forming units (CFUs) recovered (viable cells in Fig. 6A). We first asked whether *slx5Δ* and *nse5*<sup>L247A</sup> would be epistatic, and, indeed, while the loss of Slx5 compromises cell survival far more than the other single mutants, there was no additive loss of viability when combined with *nse5*<sup>L247A</sup> (Fig. 6A, light gray). This was not the case when *siz2Δ*, which reduced survival only moderately at 2 h, was combined with *slx5Δ*; in this case, the double mutant was strongly additive (Fig. 6A, dark gray). This is consistent with the notion that Siz2 has additional roles at damage, promoting survival by factors other than those that recruit and activate Slx5/Slx8. Nonetheless, Slx5 has a profound effect on survival following induction of a persistent DSB.

There were multiple pathways of repair that led to CFUs in the survival assay scored above. To get insight into which repair pathways Slx5 and pore binding affects, we performed an assay designed to monitor repair of a DSB by strand invasion into an ectopic donor (BIR). We scored for the loss of the distal arm of the invaded chromosome to ensure that we monitored BIR rather than another reciprocal recombination event. A recent study observed an ~50% drop in efficiency of survival in both the *nup84Δ* and *slx5Δ* strains after induction of a DSB in a subtelo-meric region (Chung et al. 2015). Survival was correlated with a recombination-based pathway that required Rad52 and Rad32, although it was not a specific assay for ectopic BIR, in which a one-ended DSB is repaired by an error-free mechanism involving recombination-mediated replication fork restart. Since Nup84 had already been tested in a BIR-like assay, we tested another pore component that is associated with the Nup84 complex, Nup60. Nup60 is recruited to breaks and shows similar EMAP sensitivities (Nagai et al. 2008). Monitoring a strand invasion event from chromosome V to chromosome I (Fig. 6B), we observed that *slx8Δ* and *nup60Δ* strains have a 60% and 40% drop in BIR efficiency, respectively (Fig. 6B). We propose that an irreparable or persistent DSB resembles a collapsed fork in that it has a damaged end with no immediate donor for repair (no intact sister chromatid).

The other potential pathway for repair of such lesions would be either precise NHEJ or imprecise NHEJ. Compromising the Nup84 complex did not compromise precise NHEJ at an HO-induced break to any detectable extent (Fig. 6C), but imprecise end-joining (also called alternative or microhomology-mediated end-joining) was reduced by 50%, like BIR (Fig. 6C). Both BIR and imprecise end-joining involve resection at the cut site; thus, one scenario that explains our results is that recruitment of DSBs without intact sisters to nuclear pores by Slx5/Slx8



(C) Precise NHEJ and imprecise NHEJ were performed and analyzed as described in the Materials and Methods on GA-8860 (wild type) and GA-8471 (*nup84Δ*).

triggers the degradation of a complex that might be blocking end resection. Resection would then allow alternative strand invasion or annealing pathways to proceed in a last-ditch attempt by the cell to force repair and survive. Intriguingly, sequestration at Mps3 appears to have the opposite effect: Mps3 suppresses ectopic recombination and thus may counteract the repair pathway promoted at nuclear pores (Ferreira et al. 2011; Horigome et al. 2014; Chung et al. 2015).

## Discussion

We identified two distinct SUMO-dependent pathways that trigger relocation of a DSB to the NE (Fig. 7). In G1, SUMO chain formation leads to recruitment of Slx5 and subsequent break relocation to the nuclear pore. G1 polySUMOylation depends on Siz2 and Mms21. Loss of either SUMO E3 ligase compromises relocation of DSBs to pores. In S phase, on the other hand, monoSUMOylation by Mms21 leads to DSB movement to Mps3 but not to the nuclear pore. Interestingly, Slx5 contributes to, but is not sufficient for, S-phase movement of breaks to pores and is stabilized at damage in an Nse5-dependent manner. Thus, our data also suggest that the SMC5/6 complex contributes in several ways to break relocation; in both G1 and S phase, it recruits Mms21 to mediate monoSUMOylation, but its Nse5 subunit may have additional S-phase-specific roles.

**Figure 6.** Slx8 and pore proteins favor repair by BIR and imprecise end-joining. (A) Cell survival after HO cut induction. Cleavage at the *MAT* locus by the HO endonuclease was induced by galactose for the indicated times. Cells were washed and plated on YPAD plates, and CFUs were scored after 2 d at 30°C. The rates of the viable cells in wild-type (GA-6844), *siz2Δ* (GA-6858), *nse5-L247A* (JC3161), *slx5Δ* (GA-7097), *siz2Δ slx5Δ* (GA-9206), and *nse5-L247A slx5Δ* (GA-9355) strains were normalized to cell count before cut induction. (B) BIR assay. A recipient cassette composed of a 3' truncated *LYS2* gene (*ly*), a 36-base-pair cut site for the HO endonuclease, and a *kan<sup>R</sup>* marker was incorporated into chromosome V (ChrV). A donor cassette composed of a *TRP1* marker and a 5' truncation of *LYS2* (*ys2*) was inserted 60 kb from the telomere of chromosome I (ChrI). The two mutant *lys2* fragments share 2.1 kb of homology. The HO endonuclease was expressed under the control of a galactose promoter. *Lys<sup>+</sup>* cells lacking kanamycin resistance were scored for wild-type (GA-8994), *nup60Δ* (GA-9185), *slx8Δ* (GA-9186), and *poi32Δ* (GA-9090) cells. Error bars indicate standard deviation. Significance was determined by Student's *t*-test.

Our findings allow a generalization of the phenomena to damage relocation from heterochromatin in *Drosophila* cells (Chiolo et al. 2011). Chiolo et al. (2011) similarly found that ablation of the fly Slx5/Slx8 homologs SMC5/6 and impaired SUMOylation interfered with the relocation of DSBs from heterochromatin to perinuclear sites of repair (Ryu et al. 2015). It has also been reported elsewhere that the repair of intrastrand cross-links by the Fanconi anemia complex and PML body-mediated recovery from arsenic-induced damage (Tatham et al. 2008; Kim and D'Andrea 2012) are controlled by SUMOylation, STUbL enzymes, and SMC5/6. Finally, Mms21 in parallel with Slx5/8 and SMC5/6 was shown to suppress spontaneous gross chromosomal rearrangements, although the mechanism was not clarified (Hwang et al. 2008; Albuquerque et al. 2013). Our study suggests that damage can be directed to subcompartments at the NE by distinct signals, where distinct repair activities seem to be favored. From genetic data, one would argue that the proteasome acts on the same pathway as nuclear pores and Slx5/Slx8 (Nagai et al. 2008), possibly requiring Slx8-mediated ubiquitination. Above all, we establish here for the first time a strong correlation between the spatial sequestration of damage and the extent of SUMO chain formation.

We note that ubiquitination and SMC5/6 are also necessary for telomere maintenance and PML body formation in ALT cancer cells (Potts and Yu 2007), where BIR is the primary mechanism of telomere maintenance. Consistently, Slx8 promotes type II survivor formation in

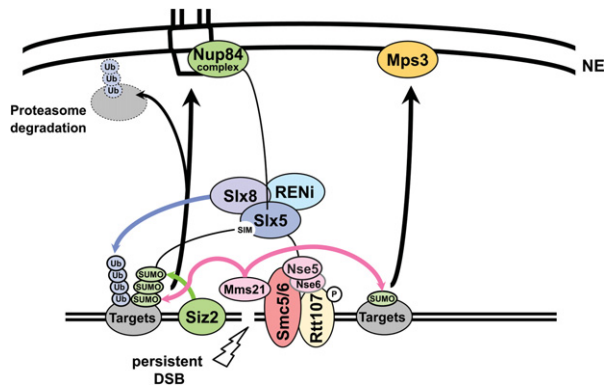


**Figure 7.** Model for the role of SUMO and the Slx5 STUbL unit in break relocation. Siz2 is damage-associated and deposits SUMO on various repair substrates that are monoSUMOylated by Mms21. Slx5/Slx8 is itself SUMOylated and recruited to the DSB in a polySUMOylation-dependent manner. Siz2, polySUMOylation, and its recognition by Slx5/Slx8 are required for DSB relocation to pores in both G1 and S. Nup84 components are recognized by Slx5. In contrast, monoSUMOylation can shift chromatin to Mps3 in an SMC5/6-dependent but Slx5/8-independent manner. Rtt107 phosphorylation by Mec1 recruits the SMC5/6 complex to DSBs. A component of SMC5/6, Nse5, interacts with Slx5. The SUMO E3 ligase Mms21 is recruited with the SMC5/6 complex. Ubiquitination of SUMOylated target proteins by the Slx5/Slx8 STUbL most likely results in subsequent degradation by the proteasome at the NE to enable repair pathways such as BIR.

yeast mutants that lack functional telomerase (Azam et al. 2006). Also, in yeast, eroded telomeres relocate to nuclear pores (V Geli, pers. comm.). These repair events all entail ectopic strand invasion, as occurs in BIR. Thus, it is tempting to speculate that a processing event that enables nonsister chromatid strand invasion is favored by shifting breaks to nuclear pores.

With respect to relocation to pores in G1-phase cells, in a gain-of-function targeting assay, we found that LexA-Slx5 can bypass the requirement for polySUMOylation. Moreover, the relocation mediated by LexA-4×Smt3 (polySUMO) fusion is dependent on Slx5 (Fig. 3). This is consistent with the notion that any number of appropriately modified targets might suffice to recruit Slx5. Indeed, it may be the extent of modification rather than the specific substrate that is critical for site-specific recruitment. Still, the question remains: Which targets of SUMOylation are relevant in this context? Do they vary with cell cycle or types of damage?

There are a number of DSB-bound factors that are targets and ligands of either Mms21, Siz2, or both. Siz2 binding at sites of damage appears to be facilitated by RPA binding to ssDNA, mediated by the Rfa2 C-terminal winged helix domain (Chung and Zhao 2015). We did not find a requirement for Rad52 in DSB relocation to nuclear pores (Horigome et al. 2014), although Rad52-KR mutants that attenuate its SUMOylation affect damage relocation out of the yeast nucleolus (Torres-Rosell et al. 2007). Similarly, whereas yKu70-SUMOylation and

yKu80-SUMOylation mediate the interaction of telomeres with Mps3, these constructs do not target DNA to Nup84 (Ferreira et al. 2011; Chung et al. 2015). Htz1 SUMOylation was implicated in DSB relocation to Mps3 (Kalocsay et al. 2009), but, given that Htz1 is a necessary chaperone for the localization of Mps3 in the inner nuclear membrane (Gardner et al. 2011), these data must be complemented with controls that show that Mps3 was properly localized in these mutants (Gardner et al. 2011). The fact that Htz1 deletion affects DSB relocation to both pores and Mps3 (Dion and Gasser 2013; Horigome et al. 2014) may argue for a role of this variant histone in break relocation. Future studies will have to address this by mapping and mutating specific interaction sites between Htz1 and Mps3. Whatever the target may be, our work illustrates the crucial importance of SUMOylation signals at DSBs for the targeting of damage to distinct nuclear subcompartments that mediate repair.

## Materials and methods

### Plasmids, yeast strains, and techniques

Standard yeast methods and media were used, and constructs, strains, growth conditions, and Y2H assays are described in detail in the Supplemental Material and Supplemental Table S2. Cut efficiencies are summarized in Supplemental Table S1.

The LexA fusions were created in the plasmid pAT4 (Taddei et al. 2004). The 4×Smt3 construct (LexA-polySUMO) was created by cloning four Smt3 genes tandemly into the vector pAT4 using a 4×Smt3 construct synthesized by Bio Basic, Inc., gene synthesis. To prevent processing of the internal SUMO proteins by Ulp1, the constructs were truncated at I<sub>96</sub> to remove the diglycine motif. The fourth SUMO residue in the chain retained the full SUMO sequence, including the diglycine motif. Targeted binding is described in Neumann et al. (2012) and Horigome et al. (2014).

### Microscopy and statistical analyses

Fluorescence microscopy and quantification were performed according to published methods (Meister et al. 2010; Horigome et al. 2015) using a Metamorph-driven spinning disk confocal system with a Yokogawa CSU-X1 scan head and an EM-CCD Cascade II (Photometrics) camera. LacI-GFP position was determined with a through-focus stack of 16–21 0.2- $\mu$ m steps and was measured by ImageJ (National Institutes of Health) and the plug-in software PointPicker (Meister et al. 2010). The numbers of nuclei scored are in Supplemental Table S1.

To determine zone enrichment, we applied a  $\chi^2$  test comparing zone 1 with a random distribution (degree of freedom, 2; confidence limit, 95%). *P*-values are listed in Supplemental Table S1. To compare the perinuclear enrichment of two different strains, we used a proportional analysis with a confidence limit of 95%. The error bars of ChIP experiments represent the SEM.

### ChIP

ChIP with anti-HA or anti-MYC epitope-tagged strains was carried out as previously described (Yoshida et al. 2010) with modifications described in the Supplemental Material. Absolute enrichment was calculated as follows: For each time point, the signal from a site near the HO DSB at *MAT* was normalized

to that from either the genomic *SMC2* locus or the mitochondrial *OLI1* locus in ChIP and input DNA samples. For each time point and site, normalized ChIP signals were normalized to input DNA signals.

#### Repair assays

Precise NHEJ and imprecise NHEJ were performed as described in van Attikum et al. (2007) using isogenic derivatives of GA-1081 (i.e., GA-8860 [wild type] and GA-8471 [*nup84Δ*]). The DSB survival assay is described in the Supplemental Material; the BIR assay was performed and the frequency of recombinants was calculated as previously described (Donnianni and Symington 2013).

#### Acknowledgments

We thank Dr. S. Nagai (Stanford University, CA) for data in Supplemental Figure S2, acquired while in the Gasser laboratory. We thank J.E. Haber for yeast strains, and the Friedrich Miescher Institute Facility for Advanced Imaging and Microscopy for technical help. C.H. was supported by a Marie Curie International Incoming Fellowship and a Japan Society for the Promotion of Science Post-doctoral Fellowship for Research Abroad. The Gasser laboratory thanks the Novartis Research Foundation, the Swiss National Science Foundation, and the Swiss Cancer League for grants awarded to S.M.G. and a student fellowship awarded to I.M. D.E.B. was supported by a graduate studentship from Alberta Innovates Health Solutions. The Cobb laboratory was supported by operating grants from Canadian Institutes of Health Research (MOP-82736) and Natural Sciences and Engineering Research Council (418122) awarded to J.A.C. C.H. performed experiments, interpreted results, and prepared figures; D.E.B., I.M., M.T.-P., and N.D. performed experiments, interpreted results, and prepared figures; J.A.C. performed experiments and supervised D.E.B.; S.M.G. interpreted results and supervised C.H., I.M., M.T.-P., and N.D.; and all contributed to writing the paper.

#### References

- Agmon N, Liefshitz B, Zimmer C, Fabre E, Kupiec M. 2013. Effect of nuclear architecture on the efficiency of double-strand break repair. *Nat Cell Biol* **15**: 694–699.
- Albuquerque CP, Wang G, Lee NS, Kolodner RD, Putnam CD, Zhou H. 2013. Distinct SUMO ligases cooperate with Esc2 and Slx5 to suppress duplication-mediated genome rearrangements. *PLoS Genet* **9**: e1003670.
- Azam M, Lee JY, Abraham V, Chanoux R, Schoenly KA, Johnson FB. 2006. Evidence that the *S. cerevisiae* Sgs1 protein facilitates recombinational repair of telomeres during senescence. *Nucleic Acids Res* **34**: 506–516.
- Bennett CB, Lewis LK, Karthikeyan G, Lobachev KS, Jin YH, Sterling JF, Snipe JR, Resnick MA. 2001. Genes required for ionizing radiation resistance in yeast. *Nat Genet* **29**: 426–434.
- Bermudez-Lopez M, Pocino-Merino I, Sánchez H, Bueno A, Guasch C, Almedawar S, Bru-Virgili S, Garí E, Wyman C, Reverter D, et al. 2015. ATPase-dependent control of the Mms21 SUMO ligase during DNA repair. *PLoS Biol* **13**: e1002089.
- Bukata L, Parker SL, D'Angelo MA. 2013. Nuclear pore complexes in the maintenance of genome integrity. *Curr Opin Cell Biol* **25**: 378–386.
- Bustard DE, Menolfi D, Jeppsson K, Ball LG, Dewey SC, Shirahige K, Sjogren C, Branzei D, Cobb JA. 2012. During replication stress, non-SMC element 5 (NSE5) is required for Smc5/6 protein complex functionality at stalled forks. *J Biol Chem* **287**: 11374–11383.
- Bylebyl GR, Belichenko I, Johnson ES. 2003. The SUMO isopeptidase Ulp2 prevents accumulation of SUMO chains in yeast. *J Biol Chem* **278**: 44113–44120.
- Bystricky K, Van Attikum H, Montiel MD, Dion V, Gehlen L, Gasser SM. 2009. Regulation of nuclear positioning and dynamics of the silent mating type loci by the yeast Ku70/Ku80 complex. *Mol Cell Biol* **29**: 835–848.
- Ceccaldi R, Rondinelli B, D'Andrea AD. 2016. Repair pathway choices and consequences at the double-strand break. *Trends Cell Biol* **26**: 52–64.
- Chang M, Bellaoui M, Boone C, Brown GW. 2002. A genome-wide screen for methyl methanesulfonate-sensitive mutants reveals genes required for S phase progression in the presence of DNA damage. *Proc Natl Acad Sci* **99**: 16934–16939.
- Chiolo I, Minoda A, Colmenares SU, Polyzos A, Costes SV, Karpen GH. 2011. Double-strand breaks in heterochromatin move outside of a dynamic HP1a domain to complete recombinational repair. *Cell* **144**: 732–744.
- Chung I, Zhao X. 2015. DNA break-induced sumoylation is enabled by collaboration between a SUMO ligase and the ssDNA-binding complex RPA. *Genes Dev* **29**: 1593–1598.
- Chung DK, Chan JN, Strecker J, Zhang W, Ebrahimi-Ardebili S, Lu T, Abraham KJ, Durocher D, Mekhail K. 2015. Perinuclear tethers license telomeric DSBs for a broad kinesin- and NPC-dependent DNA repair process. *Nat Commun* **6**: 7742.
- Cook CE, Hochstrasser M, Kerscher O. 2009. The SUMO-targeted ubiquitin ligase subunit Slx5 resides in nuclear foci and at sites of DNA breaks. *Cell Cycle* **8**: 1080–1089.
- Cremona CA, Sarangi P, Yang Y, Hang LE, Rahman S, Zhao X. 2012. Extensive DNA damage-induced sumoylation contributes to replication and repair and acts in addition to the mec1 checkpoint. *Mol Cell* **45**: 422–432.
- D'Ambrosio LM, Lavoie BD. 2014. Pds5 prevents the polySUMO-dependent separation of sister chromatids. *Curr Biol* **24**: 361–371.
- De Piccoli G, Cortes-Ledesma F, Ira G, Torres-Rosell J, Uhle S, Farmer S, Hwang JY, Machin F, Ceschia A, McAleenan A, et al. 2006. Smc5-Smc6 mediate DNA double-strand-break repair by promoting sister-chromatid recombination. *Nat Cell Biol* **8**: 1032–1034.
- Dion V, Gasser SM. 2013. Chromatin movement in the maintenance of genome stability. *Cell* **152**: 1355–1364.
- Dion V, Kalck V, Seeber A, Schleker T, Gasser SM. 2013. Cohesin and the nucleolus constrain the mobility of spontaneous repair foci. *EMBO Rep* **14**: 984–991.
- Donnianni RA, Symington LS. 2013. Break-induced replication occurs by conservative DNA synthesis. *Proc Natl Acad Sci* **110**: 13475–13480.
- Ferreira HC, Luke B, Schober H, Kalck V, Lingner J, Gasser SM. 2011. The PIAS homologue Siz2 regulates perinuclear telomere position and telomerase activity in budding yeast. *Nat Cell Biol* **13**: 867–874.
- Gardner JM, Smoyer CJ, Stensrud ES, Alexander R, Gogol M, Wiegraebe W, Jaspersen SL. 2011. Targeting of the SUN protein Mps3 to the inner nuclear membrane by the histone variant H2A.Z. *J Cell Biol* **193**: 489–507.
- Geli V, Lisby M. 2015. Recombinational DNA repair is regulated by compartmentalization of DNA lesions at the nuclear pore complex. *Bioessays* **37**: 1287–1292.
- Hazbun TR, Malmstrom L, Anderson S, Graczyk BJ, Fox B, Riffle M, Sundin BA, Aranda JD, McDonald WH, Chiu CH, et al. 2003. Assigning function to yeast proteins by integration of technologies. *Mol Cell* **12**: 1353–1365.

- Horigome C, Oma Y, Konishi T, Schmid R, Marcomini I, Hauer MH, Dion V, Harata M, Gasser SM. 2014. SWR1 and INO80 chromatin remodelers contribute to DNA double-strand break perinuclear anchorage site choice. *Mol Cell* **55**: 626–639.
- Horigome C, Dion V, Seeber A, Gehlen LR, Gasser SM. 2015. Visualizing the spatiotemporal dynamics of DNA damage in budding yeast. *Methods Mol Biol* **1292**: 77–96.
- Hustedt N, Seeber A, Sack R, Tsai-Pflugfelder M, Bhullar B, Vlamming H, van Leeuwen F, Guenole A, van Attikum H, Srivas R, et al. 2015. Yeast PP4 interacts with ATR homolog Ddc2–Mec1 and regulates checkpoint signaling. *Mol Cell* **57**: 273–289.
- Hwang JY, Smith S, Ceschia A, Torres-Rosell J, Aragon L, Myung K. 2008. Smc5–Smc6 complex suppresses gross chromosomal rearrangements mediated by break-induced replications. *DNA Repair* **7**: 1426–1436.
- Jepsson K, Kanno T, Shirahige K, Sjogren C. 2014. The maintenance of chromosome structure: positioning and functioning of SMC complexes. *Nat Rev Mol Cell Biol* **15**: 601–614.
- Kalocsay M, Hiller NJ, Jentsch S. 2009. Chromosome-wide Rad51 spreading and SUMO-H2A.Z-dependent chromosome fixation in response to a persistent DNA double-strand break. *Mol Cell* **33**: 335–343.
- Khadaroo B, Teixeira MT, Luciano P, Eckert-Boulet N, Germann SM, Simon MN, Gallina I, Abdallah P, Gilson E, Geli V, et al. 2009. The DNA damage response at eroded telomeres and tethering to the nuclear pore complex. *Nat Cell Biol* **11**: 980–987.
- Kim H, D'Andrea AD. 2012. Regulation of DNA cross-link repair by the Fanconi anemia/BRCA pathway. *Genes Dev* **26**: 1393–1408.
- Lee SE, Moore JK, Holmes A, Umezu K, Kolodner RD, Haber JE. 1998. *Saccharomyces* Ku70, mre11/rad50 and RPA proteins regulate adaptation to G2/M arrest after DNA damage. *Cell* **94**: 399–409.
- Lemaître C, Grabar A, Tsouroula K, Andronov L, Furst A, Pankotai T, Heyer V, Rogier M, Attwood KM, Kessler P, et al. 2014. Nuclear position dictates DNA repair pathway choice. *Genes Dev* **28**: 2450–2463.
- Leung GP, Lee L, Schmidt TI, Shirahige K, Kobor MS. 2011. Rtt107 is required for recruitment of the SMC5/6 complex to DNA double strand breaks. *J Biol Chem* **286**: 26250–26257.
- Loeillet S, Palancade B, Cartron M, Thierry A, Richard GF, Dujon B, Doye V, Nicolas A. 2005. Genetic network interactions among replication, repair and nuclear pore deficiencies in yeast. *DNA Repair* **4**: 459–468.
- Meister P, Gehlen LR, Varela E, Kalck V, Gasser SM. 2010. Visualizing yeast chromosomes and nuclear architecture. *Methods Enzymol* **470**: 535–567.
- Mullen JR, Brill SJ. 2008. Activation of the Slx5–Slx8 ubiquitin ligase by poly-small ubiquitin-like modifier conjugates. *J Biol Chem* **283**: 19912–19921.
- Mullen JR, Das M, Brill SJ. 2011. Genetic evidence that polysumoylation bypasses the need for a SUMO-targeted Ub ligase. *Genetics* **187**: 73–87.
- Nagai S, Dubrana K, Tsai-Pflugfelder M, Davidson MB, Roberts TM, Brown GW, Varela E, Hediger F, Gasser SM, Krogan NJ. 2008. Functional targeting of DNA damage to a nuclear pore-associated SUMO-dependent ubiquitin ligase. *Science (New York, NY)* **322**: 597–602.
- Nagai S, Heun P, Gasser SM. 2010. Roles for nuclear organization in the maintenance of genome stability. *Epigenomics* **2**: 289–305.
- Neumann FR, Dion V, Gehlen LR, Tsai-Pflugfelder M, Schmid R, Taddei A, Gasser SM. 2012. Targeted INO80 enhances subnuclear chromatin movement and ectopic homologous recombination. *Genes Dev* **26**: 369–383.
- Ohouo PY, Bastos de Oliveira FM, Almeida BS, Smolka MB. 2010. DNA damage signaling recruits the Rtt107–Slx4 scaffolds via Dpb11 to mediate replication stress response. *Mol Cell* **39**: 300–306.
- Oza P, Jaspersen SL, Miele A, Dekker J, Peterson CL. 2009. Mechanisms that regulate localization of a DNA double-strand break to the nuclear periphery. *Genes Dev* **23**: 912–927.
- Palancade B, Liu X, Garcia-Rubio M, Aguilera A, Zhao X, Doye V. 2007. Nucleoporins prevent DNA damage accumulation by modulating Ulp1-dependent sumoylation processes. *Mol Biol Cell* **18**: 2912–2923.
- Paulsen RD, Soni DV, Wollman R, Hahn AT, Yee MC, Guan A, Hesley JA, Miller SC, Cromwell EF, Solow-Cordero DE, et al. 2009. A genome-wide siRNA screen reveals diverse cellular processes and pathways that mediate genome stability. *Mol Cell* **35**: 228–239.
- Potts PR, Yu H. 2007. The SMC5/6 complex maintains telomere length in ALT cancer cells through SUMOylation of telomere-binding proteins. *Nat Struct Mol Biol* **14**: 581–590.
- Prudden J, Pebernard S, Raffa G, Slavin DA, Perry JJ, Tainer JA, McGowan CH, Boddy MN. 2007. SUMO-targeted ubiquitin ligases in genome stability. *The EMBO J* **26**: 4089–4101.
- Psakhye I, Jentsch S. 2012. Protein group modification and synergy in the SUMO pathway as exemplified in DNA repair. *Cell* **151**: 807–820.
- Ryu T, Spatola B, Delabaere L, Bowlin K, Hopp H, Kunitake R, Karpen GH, Chiolo I. 2015. Heterochromatic breaks move to the nuclear periphery to continue recombinational repair. *Nat Cell Biol* **17**: 1401–1411.
- Sarangi P, Zhao X. 2015. SUMO-mediated regulation of DNA damage repair and responses. *Trends Biochem Sci* **40**: 233–242.
- Smeenk G, van Attikum H. 2013. The chromatin response to DNA breaks: leaving a mark on genome integrity. *Annu Rev Biochem* **82**: 55–80.
- Sollier J, Driscoll R, Castellucci F, Foiani M, Jackson SP, Branzei D. 2009. The *Saccharomyces cerevisiae* Esc2 and Smc5–6 proteins promote sister chromatid junction-mediated intra-S repair. *Mol Biol Cell* **20**: 1671–1682.
- Su XA, Dion V, Gasser SM, Freudenreich CH. 2015. Regulation of recombination at yeast nuclear pores controls repair and triplet repeat stability. *Genes Dev* **29**: 1006–1017.
- Taddei A, Hediger F, Neumann FR, Bauer C, Gasser SM. 2004. Separation of silencing from perinuclear anchoring functions in yeast Ku80, Sir4 and Esc1 proteins. *EMBO J* **23**: 1301–1312.
- Tatham MH, Jaffray E, Vaughan OA, Desterro JM, Botting CH, Naismith JH, Hay RT. 2001. Polymeric chains of SUMO-2 and SUMO-3 are conjugated to protein substrates by SAE1/SAE2 and Ubc9. *J Biol Chem* **276**: 35368–35374.
- Tatham MH, Geoffroy MC, Shen L, Plechanovova A, Hattersley N, Jaffray EG, Palvimo JJ, Hay RT. 2008. RNF4 is a poly-SUMO-specific E3 ubiquitin ligase required for arsenic-induced PML degradation. *Nat Cell Biol* **10**: 538–546.
- Therizols P, Fairhead C, Cabal GG, Genovesio A, Olivo-Marin JC, Dujon B, Fabre E. 2006. Telomere tethering at the nuclear periphery is essential for efficient DNA double strand break repair in subtelomeric region. *J Cell Biol* **172**: 189–199.
- Torres-Rosell J, Machin F, Farmer S, Jarmuz A, Eydmann T, Dalggaard JZ, Aragon L. 2005. SMC5 and SMC6 genes are required



- for the segregation of repetitive chromosome regions. *Nat Cell Biol* **7**: 412–419.
- Torres-Rosell J, Sunjevaric I, De Piccoli G, Sacher M, Eckert-Boulet N, Reid R, Jentsch S, Rothstein R, Aragon L, Lisby M. 2007. The Smc5–Smc6 complex and SUMO modification of Rad52 regulates recombinational repair at the ribosomal gene locus. *Nat Cell Biol* **9**: 923–931.
- Ullal P, Vilella-Mitjana F, Jarmuz A, Aragon L. 2011. Rtt107 phosphorylation promotes localisation to DNA double-stranded breaks (DSBs) and recombinational repair between sister chromatids. *PLoS One* **6**: e20152.
- van Attikum H, Fritsch O, Gasser SM. 2007. Distinct roles for SWR1 and INO80 chromatin remodeling complexes at chromosomal double-strand breaks. *EMBO J* **26**: 4113–4125.
- Xie Y, Kerscher O, Kroetz MB, McConchie HF, Sung P, Hochstrasser M. 2007. The yeast Hex3-Slx8 heterodimer is a ubiquitin ligase stimulated by substrate sumoylation. *J Biol Chem* **282**: 34176–34184.
- Yoshida T, Shimada K, Oma Y, Kalck V, Akimura K, Taddei A, Iwahashi H, Kugou K, Ohta K, Gasser SM, et al. 2010. Actin-related protein Arp6 influences H2A.Z-dependent and -independent gene expression and links ribosomal protein genes to nuclear pores. *PLoS Genet* **6**: e1000910.
- Zhao X, Blobel G. 2005. A SUMO ligase is part of a nuclear multi-protein complex that affects DNA repair and chromosomal organization. *Proc Natl Acad Sci* **102**: 4777–4782.
- Zhao X, Wu CY, Blobel G. 2004. Mlp-dependent anchorage and stabilization of a desumoylating enzyme is required to prevent clonal lethality. *J Cell Biol* **167**: 605–611.



## PolySUMOylation by Siz2 and Mms21 triggers relocation of DNA breaks to nuclear pores through the Slx5/Slx8 STUbL

Chihiro Horigome, Denise E. Bustard, Isabella Marcomini, et al.

*Genes Dev.* 2016, **30**: originally published online April 7, 2016  
Access the most recent version at doi:[10.1101/gad.277665.116](https://doi.org/10.1101/gad.277665.116)

---

**Supplemental Material** <http://genesdev.cshlp.org/content/suppl/2016/04/07/gad.277665.116.DC1>

**References** This article cites 67 articles, 24 of which can be accessed free at:  
<http://genesdev.cshlp.org/content/30/8/931.full.html#ref-list-1>

**Creative Commons License** This article is distributed exclusively by Cold Spring Harbor Laboratory Press for the first six months after the full-issue publication date (see <http://genesdev.cshlp.org/site/misc/terms.xhtml>). After six months, it is available under a Creative Commons License (Attribution-NonCommercial 4.0 International), as described at <http://creativecommons.org/licenses/by-nc/4.0/>.

**Email Alerting Service** Receive free email alerts when new articles cite this article - sign up in the box at the top right corner of the article or [click here](#).

---

Boost NGS microRNA profiling.  
Read about 3 methods tested

**EXIQON**  
Now a QIAGEN company



**Supplementary Materials:****Figures S1- S6, Legends and Figures****Table S1, S2****Online Methods****Supplementary References****Supplementary Fig. S1. Deletions of *siz1* or *siz2* partially reduce DSB relocation**

(a) Cleavage efficiency in wild-type (GA6844), *siz1* $\Delta$  (GA-7899) and *siz2* $\Delta$  (GA-6858) strains determined by qPCR across the cleavage site. (b) Position of cleaved *MAT* in wild-type (GA-6844), *siz1* $\Delta$  (GA-7899) and *siz2* $\Delta$  (GA-6858) is shown following DSB induction (+ galactose) at indicated times. Assay was performed as described in Figure 1a-c. 33% (red dotted line) indicates random distribution.

**Supplementary Fig. S2. Deletions of *slx5* or *slx8* reduce DSB recruitment to pores**

(a) ChIP with the anti-pore monoclonal antibody, Mab414, monitors *MAT* $\alpha$  locus association with nuclear pores at the indicated time after addition of glucose (no cleavage) or galactose (HO cleavage) in wild-type (GA-3862), *slx5* $\Delta$  (GA-4105), *slx8* $\Delta$  (GA-4106) and wild-type no GAL-HO (*MATa*, GA-1080) cells. We cannot exclude that the *slx5* $\Delta$  culture was not partially diploidized in this assay, which might explain its two-fold higher level of pore recovery vs. *slx8* $\Delta$ . ChIP was carried out and results were processed as described in Nagai et al. (2008). (b) ChIP for HA-tagged Slx8 monitors *MAT* locus association with Slx8 at 1 h after cut induction on galactose in non-tagged (GA-3862) and Slx8-3HA (GA-3867) tagged cells. Distances of primers used for qPCR from the HO cut site are indicated and a probe 0.5kb from the end of telomere 6R is used as a control. ChIP was performed as in panel a.

**Supplementary Fig. S3 *Esc2* promotes DSB relocation to the nuclear pore in G1-phase cells, but is not sufficient for relocation a LexA-*Esc2* targeting assay**

(a) LexA-Slx8 complements the HU sensitivity observed in *slx8* $\Delta$ . Five-fold serial dilutions starting from  $7 \times 10^7$  cells for each indicated strain were spotted on SD-LEU medium containing indicated dose of HU and incubated at 30°C for 4 days. Two independent clones were tested per strain. (b) *MAT* position relative to CFP-Nup49 in wild-type (GA-6844), and *esc2* $\Delta$  (GA-9373) after 120 min on galactose, as described in Figure 1a-c. # , significantly non-random distribution based on cell number and confidence values from a proportional test

between random and experimental distribution. \*, significantly different distribution between wild-type and mutant. n.s., difference is not significant from random (33%), indicated by the red dotted line. (c) The position of *lacO*/LexA-tagged *PES4* was visualized by GFP-LacI and scored in the presence of LexA alone or a LexA-Esc2 fusion. Cells are classified into G1 or S phase. Strains carry GFP-Nup49 (GA-1461) and LexA fusion proteins are expressed from plasmids. Neither LexA nor LexA-Esc2 shift the tagged locus to the NE. n= cells counted; P=significance relative to a random distribution.

#### **Supplementary Fig. S4. Localization of Slx5-GFP before or after $\gamma$ -irradiation**

(a,b) Slx5-GFP (green) and CFP-Nup49 (red) are visualized by confocal microscopy in a wild-type strain (GA-8565). Cells are grown at 30°C in selective SC-L+G418 media and exposed to  $\gamma$ -irradiation (30 Gy). Prior to microscopy cells recovered during 2 h in SC-L+G418 media. Representative images (b) showing both peripheral (white arrows) and some internal Slx5 foci, particularly under conditions of irradiation, which induces nicks and oxidative damage, as well as DSBs. Spontaneous foci are of weaker intensity. Bars = 2 $\mu$ m

#### **Supplementary Fig. S5. Slx5 binds Nse5, but not nse5-L247A, of the SMC5/6 complex**

(a) Left panel compares the dimeric *S. cerevisiae* STUbL Slx5/Slx8, with its human homologue RNF4. The combination of SIM (SUMO-interacting motifs) and RING finger ubiquitin ligase function is characteristic of this class of enzyme. Right panel shows a sketch of the SMC5/6 complex with subunit names from budding yeast. (b) Analysis of Nse5 and wild-type Slx5 or Slx5 <sup>$\Delta$ SIM</sup> (in which SIMs at aa25-27 and aa93-96 are mutated) protein interactions by galactose-inducible yeast two-hybrid assays. Quantitative  $\beta$ -galactosidase assay is described in online Methods. Actual mean values of  $\beta$ -galactosidase activity are indicated beside bars. Interaction of Nse5 with Slx5 is monitored in *smt3-3KR* and the *smt3-331* loss-of-function mutant backgrounds. (c) Sketch of the Nse5 subunit. Nse5 has no recognizable SIM, although the L247 mutation interferes with both Slx5 and Smt3 interaction. Interaction of a fusion of Slx5-AD, Nse6-AD or of Smt3-AD with the wild-type Nse5 or Nse5<sup>L247A</sup>, as bait are monitored as in (b).

#### **Supplementary Fig. S6. The protein expression from yeast two-hybrid constructs**

Plasmids J038 (Nse5-LexA) and J150 (Slx5-AD) which are both galactose inducible, were co-transformed into strains JC470 (wild-type), JC2996 (*smt3-3KR*), or JC2758 (*smt3-331*). Cells were treated with glucose (-) or galactose (+) at 30°C for 6 h and protein extracts were TCA precipitated prior to denaturation for 8% SDS-PAGE. Western blots were probed with

either anti-HA (Slx5-AD) or anti-LexA (Nse5-LexA; antibodies from Santa Cruz Biotechnology). Equal loading was confirmed by probing with anti-actin (Sigma). The *smt3-331* mutation reduces but does not eliminate all SUMOylation.

**Table S1. Summary of localization assay statistics**

Figure	Experiment	Relevant genotype	min after HO	% of intact MAT	Cell cycle	# of nuclei	<i>P</i> -value (vs random/wild-type)
Fig 1c, 2b, 5a, S3b	MAT zoning	Wild-type	120	4.27 ± 0.58	G1	169	<b>1.1×10<sup>-4</sup></b>
Fig 1c, 2b, 5a, S3b	MAT zoning	Wild-type	120	4.27 ± 0.58	S	108	<b>3.6×10<sup>-8</sup></b>
Fig 1c	MAT zoning	<i>siz1Δ siz2Δ</i>	120	6.51 ± 0.05	G1	321	0.24 / <b>1.8×10<sup>-4</sup></b>
Fig 1c	MAT zoning	<i>siz1Δ siz2Δ</i>	120	6.51 ± 0.05	S	64	0.48 / <b>8.3×10<sup>-3</sup></b>
Fig 1c	MAT zoning	<i>mms21ΔC</i>	120	6.08 ± 0.28	G1	146	9.0×10 <sup>-2</sup> / <b>1.7×10<sup>-4</sup></b>
Fig 1c	MAT zoning	<i>mms21ΔC</i>	120	6.08 ± 0.28	S	146	0.56 / <b>3.2×10<sup>-4</sup></b>
Fig 1d, 2c	Pore coloc.	Wild-type	0	100	G1	301	-
Fig 1d, 2c	Pore coloc.	Wild-type	40	10.60 ± 5.30	G1	299	-
Fig 1d, 2c	Pore coloc.	Wild-type	120	3.78 ± 1.08	G1	149	-
Fig 1d, 2c	Pore coloc.	Wild-type	0	100	S	94	-
Fig 1d, 2c	Pore coloc.	Wild-type	40	10.60 ± 5.30	S	88	-
Fig 1d	Pore coloc.	<i>siz2Δ</i>	0	100	G1	206	-
Fig 1d	Pore coloc.	<i>siz2Δ</i>	40	47.47 ± 0.66	G1	150	-
Fig 1d	Pore coloc.	<i>siz2Δ</i>	120	7.95 ± 0.82	G1	129	-
Fig 1d	Pore coloc.	<i>siz2Δ</i>	0	100	S	62	-
Fig 1d	Pore coloc.	<i>siz2Δ</i>	40	47.47 ± 0.66	S	51	-
Fig 1g	MAT zoning	<i>smt3-3KR</i>	120	6.21 ± 0.37	G1	279	0.20
Fig 1g	MAT zoning	<i>smt3-3KR</i>	120	6.21 ± 0.37	S	71	0.36
Fig 2b	MAT zoning	<i>slx5Δ</i>	120	4.34 ± 0.98	G1	110	0.89 / <b>1.6×10<sup>-2</sup></b>
Fig 2b	MAT zoning	<i>slx5Δ</i>	120	4.34 ± 0.98	S	63	<b>1.6×10<sup>-2</sup></b> / <b>0.17</b>
Fig 2b	MAT zoning	<i>slx8Δ</i>	120	6.83 ± 1.06	G1	108	0.68 / <b>4.6×10<sup>-2</sup></b>

Fig 2b	MAT zoning	<i>slx8Δ</i>	120	6.83 ± 1.06	S	68	$\frac{3.2 \times 10^{-2}}{9.9 \times 10^{-2}}$
Fig 2c	Pore coloc.	<i>slx5Δ</i>	0	100	G1	202	-
Fig 2c	Pore coloc.	<i>slx5Δ</i>	40	13.11 ± 1.49	G1	152	-
Fig 2c	Pore coloc.	<i>slx5Δ</i>	120	9.32 ± 0.81	G1	133	-
Fig 2c	Pore coloc.	<i>slx5Δ</i>	0	100	S	50	-
Fig 2c	Pore coloc.	<i>slx5Δ</i>	40	13.11 ± 1.49	S	34	-
Fig 3b, 4a, S3c	Targeting, zoning	LexA/WT	-	-	G1	147	0.73
Fig 3b, 4a, S3c	Targeting, zoning	LexA/WT	-	-	S	105	0.68
Fig 3b	Targeting, zoning	LexA-polySmt3/WT	-	-	G1	116	$< 1.0 \times 10^{-30}$
Fig 3b	Targeting, zoning	LexA-polySmt3/WT	-	-	S	82	0.18
Fig 3b	Targeting, zoning	LexA-polySmt3/ <i>siz2Δ</i>	-	-	G1	139	$4.0 \times 10^{-4}$
Fig 3b	Targeting, zoning	LexA-polySmt3/ <i>siz2Δ</i>	-	-	S	92	0.30
Fig 3b	Targeting, zoning	LexA-polySmt3/ <i>slx5Δ</i>	-	-	G1	88	0.88
Fig 3b	Targeting, zoning	LexA-polySmt3/ <i>slx5Δ</i>	-	-	S	198	0.55
Fig 3c	Targeting, zoning	LexA-Slx5/WT	-	-	G1	102	$6.6 \times 10^{-5}$
Fig 3c	Targeting, zoning	LexA-Slx5/WT	-	-	S	84	0.49
Fig 3c	Targeting, zoning	LexA-Slx5/ <i>siz2Δ</i>	-	-	G1	178	$1.4 \times 10^{-8}$
Fig 3c	Targeting, zoning	LexA-Slx5/ <i>siz2Δ</i>	-	-	S	75	0.62
Fig 3c	Targeting, zoning	LexA-Slx5/ <i>slx8Δ</i>	-	-	G1	80	$3.9 \times 10^{-5}$
Fig 3c	Targeting, zoning	LexA-Slx5/ <i>slx8Δ</i>	-	-	S	95	$7.0 \times 10^{-2}$
Fig 3c	Targeting, zoning	LexA-Slx8/WT	-	-	G1	138	0.28
Fig 3c	Targeting, zoning	LexA-Slx8/WT	-	-	S	70	0.27
Fig 3d, 4b	Targeting, pore coloc.	LexA	-	-	G1	129	-
Fig 3d, 4b	Targeting,	LexA	-	-	S	101	-

	pore coloc.							
Fig 3d	Targeting, pore coloc.	LexA-polySmt3	-	-	G1	179	-	
Fig 3d	Targeting, pore coloc.	LexA-polySmt3	-	-	S	106	-	
Fig 3d	Targeting, pore coloc.	LexA-Slx5	-	-	G1	131	-	
Fig 3d	Targeting, pore coloc.	LexA-Slx5	-	-	S	104	-	
Fig 4a	Targeting, zoning	LexA-Smt3/WT	-	-	G1	110	0.20	
Fig 4a	Targeting, zoning	LexA-Smt3/WT	-	-	S	105	<b>5.3×10<sup>-6</sup></b>	
Fig 4a	Targeting, zoning	LexA-smt3- 3KR/WT	-	-	G1	84	0.35	
Fig 4a	Targeting, zoning	LexA-smt3- 3KR/WT	-	-	S	93	<b>2.1×10<sup>-3</sup></b>	
Fig 4a	Targeting, zoning	LexA-smt3- 3KR/ <i>siz2Δ</i>	-	-	G1	116	0.39	
Fig 4a	Targeting, zoning	LexA-smt3- 3KR/ <i>siz2Δ</i>	-	-	S	105	<b>3.8×10<sup>-3</sup></b>	
Fig 4b	Targeting, pore coloc.	LexA-Smt3	-	-	G1	131	-	
Fig 4b	Targeting, pore coloc.	LexA-Smt3	-	-	S	104	-	
Fig 4b	Targeting, pore coloc.	LexA-smt3-3KR	-	-	G1	145	-	
Fig 4b	Targeting, pore coloc.	LexA-smt3-3KR	-	-	S	112	-	
Fig 4c	Targeting, zoning	LexA-smt3-3KR and control vector	-	-	G1	95	0.25	
Fig 4c	Targeting, zoning	LexA-smt3-3KR and control vector	-	-	S	83	<b>2.0×10<sup>-5</sup></b>	
Fig 4c	Targeting, zoning	LexA-smt3-3KR and Mps3N'	-	-	G1	93	0.51	
Fig 4c	Targeting, zoning	LexA-smt3-3KR and Mps3N'	-	-	S	143	0.34	
Fig 5b	<i>MAT</i> zoning	<i>nse5-L247A</i>	120	8.24 ± 0.23	G1	194	<b>2.0×10<sup>-3</sup></b> / 0.50	
Fig 5b	<i>MAT</i> zoning	<i>nse5-L247A</i>	120	8.24 ± 0.23	S	95	0.35 / <b>3.7×10<sup>-3</sup></b>	
Fig 5b	<i>MAT</i> zoning	<i>smc6-9</i>	120	14.45 ± 1.19	G1	191	0.96 / <b>7.5×10<sup>-3</sup></b>	

Fig 5b	MAT zoning	<i>smc6-9</i>	120	14.45 ± 1.19	S	61	0.86 / <b>2.8×10<sup>-3</sup></b>
Fig 5b	MAT zoning	<i>rtt107Δ</i>	120	5.01 ± 0.45	G1	252	0.32
Fig 5b	MAT zoning	<i>rtt107Δ</i>	120	5.01 ± 0.45	S	106	0.28
Fig S1a, b	MAT zoning	Wild-type	0	100	G1/S/G2	198	1
Fig S1a, b	MAT zoning	Wild-type	20	20.43 ± 5.19	G1/S/G2	206	<b>4.3×10<sup>-3</sup></b>
Fig S1a, b	MAT zoning	Wild-type	40	15.95 ± 9.68	G1/S/G2	225	<b>2.0×10<sup>-10</sup></b>
Fig S1a, b	MAT zoning	Wild-type	60	6.60 ± 0.33	G1/S/G2	218	<b>&lt; 1.0×10<sup>-30</sup></b>
Fig S1a, b	MAT zoning	Wild-type	120	4.79 ± 2.14	G1/S/G2	211	<b>5.3×10<sup>-5</sup></b>
Fig S1a, b	MAT zoning	<i>siz1Δ</i>	0	100	G1/S/G2	267	0.19
Fig S1a, b	MAT zoning	<i>siz1Δ</i>	20	34.64 ± 6.92	G1/S/G2	233	0.75
Fig S1a, b	MAT zoning	<i>siz1Δ</i>	40	11.54 ± 0.79	G1/S/G2	185	<b>1.1×10<sup>-2</sup></b>
Fig S1a, b	MAT zoning	<i>siz1Δ</i>	60	8.06 ± 0.07	G1/S/G2	282	<b>3.0×10<sup>-6</sup></b>
Fig S1a, b	MAT zoning	<i>siz1Δ</i>	120	8.04 ± 0.79	G1/S/G2	191	0.26
Fig S1a, b	MAT zoning	<i>siz2Δ</i>	0	100	G1/S/G2	135	0.27
Fig S1a, b	MAT zoning	<i>siz2Δ</i>	20	40.89 ± 2.13	G1/S/G2	101	0.78
Fig S1a, b	MAT zoning	<i>siz2Δ</i>	40	20.37 ± 3.36	G1/S/G2	111	<b>4.4×10<sup>-2</sup></b>
Fig S1a, b	MAT zoning	<i>siz2Δ</i>	60	15.39 ± 1.23	G1/S/G2	124	<b>2.6×10<sup>-2</sup></b>
Fig S1a, b	MAT zoning	<i>siz2Δ</i>	120	9.93 ± 1.77	G1/S/G2	125	<b>6.5×10<sup>-3</sup></b>
Fig S3b	MAT zoning	<i>esc2Δ</i>	120	14.95 ± 4.19	G1	179	0.49 / <b>5.1×10<sup>-4</sup></b>
Fig S3b	MAT zoning	<i>esc2Δ</i>	120	14.95 ± 4.19	S	96	<b>9.7×10<sup>-5</sup></b> / <u>0.97</u>
Fig S3c	Targeting, zoning	LexA-Esc2/WT	-	-	G1	104	0.78
Fig S3c	Targeting, zoning	LexA-Esc2/WT	-	-	S	130	0.42

---

**Bold face:** significantly non-random



**Table S2. Yeast strains used in this study**

<b>Name</b>	<b>Genotype</b>	<b>Source</b>
GA-1081	JKM179; <i>MATα</i> , $\Delta$ <i>hml::ADE1 hmr::ADE1 ade3::GALHO ade1-100 leu2-3, 112 lys5 trp1::hisG ura3-52</i>	(Lee et al. 1998)
GA-6844	GA-1081 <i>CFP-NUP49 GFP-LacI:Leu2 MAT::LacO repeats:TRP1</i>	(Horigome et al. 2014)
GA-7968	GA-6844 <i>siz1::natMX4 siz2::C.a.URA3</i>	This study
JC3654	GA-6844 <i>mms21ΔC:HYG</i>	This study
GA-7314	GA-6844 <i>nup133::natMX4 pUN100-nup133ΔN:kanMX6</i>	This study
GA-7970	GA-7314 <i>siz2::C.a.URA3</i>	This study
GA-6858	GA-6844 <i>siz2::KanMX</i>	This study
GA-1259	JKM139; <i>MATa</i> , $\Delta$ <i>hml::ADE1 hmr::ADE1 ade3::GALHO ade1-100 leu2-3, 112 lys5 trp1::hisG ura3-52</i>	(Lee et al. 1998)
GA-8306	GA-1259 <i>3HA-MPS3</i>	(Lee et al. 1998; Horigome et al. 2014)
GA-8541	GA-8306 <i>siz2::natMX4</i>	This study
GA-9072 (JC3656)	GA-6844 <i>smt3-3KR:HYG</i>	This study
GA-1081 (JC727)	JKM179; <i>MATα</i> , $\Delta$ <i>hml::ADE1 hmr::ADE1 ade3::GALHO ade1-100 leu2-3, 112 lys5 trp1::hisG ura3-52</i>	(Lee et al. 1998)
JC3020	JC727 <i>SLX5-3HA::URA3</i>	This study
JC3668	JC3020 <i>siz2::KanMX6</i>	This study
JC3214	JC3020 <i>smt3-K11R,K15R,K19R::TRP1</i>	This study
GA-7097	GA-6844 <i>slx5::natMX4</i>	This study
GA-7098	GA-6844 <i>slx8::natMX4</i>	This study
GA-7969	GA-7314 <i>slx5::C.a.URA3</i>	This study
GA-8539	GA-8306 <i>slx5::natMX4</i>	This study
GA-8194	W303 <i>MATa</i> , <i>ade2-1 trp1-1 his3-11 his3-15 ura3-1 leu2-3 leu1-112 can1-100 nup133::HIS3 -pUN100-nup133ΔN:kanMX6 CFP-NUP49 ade2::lacI-GFP:ADE2 lys2::LexALacOPs:TRP</i>	This study
GA-1461	W303 <i>MATa</i> , <i>PES4:4xLexA:lacO array:TRP1 his3-15::GFP-LacI:HIS3 NUP49-GFP</i>	(Heun et al. 2001)
GA-4447	GA-1461 <i>siz2::KanMX6</i>	This study
GA-4448	GA-1461 <i>slx5::KanMX6</i>	This study
GA-4449	GA-1461 <i>slx8::KanMX6</i>	This study
JC3161	GA-6844 <i>nse5::HYG ura3:: nse5-L247A:URA3</i>	This study
JC3131	GA-6844 <i>smc6-9::KanMX4</i>	This study

GA-7092	GA-6844 <i>rtt107::natMX4</i>	This study
GA-4133	GA-1081 <i>NUP84-13MYC</i>	This study
JC3154	GA-4133 <i>nse5::HYG ura3:: nse5-L247A:URA3</i>	This study
JC3150	GA-4133 <i>smc6-9::KanMX4</i>	This study
JC3167	GA-1081 <i>3HA-MPS3:URA3</i>	This study
JC3114	JC3167 <i>nse5::HYG ura3:: nse5-L247A:URA3</i>	This study
JC3115	JC3167 <i>smc6-9::KanMX4</i>	This study
JC3621	JC3020 <i>nse5::HYG ura3:: nse5-L247A:URA3</i>	This study
JC3189	JC3020 <i>smc6-9::KanMX</i>	This study
GA-9206	GA-6844 <i>siz2::HPH slx5::natMX4</i>	This study
GA-9355	GA-6844 <i>nse5-L247A:URA3 slx5::HYG</i>	This study
GA-8994	W303 <i>MATa-inc, lys2::NatMX4 AVT2::ly-HOcs::KanMX6 ERV46::TRP1-ys2 (Ch I 60kb donor) ade3::GAL-HO URA3::TK BARI::LEU2</i>	(Donnianni and Symington 2013)
GA-9185	GA-8994 <i>nup60::hphMX4</i>	This study
GA-9186	GA-8994 <i>slx8::hphMX4</i>	This study
GA-9090	GA-8994 <i>pol32::hphMX4</i>	This study
GA-8860	GA-1081 <i>CFP-NUP49 GFP-LacI:Leu2 MAT::LacO repeats:TRP1</i>	This study
GA-8471	GA-6844 <i>nup84::natMX4</i>	This study
GA-7899	GA-6844 <i>siz1::natMX4</i>	This study
GA-3862	JKM139; <i>MATa, Δho hml::ADE1 hmr::ADE1 ade3::GALHO ade1-100 leu2-3, 112 lys5 trp1::hisG ura3-52</i>	Gift from Nevan Krogan
GA-4105	GA-3862 <i>slx5::caURA3</i>	This study
GA-4106	GA-3862 <i>slx8::caURA3</i>	This study
GA-1080	JKM115; <i>MATα, Δho hml::ADE1 hmr::ADE1 ade1-100 leu2-3, 112 lys5 trp1::hisG ura3-52</i>	Gift from James E. Haber
GA-3867	KLY3; GA-3862 <i>slx5::Slx5-3HA:KL-TRP</i>	Gift from Michael Keogh
GA-9373	GA-6844 <i>esc2::natMX4</i>	This study
GA-7451	YOK851; <i>MATα, his3-Δ200 leu2-3, 112 ura3-52 lys2-80 trp1-1 gal2 slx5::kanMX4 SLX5-GFP:LEU2/CEN</i>	(Cook et al. 2009)
GA-8565	GA-7451 <i>CFP-NUP49</i>	This study
JC470	W303 <i>MATa, ade2-1 trp1-1 his3-11 his3-15 ura3-1 leu2-3 leu2-112, RAD5+</i>	This study
JC2758	JC470 <i>smt3-331</i>	This study
JC2996	JC470 <i>smt3K11R, K15R, K19R::TRP1 (smt3-3KR)</i>	This study

## Online Methods

### Plasmids, yeast strains and yeast techniques

Yeast strains used in this study are described in Table S2. JKM139 and JKM179 are gifts from J. E. Haber and have been previously described (Lee et al. 1998). Standard methods for genetic modification of yeast were used (Longtine et al. 1998) and were verified by PCR and phenotypic analysis. Yeast strains with *3HA-MPS3* were created by using the plasmid pRS306-*3HA-MPS3* (gift from Dr. Mizuta) (Horigome et al. 2011). For DSB localization a *lacO* array initially containing 256 lacI binding sites was inserted at 4.4 kb from the HO cut site at *MAT* (Nagai et al. 2008). Note that repeat number is not stable in all strains and is usually less than 256. For DSB localization, cells were grown at 30°C for 2 days on YPAD plate (or selective SC media if required), then inoculated into synthetic media containing 0.05% glucose, 3% glycerol and 2% lactate (SCLGg) and grown overnight to obtain an exponentially growing cell population with no more than  $5\text{-}7 \times 10^6$  cells ml<sup>-1</sup>. Galactose (20%) is added to final 2% to induce the HO endonuclease. Cells were harvested, fixed with para-formaldehyde (final 4%) and washed 3 times with PBS at indicated time points. Cell cycle stages were assigned as follows: G1 cells have no bud and a round nucleus, cells in S phase have a bud up to 2/3 the size of the mother cells and a round nucleus. G2 cells have nuclei at the bud neck; such nuclei are usually distorted and therefore not reliable for position analysis.

### Targeting constructs and strains

Like the LexA-Slx5, -Slx8 and -Esc2 fusion, LexA fusions to 4xSmt3 to a single Smt3 or smt3-3KR moiety were created in and expressed from the plasmid pAT4. The 4xSmt3 construct (LexA-polySUMO) was created by cloning four Smt3 genes tandemly into the vector pAT4 using a 4xSmt3 construct synthesized by Bio Basic Inc. Gene Synthesis. To prevent processing of the internal SUMO proteins by Ulp1, the constructs were truncated at I<sub>96</sub> to remove the di-glycine motif. The fourth SUMO residue in the chain retains the full SUMO sequence including the di-glycine motif. The single Smt3 moiety is not mutated and can be a substrate for polySUMOylation while smt3-3KR cannot. Targeted binding of LexA fusions to the indicated loci is described in (Neumann et al. 2012; Horigome et al. 2014).

### Microscopy and image analysis

Fluorescence microscopy and quantification was performed according to published methods (Meister et al. 2010; Horigome et al. 2015). Images for zoning measurements were captured

on a Metamorph-driven Spinning-disk confocal system based on an Olympus IX81 microscope, Yokogawa CSU-X1 scan head, EM-CCD Cascade II (Photometrics) camera and an ASI MS-2000 Z-piezo stage. We used PlanApo  $\times 100$ , NA 1.45 total internal reflection fluorescence microscope oil objective. LacI-GFP position was determined with a through-focus stack of 16-21 0.2  $\mu\text{m}$  steps and was measured by ImageJ (NIH, USA) and the plug-in software PointPicker (Meister et al. 2010). The numbers of nuclei scored are in Table S1.

### **Statistical analyses and cutting efficiency**

To determine zone enrichment we applied a  $\chi^2$  test comparing zone1 to a random distribution (degree of freedom = 2, confidence limit = 95%). *P*-values are listed in Table S1. To compare the perinuclear enrichment of two different strains, we used a proportional analysis with a confidence limit of 95%. The error bars of all ChIP experiments represent the s.e.m.

The efficiency of DSB induction was determined by qPCR using TaqMan probes as described (van Attikum et al. 2007). The value was normalized to cut efficiency and PCR efficiency at an uncut locus, *SMC2*. Primer and probe sequences are available on request. The cutting efficiencies are available in Table S1.

### **Chromatin immunoprecipitation (ChIP) assays**

ChIP with anti-HA or anti-MYC epitope tagged strains was carried out as previously described (Yoshida et al. 2010) with the following modifications. Yeast cells cultured in 45 ml medium were cross-linked at 30°C for 20 min, and disrupted using a bead beater (TOMY) and Zirconia/Silica beads. The recovered chromatin fraction was subjected to sonication using Bioruptor Plus (Diagenode) to obtain fragmented chromatin < 500 bp in length. An anti-HA antibody (sc-7392, Santa Cruz Biotech, Inc), an anti-MYC antibody (9E10) combined with anti-mouse IgG magnetic beads (Invitrogen) or Protein G magnetic beads (Invitrogen), respectively, were used for IP. ChIP DNA was purified and was analysed by quantitative PCR using primers adapted to the *MATa* or *MAT $\alpha$*  locus (available on request). ChIP with Mab414 (Abcam) was performed basically as described (H. Van Attikum et al. 2007) using the indicated strains. Input and IP DNA were purified and analyzed by real-time (rt) PCR, using the Perkin-Elmer ABI Prism 7700 Sequence Detector System. For each ChIP, rtPCR was performed two or three times. Absolute enrichment was calculated as follows: for each time point, the signal from a site near the HO DSB at *MAT* was normalized to that from either genomic *SMC2* locus or mitochondrial *OLII* locus in ChIP and input DNA samples. For each time point and site, normalized ChIP signals were normalized to input DNA signals.

## Repair assays

Precise and imprecise NHEJ were performed as described in (van Attikum et al. 2007), using isogenic derivatives of GA-1081 (i.e. GA-8860, wild-type and GA-8471, *nup84Δ*). For imprecise NHEJ, cells were grown in YPLGg to OD600 0.6-1.2. They were plated on 2% galactose plates, and scored for CFUs after 2-3 days at 30°C. For precise NHEJ, cells were grown in YPLGg to log phase, HO was induced with 2% galactose for 75 min, cells were washed 2x and shaken in YPD for 2 h. Samples for qPCR were taken before galactose addition (0 min), after gal addition (75 min) and after YPD recovery (195 min). Genomic DNA was extracted and used for real-time PCR (primers available upon request). Formulas for NHEJ efficiency are described in van Attikum et al., 2007.. Survival after HO-induced cleavage was performed by standard induction of HO-cleavage on galactose for up to 4 h, followed by washing of the cells and plating in triplicate on YPAD. CFU were scored after 2 days at 30°C.

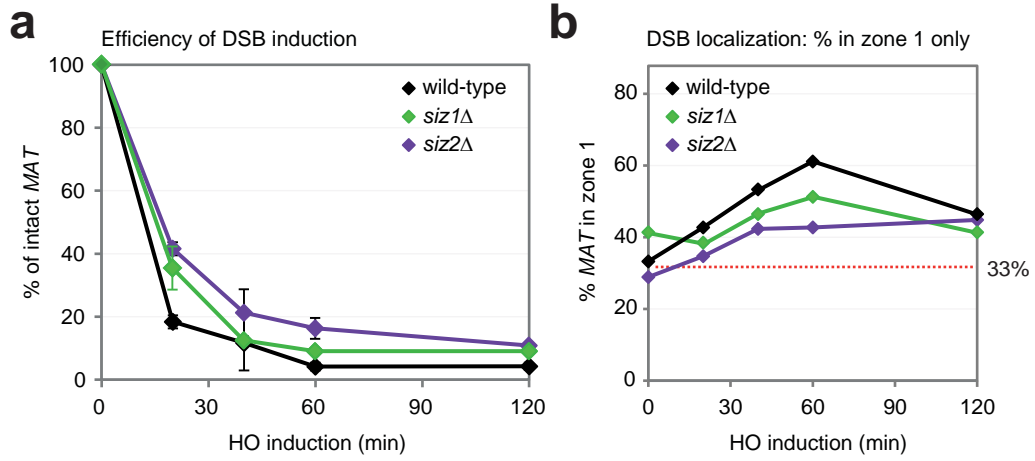
The Break-induced replication (BIR) assay was performed, and the frequency of recombinants was calculated, as previously described (Donnianni and Symington 2013). Briefly, 4 individual colonies per strain were grown to exponential phase in YPR (1% yeast extract, 2% peptone, 2% raffinose), and then plated on YP containing 2% Glucose or 2% Galactose in 3 serial dilutions. CFU were counted after 3 days. Plates were replica plated on SC-Lys and YPD+G418 to determine the frequency of BIR recombinants, which is the ratio of colonies growing on SC-Lys over those growing on YPGalactose, divided by the plating efficiency.

## Two-hybrid Analysis

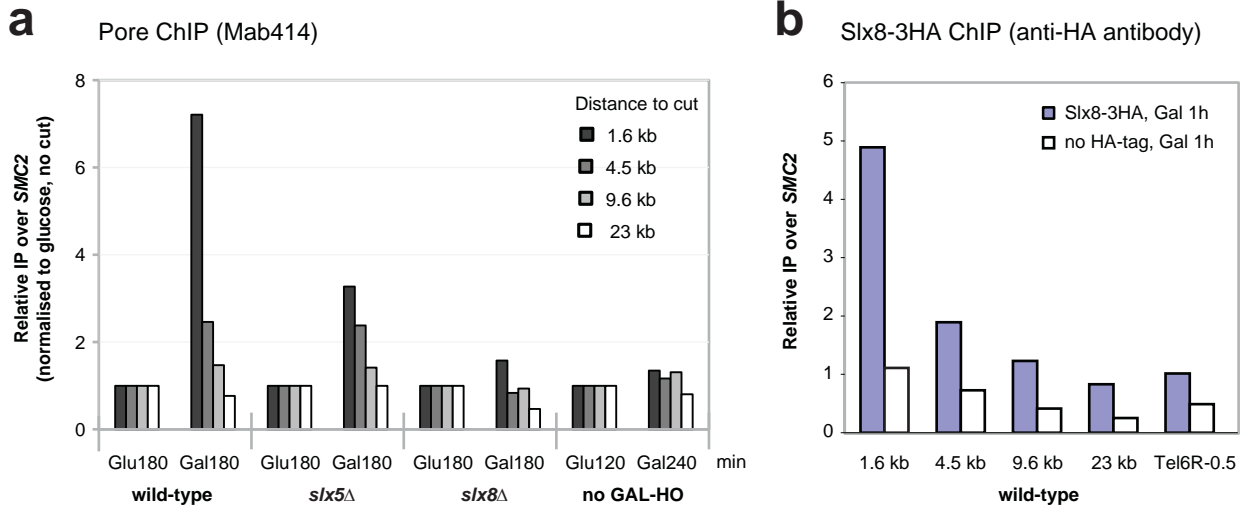
*NSE5* versions were cloned into pEG202-derived bait plasmids, creating Nse5-LexA fusion proteins, while *SLX5* genes were cloned into pJG4-6-derived prey plasmids creating Slx5-B42-activating domain fusion proteins. *nse5L247A* was generated by site-directed mutagenesis, while *slx5ΔSIM* was generated by subcloning *slx5SIMA/B* from the pAA3-derived plasmid published in (Cook et al. 2009). Bait and prey plasmids, as well as the reporter plasmid pSH18034, were transformed into W303 wild type strain JC470, JC2996 (*smt3-3KR*), or JC2758 (*smt3-331*). Protein-protein interactions were measured by quantitative  $\beta$ -galactosidase activity for permeabilized cells, and represent the averages of three independent experiments, with error bars indicating S.D.

## References

- Cook CE, Hochstrasser M, Kerscher O. 2009. The SUMO-targeted ubiquitin ligase subunit Slx5 resides in nuclear foci and at sites of DNA breaks. *Cell cycle (Georgetown, Tex)* **8**: 1080-1089.
- Donnianni RA, Symington LS. 2013. Break-induced replication occurs by conservative DNA synthesis. *Proceedings of the National Academy of Sciences of the United States of America* **110**: 13475-13480.
- Heun P, Laroche T, Shimada K, Furrer P, Gasser SM. 2001. Chromosome dynamics in the yeast interphase nucleus. *Science (New York, NY)* **294**: 2181-2186.
- Horigome C, Dion V, Seeber A, Gehlen LR, Gasser SM. 2015. Visualizing the spatiotemporal dynamics of DNA damage in budding yeast. *Methods in molecular biology* **1292**: 77-96.
- Horigome C, Okada T, Shimazu K, Gasser SM, Mizuta K. 2011. Ribosome biogenesis factors bind a nuclear envelope SUN domain protein to cluster yeast telomeres. *The EMBO journal* **30**: 3799-3811.
- Horigome C, Oma Y, Konishi T, Schmid R, Marcomini I, Hauer MH, Dion V, Harata M, Gasser SM. 2014. SWR1 and INO80 chromatin remodelers contribute to DNA double-strand break perinuclear anchorage site choice. *Molecular cell* **55**: 626-639.
- Lee SE, Moore JK, Holmes A, Umezumi K, Kolodner RD, Haber JE. 1998. Saccharomyces Ku70, mre11/rad50 and RPA proteins regulate adaptation to G2/M arrest after DNA damage. *Cell* **94**: 399-409.
- Longtine MS, McKenzie A, 3rd, Demarini DJ, Shah NG, Wach A, Brachat A, Philippsen P, Pringle JR. 1998. Additional modules for versatile and economical PCR-based gene deletion and modification in Saccharomyces cerevisiae. *Yeast (Chichester, England)* **14**: 953-961.
- Meister P, Gehlen LR, Varela E, Kalck V, Gasser SM. 2010. Visualizing yeast chromosomes and nuclear architecture. *Methods in enzymology* **470**: 535-567.
- Nagai S, Dubrana K, Tsai-Pflugfelder M, Davidson MB, Roberts TM, Brown GW, Varela E, Hediger F, Gasser SM, Krogan NJ. 2008. Functional targeting of DNA damage to a nuclear pore-associated SUMO-dependent ubiquitin ligase. *Science (New York, NY)* **322**: 597-602.
- Neumann FR, Dion V, Gehlen LR, Tsai-Pflugfelder M, Schmid R, Taddei A, Gasser SM. 2012. Targeted INO80 enhances subnuclear chromatin movement and ectopic homologous recombination. *Genes & development* **26**: 369-383.
- van Attikum H, Fritsch O, Gasser SM. 2007. Distinct roles for SWR1 and INO80 chromatin remodeling complexes at chromosomal double-strand breaks. *The EMBO journal* **26**: 4113-4125.
- Yoshida T, Shimada K, Oma Y, Kalck V, Akimura K, Taddei A, Iwahashi H, Kugou K, Ohta K, Gasser SM et al. 2010. Actin-related protein Arp6 influences H2A.Z-dependent and -independent gene expression and links ribosomal protein genes to nuclear pores. *PLoS genetics* **6**: e1000910.

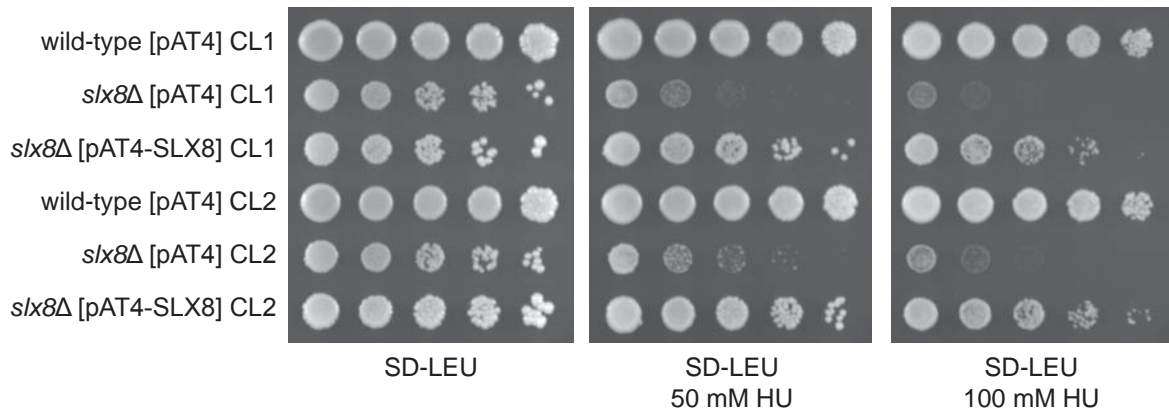
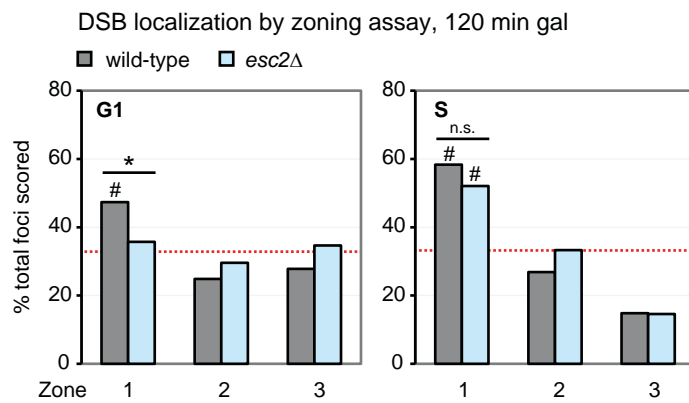
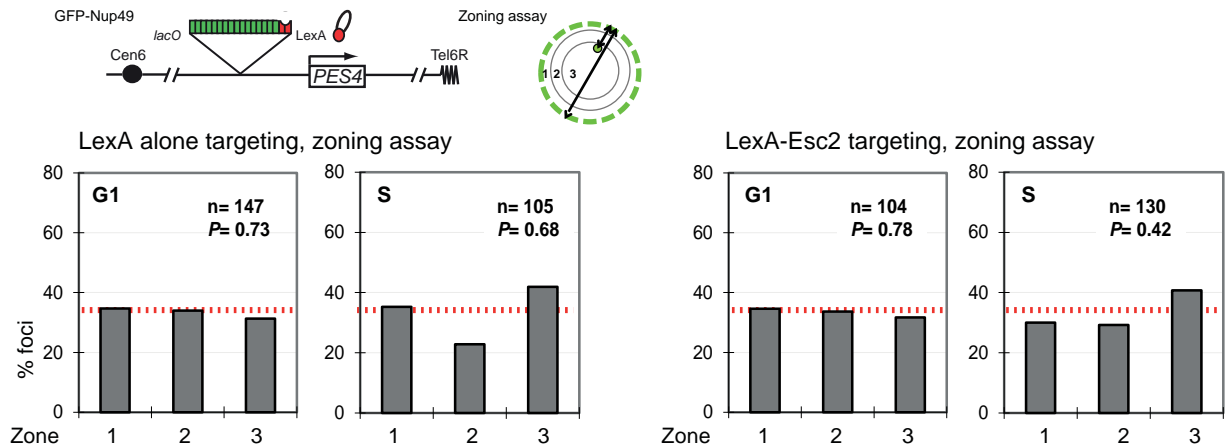


Horigome *et al.*, Figure S1

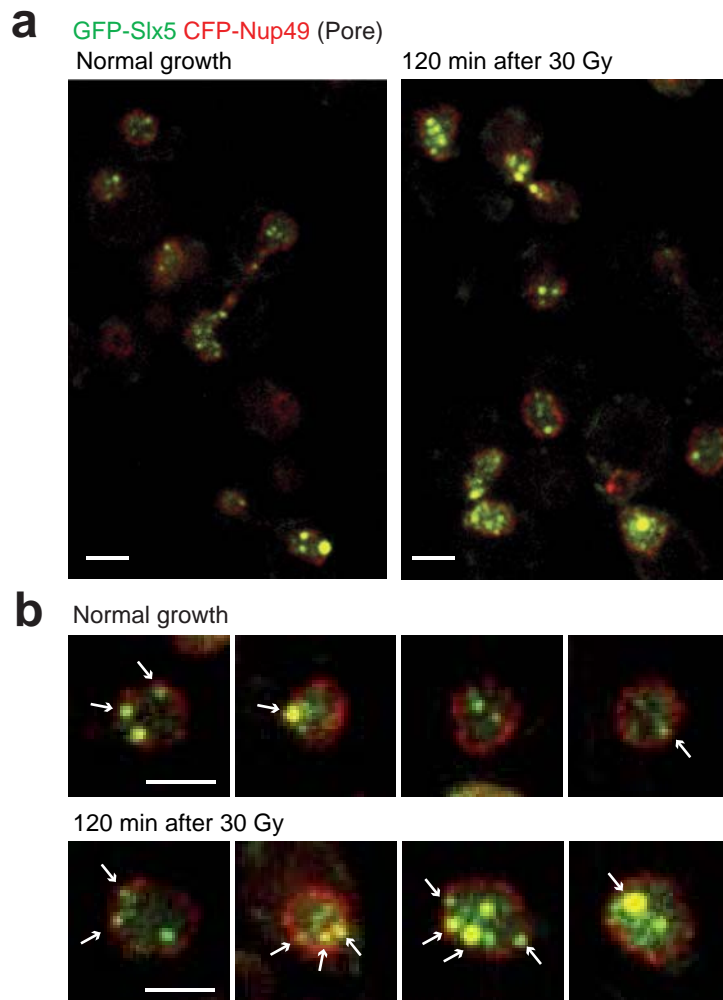


Horigome *et al.*, Figure S2



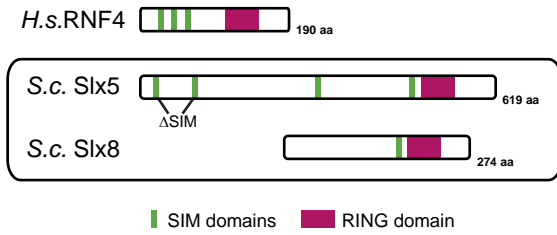
**a****b****c**

Horigome *et al.*, Figure S3

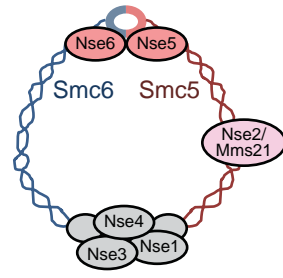


Horigome *et al.*, Figure S4

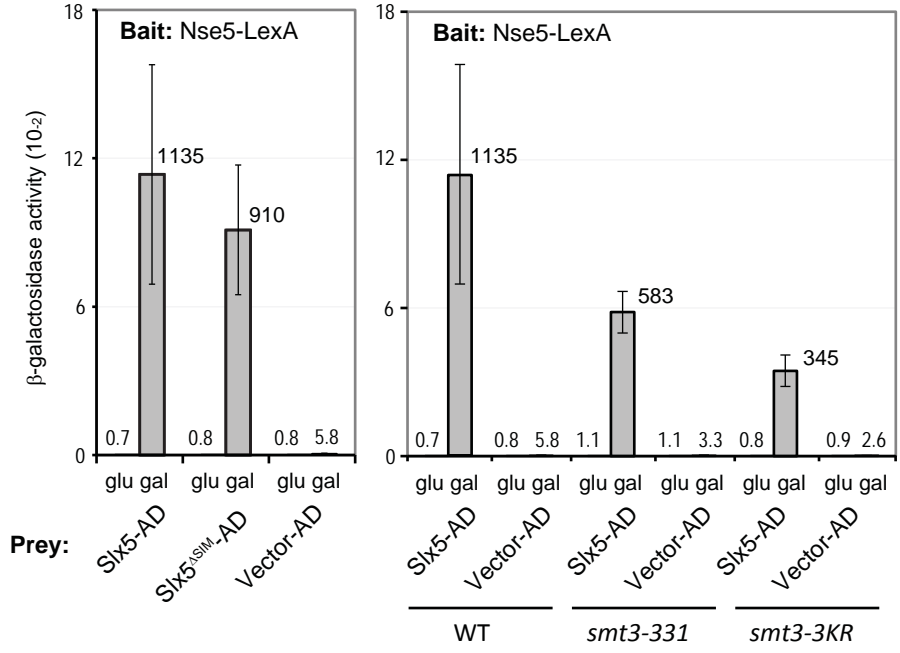
**a** STUbl: SUMO-targeted ubiquitin ligases



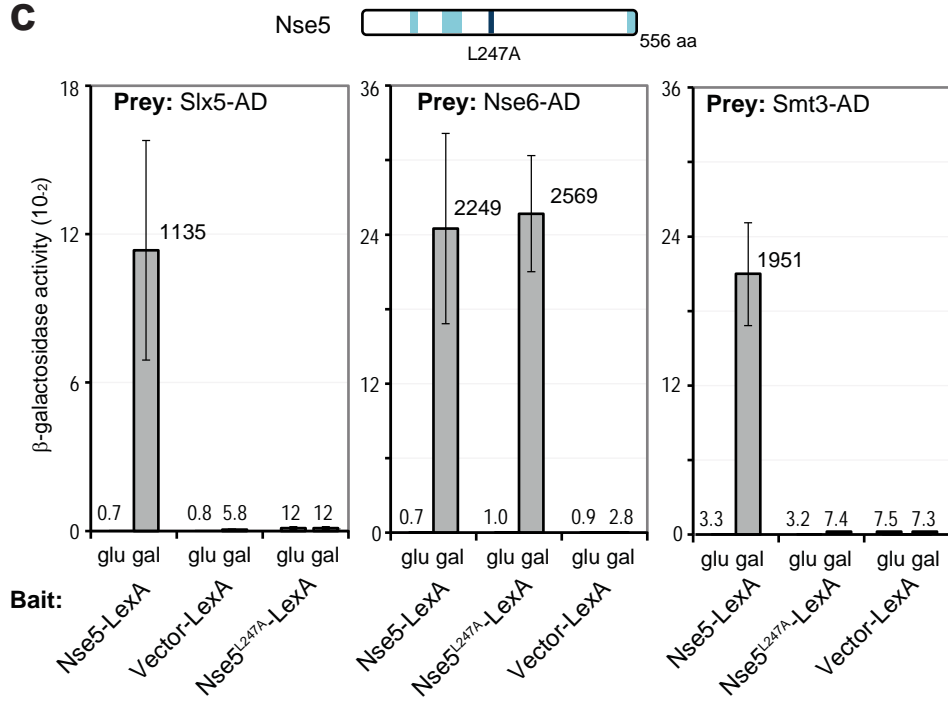
Smc5/Smc6 complex

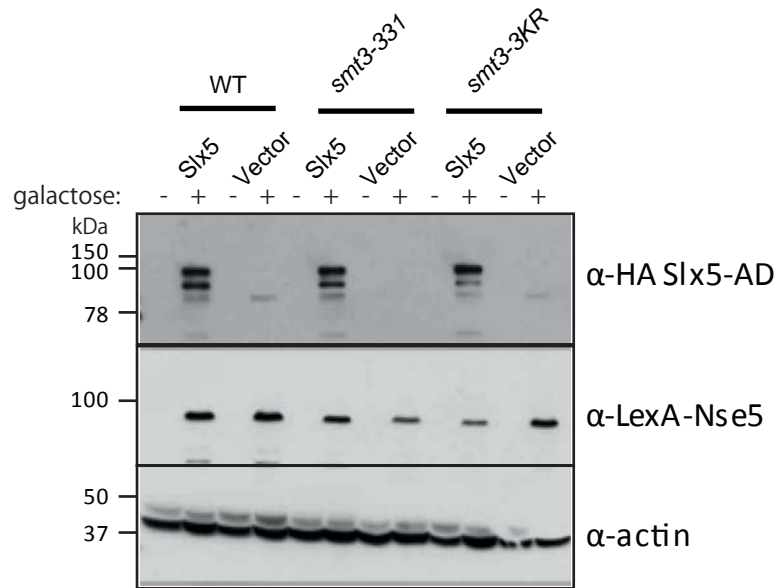


**b**



**c**





Horigome *et al.*, Figure S6

# CHAPTER 3. TELOMERIC REPEATS NEAR AN INTERNAL DOUBLE-STRAND BREAK PREVENT MRX RECRUITMENT AND ALLOW DNA END SEPARATION TO FAVOR ECTOPIC RECOMBINATION

---

Isabella Marcomini<sup>1,2</sup>, Kenji Shimada<sup>1</sup>, Neda Delgosaie<sup>1</sup>, Io Yamamoto<sup>1</sup>, Andrew Seeber<sup>1</sup>, Anais Cheblal<sup>1,2</sup>, Chihiro Horigome<sup>1,3</sup>, Ulrike Naumann<sup>4</sup> and Susan M. Gasser<sup>1,2,\*</sup>

<sup>1</sup> Friedrich Miescher Institute for Biomedical Research, Maulbeerstrasse 66, CH-4058 Basel, Switzerland

<sup>2</sup> University of Basel, Faculty of Natural Sciences, CH-4056 Basel, Switzerland

<sup>3</sup> Present address: Institute of Molecular and Cellular Biosciences; The University of Tokyo; 1-1-1, Yayoi, Bunkyo-ku, Tokyo, 113-0032, Japan

<sup>4</sup> Novartis Institute of Biomedical Research, CH-4002 Basel, Switzerland

\*Correspondence: Susan M. Gasser ([susan.gasser@fmi.ch](mailto:susan.gasser@fmi.ch))

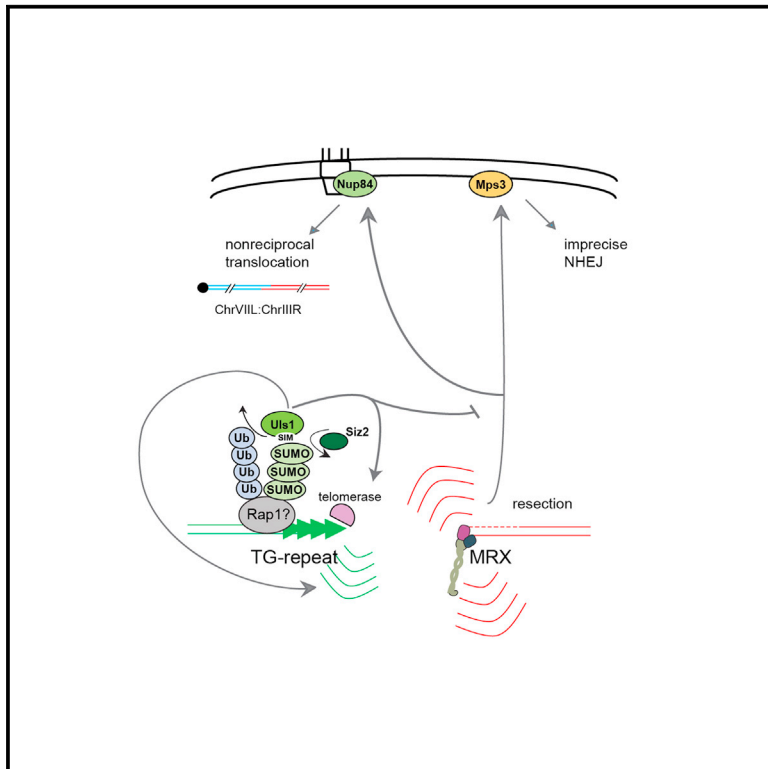
Running title: Asymmetric processing of DNA ends at a double-strand break leads to unconstrained dynamics and ectopic translocation.

Key words: Double-strand breaks, telomeric repeats, end resection, ectopic recombination, nuclear organization



## Asymmetric Processing of DNA Ends at a Double-Strand Break Leads to Unconstrained Dynamics and Ectopic Translocation

### Graphical Abstract



### Authors

Isabella Marcomini, Kenji Shimada, Neda Delgoshai, ..., Chihiro Horigome, Ulrike Naumann, Susan M. Gasser

### Correspondence

susan.gasser@fmi.ch

### In Brief

Marcomini et al. show that the presence of interstitial telomeric repeat sequences near a double-strand break alters the outcome of repair. A TG-flanked break loads MRX asymmetrically, supports resection only on one side, and allows uncoordinated movement of the break ends. The resected TG-free end invades homology on another chromosome driving a unidirectional translocation event.

### Highlights

- TG repeats near an internal break impair MRX binding and end resection
- Asymmetric MRX binding leads to enhanced end mobility
- TG repeats near an internal break promote repair by ectopic recombination
- The STUbL Uls1, not Slx5/Slx8, downregulates imprecise NHEJ at TG repeats



# Asymmetric Processing of DNA Ends at a Double-Strand Break Leads to Unconstrained Dynamics and Ectopic Translocation

Isabella Marcomini,<sup>1,2</sup> Kenji Shimada,<sup>1,5</sup> Neda Delgoshai,<sup>1,5</sup> Io Yamamoto,<sup>1</sup> Andrew Seeber,<sup>1</sup> Anais Cheblal,<sup>1,2</sup> Chihiro Horigome,<sup>1,4</sup> Ulrike Naumann,<sup>3</sup> and Susan M. Gasser<sup>1,2,6,\*</sup>

<sup>1</sup>Friedrich Miescher Institute for Biomedical Research, Maulbeerstrasse 66, 4056 Basel, Switzerland

<sup>2</sup>University of Basel, Faculty of Natural Sciences, 4056 Basel, Switzerland

<sup>3</sup>Novartis Institutes of Biomedical Research, 4002 Basel, Switzerland

<sup>4</sup>Present address: Institute of Quantitative Biology, University of Tokyo, Bunkyo-ku, Tokyo 113-0032, Japan

<sup>5</sup>These authors contributed equally

<sup>6</sup>Lead Contact

\*Correspondence: [susan.gasser@fmi.ch](mailto:susan.gasser@fmi.ch)

<https://doi.org/10.1016/j.celrep.2018.07.102>

## SUMMARY

Multiple pathways regulate the repair of double-strand breaks (DSBs) to suppress potentially dangerous ectopic recombination. Both sequence and chromatin context are thought to influence pathway choice between non-homologous end-joining (NHEJ) and homology-driven recombination. To test the effect of repetitive sequences on break processing, we have inserted TG-rich repeats on one side of an inducible DSB at the budding yeast *MAT* locus on chromosome III. Five clustered Rap1 sites within a break-proximal TG repeat are sufficient to block Mre11-Rad50-Xrs2 recruitment, impair resection, and favor elongation by telomerase. The two sides of the break lose end-to-end tethering and show enhanced, uncoordinated movement. Only the TG-free side is resected and shifts to the nuclear periphery. In contrast to persistent DSBs without TG repeats that are repaired by imprecise NHEJ, nearly all survivors of repeat-proximal DSBs repair the break by a homology-driven, non-reciprocal translocation from ChrIII-R to ChrVII-L. This suppression of imprecise NHEJ at TG-repeat-flanked DSBs requires the Uls1 translocase activity.

## INTRODUCTION

Eukaryotic genomes are riddled with repeat sequences. Simple sequence repeats include mini-, micro-, and centromeric satellites, as well as telomeric repeats. Complex repeats include protein-encoding RNA and DNA transposons. Collectively, repeats comprise up to 70% of the human genome (Padeken et al., 2015). While the functions served by repeats are unclear, it is unequivocally established that they are a source of genomic instability (Kim and Mirkin, 2013; Leffak, 2017). Replication-induced

insertions, deletions, and breaks are enhanced at repeats, and spontaneous breaks within repeat elements compromise genome integrity, as they are prone to inappropriate translocations (Aksenova et al., 2013). In mammals, such events can lead to loss of heterozygosity, which in the case of oncogenes or tumor suppressor genes contributes to oncogenic transformation.

To suppress the risk of nonreciprocal or unequal crossovers, the repair of double-strand breaks (DSBs) in repetitive DNA is accompanied by the relocation of the repeat-flanked DSB away from the repetitive sequence domain prior to resection and the loading of Rad51 (Amaral et al., 2017). Only then can single-strand invasion and homologous recombination (HR) occur. This was shown for budding yeast, where breaks in the repetitive rDNA shift from the nucleolus prior to repair by HR (Torres-Rosell et al., 2007), and for breaks that occur within centromeric heterochromatin of both *Drosophila* (Chiolo et al., 2011) and mouse cells (Tsouroula et al., 2016). In both yeast and flies, this relocation has been shown to depend on sumoylation of break-associated factors (Horigome et al., 2016; Amaral et al., 2017). In budding yeast, poly-sumoylation is implicated in the relocation of irreparable DSBs to the nuclear pore complex, which favors alternative recombination-mediated repair pathways like break-induced replication (BIR) (Horigome et al., 2016). Satellite-embedded breaks in *Drosophila* similarly relocate to nuclear pores, although repair outcomes were not monitored (reviewed in Amaral et al., 2017).

Telomeric repeats pose a special case as they normally demarcate a natural DNA end that must be protected from both non-homologous end joining (NHEJ) and HR, in order to prevent chromosomal end-to-end fusions. In most eukaryotes, telomeres contain tandem TG-rich repeats. In budding yeast, the irregular (TG<sub>1-3</sub>)<sub>n</sub> repeat covers 300 to 600 bp, while the mammalian terminal TTAGGG repeat can extend hundreds of kilobases (Palm and de Lange, 2008). These sequences are bound by sequence-specific DNA binding proteins and their ligands, forming the telosome. The telosome protects the eukaryotic genome from erosion during genomic replication, mediates short telomere elongation in S phase by nucleating





telomerase-mediated repeat extension, and prevents the recognition of chromosome ends as breaks. All three actions attenuate DNA damage checkpoint activation that would arrest the cell cycle to promote recombination-mediated repair (Symington and Gautier, 2011).

In contrast to telomeric ends, proteins recruited to internal DSBs process the ends for repair and trigger a checkpoint response. In budding yeast, DSBs are initially sensed by both yKu and the Mre11-Rad50-Xrs2 (MRX) complex (Mre11, Rad50, Nbs1 in mammals); MRX in turn recruits Tel1 kinase (ATM). If end ligation is not immediate, MRX makes a single-strand nick distal to the break, to initiate short-range resection (Cannavo and Cejka, 2014). The single-stranded DNA (ssDNA) is then extended by a second set of partially redundant enzymes, namely, Exo1, Dna2, and Sgs1 (Nicolette et al., 2010). Resection is more efficient in S phase than in G1 phase, and robust resection favors repair by HR over NHEJ, as long as a homologous template is available (Symington and Gautier, 2011). The Ku70/80 heterodimer competes for MRX and favors NHEJ (Langerak et al., 2011), which can either be precise or imprecise. Precise NHEJ entails error-free religation, while imprecise NHEJ occurs after limited resection or trimming and leads to short deletions (Sfeir and Symington, 2015). Independent of the repair pathway, the two sides of a break must be held together. This is achieved in part by MRX, which can be recruited to breaks by the single-strand DNA binding factor, replication protein A (Seeber et al., 2016).

It is noteworthy that short yeast telomeres in telomerase-deficient strains and internal HO endonuclease-induced DSBs that lack homologous donors behave similarly with respect to nuclear organization: both shift to the nuclear envelope (NE) (Nagai et al., 2008). Short telomeres bound by recombination proteins accumulate at nuclear pores (Khadaroo et al., 2009), as do difficult-to-repair DSBs. Both depend on sumoylation and the SUMO-targeted ubiquitin ligase (STUbL) Slx5/Slx8 (Horigome et al., 2016; Churikov et al., 2016). Slx5/Slx8 is also required to maintain telomere length by asymmetric strand invasion and elongation, called ALT (alternative lengthening of telomeres) or BIR (Azam et al., 2006). Differentiating internal DSBs from short telomeres is the fact that short telomeres present a free end, while at DSBs two ends are held together.

There are many sumoylated proteins found at DSBs, including Htz1, Ku, RPA, Rad51, and Rad52 (Cremona et al., 2012; Kalocsay et al., 2009), while at short telomeres, Rap1 is also sumoylated (Lescasse et al., 2013). The binding of SUMO-targeted ubiquitin ligase subunit Slx5 to both poly-SUMO chains and to Nup84 are needed for the localization of telomeres (Churikov et al., 2016) and DSBs (Horigome et al., 2016) to nuclear pores for BIR or ALT, and the impaired relocation and damage survival phenotypes of *slx5* or *slx8* strains are epistatic with *nup84Δ* (Nagai et al., 2008). This mechanism is conserved, as homologs of the SUMO E3 ligase Siz2 and Slx5/Slx8 are similarly implicated in the sequestration of heterochromatic DSBs to nuclear pore complexes in *Drosophila* (Amaral et al., 2017).

Here, we sought to understand how a repetitive TG-rich sequence alters the processing and repair of an internal DSB in budding yeast. We added a telomeric TG-rich sequence to the centromere-proximal side of the natural HO endonuclease cleavage site at the *MAT* locus on ChrIII. Only the TG-rich side

of the break showed no MRX recruitment nor end resection, which allowed the two ends to separate and acquire very high levels of local movement. The non-repetitive, distal side of the break was efficiently resected and then bound by Mps3 at the nuclear envelope, whereas the TG-rich side resisted resection and was elongated by telomerase. Imprecise NHEJ was suppressed by the TG sequence and the surviving yeast colonies underwent homology-dependent, nonreciprocal translocation of the distal arm of ChrIIIR to ChrVIII. This required a putative SUMO-targeted ubiquitin ligase, Uls1. In the absence of Uls1 there is no increased movement despite normal end resection, and ablation of the Uls1-associated translocase activity increased imprecise NHEJ efficiency. Thus, the presence of Rap1-binding TG repeats near breaks alters MRX recruitment and end-to-end tethering, and impairs imprecise NHEJ, favoring nonreciprocal translocations. The latter event resembles genome rearrangements observed in human cancers.

## RESULTS

### TG Repeats Affect Nuclear Envelope Interactions of a Persistent DSB

The budding yeast genome has relatively little interstitial repeat sequence and lacks centromeric satellite arrays. The introduction of internal repeats leads to replication fork stalling and both the expansion and reduction of the initial repeat (Kim and Mirkin, 2013; Leffak, 2017). Inserts of 120 bp of (TGTGTGGG)<sub>15</sub> can lead to gross chromosomal rearrangements, translocations, and acentric minichromosomes (Aksenova et al., 2013), yet how internal repeats influence break processing was never determined. To examine this, we inserted telomeric repeats on the centromeric side of the HO endonuclease cleavage site at the *MAT* locus on yeast chromosome III (Figure 1A), such that the G-rich strain is oriented 5' to 3' and would create a TG-rich overhang if resected.

The induction of Gal1p:HO by galactose led to rapid cleavage at the HO cut site with efficiencies that were comparable with or without inserted repeats (Figure 1B). We note that the presence of 250 bp of TG (Tg250), unlike 80 bp (Tg80), tethers the intact *MAT* locus at the nuclear envelope prior to cleavage (Figures 1C and S1), likely reflecting Sir4 binding and SIR-mediated transcriptional repression (Gartenberg et al., 2004).

We examined whether the short Tg80 insert would affect the efficiency of DSB relocation to the nuclear envelope by tracking LacI-GFP after Gal1p:HO induction. After 100 min of continuous HO induction, the *lacO*-tagged Tg0 and Tg80 constructs had both shifted significantly toward the Nup49-CFP tagged nuclear rim. However, the kinetics of relocation differed: at time points of 40 and 70 min, the Tg80 DSB was not enriched at the nuclear envelope, unlike the Tg0 break (Figure 1D). The Tg250 locus, on the other hand, was peripheral prior to cleavage and remained there after HO induction (Figure S1).

There are at least two characterized sites of damage binding at the nuclear envelope, the nuclear pore complex and the SUN domain protein Mps3 (Horigome et al., 2014). Persistent breaks in G1- and S-phase cells shift to nuclear pores, while resected ends in cells lacking a homologous template bind Mps3 in S or G2 phase (Horigome et al., 2014). We therefore examined

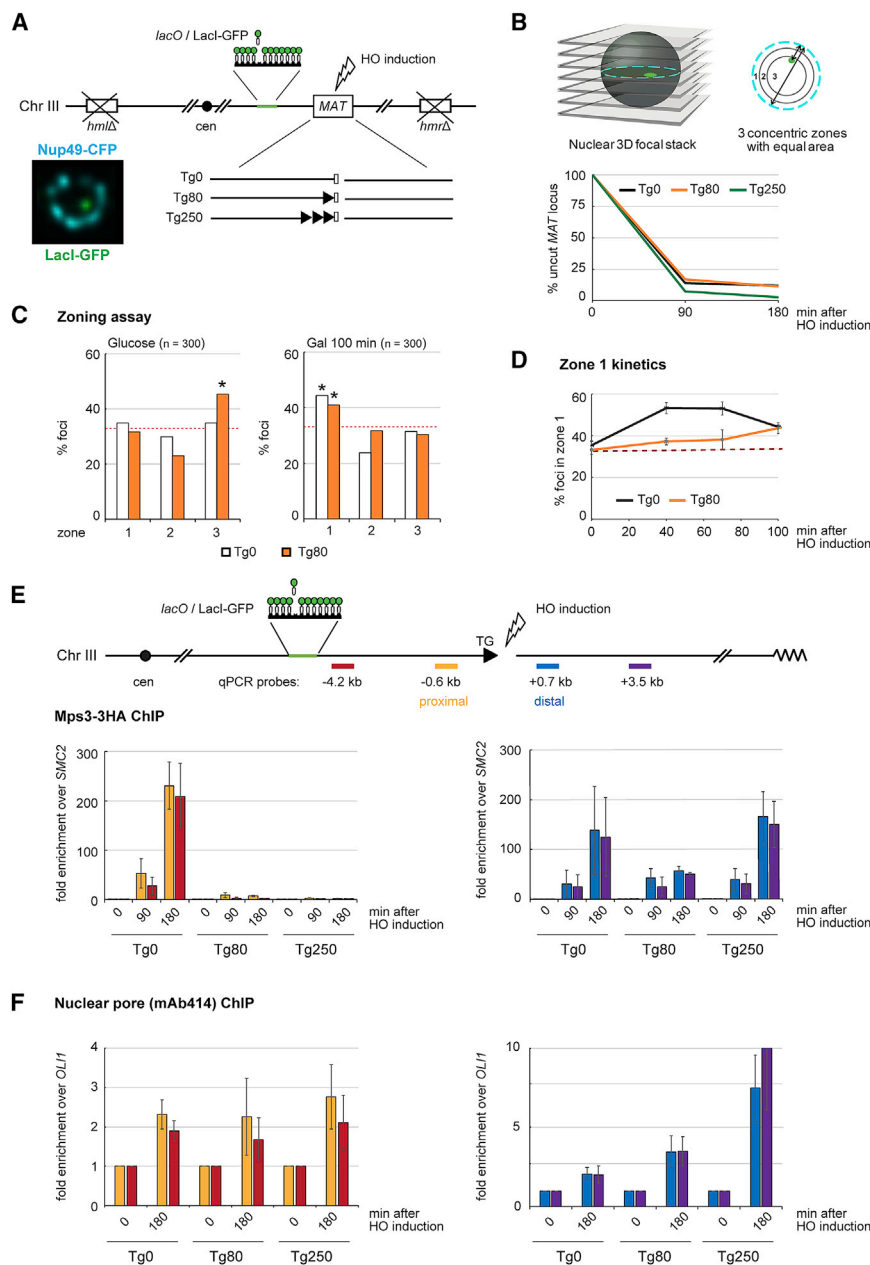


**Figure 1. Telomeric Repeats at a Persistent DSB Affect Relocalization Timing and Anchorage Site**

(A) TG-flanked DSB constructs with 80 or 250 bp of  $(TG_{1-3})_n$  (Gilson et al., 1993) as shown at the *MAT* locus (ChrIII) with 256 *lacO* repeats at 4.6 kb. *HML* and *HMR* loci are deleted, and CFP-Nup49, Lacl-GFP, and Gal1p::HO-expressing constructs are integrated. A single-plane confocal image with Nup49 and *MAT* signals is shown at left.

(B) Zoning assay used in (C): the ratio of locus distance to nuclear envelope divided by the nuclear diameter is determined in the focal plane in which the Lacl-GFP spot is brightest. Ratios are binned into three equal concentric zones of equal surface. HO cleavage efficiency at 90 and 180 min of HO induction monitored by qPCR in GA-8860 (Tg0), GA-8119 (Tg80), and GA-8502 (Tg250). HO-cut site Ct values were normalized to an amplicon in *SMC2* and were further normalized to the ratio at time point 0. Experiments were done in triplicate, and error bars are not shown as  $SD < 5\%$ .

(C) Zoning assay for GFP-tagged *MAT* locus as in (B), on glucose (left) or 100 min after HO induction on galactose (right) in Tg0 (GA-8861, white) and Tg80 (GA-8119, orange) strains.  $n$  = nuclei scored. Red dotted line indicates a random distribution, or 33% in each zone. \*significantly non-random distribution using  $\chi^2$  test versus random (degree of freedom, 2; confidence limit, 95%).

(D) Percentage of GFP-tagged foci in zone 1 after HO induction in Tg0 (GA-8861) and Tg80 (GA-8119). Error bars, mean values of three independent experiments  $\pm$  SEM.  $n$  = 80 for each strain and experiment; red dotted line, random.

(E) ChIP of HA-tagged Mps3 in Tg0 (GA-8306), Tg80 (GA-8633), and Tg250 (GA-8845) at 0, 90, and 180 min after HO induction. The four qPCR probes (color-coded) are shown relative to the DSB.

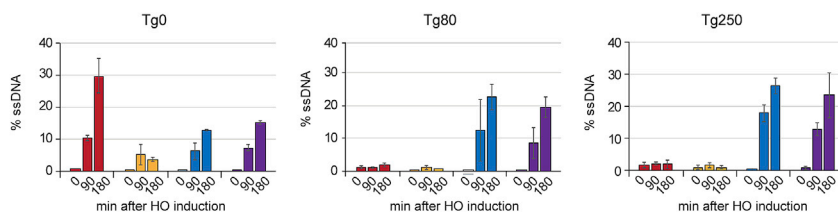
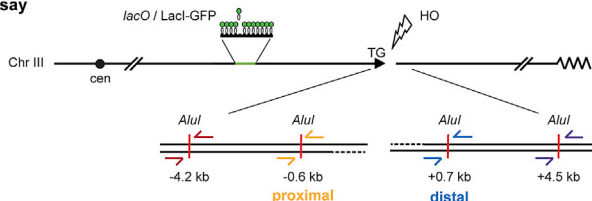
(F) Nuclear pore ChIP using Mab414 in Tg0 (GA-8860), Tg80 (GA-8119), and Tg250 (GA-8502) at 0 and 180 min after HO induction is quantified using qPCR probes; (E) and (F) each show data from two biological replicates, amplified in triplicate and presented as mean values  $\pm$  SEM.

whether the presence of Tg80 or Tg250 near a DSB alters perinuclear anchorage site. Using chromatin immunoprecipitation (ChIP) for nuclear pores and Mps3, we scored for interaction on either side of the break (Figure 1E). The Tg0 DSB interacted with Mps3 on both sides at 90 and 180 min after HO induction, while the Tg80-flanked break bound Mps3 exclusively on the non-TG side (Figure 1E). The same was observed for the cleaved Tg250 construct (Figure 1E). Thus, the presence of TG repeats led to asymmetric Mps3 binding, with the TG-containing end failing to bind Mps3. Low-level interaction with nuclear pores was detected in all constructs for both break sides (Figure 1F).

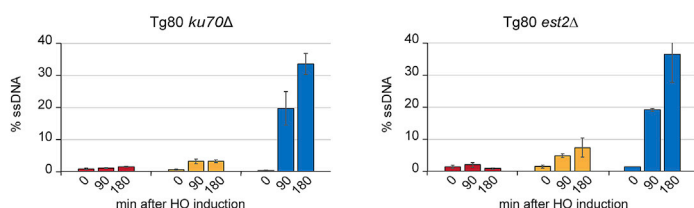
### Resection and MRX Binding Are Blocked by TG Repeats at an Internal HO-Induced DSB

Given that the interaction of a DSB with Mps3 requires end resection (Horigome et al., 2014), we hypothesized that the TG-rich inserts might impair resection at the HO cut site. We therefore monitored the amount of exposed ssDNA following HO endonuclease induction at either 90 or 180 min, using a restriction enzyme-based method (Zierhut and Diffley, 2008). Because *Alu1* only cleaves dsDNA, the generation of ssDNA by end resection will block cleavage at its cognate sites near a resected DSB. By monitoring amplification efficiency at *Alu1* consensus, we could score the extent and efficiency of resection

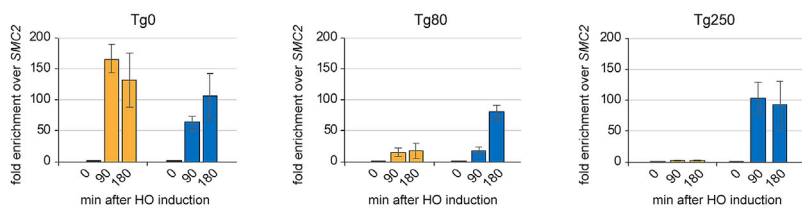
**A Resection assay**



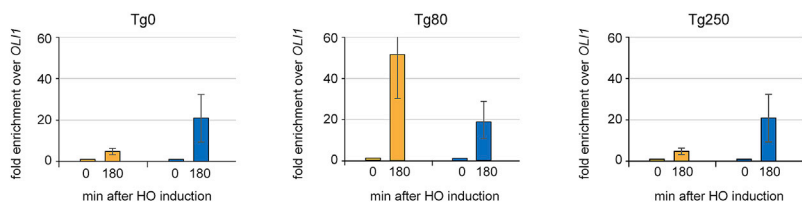
**B Resection assay**



**C Rad50-PK ChIP**



**D Ku70 ChIP**



around the break, which was proportional to the intensity of the *Alu1*-spanning qPCR bands (Figure 2A).

In the Tg0 strain, we detected nearly equal resection on both sides of the break after 90 min on galactose (Figure 2A), with the centromere-proximal side showing more extensive resection by 180 min. In contrast, in the strains bearing a Tg80 or Tg250 insert, little or no resection was scored on the TG-containing side of the break, even after 180 min, although resection proceeded efficiently on the distal side of the same break (Figure 2A). We hypothesized that yKu or telomerase might bind and block the Tg80 repeats, given that Tg80 in a subtelomeric location is recognized as short telomere in need of elongation (Negrini et al., 2007). However, the resection block was not alleviated by deletion of yKu nor of the catalytic subunit of telomerase, Est2 (Figure 2B). There was limited improvement in resection

**Figure 2. TG Repeats at a DSB Impose a Strong Block to 5'-End Resection and Inhibit MRX Binding**

(A) A resection assay monitors ssDNA at indicated *Alu1* sites in Tg0 (GA-8861), Tg80 (GA-8119), and Tg250 (GA-8502) strains, following 0, 90, and 180 min of HO induction. Results were normalized to an *Alu1*-free region in *SMC2*. Two biological replicates, amplified in triplicate, are presented as mean values  $\pm$  SEM.

(B) Absence of either yKu70 (Tg80 *ku70Δ*; GA-9553) or telomerase (Tg80 *est2Δ*; GA-9005) does not release the resection block on the TG side of the DSB. Resection from two biological replicates, amplified in triplicate and presented as mean values  $\pm$  SEM.

(C) Anti-PK ChIP of MRX subunit Rad50-PK in Tg0 (GA-9519), Tg80 (GA-9549), and Tg250 (GA-9521) at the indicated times after HO induction.

(D) ChIP as in (C), but for Ku70 in Tg0 (GA-8861), Tg80 (GA-8119), and Tg250 (GA-8502) strains, 0 and 180 min after HO induction. Fold enrichments over the mitochondrial locus *OLI1* were normalized to levels at time 0. (C) and (D) are three experiments shown as mean  $\pm$  SEM.

on the Tg80 side of the break upon over-expression of Exo1, which drives the extended resection at DSBs (Figure S2).

The 5'-end resection is generally initiated by the MRX complex and requires the ATPase activity of Rad50 (Deshpande et al., 2014). Therefore, we monitored the recruitment of MRX to the DSB by performing ChIP for a fully complementing PK-tagged Rad50 (Seeber et al., 2016). As expected, we find Rad50 recruited equally to both sides of the break in the Tg0 strain, enabling MRX to bridge the DNA ends and initiate resection on both sides (Figure 2C, left graph). In contrast, in strains carrying either the Tg80 or Tg250 insert, we observe strongly reduced Rad50 binding on the TG side

of the break, while its recruitment to the distal side was readily detected, at levels equivalent to the Tg0 strain (Figure 2C). Previous studies suggested that natural short telomeres have a reduced complement of Rap1-Rif1-Rif2, which allows more MRX recruitment (Shore and Bianchi, 2009). This appears not to occur at a Tg80-proximal DSB at *MAT*, where the TG repeats block MRX binding, leading to an asymmetrical processing of the two sides of the break.

Although Ku does not affect resection, it might influence MRX association. Therefore, we monitored the presence of yKu on either the TG-rich or the distal side of Tg80- or Tg250-flanked HO cuts by ChIP-qPCR. As presented in Figure 2D, in Tg0, Tg80, and Tg250-bearing strains, yKu70 showed equal enrichment by ChIP at 180 min on the distal side of the break. yKu70 levels were equal between Tg0 and Tg250 on the TG-rich side

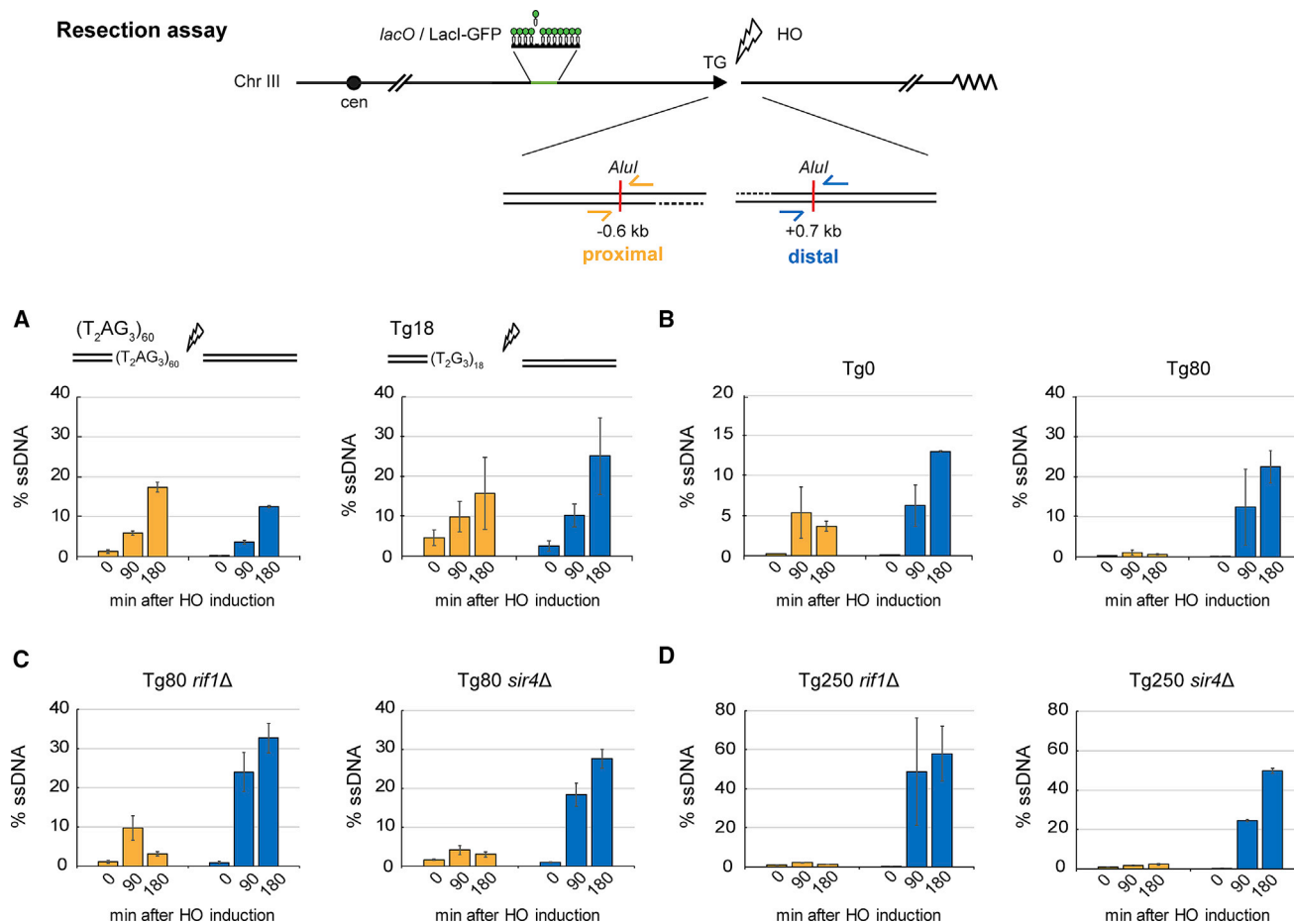


**Figure 3. TG Resection Block Requires Multiple Rap1 Motifs but Not Major Rap1 Ligands**

(A) Resection assay as Figure 2A after HO induction, using color-coded probes. Strain (T<sub>2</sub>AG<sub>3</sub>)<sub>60</sub> (GA-9823) contains human TTAGGG repeats that cannot bind Rap1, while Tg18 (GA-9824) harbors one Rap1 consensus. Two biological replicates, amplified in triplicate, are presented (mean values ± SEM).

(B–D) Resection assay at the DSB in Tg0 and Tg80 strains as in Figure 2A, in isogenic Tg80 and Tg250 strains (B); Tg80 *rif1*Δ (GA-9449), Tg80 *sir4*Δ (GA-9158) in (C); Tg250 *rif1*Δ (GA-8596) and Tg250 *sir4*Δ (GA-8587) in (D). Loss of Rif1 partially relieved the TG-resection block in Tg80 but not Tg250. Loss of Sir4 had no effect in either background. Data of GA-8596 and GA-8587 are mean values of three technical replicates ± SEM; data of GA-9449 and GA-9158 are mean values of three biological replicates ± SEM.

but were strikingly enriched in Tg80 (Figure 2D). This latter may reflect Ku's role in telomerase recruitment (Bertuch and Lundblad, 2003), because Tg80, but not Tg250, triggers elongation (Ribeyre and Shore, 2012).

### Sequence and Length of TG Repeats Control the Resection Block at TG-Flanked DSBs

The asymmetric binding of MRX at the Tg80 DSB is a likely cause of the differential processing of the two DNA ends, yet why should MRX bind asymmetrically? To ask whether it stems from the repetitive nature of the Tg80 DNA or the binding of Rap1, the (TG<sub>1-3</sub>)<sub>n</sub> ligand, we replaced the yeast repeat with 60 bp of human telomeric repeat and monitored end resection. The human (TTAGGG)<sub>n</sub> repeat is known to recruit telomerase for elongation in yeast, although Rap1 does not bind it with significant affinity (Brevet et al., 2003; Ribaud et al., 2012). Using the *Alu1*-amplicon method, we found that the human repeat allowed

efficient resection on both sides (Figure 3A), unlike the Tg80 insert (Figure 3B), arguing that Rap1 binding, rather than a G-quartet forming sequence, blocks end resection. Consistently, the Tg250 insert with 14 Rap1 binding sites (Gilson et al., 1993), was an even more effective barrier to resection and MRX binding than Tg80, while a single high-affinity Rap1 consensus (Tg18) functioned like Tg0 (Figures 3A and 3B).

A previous study inserted a similar Tg80-flanked HO cleavage site in a telomere-proximal region and found that the C terminus of Rap1 inhibits MRX binding to the break in a Rif1-dependent manner (Hirano et al., 2009). A second Rap1C ligand, Sir4, competes for Rif1 binding (Moretti et al., 1994; Wotton and Shore, 1997) and is recruited to DSBs (Martin et al., 1999). Therefore, we tested the effect of either Rif1 or Sir4 deletion on Tg80 resection. While the loss of Rif1 slightly improved resection on the Tg80 side at 90 min, this impact did not persist at 180 min and was not detectable at the Tg250-flanked break. Loss of Sir4

also showed no significant increase in resection (Figures 3C and 3D), and neither Tg80 nor Tg250 flanked sites showed any resection at the distal probe at  $-4.2$  kb in these mutants (data not shown). Given that the HO cleavage was equally efficient in all strains (Figure S3) and that resection on the non-TG side occurred, we conclude that the asymmetric resection pattern at the Tg80 DSB reflects the binding of Rap1, but not Rif1 or Sir4.

Rap1 is encoded by an essential gene in yeast, and it plays a major role in controlling the transcription of growth-regulatory genes. Because telomeres become dramatically extended upon loss of the Rap1 C-terminal domain, we next tried to monitor DSB resection at Tg80 either in a *rap1 $\Delta$ C* background or after depletion of a degron-tagged Rap1 protein. However, galactose-induced transcription of Gal1p:HO was compromised under both conditions, obviating this approach (data not shown). We cannot exclude that Rap1's affinity for (TG<sub>1-3</sub>)<sub>n</sub> itself impairs resection, although we note that Tbf1 binds the TTAGGG repeat with similar avidity without blocking resection.

### The TG-Rich and Non-TG Sides of the DSB Separate, Allowing Increased Break Movement

Recent work has shown that the binding of MRX to short ssDNA stretches at DSBs through the N-terminal OB fold of RPA1 contributes to holding the two break ends together (Seeber et al., 2016). Given that MRX is missing from the proximal side of the break in the Tg80 strain, we next asked whether the association of the two ends is affected by the Tg80 insert. We tracked the proximal TG-containing side of the break through the binding of Lacl-GFP to the *lacO* array, and of the distal non-TG side through Rad52-Ruby2, which binds after cleavage and resection (Dion et al., 2012; Lisby et al., 2004). Visible Rad52 foci assemble within 1 hr after HO induction (Miyazaki et al., 2004).

To estimate the impact of TG-repeats on end tethering, we first quantified the level of Rad52 and Lacl-GFP colocalization at 135 min after cut induction. Whereas 55% of the green and the red signals coincide in the Tg0 cells bearing both Lacl-GFP and Rad52-Ruby2 foci, only 14% of foci showed coincidence in Tg80 cells and 70% were fully separated (Figure 4A). This striking loss of tethering of Rad52 and Lacl-GFP tagged sides is consistent with the observed asymmetry in MRX binding to only one side of the break in the Tg80 strain (Figure 2D) and contrasts with break behavior at normal HO cut sites (Tg0), where 97% of the ends remained together (Seeber et al., 2016).

The induction of a persistent DSB increases local chromatin movement (Dion et al., 2012; Miné-Hattab and Rothstein, 2012), even though the ends remain linked through a protein bridge. Our ability to visualize the two sides of the same break by fluorescence microscopy (Lacl-GFP on the TG-side and Rad52-Ruby2 on the resected side) allowed us to monitor their dynamics independently using through-focal three-dimensional (3D) stacks acquired at 80-ms intervals on a total internal fluorescence (TIRF) microscope (Figure 4B). From the single-particle tracking (SPT) data taken at 2 hr after HO induction, we extracted characteristic statistical parameters of movement of either end, and calculated the extent of nuclear volume explored by either focus using mean square displacement (MSD) curves. From the plateau of constrained diffusive movement of multiple SPTs, we estimated the radius of the maximal volume of particle

movement, or  $R_c$ , before and after HO cut induction (Figure 4C). As expected, prior to DSB induction, the Lacl-GFP foci had similar subdiffusive movement in both Tg0 and Tg80 strains, and the Rad52-Ruby2 marker was not present (Figure 4C, left, uncut). Upon cut induction, movement of the Lacl-tagged focus increased more significantly at the Tg80 DSB than at the Tg0 break ( $R_c = 0.41 \mu\text{m}^2$  versus 0.37; Figures 4C and 4D; Figure S4 for SEs). Moreover, the Rad52-tagged distal side of the break had extremely robust movement in Tg80 cells, with  $R_c$  and diffusion constant ( $D_c$ ) values much larger than those of the Rad52 focus in Tg0. As expected, the Tg0 Rad52-Ruby2 and Lacl-*lacO* foci coincided and moved coordinately ( $R_c = 0.34$  versus 0.37; Figure 4D), in contrast to the uncoordinated movement observed at the Tg80 break.

Statistical parameters from time-lapse imaging (Amitai et al., 2017) confirm that the movement of the resected Rad52-bound side has thrice the diffusion coefficient and one-half the spring constant ( $K_c$ ) in the Tg80 background (Figure 4D). A particularly informative parameter of SPTs is the anomalous exponent ( $\alpha$ ), which indicates whether movement is directed, diffusive, or subdiffusive in character (Amitai et al., 2017). Intriguingly, the change in  $\alpha$  is significantly different on the two sides of the Tg80 break, but not of the Tg0 break;  $\alpha$  increases from 0.409 to 0.479 on the Tg80 side, while it decreases to 0.328 on the resected distal end (Figure 4D). Thus, the resected end not only moves more, but in a more diffusive manner. This coincides with the loading of Rad51, which is proposed to form a damage-induced stiffening of the ssDNA distal to DSB site (Miné-Hattab and Rothstein, 2012). This asymmetrical behavior of the two DNA ends in the Tg80 strain underscores the fact that the break ends are not tethered and are differentially processed for repair (Figure 4E). Given that increased chromatin mobility is thought to favor homology-dependent repair (Dion et al., 2012; Miné-Hattab and Rothstein, 2012), the increased mobility of the non-TG side at the Tg80 break suggests that it may be engaging in early steps of HR.

### Telomeric Repeats Near a Persistent DSB Inhibit Imprecise End Joining but Allow Alternative Repair

Haploid colony survival in face of persistent HO endonuclease expression requires a repair event that eliminates the HO consensus but retains the distal arm of ChrIII, which bears many essential genes. Given that the test strain lacks the homologous mating type loci that provide donor sequences for repair (Figure 5A), no intrachromosomal gene conversion events can occur. Thus, in a wild-type background, most survivors of continuous HO endonuclease expression repair the cut site by imprecise NHEJ, generating survivors with mutated cleavage consensus that resist HO endonuclease cleavage.

As shown in Figure 5B, the introduction of TG repeats on one side of the break reduced the frequency of colony formation on galactose by 76% (Tg80\*), in comparison to the survivor frequency at the native *MAT* (Tg0, wild-type [WT] *MAT*). Since survivor colony number was very low, we provided 300 bp of homology to the 3' of *MNT2*, a non-essential gene located in the left subtelomeric region of ChrVII, to the distal side of the HO consensus. Addition of this sequence restored the survival frequency of TG-flanked DSBs to a level roughly equivalent to the

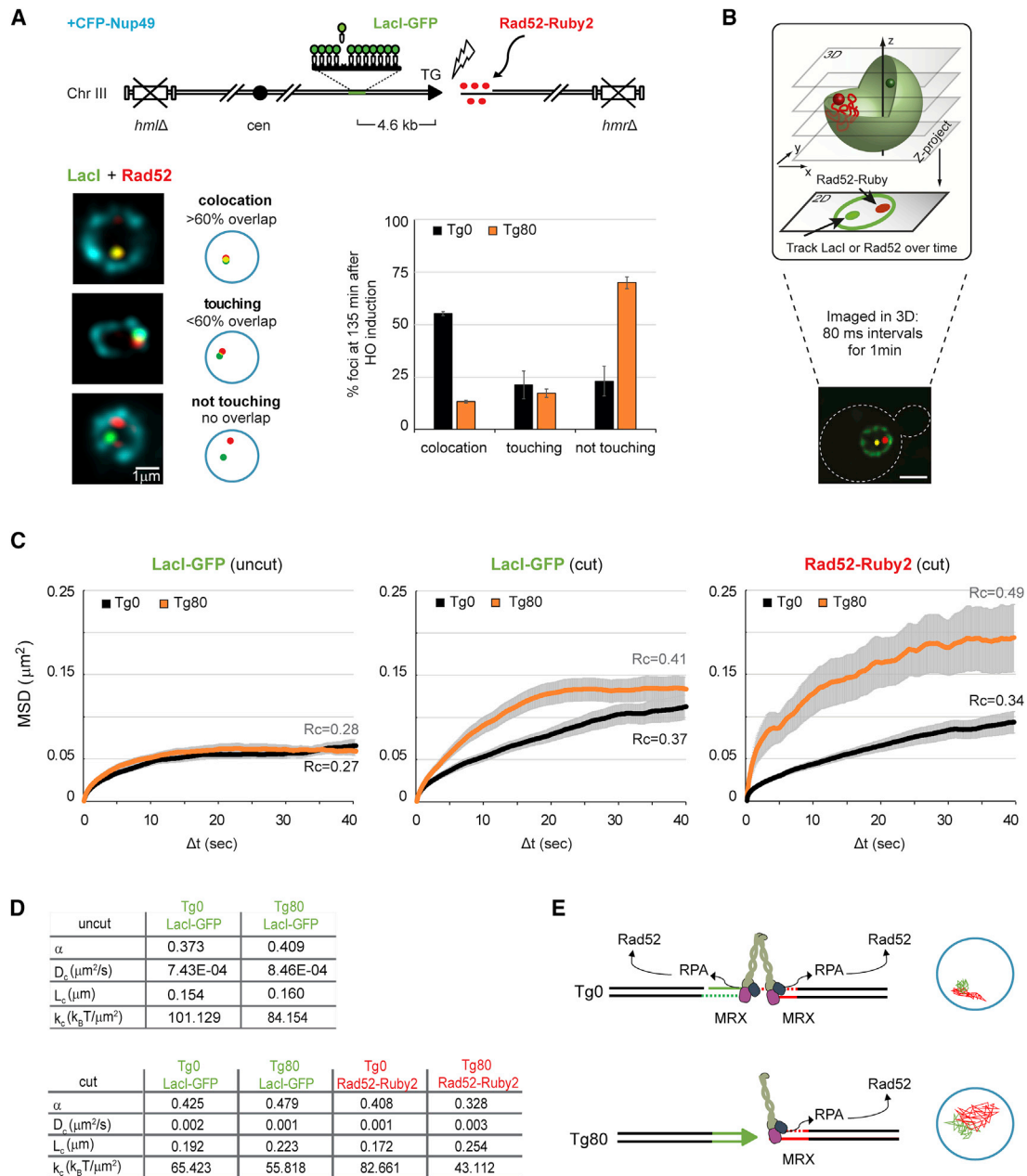


**Figure 4. Break Ends at TG-Flanked DSBs Separate and Move in an Uncoordinated Fashion**

(A) System used to visualize Rad52-Ruby2 on one side of the resected HO-induced non-TG break side, while the TG side was visualized by LacI-GFP. Criteria for juxtaposition of foci are shown. Percentage of colocalization of LacI-GFP and Rad52-Ruby2 foci in Tg0 (GA-9948) and Tg80 (GA-9912) are quantified at 135 min after HO induction. Cleavage efficiency is >95%.  $n = 80$  cells per strain per experiment; mean values of three independent experiments  $\pm$  SEM are shown.

(B) Scheme of LacI-GFP and Rad52-Ruby2 locus tracking by TIRF microscopy acquired at 80-ms time intervals for 1 min, starting 2 hr after HO induction.

(C) MSD analysis based on SPTs of LacI-GFP and Rad52-Ruby2 using Tg0 (GA-9948, black) and Tg80 (GA-9913, orange) strains, with and without HO cut. SPTs per strain and conditions are as follows: Tg0 uncut, 20; Tg0 Rad52-Ruby2, 23; Tg80 uncut, 23; Tg0 LacI-GFP, 25; Tg80 Rad52-Ruby2, 24; and Tg80 LacI-GFP, 24.  $R_c$ , radii of constrained movement ( $\mu\text{m}$ ), are indicated above each averaged track.

(D) Statistical biophysical parameters (Amitai et al., 2017) determined from single-particle trajectories as in (C). Numbers are means of at least 20 trajectories.  $\alpha$ , anomalous exponent;  $D_c$ , diffusion coefficient;  $k_c$ , effective spring constant;  $L_c$ , length of constraint (Amitai et al., 2017).

(E) In the absence of TG repeats, ends are held together by the MRX complex, which leads to end resection, RPA, Rad51, and Rad52 binding. In Tg80, MRX binds only the non-TG side. Ends separate, moving without constraint.

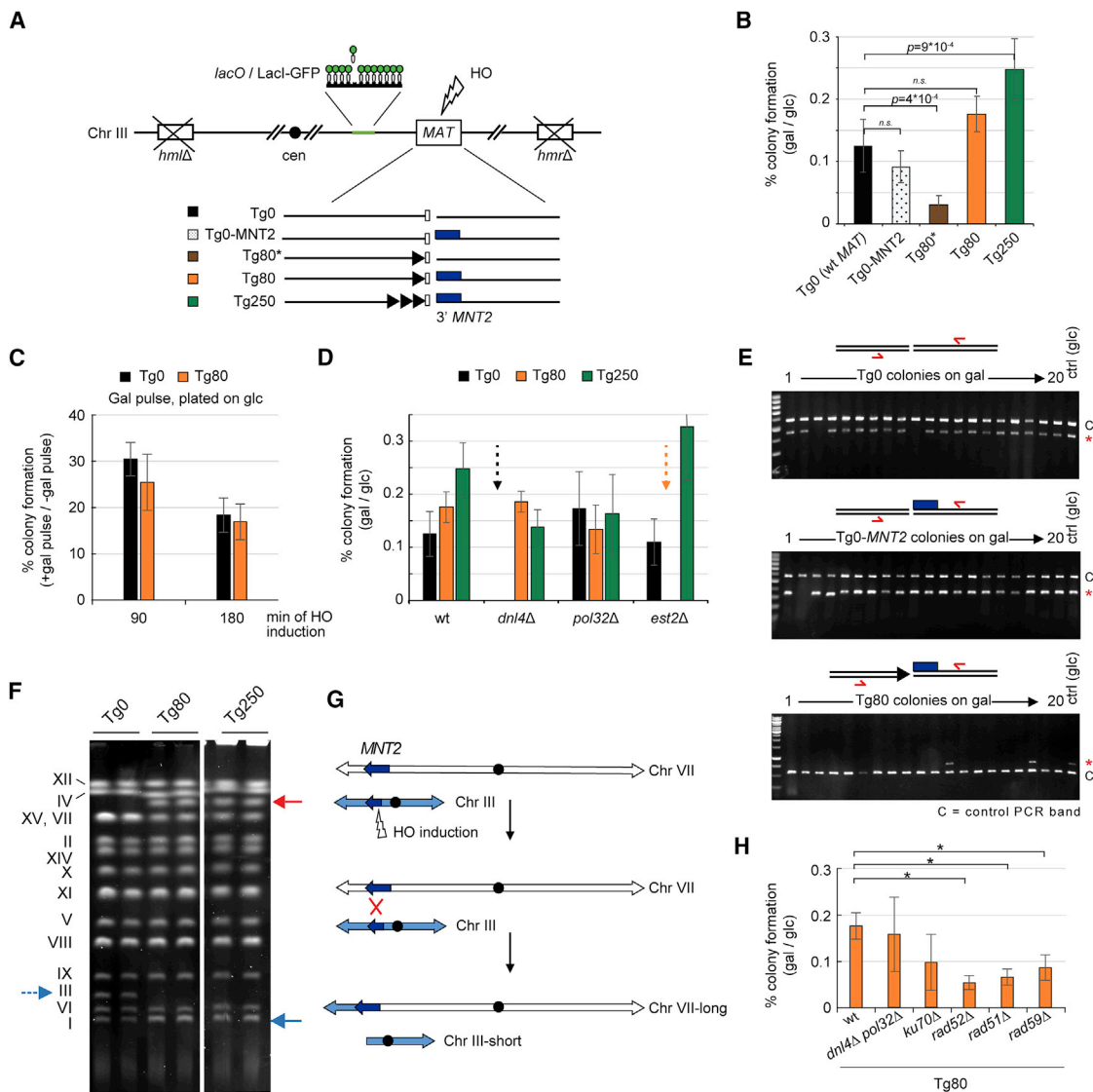


**Figure 5. Telomeric-Like Repeats Flanking a Persistent DSB Determine Repair Outcome**

(A) Scheme of TG-flanked DSB constructs at the *MAT* locus (Figure 1A): blue box, 300-bp *MNT2* homology relative to the HO cut site. (B) Colony formation on galactose (HO on, DSB cut) normalized to colony growth on glucose (HO off, DSB uncut) in GA-8861 (Tg0), GA-10085 (Tg0-MNT2), GA-9918 (Tg80\*), GA-8119 (Tg80), and GA-8502 (Tg250). Colony growth on galactose requires mutation of HO consensus. Mean ratios of four or more experiments  $\pm$  SD are shown; p values from a t test with 95% confidence interval between Tg0 and test constructs. n.s., nonsignificant ( $p > 0.05$ ). (C) Cultures of Tg0 and Tg80 were grown in 3% galactose for 90 or 180 min and then plated on glucose; colony outgrowth mostly represents precise end joining. Percentage of colony formation rate after the galactose pulse is normalized to colony formation rate on glucose without galactose. Mean  $\pm$  SD of three independent experiments is presented. (D) As (B) for the indicated Tg0, Tg80, and Tg250 strains with indicated mutations. Arrows mark no growth on galactose (Tg0 *dnl4Δ*; Tg80 *est2Δ*) based on three independent experiments (mean  $\pm$  SD). (E) For each construct, genomes from 20 colonies grown on galactose were used in parallel PCRs across the HO cut site (red asterisk), and within *SMC2* (labeled C). Pooled PCR products were resolved on agarose gels. Uncut control from the same strain (on glucose; uncut) is indicated. (F) CHEF gel analysis of two of ten independent galactose-grown colonies of Tg0, Tg80, and Tg250 survivors on galactose. For each strain, all ten karyotypes resembled the two shown. Dotted blue arrow, ChrIII; solid blue arrow, ChrI signal; red arrow, new band in Tg80 and Tg250 survivors. (G) Scheme for the *MNT2*-mediated nonreciprocal translocation from ChrIII to subtelomeric ChrVII. (H) As (B) in indicated mutants. Each column represents the mean of four independent experiments  $\pm$  SD. \*Statistical significance with a p value  $< 0.001$  (t test with 95% confidence interval, wild-type versus mutant).

Tg0 strain, while the presence of Tg250 instead of Tg80 at the DSB further increased survivor frequency (Figure 5B).

To see whether the presence of Tg80 affects rates of precise end joining, we first checked whether Tg80 inhibits NHEJ generally. For precise or imprecise end-joining reactions to occur, unblocked 3' OH and 5' PO<sub>4</sub> groups are needed together with DNA ligase 4 (Dnl4), resulting in end-to-end ligation and an intact ChrIII (Boulton and Jackson, 1996; Matsuzaki et al., 2008). Ligation following limited resection generates a mutated HO consensus, which prevents the continuous cleavage-ligation cycle that provokes cell-cycle arrest. To score NHEJ events in the presence of Tg80, we placed cells on galactose to induce the HO endonuclease for a limited time (90 or 180 min), and then plated the cells on glucose to repress HO endonuclease expression. This allows cells in which the DSB is repaired by precise NHEJ to grow, as well as those repaired by imprecise end joining. Intriguingly, we scored statistically equivalent rates of colony outgrowth in Tg0 and Tg80 strains under these conditions (Figure 5C). Given that cleavage was equally efficient (Figure S5A), we argue that Tg80 per se does not inhibit precise NHEJ.

As mentioned above, Gal1p:HO strains that survive on galactose generally undergo imprecise NHEJ, and thus survivor rates drop upon ablation of DNA ligase 4 (*dnl4Δ*). For the Tg0 strain on galactose, this is indeed the case (Figure 5D). However, the Tg80 and Tg250 survivor colonies on galactose were insensitive to the loss of DNA ligase 4 (Figure 5D). We further tested the deletion of *POL32*, which encodes the regulatory subunit of DNA polymerase  $\delta$  required for BIR (Lydeard et al., 2007). Neither altered the rate of survivor formation, arguing that neither NHEJ nor BIR mediates the repair in Tg80 DSB survivors.

We next tested directly for end-to-end re-ligation events in the galactose-grown survivors of Tg80 and Tg0 strains. Using colony PCR with primers that span the HO cut site, we scored for the regeneration of an intact *MAT* fragment, which arises from either precise or imprecise NHEJ (Figure 5E). As an internal control for PCR efficiency, we amplified the *SMC2* gene on ChrVI, and the PCR products were pooled for analysis by agarose gel electrophoresis. As shown for 20 randomly chosen Tg80 survivors (from 80 tested per strain), 18 had no PCR product from primers that span the HO consensus (Figure 5E). This argues for a repair event that does not restore an intact ChrIII (Figure 5E). In contrast, nearly all Tg0 and Tg0-HO-MNT2 survivors of continuous HO induction restored a contiguous *MAT* locus, as expected for repair by imprecise NHEJ (Figure 5E). We ruled out the possibility of cleavage site deletion by performing PCR on DNA isolated from the strain prior to galactose exposure (ctrl gic). These results argue that the Tg80 insert profoundly alters DSB repair of a persistent HO cut, possibly by suppressing imprecise NHEJ.

We checked the karyotypes of the survivors by pulsed-field gel electrophoresis (clamped homogeneous electric fields [CHEFs]) to examine karyotype after Gal1p:HO-induced cleavage. Genomic DNA from galactose-growth survivors for Tg0, Tg80, and Tg250 strains (ten each) was analyzed, and representative CHEF gels are shown (Figure 5F). Tg0 survivor karyotypes were identical to the reference genome, while all Tg80 and Tg250 survivors shared exactly the same changes: an additional chromosomal band appears above the doublet of ChrVII and

ChrXV (~1.1 Mb), and loss of ChrIII at 320 kb (Figure 5G). None of these changes was detected in cells that were grown continuously on glucose (Figure S5B).

We determined the precise chromosome rearrangements by performing whole Pacific Biosciences (PacBio) genome sequencing on three Tg80 and three Tg250 galactose survivors. In all those analyzed, the distal 100 kb of ChrIII had been translocated to the native *MNT2* gene in the left subtelomere of ChrVII. The recombination restored the intact *MNT2* reading frame precisely, indicating that strand invasion must have been initiated by the 300 bp of *MNT2* homology inserted at *MAT* (Figure 5G, PacBio data in Figure S5C). This explains the upshift of ChrVII to a slower migrating band, and the loss of full-length ChrIII. Loss of the ChrIII sequences distal to *MAT* results in a chromosome the size of ChrI (230 kb), explaining the increase in intensity of a band at 220 kb. No other recurrent variations were detected in the six colonies sequenced.

We examined the repair pathway/factors needed for this nonreciprocal translocation event in Tg80, by testing for survivors in strains lacking genes involved in HR, and in the *dnl4Δ pol32Δ* double mutant, which ablate NHEJ and BIR, respectively. The rate of Tg80 survivors in the *pol32Δ dnl4Δ* double mutant was like wild-type, but we found a significant reduction of survivors in strains lacking Rad51 and Rad52 (Figure 5H). Deletion of yKu or Rad59 had more minor effects (Figure 5H). In conclusion, the presence of TG repeats at a DSB blocked imprecise NHEJ and drove repair toward ectopic recombination, generating a nonreciprocal chromosomal translocation (Figure 5G).

### Telomerase Elongates the Tg80 Side of the DSB

The stability of ChrIII in the TG-DSB survivors requires that the TG-flanked end is stabilized or capped. While Tg250 is sufficient to serve as a telomere, Tg80 has been previously shown to be "critically short" and seed telomerase-mediated elongation. In the absence of telomerase (*est2Δ*), we no longer recovered survivors in the Tg80 background, while both the Tg0 and Tg250 yielded normal colony outgrowth (Figure 5D). To confirm that the right arm of ChrIII is elongated by *de novo* telomere extension at the Tg80-flanked cut, we performed telomere-specific PCR to monitor terminal TG-repeat length on DNA extracted from cells at specific time points after HO induction (Förstemann et al., 2000). Without telomere elongation, a single stable band is amplified, as shown in the left-hand gel for the Tg0 DSB (Figures S5D and S5E). The population of fragments larger than the expected PCR band in the Tg80 strain was absent upon mutation of the catalytic telomerase subunit, Est2 (Figure S5D), confirming that the Tg80 end is a substrate for telomerase.

Previous work argued that the activation of telomerase in S-phase cells leads to a release of telomeres from Mps3, their perinuclear anchorage site (Schober et al., 2009), which was restored only after telomere elongation (Ferreira et al., 2011). We therefore tested whether telomerase binding was responsible for the delayed relocation of the Tg80 end to the nuclear envelope (Figure 1). Upon deletion of the telomerase catalytic subunit Est2, the Tg80 side of the DSB shifted more rapidly to zone 1 (Figure S5F), confirming that telomerase action delayed Tg80 binding at the nuclear envelope (Ferreira et al., 2011).



## Sumoylation and the Translocase Uls1 Affect Nuclear Envelope Relocation of the Tg80 DSBs and Repair Outcome

The Tg80 break localization data argue that the TG insert initially prevents both resection and Mps3 binding (Figures 1B and 1C), while the TG-free side of the break showed strong association with Mps3, much like normal S-phase resected DSBs that lack an intact sister for repair (Horigome et al., 2014). Earlier work has implicated sumoylation and the poly-SUMO targeted ubiquitin ligase Slx5/Slx8 (a SUMO-targeted ubiquitin ligase enzyme) in the shift of damage to the Nup84 complex at pores, while mono-sumoylation was implicated in Mps3 binding (Horigome et al., 2016). The importance of SUMO recognition by SUMO-targeted ubiquitin ligase enzymes extends to the human homolog RNF4 in the relocation of damage to PML bodies for repair (Prudden et al., 2007), as well as to DSB relocation to nuclear pores in *Drosophila* (Amaral et al., 2017).

We therefore tested the role of the SUMO E3 ligase Siz2 and the Slx5/Slx8 SUMO-targeted ubiquitin ligase on the relocation of the Tg80 DSBs (Horigome et al., 2016). Surprisingly, the loss of Slx5/Slx8 had no effect, while the loss of the SUMO E3 ligase Siz2 completely impaired relocation to the nuclear envelope (Figure 6B). This suggests that sumoylation, but not the Slx5/Slx8 SUMO-targeted ubiquitin ligase, mediates Tg80 end relocation. We therefore examined the second putative SUMO-targeted ubiquitin ligase in yeast, Uls1 (or Ris1, Figure 6A), which in addition to harboring SUMO-interacting motifs (SIMs) and the ubiquitin E3 ligase RING finger, has a SNF2 DNA-dependent ATPase domain. Uls1 has been reported to be recruited to short telomeres in yeast, potentially recognizing sumoylated Rap1 (Lescasse et al., 2013). Indeed, deletion of the *ULS1* gene completely blocked relocation of the Tg80-proximal side of the DSB at *MAT* (Figure 6B).

Next, we examined whether Uls1 plays a role in the relocation of normal DSBs to either Mps3 or nuclear pores, by monitoring DSB association with Mps3 by ChIP in the *uls1Δ* strain, and by performing DSB colocalization with clustered pores (Horigome et al., 2014). This assay makes use of a well-characterized pore-clustering strain (*nup133ΔN*) as previously reported (Horigome et al., 2014), in which we monitor colocalization of the GFP-tagged break with the CFP-Nup49 tagged pore cluster. Figure 6C shows the percentage of cells in which the DSB was in contact with the Nup49-CFP pore cluster at the indicated times after HO induction. In the Tg0 strain, interaction increased from a background level of 20% to roughly 40% after HO cut induction. For Tg0, the increase required Slx5/Slx8 and the E3 SUMO ligase Siz2 (Horigome et al., 2016), but not Uls1 (Figure 6C). In contrast, for the Tg80 DSB, both *uls1Δ* and *siz2Δ* reduced DSB association with the periphery, while *slx8Δ* did not (Figure 6B). This suggests a unique role for the Uls1 ubiquitin ligase at breaks harboring telomeric repeats, consistent with the reported ability of Uls1 to bind sumoylated Rap1 at telomeres (Lescasse et al., 2013).

Because *uls1Δ* and *siz2Δ* reduce pore relocation, we next asked whether these mutants influence the pathway of repair at the Tg80-flanked DSB. We scored for NHEJ in survivor colonies grown on galactose by monitoring for a PCR band across the cleavage consensus. While the overall rate of survivor colony formation on galactose is roughly equal in all Tg80 strains (Figure S6B), the frequency of imprecise NHEJ over ectopic recombination events

increased 10-fold in either the *uls1Δ* or *siz2Δ* Tg80 strain (from 5% to 55%), but not in *slx8Δ* (Figure 6D), correlating reduced relocation with enhanced NHEJ. Although previous studies reported a role for Rif1 in facilitating NHEJ at normal DSBs (Mattarocci et al., 2017), we scored only a slight increase in NHEJ in *rif1Δ*, while *sir4Δ* mutants enhanced NHEJ much like the mutants *uls1Δ* and *siz2Δ* (Figure 6D). Rif1 may play a minor role in suppressing NHEJ at Tg80-flanked breaks, probably acting only at early-stage processing. In contrast, the 10-fold increase of imprecise NHEJ observed in the Tg80 *uls1Δ* and *sir4Δ* mutants suggests that Uls1 and Sir4 strongly inhibit NHEJ at Tg80 DSBs in wild-type strains. We examined whether this might be due to altered resection, yet loss of these factors had no effect on 5'-end resection at Tg80 breaks (Figures 3C and 6E). Importantly, in the case of Uls1, the suppression of NHEJ required its translocase activity (Figure S6C).

The increased chromatin movement observed at DSBs correlates with increased rates of recombination (Hauer et al., 2017; Dion et al., 2012), as enhanced diffusive movement is thought to enhance the efficiency of homology search. The Swi2/Snf2-like domain at the Uls1 C terminus could mediate chromatin remodeling and enhance movement; thus, we monitored break-induced chromatin movement at the Tg80 DSB in the absence of Uls1. MSD analysis of LacI-GFP (TG side) and Rad52-Ruby2 (non-TG side) foci was performed (as Figure 4D). *ULS1* deletion slightly reduced the basal subdiffusive chromatin movement even before HO induction (Figure 6F, left panel) and strongly reduced DSB movement on both sides of the HO-induced break in the Tg80 strain (Figure 6F, dotted lines). Moreover, the level of Rad52 foci in *uls1Δ* cells was reduced. Both of these observations correlate with the elevated rate of NHEJ repair in *uls1Δ* cells (Figure 6D). Thus more NHEJ correlates with less movement, and both were favored by *uls1Δ*.

In wild-type backgrounds, the TG-rich side of the Tg80 DSB failed to bind Mps3, and this coincided with reduced imprecise NHEJ. Consistent with earlier work, this argues that Mps3-mediated sequestration of resected breaks favors imprecise NHEJ over ectopic recombination. To see whether deletion of the Mps3 nucleoplasmic domain (*meps3ΔN*) reduces NHEJ, we monitored end joining by qPCR across the cut site in a strain with efficient NHEJ, that is, the Tg18 strain (Figure S6D). Indeed, imprecise end-joining repair of the Tg18-proximal break dropped by 50% in *meps3ΔN* cells compared to cells bearing intact Mps3 (Figure S6D). This confirms that DSB association with Mps3 protects from ectopic recombination after resection, and in some cases favors imprecise NHEJ.

Taken together, our results argue that poly-sumoylation and Uls1 binding at a TG-flanked DSB protect the end from NHEJ, while helping load telomerase (Figure 7). The binding of a resected DSB to Mps3 favors imprecise NHEJ, as long as the ends are held together, which is not the case at the Tg80-flanked break. At these, Uls1 counters NHEJ by antagonizing end-to-end tethering and increasing chromatin movement. This in turn enhances the homology search and the observed nonreciprocal translocation.

## DISCUSSION

Interstitial telomeric sequences (ITs) are present in many organisms and are recognized as markers of chromosome fragile

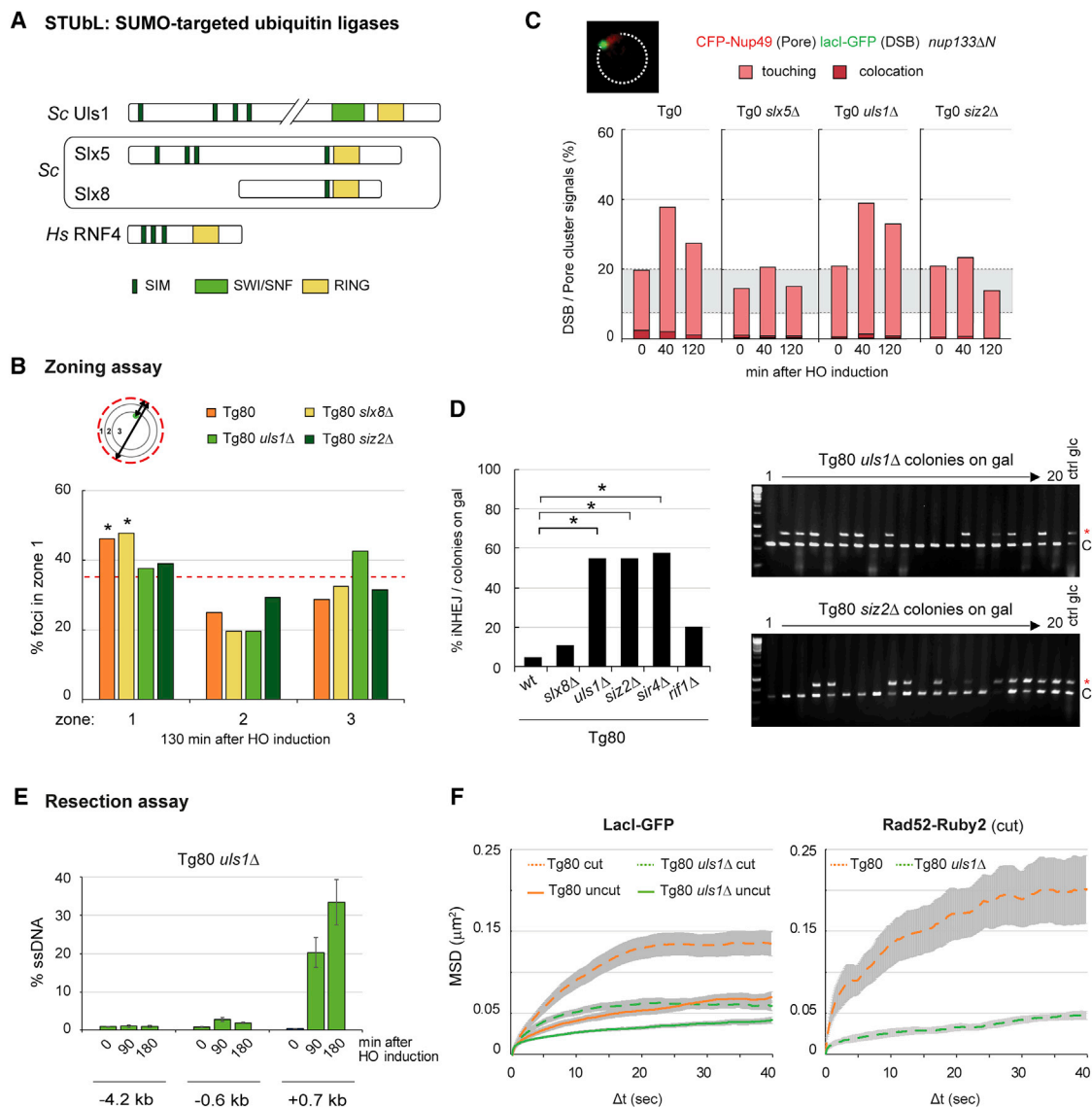


**Figure 6. Siz2 and Uls1 Control Relocation of the TG Side at the Tg80 DSB and Suppress NHEJ**

(A) Scheme of major yeast SUMO-dependent ubiquitin ligases (STUbLs) and RNF4 in man. Uls1 contains a SNF2-like ATPase as well as SUMO-interacting motifs (SIMs) and RING finger ubiquitin ligase domain.

(B) Zoning assay (Figure 1B) for DSB distribution at 130 min after galactose-induced HO expression. Strains used were Tg80 (GA-8119), Tg80 *slx8*Δ (GA-10050), Tg80 *uls1*Δ (GA-9855), and Tg80 *siz2*Δ (GA-9794). Mean values of three independent experiments ± SEM are shown. \*Non-random distribution in zone 1 ( $\chi^2$  test of random versus experimental distribution; degree of freedom, 2; confidence limit, 95%),  $p = 0.048$ .

(C) Co-localization of MAT with the pore cluster in *nup133*ΔN background, in wild-type (GA-7314), *slx5*Δ (GA-7969), *uls1*Δ (GA-8475), and *siz2*Δ (GA-7970) strains at specific times after HO induction. Pink and red colors indicate adjacency and colocalization, respectively (Horigome et al., 2016). Gray, random distribution zone based on theoretical tests.

(D) Indicated genes were deleted in the Tg80 strain (wild-type, GA-8119) generating GA-10050, GA-9855, GA-9794, GA-9158, and GA-9449. Graph presents the percentage of colonies repaired by imprecise NHEJ out of all survivors on galactose, as scored by qPCR across the HO cut site (Figure 1C).  $n = 60$  per strain. \*Statistical significance with a  $p$  value  $< 10^{-4}$  in a  $\chi^2$  test of wild-type and mutant with 95% confidence interval. Example gels showing 20 colonies of indicated strains are shown.

(E) Loss of Uls1 does not release the resection block on the TG side of the DSB in Tg80. Resection scored by ssDNA *AluI* assay (Figure 2A) with Tg80 *uls1*Δ (GA-9555). Probe distance from the HO consensus is shown. Three biological replicates, assayed in triplicate, are presented as mean values ± SEM.

(F) MSD analysis based on single-particle trajectories of Lacl-GFP and Rad52-Ruby2 in Tg80 (GA-9913, orange) and Tg80 *uls1*Δ (GA-10435, green), with and without HO induction (cut versus uncut). Tg80 control data are from Figure 4C. Videos analyzed per strain are as follows: Tg80 lacl-GFP uncut, 23; Tg80 Rad52-Ruby2, 28; Tg80 lacl-GFP cut, 28; Tg80 *uls1*Δ Lacl-GFP uncut, 43; Tg80 *uls1*Δ Rad52-Ruby2 cut, 25; Tg80 *uls1*Δ Lacl-GFP cut, 9. Rad52 foci in the Tg80 *uls1*Δ are rare due to elevated rates of NHEJ.

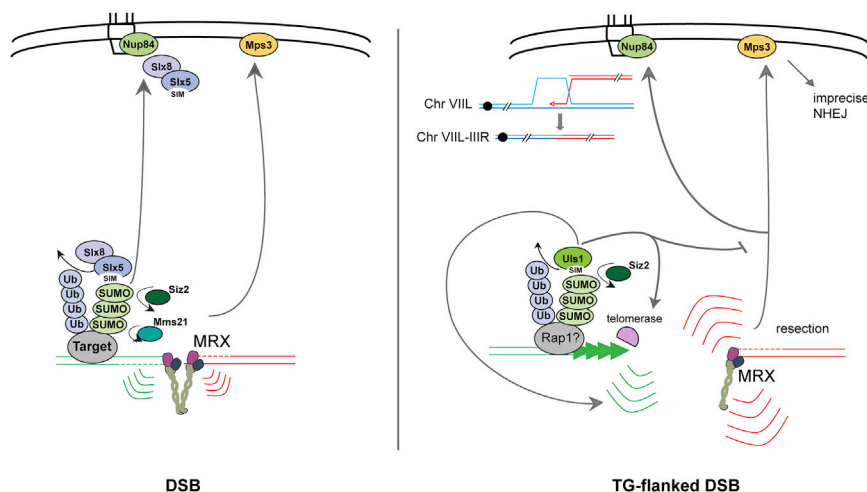


**Figure 7. Model for the Effect of TG-Rich Repeats on DSB Repair**

MRX binds and helps tether the ends of a Tg0 DSB together (Seeber et al., 2016). On the TG-rich side of a TG-flanked DSB, MRX binding is reduced, allowing the two ends to separate. Tg80 seeds telomerase, and once elongated, the end moves to the nuclear envelope, while the TG-free side, lacking end-to-end tethering, moves freely, favoring homology-driven ectopic recombination. The processing of Tg0 and Tg80 ends requires the translocase activity of Uls1 and sumoylation by the SUMO E3 ligase Siz2. Siz2 and Uls1 antagonize NHEJ.

on repair outcome in the Tg0 strain (Figure 5B). Thus, it is not sufficient to promote end movement. Rather, we argue that the asymmetrical binding of MRX coupled with the telomerase-seeding

sites (Ruiz-Herrera et al., 2009), hot spots for replication fork stalling, repeat expansion, deletion events (Aksenova et al., 2013), and nonreciprocal chromosomal rearrangements. It has been unclear whether ITSs influence the repair pathway or only generate more damage. By inserting a short stretch of yeast telomeric repeats next to a controlled HO cleavage site at the *MAT* locus, 80 bp of a TG-rich repeat was shown sufficient to significantly alter DSB repair outcome. Five Rap1 binding sites blocked resection of the TG-rich side of the break, allowing separation of the two break ends and enabling distinct repair mechanisms to act. MRX binding was reduced only on the repeat-containing side, while the opposite side was resected normally for HR and Rad52-mediated Rad51 loading. The distal side of the break shows dramatically increased subnuclear movement, which correlates with a nonreciprocal ectopic recombination event or chromosomal translocation. All survivor colonies of persistent HO endonuclease expression underwent the ChrIII-ChrVII translocation, while without the TG-rich insert, almost all undergo repair by imprecise NHEJ (Figure 5). This is striking because asymmetric chromosomal translocation at repeats is a frequent form of genomic instability in cancer cells. Mechanisms that suppress their occurrence are unknown.

We propose that the absence of MRX, which holds DSB ends together at TG-free DSBs (Seeber et al., 2016), and the ensuing increase in DSB movement, both attenuate NHEJ and enable the distal side of the break to engage in homology search. We note that loss of the translocase activity of the SUMO-targeted ubiquitin ligase, Uls1, or silencing factor Sir4, increase the rate of imprecise NHEJ over translocation (Figure 6 and S6C), but does not increase end resection on the TG-rich side of the break (Figures 3C and S5A). Thus, the resection-initiating role of MRX may not be the definitive parameter in repair pathway choice. Instead, MRX may influence repair outcome by recruiting Sae2 or Tel1, or it may simply hold the two sides of the break together, reducing their uncoordinated mobility (Seeber et al., 2016). We cannot exclude a role for the *MNT2* homology present at *MAT* in the enhanced end movement, yet the *MNT2* insert did not have a significant effect

capacity of  $(TG_{1-3})_n$  suppress imprecise NHEJ and promote ectopic HR.

Importantly, the nature of the repeat sequence present at the DSB can influence the pathway of repair. TTAGGG can seed telomerase, yet it does not significantly increase ectopic HR when it flanks the HO-induced break. Moreover, a single Rap1 binding site fails to have the same effect as a cluster of 5. We cannot attribute the repair outcome to the Rap1 ligand, Rif1, given that *rif1Δ* only slightly enhances imprecise NHEJ at the Tg80 break (Figure 6D). Stronger effects on repair were seen upon ablation of either the SUMO E3 ligase, Siz2, or the SUMO binding ATPase, Uls1. Both factors significantly suppress imprecise NHEJ (Figure 6). The recognition of poly-sumoylated Rap1 by Uls1 (Lescasse et al., 2013) may lead to the ubiquitination and degradation of Rap1 or other sumoylated targets at break sites. We note that the loss of Uls1 also reduces the exaggerated movement of the untethered ends, suggesting that its loss may restore MRX binding to the Tg80 end.

While the Siz2 SUMO ligase acts at both Tg0 and Tg80 DSBs, the effect of Uls1 appears to be specific for Tg80-adjacent breaks. At TG-free DSBs, it was shown that poly-sumoylation recruits the SUMO-targeted ubiquitin ligase Slx5/Slx8, which then mediates relocation of the DSB to nuclear pores (Horigome et al., 2016). This does not require Uls1 (Figure 6C). The opposite is true for the shift of Tg80 to pores: repeat-flanked damage depends on Uls1 and not on Slx5/Slx8 (Figure 6B). Uls1 has, in addition to SUMO binding motifs and a E3-like Ring finger, a unique ATP-dependent translocase activity, which is required to impair NHEJ at the Tg80 end (Figure S6C).

Besides these break-binding factors, we find that nuclear envelope binding sites influence repair outcome. The loss of the nucleoplasmic domain of the yeast Mps3 protein (*mps3ΔN*) led to increased spontaneous sister chromatid exchange (Horigome et al., 2014) and less imprecise NHEJ (Figure S6A). In contrast, DSB-pore interaction favored ectopic recombination pathways, BIR, and other nonreciprocal homology-driven events (Chung et al., 2015; Horigome et al., 2014).

### Telomeric Identity and DNA Repair Outcome

This work sheds new light on how cells safeguard telomeres: the (TG<sub>1-3</sub>)<sub>n</sub> sequence inhibits imprecise end joining in yeast, in a length-dependent manner. This explains why TG repeats are primarily found at telomeres; the largest internal (TG<sub>1-3</sub>)<sub>n</sub> stretch in budding yeast is <34 bp (Mangahas et al., 2001). From an evolutionary perspective, ITSs of (TG<sub>1-3</sub>)<sub>n</sub> repeats ≥ 80 bp would be destabilizing, inducing translocations at spontaneous DSBs. Whereas other researchers have invoked folded G-structures as an intrinsic means to block NHEJ and/or recombination at telomeres (Moriyama et al., 2017), the effect we see does not stem solely from TG richness. Human and yeast telomere repeats are similarly TG-rich, yet did not have the same impact. Intriguingly, an earlier study still saw MRX bound to a subtelomeric TG-flanked DSB, although end resection was reduced (Ribeyre and Shore, 2012). These authors did not score repair pathway choice, however, since all survivors simply lost the distal part of the chromosome, a nonlethal event in their strain. Because the ChrIII sequences distal to *MAT* are essential, our internal TG-flanked DSB more closely reflects ITS-associated breaks in mammalian cells.

In the human genome, short ITSs have been correlated with jumping translocations, a rare case of cytological aberrations in which a fragment of donor chromosome is translocated onto more than one recipient chromosome. This kind of nonreciprocal translocation is frequent in Prader-Willi syndrome and hematological malignancies (Miller et al., 2015; Rivera et al., 1990; Vermeesch et al., 1997). Previous work also reported several kinds of chromosome rearrangements favored by internal telomeric sequences in yeast (Aksenova et al., 2013). While fork stalling was suggested to drive these rearrangements, they may stem from TG-specific factors that favor ectopic recombination over end joining, by competing with MRX and preventing end-to-end tethering. We show in yeast that this correlates with an asymmetrical processing of DNA ends and nonreciprocal translocation events. We propose that asymmetrical end processing may be the critical feature that drives recombination-dependent, nonreciprocal translocations at a TG-flanked DSB. In our system, this required the activity of the SNF2-ATPase containing putative SUMO-targeted ubiquitin ligase, Uls1, which disfavors imprecise NHEJ. We speculate that, in mammals, the repair of repeat-flanked DSBs may be influenced by ATRX, a mammalian AAA+ translocase (Lovejoy et al., 2012), which suppresses repeat-induced translocations at ITSs.

### STAR★METHODS

Detailed methods are provided in the online version of this paper and include the following:

- KEY RESOURCES TABLE
- CONTACT FOR REAGENT AND RESOURCE SHARING
- EXPERIMENTAL MODEL AND SUBJECT DETAILS
  - Yeast Strains and Construction
- METHOD DETAILS
  - DNA Extraction for PCR
  - Fluorescence Microscopy
  - DSB Survival Assay by Colony Formation
  - Pulsed-Field Gel Electrophoresis (PFGE)

- Telomerase PCR at a Double Strand Break
- Chromatin Immunoprecipitation (ChIP)
- Resection Assay
- SMRTbell Library Construction for Sequencing
- PacBio RSII Sequencing
- QUANTIFICATION AND STATISTICAL ANALYSIS
- DATA AND SOFTWARE AVAILABILITY

### SUPPLEMENTAL INFORMATION

Supplemental Information includes six figures and three tables and can be found with this article online at <https://doi.org/10.1016/j.celrep.2018.07.102>.

### ACKNOWLEDGMENTS

We thank H. Ferreira for the Uls1 plasmids, J.E. Haber for yeast strains, and D. Shore for constructs and these three and J. Lingner (EPFL) for helpful advice. We thank E. Oakeley for supervising the PacBio sequencing, J. Eglinger, S. Bourke, and L. Gelman for advanced imaging, and M. Tsai-Pflugfelder for experimental support. I.M. was supported by the Swiss National Science Foundation NCCR Frontiers in Genetics PhD program, C.H. by a Marie Curie International Fellowship, and the Gasser laboratory by the Novartis Research Foundation and Swiss National Science Foundation Research Grant 310030B\_156936 awarded to S.M.G.

### AUTHOR CONTRIBUTIONS

I.M. performed experiments, interpreted results, and prepared figures and text. K.S. and N.D. performed experiments, interpreted results, and edited figures and text. A.S., A.C., I.Y., and C.H. performed experiments, interpreted results, and made figures. U.N. performed deep sequencing. S.M.G. supervised, interpreted results, and helped write the paper.

### DECLARATION OF INTERESTS

The authors declare no competing interests.

Received: March 24, 2018

Revised: June 7, 2018

Accepted: July 27, 2018

Published: September 4, 2018

### REFERENCES

- Aksenova, A.Y., Greenwell, P.W., Dominska, M., Shishkin, A.A., Kim, J.C., Petes, T.D., and Mirkin, S.M. (2013). Genome rearrangements caused by interstitial telomeric sequences in yeast. *Proc. Natl. Acad. Sci. USA* *110*, 19866–19871.
- Amaral, N., Ryu, T., Li, X., and Chiolo, I. (2017). Nuclear dynamics of heterochromatin repair. *Trends Genet.* *33*, 86–100.
- Amitai, A., Seeber, A., Gasser, S.M., and Holman, D. (2017). Visualization of chromatin decompaction and break site extrusion as predicted by statistical polymer modeling of single-locus trajectories. *Cell Rep.* *18*, 1200–1214.
- Azam, M., Lee, J.Y., Abraham, V., Chanoux, R., Schoenly, K.A., and Johnson, F.B. (2006). Evidence that the *S. cerevisiae* Sgs1 protein facilitates recombinational repair of telomeres during senescence. *Nucleic Acids Res.* *34*, 506–516.
- Bertuch, A.A., and Lundblad, V. (2003). The Ku heterodimer performs separable activities at double-strand breaks and chromosome termini. *Mol. Cell Biol.* *23*, 8202–8215.
- Boulton, S.J., and Jackson, S.P. (1996). Identification of a *Saccharomyces cerevisiae* Ku80 homologue: roles in DNA double strand break rejoining and in telomeric maintenance. *Nucleic Acids Res.* *24*, 4639–4648.
- Brevet, V., Berthiau, A.S., Civitelli, L., Donini, P., Schramke, V., Géli, V., Ascenzi, F., and Gilson, E. (2003). The number of vertebrate repeats can be

- regulated at yeast telomeres by Rap1-independent mechanisms. *EMBO J.* 22, 1697–1706.
- Cannavo, E., and Cejka, P. (2014). Sae2 promotes dsDNA endonuclease activity within Mre11-Rad50-Xrs2 to resect DNA breaks. *Nature* 514, 122–125.
- Chiolo, I., Minoda, A., Colmenares, S.U., Polyzos, A., Costes, S.V., and Karpen, G.H. (2011). Double-strand breaks in heterochromatin move outside of a dynamic HP1a domain to complete recombinational repair. *Cell* 144, 732–744.
- Chung, D.K., Chan, J.N., Strecker, J., Zhang, W., Ebrahimi-Ardebili, S., Lu, T., Abraham, K.J., Durocher, D., and Mekhail, K. (2015). Perinuclear tethers license telomeric DSBs for a broad kinesin- and NPC-dependent DNA repair process. *Nat. Commun.* 6, 7742.
- Churikov, D., Charifi, F., Eckert-Boulet, N., Silva, S., Simon, M.N., Lisby, M., and Géli, V. (2016). SUMO-dependent relocalization of eroded telomeres to nuclear pore complexes controls telomere recombination. *Cell Rep.* 15, 1242–1253.
- Cremona, C.A., Sarangi, P., Yang, Y., Hang, L.E., Rahman, S., and Zhao, X. (2012). Extensive DNA damage-induced sumoylation contributes to replication and repair and acts in addition to the mec1 checkpoint. *Mol. Cell* 45, 422–432.
- Deshpande, R.A., Williams, G.J., Limbo, O., Williams, R.S., Kuhnlein, J., Lee, J.H., Classen, S., Guenther, G., Russell, P., Tainer, J.A., and Paull, T.T. (2014). ATP-driven Rad50 conformations regulate DNA tethering, end resection, and ATM checkpoint signaling. *EMBO J.* 33, 482–500.
- Dion, V., Kalck, V., Horigome, C., Towbin, B.D., and Gasser, S.M. (2012). Increased mobility of double-strand breaks requires Mec1, Rad9 and the homologous recombination machinery. *Nat. Cell Biol.* 14, 502–509.
- Ferreira, H.C., Luke, B., Schober, H., Kalck, V., Lingner, J., and Gasser, S.M. (2011). The PIAS homologue Siz2 regulates perinuclear telomere position and telomerase activity in budding yeast. *Nat. Cell Biol.* 13, 867–874.
- Förstemann, K., Höss, M., and Lingner, J. (2000). Telomerase-dependent repeat divergence at the 3' ends of yeast telomeres. *Nucleic Acids Res.* 28, 2690–2694.
- Gartenberg, M.R., Neumann, F.R., Laroche, T., Blaszczyk, M., and Gasser, S.M. (2004). Sir-mediated repression can occur independently of chromosomal and subnuclear contexts. *Cell* 119, 955–967.
- Gilson, E., Roberge, M., Giraldo, R., Rhodes, D., and Gasser, S.M. (1993). Distortion of the DNA double helix by RAP1 at silencers and multiple telomeric binding sites. *J. Mol. Biol.* 237, 293–310.
- Hage, A.E., and Houseley, J. (2013). Resolution of budding yeast chromosomes using pulsed-field gel electrophoresis. *Methods Mol. Biol.* 1054, 195–207.
- Hauer, M.H., Seeber, A., Singh, V., Thierry, R., Sack, R., Amitai, A., Kryzhanovska, M., Eglinger, J., Holcman, D., Owen-Hughes, T., and Gasser, S.M. (2017). Histone degradation in response to DNA damage enhances chromatin dynamics and recombination rates. *Nat. Struct. Mol. Biol.* 24, 99–107.
- Hirano, Y., Fukunaga, K., and Sugimoto, K. (2009). Rif1 and rif2 inhibit localization of tel1 to DNA ends. *Mol. Cell* 33, 312–322.
- Horigome, C., Oma, Y., Konishi, T., Schmid, R., Marcomini, I., Hauer, M.H., Dion, V., Harata, M., and Gasser, S.M. (2014). SWR1 and INO80 chromatin remodelers contribute to DNA double-strand break perinuclear anchorage site choice. *Mol. Cell* 55, 626–639.
- Horigome, C., Bustard, D.E., Marcomini, I., Delgosaie, N., Tsai-Pflugfelder, M., Cobb, J.A., and Gasser, S.M. (2016). PolySUMOylation by Siz2 and Mms21 triggers relocation of DNA breaks to nuclear pores through the Slx5/Slx8 STUbL. *Genes Dev.* 30, 931–945.
- Kalocsay, M., Hiller, N.J., and Jentsch, S. (2009). Chromosome-wide Rad51 spreading and SUMO-H2A.Z-dependent chromosome fixation in response to a persistent DNA double-strand break. *Mol. Cell* 33, 335–343.
- Khadaroo, B., Teixeira, M.T., Luciano, P., Eckert-Boulet, N., Germann, S.M., Simon, M.N., Gallina, I., Abdallah, P., Gilson, E., Géli, V., and Lisby, M. (2009). The DNA damage response at eroded telomeres and tethering to the nuclear pore complex. *Nat. Cell Biol.* 11, 980–987.
- Kim, J.C., and Mirkin, S.M. (2013). The balancing act of DNA repeat expansions. *Curr. Opin. Genet. Dev.* 23, 280–288.
- Langerak, P., Mejia-Ramirez, E., Limbo, O., and Russell, P. (2011). Release of Ku and MRN from DNA ends by Mre11 nuclease activity and Ctp1 is required for homologous recombination repair of double-strand breaks. *PLoS Genet.* 7, e1002271.
- Lee, S.E., Bressan, D.A., Petrini, J.H., and Haber, J.E. (2003). Complementation between N-terminal S. cerevisiae mre11 alleles in DNA repair and telomere length maintenance. *DNA Repair* 7, 27–40.
- Leffak, M. (2017). Break-induced replication links microsatellite expansion to complex genome rearrangements. *BioEssays* 39, 1700025.
- Lescasse, R., Pobiega, S., Callebaut, I., and Marcand, S. (2013). End-joining inhibition at telomeres requires the translocase and polySUMO-dependent ubiquitin ligase Uls1. *EMBO J.* 32, 805–815.
- Lisby, M., Barlow, J.H., Burgess, R.C., and Rothstein, R. (2004). Choreography of the DNA damage response: spatiotemporal relationships among checkpoint and repair proteins. *Cell* 118, 699–713.
- Lovejoy, C.A., Li, W., Reisenweber, S., Thongthip, S., Bruno, J., de Lange, T., De, S., Petrini, J.H., Sung, P.A., Jasin, M., et al.; ALT Starr Cancer Consortium (2012). Loss of ATRX, genome instability, and an altered DNA damage response are hallmarks of the alternative lengthening of telomeres pathway. *PLoS Genet.* 8, e1002772.
- Lydeard, J.R., Jain, S., Yamaguchi, M., and Haber, J.E. (2007). Break-induced replication and telomerase-independent telomere maintenance require Pol32. *Nature* 448, 820–823.
- Mangahas, J.L., Alexander, M.K., Sandell, L.L., and Zakian, V.A. (2001). Repair of chromosome ends after telomere loss in *Saccharomyces*. *Mol. Biol. Cell* 12, 4078–4089.
- Martin, S.G., Laroche, T., Suka, N., Grunstein, M., and Gasser, S.M. (1999). Relocalization of telomeric Ku and SIR proteins in response to DNA strand breaks in yeast. *Cell* 97, 621–633.
- Matsuzaki, K., Shinohara, A., and Shinohara, M. (2008). Forkhead-associated domain of yeast Xrs2, a homolog of human Nbs1, promotes nonhomologous end joining through interaction with a ligase IV partner protein, Lif1. *Genetics* 179, 213–225.
- Mattarocci, S., Reinert, J.K., Bunker, R.D., Fontana, G.A., Shi, T., Klein, D., Cavadini, S., Faty, M., Shyian, M., Hafner, L., et al. (2017). Rif1 maintains telomeres and mediates DNA repair by encasing DNA ends. *Nat. Struct. Mol. Biol.* 24, 588–595.
- Meister, P., Gehlen, L.R., Varela, E., Kalck, V., and Gasser, S.M. (2010). Visualizing yeast chromosomes and nuclear architecture. *Methods Enzymol.* 470, 535–567.
- Miller, C.R., Stephens, D., Ruppert, A.S., Racke, F., McFaddin, A., Breidenbach, H., Lin, H.J., Waller, K., Bannerman, T., Jones, J.A., et al. (2015). Jumping translocations, a novel finding in chronic lymphocytic leukaemia. *Br. J. Haematol.* 170, 200–207.
- Miné-Hattab, J., and Rothstein, R. (2012). Increased chromosome mobility facilitates homology search during recombination. *Nat. Cell Biol.* 14, 510–517.
- Miyazaki, T., Bressan, D.A., Shinohara, M., Haber, J.E., and Shinohara, A. (2004). In vivo assembly and disassembly of Rad51 and Rad52 complexes during double-strand break repair. *EMBO J.* 23, 939–949.
- Moretti, P., Freeman, K., Coodly, L., and Shore, D. (1994). Evidence that a complex of SIR proteins interacts with the silencer and telomere-binding protein RAP1. *Genes Dev.* 8, 2257–2269.
- Moriyama, K., Lai, M.S., and Masai, H. (2017). Interaction of Rif1 protein with G-quadruplex in control of chromosome transactions. *Adv. Exp. Med. Biol.* 1042, 287–310.
- Nagai, S., Dubrana, K., Tsai-Pflugfelder, M., Davidson, M.B., Roberts, T.M., Brown, G.W., Varela, E., Hediger, F., Gasser, S.M., and Krogan, N.J. (2008). Functional targeting of DNA damage to a nuclear pore-associated SUMO-dependent ubiquitin ligase. *Science* 322, 597–602.

- Negrini, S., Ribaud, V., Bianchi, A., and Shore, D. (2007). DNA breaks are masked by multiple Rap1 binding in yeast: implications for telomere capping and telomerase regulation. *Genes Dev.* *21*, 292–302.
- Nicolette, M.L., Lee, K., Guo, Z., Rani, M., Chow, J.M., Lee, S.E., and Paull, T.T. (2010). Mre11-Rad50-Xrs2 and Sae2 promote 5' strand resection of DNA double-strand breaks. *Nat. Struct. Mol. Biol.* *17*, 1478–1485.
- Padeken, J., Zeller, P., and Gasser, S.M. (2015). Repeat DNA in genome organization and stability. *Curr. Opin. Genet. Dev.* *31*, 12–19.
- Palm, W., and de Lange, T. (2008). How shelterin protects mammalian telomeres. *Annu. Rev. Genet.* *42*, 301–334.
- Prudden, J., Pebernard, S., Raffa, G., Slavin, D.A., Perry, J.J., Tainer, J.A., McGowan, C.H., and Boddy, M.N. (2007). SUMO-targeted ubiquitin ligases in genome stability. *EMBO J.* *26*, 4089–4101.
- Ribaud, V., Ribeyre, C., Damay, P., and Shore, D. (2012). DNA-end capping by the budding yeast transcription factor and subtelomeric binding protein Tbf1. *EMBO J.* *31*, 138–149.
- Ribeyre, C., and Shore, D. (2012). Anticheckpoint pathways at telomeres in yeast. *Nat. Struct. Mol. Biol.* *19*, 307–313.
- Rivera, H., Zuffardi, O., and Gargantini, L. (1990). Nonreciprocal and jumping translocations of 15q1–qter in Prader-Willi syndrome. *Am. J. Med. Genet.* *37*, 311–317.
- Ruiz-Herrera, A., Nergadze, S.G., Santagostino, M., and Giulotto, E. (2009). Telomeric repeats far from the ends: mechanisms of origin and role in evolution. *Cytogenet. Genome Res.* *122*, 219–228.
- Sage, D., Neumann, F.R., Hediger, F., Gasser, S.M., and Unser, M. (2005). Automatic tracking of individual fluorescence particles: application to the study of chromosome dynamics. *IEEE Trans. Image Process.* *14*, 1372–1383.
- Schober, H., Ferreira, H., Kalck, V., Gehlen, L.R., and Gasser, S.M. (2009). Yeast telomerase and the SUN domain protein Mps3 anchor telomeres and repress subtelomeric recombination. *Genes Dev.* *23*, 928–938.
- Seeber, A., Hegnauer, A.M., Hustedt, N., Deshpande, I., Poli, J., Eglinger, J., Pasero, P., Gut, H., Shinohara, M., Hopfner, K.P., et al. (2016). RPA mediates recruitment of MRX to forks and double-strand breaks to hold sister chromatids together. *Mol. Cell* *64*, 951–966.
- Sfeir, A., and Symington, L.S. (2015). Microhomology-mediated end joining: a back-up survival mechanism or dedicated pathway? *Trends Biochem. Sci.* *40*, 701–714.
- Shore, D., and Bianchi, A. (2009). Telomere length regulation: coupling DNA end processing to feedback regulation of telomerase. *EMBO J.* *28*, 2309–2322.
- Storici, F., and Resnick, M.A. (2006). The delitto perfetto approach to in vivo site-directed mutagenesis and chromosome rearrangements with synthetic oligonucleotides in yeast. *Methods Enzymol.* *409*, 329–345.
- Symington, L.S., and Gautier, J. (2011). Double-strand break end resection and repair pathway choice. *Annu. Rev. Genet.* *45*, 247–271.
- Torres-Rosell, J., Sunjevaric, I., De Piccoli, G., Sacher, M., Eckert-Boulet, N., Reid, R., Jentsch, S., Rothstein, R., Aragón, L., and Lisby, M. (2007). The Smc5-Smc6 complex and SUMO modification of Rad52 regulates recombinational repair at the ribosomal gene locus. *Nat. Cell Biol.* *9*, 923–931.
- Tsouroula, K., Furst, A., Rogier, M., Heyer, V., Maglott-Roth, A., Ferrand, A., Reina-San-Martin, B., and Soutoglou, E. (2016). Temporal and spatial uncoupling of DNA double strand break repair pathways within mammalian heterochromatin. *Mol. Cell* *63*, 293–305.
- Vermeesch, J.R., Petit, P., Speleman, F., Devriendt, K., Fryns, J.P., and Marynen, P. (1997). Interstitial telomeric sequences at the junction site of a jumping translocation. *Hum. Genet.* *99*, 735–737.
- Wotton, D., and Shore, D. (1997). A novel Rap1p-interacting factor, Rif2p, cooperates with Rif1p to regulate telomere length in *Saccharomyces cerevisiae*. *Genes Dev.* *11*, 748–760.
- Zierhut, C., and Diffley, J.F. (2008). Break dosage, cell cycle stage and DNA replication influence DNA double strand break response. *EMBO J.* *27*, 1875–1885.

## STAR★METHODS

### KEY RESOURCES TABLE

REAGENT or RESOURCE	SOURCE	IDENTIFIER
<b>Antibodies</b>		
Mab414 nuclear pore antibody	abcam	Mab414, ab24609
Sheep anti-mouse IgG magnetic beads	Invitrogen	11031
Anti-HA antibody	Santa Cruz Biotech	F-7, sc-7392
Anti-PK antibody	Acris Antibodies	SV5-PK1, SM1691
Sheep anti-rabbit IgG Dynabeads	Invitrogen	11203D
anti-yKu70 rabbit polyclonal antibody	A. E. Tomkinson	anti-Hdf1
<b>Critical Commercial Assays</b>		
SMRTbell Template Prep Kit	Pacific Biosciences	100-259-100
PippinHT	Sage Science	HTP0001
protease inhibitors (cOmplete EDTA-free)	Roche	04693159001
AccuPrep DNA extraction kit	Bioneer	K-3034
MagBead-binding One Cell Per Well	Pacific Biosciences	100-267-800-03
Binding Kit P6 v2	Pacific Biosciences	100-372-700
DNA Sequencing Kit 4.0	Pacific Biosciences	100-364-600
<b>Deposited Data</b>		
Pacific Biosciences sequencing datasets	NCBI Bioproject database	Submission ID SUB4312748, under Bioproject ID PRJNA482327
<b>Experimental Models: Organisms/Strains</b>		
Budding yeast: see <a href="#">Table S1</a>	Susan Gasser, FMI	<a href="#">Table S1</a>
<b>Oligonucleotides</b>		
Primer lists: see <a href="#">Tables S2</a> and <a href="#">S3</a>	different suppliers, this paper	<a href="#">Tables S2</a> and <a href="#">S3</a>
<b>Recombinant DNA</b>		
Plasmid expressing wild-type ULS1	HFP269, H. Ferreira, St. Andrews University	p416-FLAG-ULS1
Plasmid expressing translocase mutant uls1-K975A	HFP282, H. Ferreira, St. Andrews University	p416-FLAG-uls1-K975A
Plasmid containing EXO1	<a href="#">Lee et al., 2003</a>	pJH1772
Plasmid containing Ruby2 fluorophore	Addgene	pFA6a-link-yomRuby2-Kan
Plasmid containing TG80-HO-3'MNT2	<a href="#">Ribeyre and Shore, 2012</a>	pIM35
Plasmid containing (TTAGGG)60-HO-3'MNT2	<a href="#">Ribaud et al., 2012</a>	pVR4
Plasmid 3571 containing TG250-HO-3'MNT2	This paper	pUC57-TG250
Plasmid 3892 containing TG18-HO-3'MNT2	This paper	pUC57-TG18
<b>Software and Algorithms</b>		
SPT analysis and biophysical parameter extraction	S. Gasser, <a href="#">Amitai et al., 2017</a>	NA
Spot tracker ImageJ (FIJI) plug-in	S. Gasser, <a href="#">Sage et al., 2005</a>	NA
PointPicker	S. Gasser, <a href="#">Meister et al., 2010</a>	NA

### CONTACT FOR REAGENT AND RESOURCE SHARING

All reagents and resources can be obtained by contacting Susan M. Gasser, at the Friedrich Miescher Institute for Biomedical Research, Maulbeerstr. 66, 4058 Basel, Switzerland; [Susan.gasser@fmi.ch](mailto:Susan.gasser@fmi.ch)

## EXPERIMENTAL MODEL AND SUBJECT DETAILS

### Yeast Strains and Construction

All strains were derived from JKM179 and are listed in [Table S1](#). Strain GA-8119 (TG80-HO-3'MNT2 construct at *MAT*) and strain GA-9823 ((TTAGGG)60-HO-3'MNT2 construct at *MAT*) were constructed by *delitto perfetto* ([Storici and Resnick, 2006](#)), followed by insertion of the TG-HO-3'MNT2 PCR fragment obtained from plasmid pIM35 ([Ribeyre and Shore, 2012](#)) and pVR4 ([Ribaud et al., 2012](#)) respectively, using primers SG-6571 and SG-6572. Strain GA-9918 was constructed by subsequent deletion of the 3' *MNT2* fragment present in GA-8119. The strains GA-8502 and GA-9824 were constructed the same as GA-8119, except that the PCR products containing TG250-HO-3'MNT2 or TG18-HO-3'MNT2 were amplified from plasmids 3571 (pUC57-TG250) and 3892 (pUC57-TG18), respectively (available upon request). These constructs differ from TG80-HO-3'MNT2 only by the presence of either 250 bp or 18 bp of TG repeats, instead of 80. The Ruby2 fluorophore plasmid used to create GA-9912 and GA-9948 was obtained from Addgene. For all live microscopy and localization assays, SC medium was used instead of YP. For DSB localization assays, 1 ml of cells was harvested at each time point, fixed in 4% paraformaldehyde (final concentration) for 5 min and washed three times with PBS before microscopy.

### METHOD DETAILS

The primers used in this work are listed in [Tables S2](#) and [S3](#). The plasmid containing *EXO1* in [Figure 2C](#) is pJH1772 ([Lee et al., 2003](#)). The plasmid expressing wild-type *ULS1* (p416-FLAG-ULS1) and translocase mutant *uls1-K975A* (p416-FLAG-uls1-K975A) were cloned into pRS416 from HFP269 and HFP282 (gifts from Dr. H. Ferreira), respectively.

### DNA Extraction for PCR

Unless otherwise specified, DNA for PCR and quantitative PCR was extracted by spinning down 1 ml of cells and resuspending them in 200  $\mu$ l DNA isolation buffer (2% v/v Triton X-100, 1% w/v SDS, 100 mM NaCl, 10 mM Tris-HCl pH 8, 1 mM EDTA). Cell lysis was performed by addition of 200  $\mu$ l zirconia/silica beads and 200  $\mu$ l phenol:chloroform:isoamylalcohol (25:24:1), followed by vortexing for 5 min at room temperature. 200  $\mu$ l TE buffer pH 8 was added to each sample, and samples were centrifuged for 5 min at 16,000 g. DNA was precipitated by addition of 1 ml 100% ethanol and 50  $\mu$ l of 3 M sodium acetate to the aqueous phase. Samples were incubated at  $-70^{\circ}\text{C}$  for 40 min, then centrifuged for 10 min at 16,000 g. The pellet was washed once in 70% ethanol, dried and resuspended in 100  $\mu$ l sterile water for use in PCR reactions.

### Fluorescence Microscopy

Images for assessment of DSB localization by performing zoning or colocalization measurements were captured on a Metamorph-driven Spinning-disk confocal system based on an Olympus IX81 microscope, Yokogawa CSU-X1 scan head, EM-CCD Cascade II (Photometrics) camera and an ASI MS-2000 Z-piezo stage. We used a PlanApo  $\times$  100, NA 1.45 total internal reflection fluorescence microscope oil objective.

Live microscopy was done at  $25^{\circ}\text{C}$  on a Nikon Eclipse Ti microscope, two EM-CCD Cascade II (Photometrics) cameras, an ASI MS-2000 Z-piezo stage and a PlanApo  $\times$  100, NA 1.45 total internal reflection fluorescence microscope oil objective and Visiview software. Fluorophores were excited at 561 nm (for Ruby2) and at 491 nm (for GFP), and emitted fluorescence was acquired simultaneously on separate cameras (Semrock FF01-617/73-25 filter for mCherry/ Ruby2 and Semrock FF02-525/40-25 filter for GFP). Time-lapse series were streamed taking 8 optical slices per stack every 80 ms for 60 s with 10 ms exposure times per slice respectively with laser powers set to  $\sim$ 7%–12% for either laser line. Gain was set to 800.

### DSB Survival Assay by Colony Formation

Cultures were grown in YPLGg medium (2% glycerol lactate, 0.05% glucose) at  $30^{\circ}\text{C}$  overnight to late log phase ( $1 \times 10^7$  cells/ml). For colony formation assays (e.g., [Figure 5](#)), cells were counted and diluted as follows: for each strain, 10 and 100 cells were plated on two YPAD (Yeast extract, bactopectone, adenine, and 2% dextrose (glucose)) plates, while 10,000, 20,000 and 50,000 cells were plated on YPGal (2% galactose instead of dextrose) plates and incubated at  $30^{\circ}\text{C}$ . Survivor colonies were counted after 4 days at  $30^{\circ}\text{C}$ . In [Figure S6C](#), cells were grown in synthetic LGg-uracil medium, and survivors were obtained on synthetic-2% galactose-uracil medium after 5 days at  $30^{\circ}\text{C}$ . Total survivor numbers were calculated by normalizing colony number on YPGal to colony number on YPD. For the experiment in [Figure 5C](#): in late log phase, HO cut was induced by addition of 2% galactose in liquid cultures. Before induction (time 0'), cells were counted and diluted. For each culture, 10 or 100 cells were plated in duplicate on YPAD plates. At 90 and 180 min after cut induction, 250 and 500 cells for each strain were plated in duplicate on YPAD plates, respectively. Plates were incubated at  $30^{\circ}\text{C}$ . Survivor colonies were counted after 3 days of incubation, and the total survivor numbers were determined at each time point by normalizing number of colonies from that time point to number of colonies at time 0 (before HO induction).

### Pulsed-Field Gel Electrophoresis (PFGE)

PFGE was performed as previously described ([Hage and Houseley, 2013](#)). Yeast genomic DNA was prepared in an agarose plug as described in the instruction manual of the Pulsed Field Electrophoresis System (Bio-Rad, CHEF-DR II) with the following



modifications. Cultures were grown in YPLGg overnight to log phase. About  $5 \times 10^5$  cells were harvested and washed in ice-cold 0.05 M EDTA pH 8.0 and pelleted. Cell pellets were resuspended in Zymolyase buffer (50 mM Na-PO<sub>4</sub> [pH 7.0], 50 mM EDTA, 1 mM dithiothreitol [DTT]) and embedded in a 2% agarose plug (Cleancut agarose, Biorad): 50  $\mu$ l agarose was mixed with 50  $\mu$ l of cells. Genomic DNA was prepared by treating the plug with 0.4 mg/ml Zymolyase (20T, Seikagaku) in Zymolyase buffer at 37°C for 1 h, followed by 1 mg/ml proteinase K digestion in 10 mM Tris-HCl (pH 7.5), 50 mM EDTA, 1% sodium N-lauroylsarcosinate at 50°C or 30°C for 15–20 h. After 4 washes in 20 mM Tris-50 mM EDTA pH 8.0, plugs were loaded in 0.8% agarose/0.5  $\times$  Tris-Borate-EDTA (TBE) on the CHEF-DR II (Bio-Rad) and chromosomal DNA was migrated at 14°C, 6V/cm, 60 s switch time for 15 h, then 90 s for 9 h. The gel was stained for 1 h at room temperature with RedSafe (Fisher Scientific), destained for 2 h and imaged on c400 Imaging System (Azure Biosystems).

### Telomerase PCR at a Double Strand Break

Telomerase PCR was performed as previously described (Förstemann et al., 2000). DNA was extracted from 1.5 ml of culture collected at each time point indicated (Figure S5D). A starting amount of 150 ng/ $\mu$ l of DNA was used in each C-tailing reaction: first, DNA was diluted in CutSmart buffer (NEB) to a final volume of 8  $\mu$ l and denatured at 96°C for 10 min on a PCR block. Once samples cooled down to 37°C, 1  $\mu$ l of tailing mix was quickly added to each reaction: the tailing mix contained 1 U of terminal transferase (NEB), 0.1 mM dCTP and 1 $\times$  CutSmart buffer. The tailing reaction was performed using the following program: 37°C for 30 min, 65°C for 10 min and 95°C for 5 min. Immediately afterward, telomerase PCR was started by addition of 30  $\mu$ l PCR mix to each tube. The PCR mix contained 0.5 mM fresh dNTPs, 0.75  $\mu$ M G18 primer (SG-7613), 2.5 U ExTaq polymerase (Takara), 0.75  $\mu$ M forward primer (SG-2659 for Tg0, SG-6611 for Tg80), 4  $\mu$ l 10 $\times$  telomerase PCR buffer. 10 $\times$  PCR buffer containing 50% glycerol, 670 mM Tris-HCl (pH 8.8), 160 mM (NH<sub>4</sub>)<sub>2</sub>SO<sub>4</sub>, 0.1% Tween-20, 0.74% HCl. The telomerase PCR program was as follows: 95°C 3 min, [95°C for 30 s, 62°C for 20 s, 72°C for 20 s] for 35 cycles, and 72°C for 5 min. PCR products were separated on a 2.5% agarose gel (10  $\mu$ l PCR product with 2  $\mu$ l 6 $\times$  loading dye) and imaged with Azure c400 Imaging Systems. The control band was obtained in a standard PCR reaction using the same DNA, and primers SG-525 and SG-526 for the SMC2 gene.

### Chromatin Immunoprecipitation (ChIP)

ChIP using the Mab414 nuclear pore antibody (Abcam) was performed as previously described (Horigome et al., 2014) with slight modifications. At each time point about  $15 \times 10^8$  cells were sampled, crosslinked with 1% formaldehyde for 20 min while rotating at rt, then washed twice in ice cold 1 $\times$  PBS. 40  $\mu$ l of sheep anti-mouse IgG magnetic beads (Invitrogen) per sample were washed twice in 500  $\mu$ l PBS, 5 mg/ml bovine serum albumin (BSA, A-4503 Sigma Aldrich), and blocked in the same solution for 30 min while rotating at 4°C. Beads were washed with 500  $\mu$ l PBS, and 1  $\mu$ g nuclear pore antibody (mAB414) per sample was added to the beads followed by 4 h incubation while rotating at 4°C. After incubation, antibody-coupled beads were washed twice in 1 ml lysis buffer (50 mM HEPES-KOH pH 7.5, 140 mM NaCl, 1 mM EDTA, 1% Triton X-100, 0.1% sodium deoxycholate) and then added to cell lysates, which were prepared as follows. Cell pellets were resuspended in 600  $\mu$ l lysis buffer and lysed by addition of 200  $\mu$ l zirconia-silica beads and bead beating in a bead beater (Fastprep-24 5G, MP Biomedicals) for 1 min at 6.5 m s<sup>-1</sup> for 3 times. Lysates were recovered from beads by centrifugation at 2000 g for 10 min at 4°C. The pellet fraction containing cross-linked chromatin was then resuspended in 1 mL of lysis buffer and sonicated on a (Bioruptor) for 20 cycles (30 s on, 30 s off). Samples were centrifuged at 7000 g for 2 min and the supernatant containing released chromatin proteins was recovered: 50  $\mu$ l of the supernatant was collected as input and stored at –20°C until the crosslinking reversal step, and the rest was added to antibody-coupled beads and incubated on a rotating wheel at 4°C overnight (about 16 h). The next day, beads were washed 3 times 5 min in lysis buffer, and once in wash buffer (10 mM Tris-HCl pH 8.0, 250 mM LiCl, 0.5% Nonidet P40 (Igepal), 0.5% sodium deoxycholate, 1 mM EDTA) for 10 min, and lastly once in Tris-EDTA (TE) pH 8.0 for 1 min. All washes were done on a rotating wheel at 4°C. DNA was eluted from beads in 100  $\mu$ l 1% SDS-TE by incubation at 65°C for 10 min, and repeated once (200  $\mu$ l total elute). 200  $\mu$ l 1% SDS-TE was also added to input samples, and crosslinking was reversed for all samples by an overnight incubation at 65°C.

ChIP with anti-yKu70 rabbit polyclonal antibody was performed as follows. Briefly, after sonication 1  $\mu$ l primary antibody anti-yKu70 (kind gift of Dr. A. E. Tomkinson) was added directly to each lysate and samples were incubated for 10 h at 4°C. 40  $\mu$ l M-280 sheep anti-rabbit IgG Dynabeads (Invitrogen) were added to each sample followed by 2h incubation while rotating at 4°C for to capture Ab-bound species. Bead washes, elution and crosslink reversal were performed as for pore ChIP. HA-tagged Mps3 ChIP was performed similarly as pore ChIP using 50  $\mu$ l sheep anti-mouse IgG magnetic beads (Invitrogen) and 6  $\mu$ g anti-HA antibody (sc-7392, Santa Cruz Biotech), per sample. Slight modifications were made in the washing steps, after overnight incubation of antibody-coupled beads with lysates: samples were washed 3 times in lysis buffer for 10 min at 4°C, once with high salt buffer (1% Triton X-100, 0.1% sodium deoxycholate, 1 mM EDTA pH 8.0, 10 mM Tris-HCl pH8.0, 0.5 M NaCl) for 5 min, two washes in standard wash buffer for 10 min on rotation, and one wash in Tris-EDTA (TE) pH 8.0 for 1 min. Elution and decrosslinking were performed as for pore ChIP.

ChIP for PK-tagged Rad50 was done as described (Seeber et al., 2016) and with the same procedure as pore ChIP, except that immunoprecipitation required only 2 h rotation at 4°C, given the high efficiency of the antibody. 1  $\mu$ l of SV5-PK1 antibody (Acris Antibodies) was used per sample. All ChIP buffers contained protease inhibitors (cOmplete EDTA-free, Roche). In all ChIP experiments, DNA was recovered after reversal of crosslinking using the AccuPrep DNA extraction kit (Bioneer), and DNA was eluted in

20% kit elution buffer (diluted with deionized water). This DNA was analyzed by quantitative PCR on StepOnePlus machine (Applied Biosystem) using Taqman or SYBR green detection methods. Primers were used at 0.3  $\mu$ M concentration, probes at 0.04  $\mu$ M.

### Resection Assay

For this technique, it is important to use a robust DNA extraction method that produces very clean DNA. For each time point,  $6 \times 10^7$  cells grown at 30°C to late log phase were harvested and washed once in cold phosphate-buffered saline (PBS). Cells were resuspended in 500  $\mu$ l buffer L (50 mM Tris-HCl pH 8.0, 7 mM  $\beta$ -mercaptoethanol, 150 mM NaCl, 1 mM EDTA, 1% v/v SDS), transferred to cryotubes with 300  $\mu$ l zirconia silica beads and 500  $\mu$ l phenol: chloroform:isoamylalcohol (PCI) 25:24:1. Samples were vortexed for 2 min, beat in a cell lyser (Fastprep-24 5G, MP Biomedicals) for 90 s at 6.5 m s<sup>-1</sup>, placed on ice for 2 min and centrifuged at 16,000 g for 5 min. The top aqueous layer was isolated, and 500  $\mu$ l PCI was added to it. Samples were vortexed for 2 min, centrifuged for 5 min at 16,000 g. The aqueous layer was isolated and 1 ml ethanol was added to it. DNA was precipitated at -70°C for 40 min. Samples were centrifuged at 4°C for 10 min at 16,000 g. The pellet was dried briefly, then resuspended in 300  $\mu$ l TE buffer + 15  $\mu$ g RNase A (BioBasic) and incubated at 37°C for 2 h. DNA was precipitated by addition of 600  $\mu$ l isopropanol and 0.15 mM NaCl. Samples were centrifuged at 4°C for 10 min at 16,000 g. The pellet was washed once in 70% ethanol and dried, then resuspended in TE pH 8.0. The amount of DNA isolated was quantified by Nanodrop measurement and all samples were diluted to a 200 ng/ $\mu$ l for the resection assay, which was carried out as previously described (Zierhut and Diffley, 2008). The only exception was that *Alu1* (NEB) was used as the restriction enzyme. For each sample, a mock digestion and an *Alu1* digestion were set up in 25  $\mu$ l overnight at 37°C with 3  $\mu$ g DNA per sample. Digestions were diluted 1:10 in sterile water and used directly in quantitative PCR. DNA was analyzed by quantitative PCR with StepOnePlus machine (Applied Biosystem) and SYBR green detection method. For each time point, Ct values were normalized to those obtained from the mock sample, and then further normalized to values obtained from an amplicon in *SMC2* control gene.

### SMRTbell Library Construction for Sequencing

The amount of 20  $\mu$ g of genomic DNA were needle-sheared with a 26-gauge blunt-end needle (BD), and used as input for SMRTbell library construction using the SMRTbell Template Prep Kit (Pacific Biosciences), following Pacific Biosciences' 20 kb Template Preparation protocol. The final libraries were size-selected on a PippinHT (Sage Science) using the 0.75% 6-10 kb High-Pass 75D method, with a starting size of 9900 bp. The final average library size was about 60,000 bp as judged on an Agilent Genomic DNA ScreenTape (Agilent).

### PacBio RSII Sequencing

Each SMRTbell library was sequenced on three to four Pacific Biosciences RSII SMRTcells at loading concentrations ranging from 300 to 450 pM using the MagBead-binding One Cell Per Well workflow, the Binding Kit P6 v2 and DNA Sequencing Kit 4.0 (all Pacific Biosciences). Data was acquired for a duration of 240 min, with Stage Start enabled.

## QUANTIFICATION AND STATISTICAL ANALYSIS

Time-lapse image stacks were analyzed as in (Dion et al., 2012) and in (Amitai et al., 2017) using a custom made ImageJ (FIJI) plug-in (Sage et al., 2005), to correct for translational movement and to extract the coordinates of locus position. Only S phase cells were tracked. The error bars of all mean square displacement (MSD) plots represent the s.e.m. In all microscopy experiments, cut induction was verified by quantitative PCR using primers flanking the cut site. The derivation and extraction of biophysical parameters of the single particle tracking data was performed exactly as described in the supplemental methods of Amitai et al. (2017). MSD graphs were calculated as described in Hauer et al. (2017). Three-zone position analysis for LacI- GFP foci was performed using a through-focus stack of 16-21 0.2  $\mu$ m steps and was measured by ImageJ (NIH, USA) and software PointPicker (Meister et al., 2010). Standard tests for significance are described in the corresponding figure legends.

For quantification of ChIP results, the absolute enrichment was calculated as follows. For each time point, the signal from a PCR reaction near the DSB was normalized to the signal from the control genomic locus, *SMC2* or the mitochondrial gene, *OLI1*, in the same sample. For each time point and probe, the normalized IP signal was then normalized to the input signal.

## DATA AND SOFTWARE AVAILABILITY

The accession number for the Pacific Biosciences sequencing data sets reported in this paper is NCBI: PRJNA482327.

All sequencing data and software used are available from the lead author, upon request.

**Cell Reports, Volume 24**

**Supplemental Information**

**Asymmetric Processing of DNA Ends  
at a Double-Strand Break Leads to Unconstrained  
Dynamics and Ectopic Translocation**

**Isabella Marcomini, Kenji Shimada, Neda Delgoshaiie, Io Yamamoto, Andrew Seeber, Anais Cheblal, Chihiro Horigome, Ulrike Naumann, and Susan M. Gasser**

## Supplementary Material

### Asymmetric processing of DNA ends at a double-strand break leads to unconstrained dynamics and ectopic translocation

Isabella Marcomini, Kenji Shimada, Neda Delgosaie, Io Yamamoto, Andrew Seeber, Anais Cheblal, Chihiro Horigome and Susan M. Gasser

#### Inventory

##### 1 - Supplemental Tables

<i>Table S1: Strains used in this study</i>	<b>p 1</b>
A list of the yeast strains, index number and original citation.	<i>p 1</i>
<i>Table S2: PCR primers used in this study</i>	<b>p 2</b>
Primers required for completing described experimental procedures	<i>p 2</i>
<i>Table S3: Real-time PCR primers used in this study</i>	<b>p 2</b>
Primers used for quantifying ChIP data and telomere elongation	<i>p 2</i>

##### 2 - Supplemental Figures

<i>Figure S1: Tg250 is at the nuclear periphery before and after HO cleavage.</i>	<b>p 3</b>
Relates to Figure 1C. Position scoring of Tg250-flanked MAT locus in the 3 zone assay shows perinuclear positioning.	<i>p 3</i>
<i>Figure S2: Overexpression of Exo1 exonuclease partially rescues the resection block of the TG-flanked end in Tg80 strains.</i>	<b>p 3</b>
Relates to Figure 2. Quantification of 5' end resection at Tg80 with overexpressed EXO1	<i>p 3</i>
<i>Figure S3: HO cleavage efficiency is not affected by TG-rich insertions nor by rif1 or sir4 mutations.</i>	<b>p 4</b>
Relates to Figure 3. The MAT locus is cut with comparable efficiencies by HO endonuclease	<i>p 4</i>
<i>Figure S4: Standard deviation values for the biophysical parameters defining DSB end movement.</i>	<b>p 5</b>
Relates to Figure 4D. Derivation of movement values is described in Amitai et al., 2017.	<i>p 5</i>
<i>Figure S5: While the TG-flanked DSB is repaired by an ectopic homology-mediated recombination event, the non-TG side is elongated by telomerase.</i>	<b>p 6</b>
Panels A-F relate to Figure 5C-F. A) Cut efficiency; B) CHEF gel analysis for Tg80 (GA-8119) grown always on glucose; D,E) Telomere PCR at a DSB F) Cut efficiency calculated	<i>p 6</i>
<i>Figure S6: DSB-Mps3 anchorage is not Siz2 nor Uls1 dependent and enhances NHEJ over ectopic HR.</i>	<b>p 7</b>
Relates to Figure 6. A) ChIP for HA-tagged Mps3; B) Ratio of colonies formed on galactose; C) Requirement of Uls1 translocase activity to suppress NHEJ; D) NHEJ pathway efficiency	<i>p 7</i>

## Marcomini et al. Supplementary tables

**Table S1. Strains used in this study (related to Fig. 1-7, S1-4).**

Name	Genotype	Source
GA-8861	JKM179: <i>MAT</i> $\alpha$ , $\Delta$ <i>ho hml::ADE1 hmr::ADE1 ade3::GALHO ade1-100 leu2-3, 112 lys5 trp1::hisG ura3-52 CFP-NUP49 GFP-LacI:Leu2 MAT::LacO</i> repeats: <i>TRP1</i>	Horigome et al., 2014
GA-8119	GA8861 TG80-HO-MNT2	This study
GA-8502	GA8861 TG250-HO-MNT2	This study
GA-10085	GA8861 HO-MNT2	This study
GA-9005	GA-8119 <i>est2::natMX4</i>	This study
GA-9502	GA-8119 <i>pol32::natMX4</i>	This study
GA-9511	GA-8119 <i>dnl4::natMX4</i>	This study
GA-8561	GA-8861 <i>dnl4::natMX4</i>	This study
GA-9551	GA-8561 <i>pol32::hphMX4</i>	This study
GA-9512	GA-8502 <i>dnl4::natMX4</i>	This study
GA-9918	GA-8861 TG80-HO	This study
GA-9549	GA-8119 <i>rad50-9PK-k.i.</i>	This study
GA-9519	GA-8861 <i>rad50-9PK-k.i.</i>	This study
GA-9521	GA-8502 <i>rad50-9PK-k.i.</i>	This study
GA-9948	GA-8861 <i>yom-Ruby2-kanMX6</i>	This study
GA-9913	GA-8119 <i>yom-Ruby2-kanMX6</i>	This study
GA-9449	GA-8119 <i>rif1::hphMX4</i>	This study
GA-9158	GA-8119 <i>sir4::natMX4</i>	This study
GA-8596	GA-8502 <i>rif1::hphMX4</i>	This study
GA-8587	GA-8502 <i>sir4::natMX4</i>	This study
GA-9553	GA-8119 <i>yku70::natMX4</i>	This study
GA-9823	GA-8861 (TTAGGG) <sub>60</sub> -HO-MNT2	This study
GA-9824	GA8861 TG18-HO-MNT2	This study
GA-8306	JKM139: <i>MAT</i> $\alpha$ $\Delta$ <i>ho hml::ADE1 hmr::ADE1 ade3::GALHO ade1-100 leu2-3,112 lys5 trp1::hisG ura3-52 Mps3-3HA</i>	Horigome et al., 2014
GA-8633	GA8119 <i>Mps3-3HA</i>	This study
GA-8845	GA8502 <i>Mps3-3HA</i>	This study
GA-10054	GA-9824 <i>mps3<math>\Delta</math>65-145</i>	This study
GA-8334	GA8119 <i>nup84::natMX4</i>	This study
GA-9855	GA8119 <i>uls1::kanMX6</i>	This study
GA-10050	GA8119 <i>slx8::natMX4</i>	This study
GA-9794	GA-8119 <i>siz2::hphMX4</i>	This study
GA-10435	GA9913 <i>uls1::natMX4</i>	This study
GA-7314	GA-8861 <i>nup133::natMX4 pUN100-nup133<math>\Delta</math>N:kanMX6</i>	Horigome et al., 2014
GA-7969	GA-7314 <i>slx5::C.a. URA3</i>	Horigome et al., 2016
GA-8475	GA-7314 <i>uls1::C.a. URA3</i>	This study
GA-7970	GA-7314 <i>siz2::C.a. URA3</i>	Horigome et al., 2016

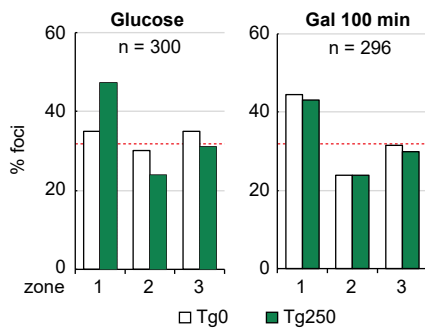
**Table S2. PCR Primers used in this study. Related to Fig. 1, 2, 7.**

Name	Sequence
SG-7613	CGGGATCCGGGGGGGGGGGGGGGGGGGG
SG-6611	CGCTGGTTTGCATAAAGGTA
SG-2659	CACAGTTTGGCTCCGGTGTA
SG-5771	ACAAAGAATGATGCTAAGAATT
SG-475	GACGACCTT GTAACAGTCC AGACAG
SG-476	TACGTCCTTACCTTCGCATGGAACC
SG-525	AATTGGATTTGGCTAAGCGTAATC
SG-526	CTCCAATGTCCCTCAAAATTTCTT

**Table S3. Real-time PCR Primers used in this study. Related to Fig. 3, 5, 6, 7, S1, S2, S4.**

Name	Sequence	Target
SG-525	AATTGGATTTGGCTAAGCGTAATC	<i>SMC2</i>
SG-526	CTCCAATGTCCCTCAAAATTTCTT	
TQ-3 (probe)	CGACGCGAATCCATCTTCCCAAATAATT	
SG-2918	CAAGAAACCCATCAATTAAGACCTAGT	<i>OL11</i>
SG2919	ATGAAACCATTAACAGAATAAACCTGTAG	
SG-6695	GTAGTTGTGTGCCAGAAGGC	HOcs (TG strains)
SG-6696	GGCAGGGGAATTCTTATACT	
SG-2285	AATATGGGACTACTTCGCGCAACA	HOcs (wt <i>MAT</i> )
SG-2286	CGTCACCACGTACTIONCAGCATAA	
SG-563	TCAACCATATATAATAACTTAATAGACGACATTC	-0.6kb from HOcs
SG-564	CTAGACGTTTTTCTTTCAGCTTTTTTG	
TQ-2 (probe)	CTTTCAAAATTAAGAACAAAGCATCCAAATCATAACAGAA	
SG-2912	TCACGCTTTATAACAATATCAAGTTTACCT	+0.7 kb from HOcs
SG-2913	ATTGGAAACACCAAGGGAGAGA	
TQ-44 (probe)	TCATTACTATTCATCTTCGCCACAAG	
SG-8444	CCCAAACAAAACCCAGACAT	-0.6kb from HOcs
SG-8445	TGCTGGATTTAAACTCATCTGTG	
SG-8440	CTCTCCCTGGTGTTCCTCAA	+0.7kb from HOcs
SG-8441	GAAAAGATTGGCCGTCAAAA	
SG-8448	CAATGCCTTCCTTCTCCAAA	-4.2kb from HOcs
SG-8449	ACCTGAGCGACGAGAAATTG	
SG-8459	TGCGATGAAGTCAACGAATTA	+4.5kb from HOcs
SG-8460	GAGCACTTTTACCGGCAGTT	
SG-7702	CACACAATCACATCCCTCAAAC	+3.5 kb from HOcs
SG-7703	AGAAGAAGAGGAAGGCGAAAG	
TQ-56 (probe)	CCTCAATATTCCGCCTTTCCTTTCCTCC	
SG-6761	ACATTAATAAAGAGAAGAGCCCAAAG	-0.24 kb from HOcs
SG-6762	GCCACATTTCTTTGCAACTTC	
TQ-54 (probe)	AGCACGGGCATTTTTAGAACAGGTTTTTAGAAG	

## Zoning assay

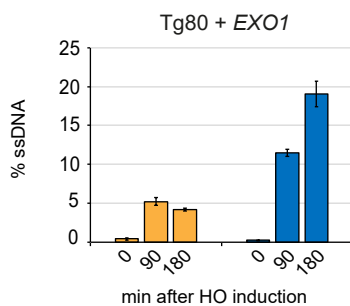


Marcomini et al., Figure S1

### Figure S1. Tg250 is at the nuclear periphery before and after HO cleavage.

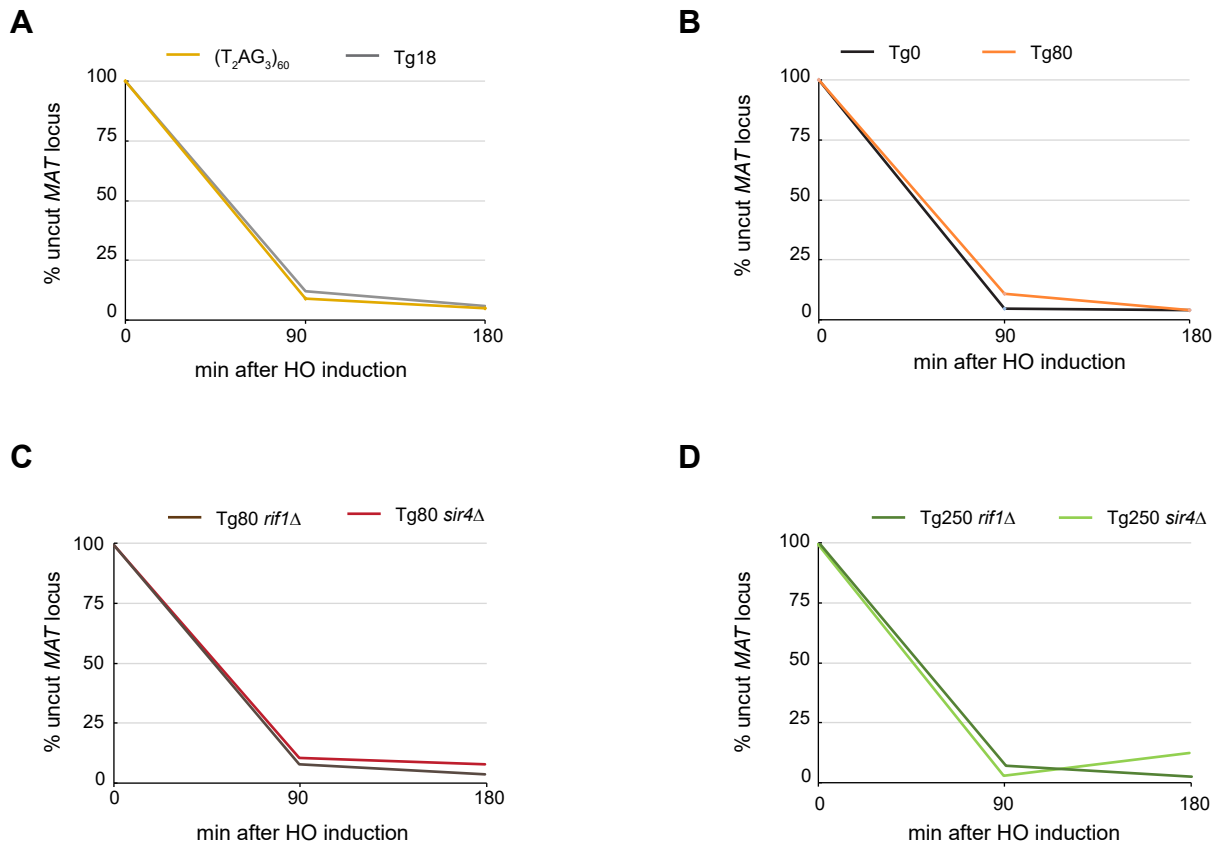
a) Relates to Figure 1C. Results from scoring the position of the *MAT* locus in the 3 zoning assay in panel 1B, for an exponentially growing culture in glucose (left graph) or 100 min after HO induction on galactose (right graph) in Tg0 (GA-8861, white) and Tg250 (GA-8502, green) strains. n=number of nuclei scored per condition. A random distribution of a locus results in 33% of cells with the locus in each zone, as indicated by the red dotted line. The *lacI*-GFP focus in Tg250 strains is significantly perinuclear before and after HO cut induction, presumably due to the binding of Sir4.

## Resection assay



Marcomini et al., Figure S2

**Figure S2. Overexpression of Exo1 exonuclease partially rescues the resection block at the TG-flanked end in Tg80 strains.** Relates to Figure 2. Quantification of ssDNA generated by 5' end resection as in panel 2A, in a Tg80 strain overexpressing EXO1 from a galactose-inducible 2 $\mu$  plasmid (pJH1772). Data from 2 biological replicates, amplified in triplicate are presented as mean values +/- s.e.m.



Marcomini et al., Figure S3

**Figure S3. HO cleavage efficiency is not affected by TG-rich insertions nor by *rif1* or *sir4* mutation.**

A) – D) Relates to Figure 3. The *MAT* locus is cut with comparable efficiencies by HO endonuclease upon galactose addition to exponentially growing cultures of GA-9823, GA-9824, GA-8861, GA-8119, GA-9449, GA-9158, GA-8596, GA-8587. DNA samples were collected at 0, 90 and 180 mins after HO induction and were used to quantify the percentage of intact *MAT* locus by qPCR. Ct values of amplicons across the HO cut site were normalized for those obtained by amplification of the control locus *SMC2* at 90 and 180 minutes after galactose addition, and these ratios were further normalized for the ratio obtained at time point 0. Mean of 3 replicates are shown. Standard deviation is not shown, as it was lower than 2% for each strain and time point.



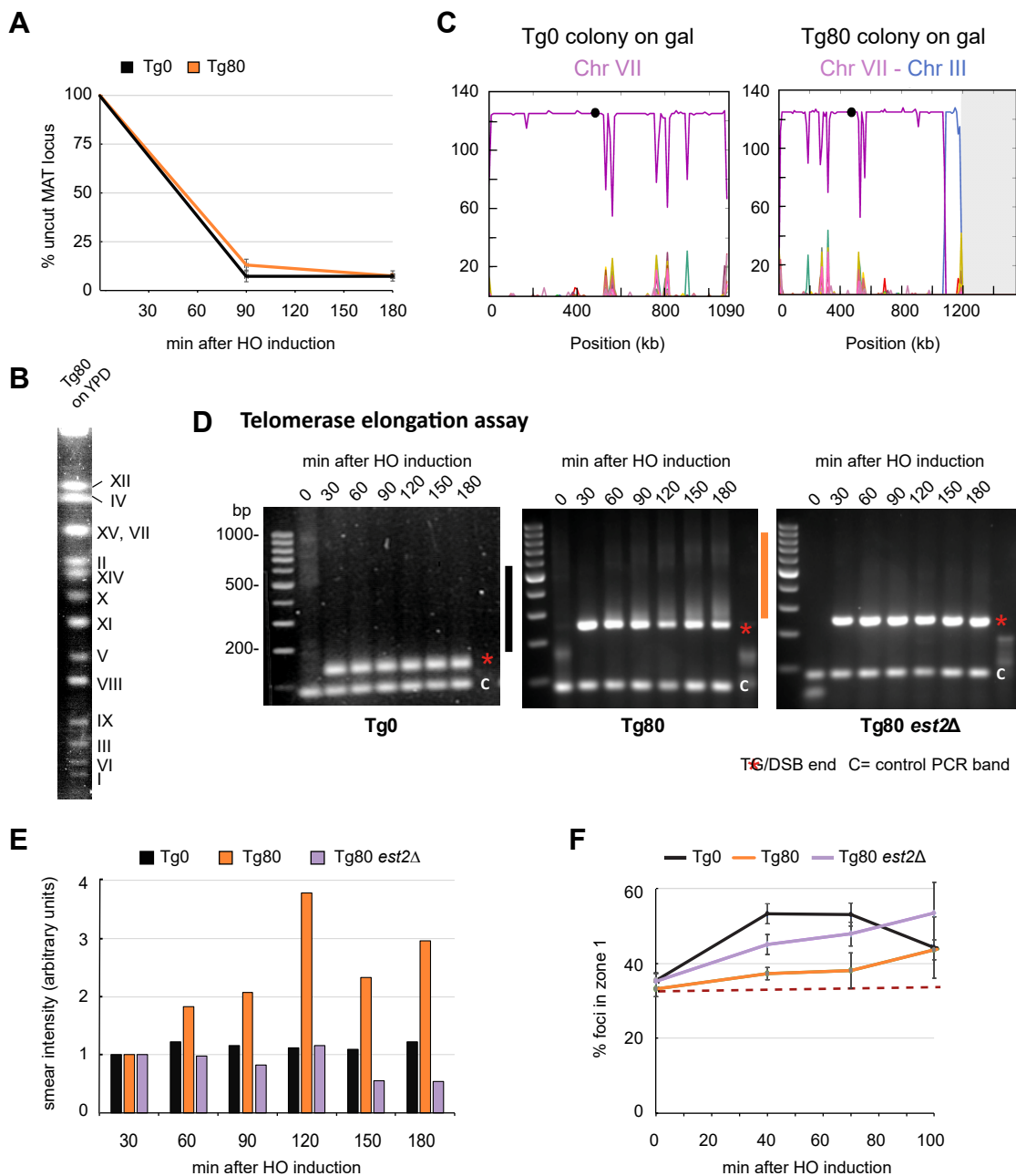
Movement parameters - standard errors of the mean (s.e.m.)

uncut	Tg0	Tg80
	lacI-GFP	lacI-GFP
$\alpha$ ( $\mu\text{m}$ )	0.036	0.024
$D_c$ ( $\mu\text{m}^2/\text{s}$ )	8.28E-03	5.77E-05
$L_c$ ( $\mu\text{m}$ )	7.38E-03	5.54E-03
$k_c$ ( $k_B T/\mu\text{m}^2$ )	13.382	5.579

cut	Tg0	Tg80	Tg0	Tg80
	lacI-GFP	lacI-GFP	Rad52-Ruby2	Rad52-Ruby2
$\alpha$ ( $\mu\text{m}$ )	0.032	0.039	0.039	0.047
$D_c$ ( $\mu\text{m}^2/\text{s}$ )	7.6E-04	4.3E-05	1.5E-04	3.7E-04
$L_c$ ( $\mu\text{m}$ )	0.010	0.011	0.009	0.020
$k_c$ ( $k_B T/\mu\text{m}^2$ )	6.075	13.053	9.117	4.920

Marcomini et al., Figure S4

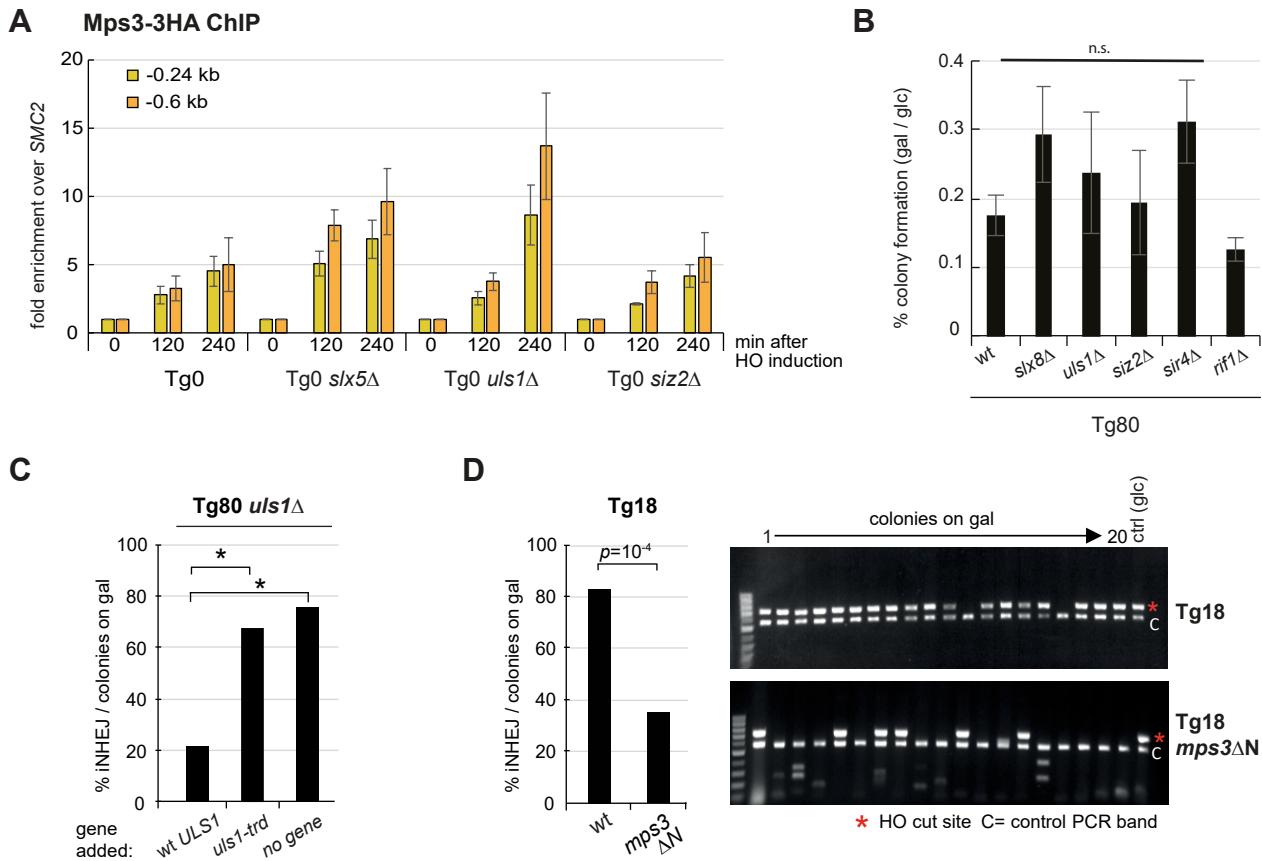
**Figure S4. Standard deviation values for the biophysical parameters defining DSB end movement.** Relates to Figure 4D. Derivation of these values is described in Amitai et al., 2017. See text for details.



Marcomini et al., Figure S5

**Figure S5. Processing of the Tg80 break by telomerase.**

A) Relates to Figure 5C. Cut efficiency calculated by qPCR as percentage of intact *MAT* locus in Tg0 (GA-8861) and Tg80 (GA-8119). Ct values from qPCR of cut locus at 90 and 180 minutes HO induction were normalized to a control locus *SMC2*, and were further normalized to the ratio at t=0. Results show the mean of 3 independent experiments, +/- s.d. B) Relates to Figure 5F. CHEF gel of wild-type chromosomal pattern for Tg80 (GA-8119) grown always on glucose. C) Relates to Figure 5F,G. Sequencing analysis by PacBio for aTg0 and aTg80 colony grown on galactose, out of 3 analyzed by SMRT sequencing with identical results. This shows homology-mediated ectopic recombination between the non-TG side of the Tg80 DSB on Chr III with the *MNT2* gene on Chr VII-L. D,E) Relates to Figure 5F,G. Telomere PCR at a DSB in Tg0 (GA-8860), Tg80 (GA-8119) and Tg80 *est2Δ* (GA-9005), at indicated time points after HO induction in exponentially growing cultures. Extracted DNA samples was used as template for two PCR reactions: the control amplicon in *SMC2* (marked as C), and the amplified telomeric repeat extension which generates an upward smear of varying sizes (red asterisk plus bar). Shown is a 1.5% agarose gel and stained with RedSafe nucleic acid staining solution (ChemBio). The graph in panel E represents the quantification of the smear in arbitrary units for the color-coded indicated zone over background values. F) Relates to Fig. 5 and Fig. 1D. Deletion of telomerase catalytic subunit Est2 rescues the delay in relocation to the nuclear periphery of Tg80. Quantitation of focus number in zone 1 of the nuclear volume as in Fig. 1D at indicated time-points after HO induction in Tg0 (GA-8861), Tg80 (GA-8119) and Tg80 *est2Δ* (GA-9005). Error bars represent mean values of 3 independent experiments, +/- s.e.m. n=80 nuclei for each strain and experiment. The red dotted line indicates a random distribution.



Marcomini et al., Figure S6

**Figure S6. DSB-Mps3 anchorage is Siz2 and Uls1 independent and enhances NHEJ over ectopic HR.**

A) Relates to Figure 6B,C. ChIP for HA-tagged Mps3 monitors *MAT* locus association with Mps3 at indicated time points after HO cut induction on galactose in Tg0 wild-type (GA-8306), *slx5Δ* (GA-8539) and *uls1Δ* (GA-8542) cells. Data from two- (Tg0) or three- (*slx5Δ*, *uls1Δ*, *siz2Δ*) independent experiments are presented as mean +/- s.e.m. B) Relates to Figure 6D. The indicated mutants do not compromise overall survival on galactose of a cut at Tg80. Ratio of colonies on galactose normalized to colony numbers on glucose was calculated for the indicated Tg80 mutants. Each column represents the mean of at least three independent experiments, +/- s.d. C) Relates to Figure 6D. The *uls1Δ* strain (GA-9855) was complemented with a plasmid expressing either no *ULS1* (no gene, pRS416), wt *ULS1* (p416-FLAG-*ULS1*) or translocase-dead *uls1* (p416-*uls1*-K975A, *uls1-trd*). Survivor colonies after 5 days on galactose from each strain were monitored by PCR for repair by imprecise NHEJ (as in Fig. 6D, n= 40, wt *ULS1*; 40, *uls1-trd*; 37, no gene). Whereas wt *ULS1* reduces imprecise NHEJ events, the translocase deficient *uls1* mutant does not. The asterisk indicates statistical significance with a p value < 10<sup>-4</sup> in a Chi square test with 95% confidence interval. D) Relates to Fig. 6. The assay for NHEJ pathway efficiency (Fig. 6D) was performed on exponentially growing cultures of Tg18 (GA-9824) and Tg18 *mps3ΔN* (GA-10054). NHEJ is highly efficient in the Tg18 strain which allows us to monitor a drop in *mps3ΔN* (GA-10054). The graph presents the % of colonies resulting from NHEJ over all galactose-grown survivor colonies (n= 40). The p value is indicated for a Chi square test with 95% confidence interval between wt and mutant. Alongside are examples of agarose gels obtained as in Fig. 6D, from DNA of galactose-grown colonies of Tg18 and Tg18 *mps3ΔN*. 20 colonies grown on galactose were selected and their genomic DNA was used in two PCR reactions to amplify the region encompassing the HO cut site (asterisk), as well as a control region in *SMC2* gene (marked with C). For each colony pooled PCR products were resolved on an agarose gel. The last lane represents a colony of the same strain grown on glucose (uncut).



## CHAPTER 4. CONCLUSIONS AND FUTURE PERSPECTIVES

---

### Processing of a persistent DSB

This PhD thesis investigated two main questions in the field of cell biology: one is the newly discovered participation of the nuclear periphery in DNA repair. The other is what differentiates a telomere as such from a DSB for the repair machinery. At the beginning of my PhD I contributed to two papers that stem from an initial observation that a persistent DSB, in absence of a partner for homologous recombination, moves to the nuclear periphery (Nagai et al. 2008). The first paper (Horigome et al. 2014) analyzes dynamics of break movement and requirements for binding to either pores or Mps3. The second paper (Horigome et al. 2016) concentrates specifically on the SUMO role in the DNA break relocation. These papers have made the first steps towards uncovering the role of the nuclear periphery in break repair. In fact, we know now that a persistent DSB moves to the NE within 40 min after break induction. This movement is dependent on SUMOylation. DSBs bind pores and Mps3 with different requirements: binding to pores occurs throughout the cell cycle, binding to Mps3 occurs only in S phase in a resection-dependent manner. SUMOylation plays an important role in the relocation of a persistent DSB to the NE: whereas pore binding requires Slx5 recruitment and polySUMOylation at the break site, Mps3 binding is independent of Slx5, but dependent on monoSUMOylation by the E3 SUMO ligase Mms21. In relation to chromatin remodeling, while Ino80 is required to bind Mps3, Swr1 and histone Htz1 are required for relocation to either site, possibly for different reasons. Finally, we have learned that DSB relocation and chromatin mobility are processes with different genetic requirements.

Despite the advances made in the past few years towards understanding the role of the nuclear envelope in repair, the fundamental question still remains: which downstream events are dependent on localization at nuclear pores or Mps3? Given the role of SUMO-dependent ubiquitin ligases in these processes, it is speculated that the targeting of proteins to the proteasome, which is enriched at the nuclear envelope, may be a key step in repair pathway choice. Alternatively, deSUMOylation by the pore-associated SUMO protease Ulp1 in yeast, may be required to initiate an alternative pathway of repair. On the other hand, Mps3 appears to sequester ssDNA from ectopic recombination and its role may simply be structural. Further studies are needed to test these hypotheses (discussed in Horigome et al. 2014, 2016).

## **A different approach to investigate repair at the nuclear periphery**

Given the numerous players recruited to break sites, and the large number of proteins that are SUMOylated at DSBs, it is difficult to determine which target might be most crucial for DSB repair or for relocation. Moreover, SUMO ligase/protease and STUbL mutants have pleiotropic effects that make it quite hard to dissect single events and causality at the nuclear pore. Most of the progress has been made through the use of mutants, and this genetic approach has natural limitations. First, the mutants have variable viability, and second, there are multiple potential interpretations of the readout. While high-resolution microscopy provides some insight, it is hard to determine the relevance and significance of biological observations on the single cell level, for repair events that might represent a very small fraction of the total cells in a population. In most cases a DSB without an homologous donor for repair will cause cell death.

The bottom up genetic approach, which leads from DSB to NE function, is based on educated guesses and seeks to find some biological relevance for the events observed. An alternative approach that might yield major contributions could be a top down systematic analysis of several repair pathways and their components with respect to the nuclear periphery, or at the known sites for repair at the nuclear periphery. This was done in part by localizing Rad52 foci, which were systematically excluded from the nuclear periphery (Bystricky et al. 2008), except -surprisingly - in the case of short telomeres, for which Rad52 foci could be observed at nuclear pores (Khadaroo et al. 2009; Churikov et al. 2016). Some nuclear pore mutants do affect repair pathways (Loeillet et al. 2005; Nagai et al. 2008; Bukata et al. 2013; Chung et al. 2015), as does the *mps3 $\Delta$ N* mutant (Horigome et al. 2014), yet it is difficult to exclude indirect effects of these mutations that stem from impaired nuclear trafficking and related functions. In my thesis I contributed by testing NHEJ and break-induced replication, given that unequal sister chromatid recombination (uSCR) was already tested. However, there is as yet no analysis of NE contribution to synthesis-dependent strand annealing (SDSA) or single strand annealing (SSA), although assays for these repair pathways exist (Moore et al. 2009a; Korbelt et al. 2017). By testing all possible pathways of repair for comparative effects on damage outcome, one may be able to identify new determinants and rate limiting steps in repair pathway choice.

Understanding how cells control repair pathway choice is important because the classic chemotherapeutic drugs are based on provoking DNA damage that overwhelms repair pathways, which themselves are often mutated in cancers. Although it was shown in a chemical screen that drugs that target nuclear pores are synthetic lethal with compromised recovery from replication stress (*mec1-100* or *sgs1 $\Delta$*  mutants in budding yeast on HU, K. Shimada and SM Gasser, unpublished),

it is unclear what aspects of pore function they affect. This approach has not been exploited for cancer therapeutics because the exact contributions made by nuclear structure and the spatial organization of repair are still poorly understood. For example, it is intriguing that precise end joining is not perturbed by deletion of Nup84 (Horigome et al. 2016, Fig.6), while imprecise end-joining is. This would suggest that something specific to the imprecise pathway requires the pore: it could be the initiation of resection, or the trimming of 3' ends by the Rad1-10 complex, a step that is also involved in nuclear excision repair (NER). NER however does not require resection. So, if *nup84Δ* did not have a clear NER phenotype, this would suggest that end trimming is not the limiting factor in imprecise NHEJ in *nup84Δ*. If it did have such phenotype, in the context of an induced DSB, one could look at fluorescently tagged Rad10 localization. Rad10 was already shown to form foci in response to DSBs (Moore et al. 2009b), but their nuclear location was not analyzed. On the other hand, if repair proteins are present in excess of the lesions, it may be difficult to see any preferred localization at pores or other substructures.

Another aspect that reveals the limitations of our understanding is that to date only nuclear pores and Mps3 have been described as NE compartments with a role in DSB repair. Recently, a novel sub-pore particle that consists of Nup170, Siz2, Esc1 and Sir4 has been proposed (Lapetina et al. 2017). Given the effects we observe of the *sir4Δ* on NHEJ frequency, it would be interesting to test a mutation in Nup170 for its role in creating a novel NE subcompartment for repair.

It is possible that other unsuspected or unknown NE partners are involved in DSB repair, which might be discovered by detecting DSB binding proteins at the NE in an unbiased way. A generic screen for NE proteins binding a single DSB would not be easy, because these proteins would likely be hydrophobic and difficult to solubilize. To surmount the intrinsic difficulties of catching transient interactions, Bio-ID has been successfully applied in many contexts in mammalian cells. Although there are only a few reports in yeast (Williams et al. 2014; Kim et al. 2016), Bio-ID provides a mean to identify proteins that are difficult to purify. It involves fusion of the biotin ligase BirA with a protein of interest and consequent biotinylation of proximal endogenous proteins, that can then be recovered by a standard biotin-affinity column. Alternatively, one could try to pull down GFP in the strains with GFP-tagged DSB, in a SILAC condition +/- DSB induction. This pulldown would have the advantage that the system is not affected by any modifications. Either of these assays could yield novel players in DSB processing and repair at the NE.

## **The nucleo- to cytoskeleton connection**

MonoPolar Spindle 3 (Mps3) is a mysterious protein. On the one hand it is a component of the spindle pole body (SPB) half bridge, where it is important for meiotic bouquet formation and correct chromosome segregation(Jaspersen et al. 2002; Conrad et al. 2008). On the other hand, it has a recently described role in DSB repair(Oza et al. 2009; Peterson and Craig 2010). Intriguingly, Mps3 is one of two binding sites that an irreparable DSB will move to with the other being the nuclear pore (NPC)(Oza et al. 2009; Horigome et al. 2014). The choice of repair site is regulated by the cell cycle. While DSBs can bind pores throughout the cell cycle, DSBs will not be recruited to Mps3 in G1 phase because binding to Mps3 requires resection, which occurs mostly in S phase(Horigome et al. 2014). However, Mps3 affects the interaction of a DSB also with nuclear pores, for unknown reasons. The N-terminal domain of Mps3 is of particular interest. This domain can be cleaved during meiosis, which changes the conformation of the protein and facilitates segregation(Li et al. 2017). In addition, the N-terminus is necessary to anchor telomeres, bind DSBs and prevent ectopic recombination events(Schober et al. 2009).

Mps3 is a member of a large family of transmembrane proteins called Sad1-UNC-84 homology (SUN) family. It is conserved from yeast to man. Recent work with mammalian SUN domain-containing proteins (SUN1/2) that are themselves components of the greater Linker of Nucleoskeleton and Cytoskeleton Complex (LINC), has shown that these proteins are important for increased movement of dysfunctional telomeres as well as DSBs(Lottersberger et al. 2015). Moreover, degenerative laminopathies have been shown to be suppressed by loss of SUN1(Chen et al. 2012). In mammalian cells, microtubules connect to the nucleus through the LINC complex. In the same study, depolymerization of microtubules through toxins such as Taxol or Nocodazole prevented increased movement of dysfunctional telomeres and decreased the frequency of telomere end-end fusions. These observations have led to the hypothesis that external forces transmitted from cytoplasmic microtubules to the nucleus can contribute to ectopic repair events.

In yeast, chromosomes are constitutively tethered to the SPB through their centromeres by kinetochore microtubules, and Nocodazole treatment in yeast actually increases - rather than blocks - the chromatin movement (Marshall et al. 1998; Amitai et al. 2017). Nocodazole also triggers the release of centromeres from the SPB(Bystricky et al. 2004), which could be another source of altered movement. However, one observation that may support a role for external microtubules affecting the internal movement of a DSB is that increased movement of a DSB is prevented by nocodazole treatment(Amitai et al. 2017; Lawrimore et al. 2017)



Lately, there has been evidence for a role of nuclear actin in repair, not only limited to its role in chromatin remodelers. A recent study analyzed the subdiffusive movement of chromatin in response to actin depolymerization in the nucleus (Spichal and Fabre 2017). They demonstrated that chromatin movement in yeast is decreased by an actin polymerization inhibitor, in a way that is independent of the putative LINC component Csm4. Importantly, this study did not look at a DSB movement. In addition, they showed that tethering actin to the nuclear envelope increased the movement of pores within the envelope itself. In the nucleus of *S. cerevisiae*, most of G-actin was shown to be in complex with Arp4 (Miyamoto and Gurdon 2013), which blocks the formation of a polymer fiber, but in other model systems there is some evidence supporting intranuclear oligomeric structures different from cytoplasmic F-actin (Görllich et al. 2006; McDonald et al. 2006; Kalendová et al. 2014; Belin et al. 2015). A very speculative scenario in case of a persistent DSB is that the interaction with the LINC complex member Mps3 could provide a link between the nuclear actin and the cytoplasmic cytoskeleton, promoting NPC movement. An interaction of Mps3 with actin was not reported, but Mps3 was shown to interact with formin (Bnr1 and Bni1) by yeast two-hybrid assays (Wang et al. 2012), and formin is important to nucleate actin filaments (Baarlink and Grosse 2014). Perhaps the ability of nuclear pores to shift in the membrane would facilitate interaction with the DSB or partial clustering of a subset of pores. Association of a subset of nucleoporins of the outer and inner pore ring in a complex distinct from NPC was recently reported (Lapetina et al. 2017). Such a model would explain why Mps3 deletion affects relocation of a DSB to pores. Mps3 could therefore mediate the link between DSB signaling and nuclear actin oligomers thereby favoring mobilization of pores.

It was recently shown that treatment of cells with Latrunculin A, which inhibits actin polymerization, only partially attenuates the damage-dependent increase in locus movement (Amitai et al. 2017). However, this study did not look at NE interactions or repair efficiency: if actin is required to transmit the cytoskeleton-to-Mps3-to-pore signal, a DSB upon Latrunculin A treatment would still be able to bind Mps3 but maybe not pores. These aspects are ripe for exploration.

## **Processing of TG-flanked double strand breaks**

My main project tackled the long-standing question of what defines a telomere and protects it from the repair machinery. The main advantage of my system is that the telomeric repeats I used are isolated from their natural location at chromosome ends, allowing for unbiased investigation on how the repeats affect repair. I could show that 80bp of telomeric repeats are sufficient to block long-range resection and strongly inhibit the binding of the MRX complex. This is sufficient to disengage

the destiny of the two DNA ends: one gets elongated by telomerase, the other translocates onto another chromosome. The separation of ends also allows them to explore a larger portion of the nuclear volume. Particularly on the non-TG end we observe increased movement which theoretically should favor homology search. Furthermore, TG repeats affect binding of the DSB to the nuclear periphery: they completely abolish interaction with Mps3, consistent with their ability to block resection. Interaction with the periphery is affected by SUMO: the SUMO dependent ubiquitin ligase Uls1 has the strongest effect on repair outcome. Mutations of the NE binding sites, Nup84 and Mps3, have opposite effects in repressing and favoring the translocation, respectively. In conclusion, the presence of MRX at both sides of a DSB is a key determinant of genomic stability.

### **The resection block imposed by TG repeats**

The most pressing question arising from these observations is: what imposes such a strong block to resection at TG-flanked breaks? A recent study analyzed TG-flanked breaks and telomeres of different lengths: they pinpointed a threshold in telomere addition at TG34. They propose a model where, at TG tracts of less than 34 bp, Pif1 helicase inhibits telomerase recruitment, whereas when TG repeats are over 34bp, Cdc13 outcompetes Pif1 and promotes elongation by telomerase, both at telomeres and at TG-flanked breaks(Strecker et al. 2017). However, a follow up paper shows that Pif1 inhibitory effect on telomerase activity is not dependent on telomere length, indicating that Pif1 itself is not responsible for setting a threshold of repeats elongation(Stinus et al. 2017). Since the threshold is also not dependent on the Cdc13-Est1 interaction, the authors suggested a specific role for Cdc13 binding alone. While Cdc13 is a player that should be tested in a rapid timecourse in my TG-HO system, binding of Cdc13 at Tg80 would imply ssDNA exposure, hence Mre11 binding, which is barely detectable at TG80-flanked DSBs by ChIP 90 mins after break induction. Furthermore, nuclear Pif1 is involved in several biological processes, like Okazaki fragment processing, telomeres replication, and BIR(Geronimo and Zakian 2016). Binding partners in any of these processes, brought in by Pif1, could play a direct role in telomerase regulation.

A likely candidate responsible for blocking resection is Rap1: this protein in yeast binds tightly to telomeric repeats in a sequence-specific manner, through a bipartite binding site that resembles the Myb domain(Gilson et al. 1993; Konig et al. 1996). Rap1 molecules bind continuously along the repetitive telomeric consensus sequence with a spacing of about 18bp(Gilson et al. 1993). Negrini and colleagues showed that, when long TG telomeric tracts (250bp) were exposed by induction of a nearby DSB in the subtelomeric region of chromosome V, the binding of Mre11 and Cdc13 along the repeats was inhibited. To test if Rap1 was the cause of this inhibition they incorporated synthetic

arrays of 16 Rap1 binding sites, either the precise consensus or sequences with a critical mutation that would prevent Rap1 binding. In the latter case, in absence of Rap1 binding the binding of Cdc13 and Mre11 to the sequence upon DSB was rescued. However, in the subtelomeric region, Rap1 seems to block Mre11 and Cdc13 binding only at long TG tracts (more than 4 Rap1 binding sites), as showed by ChIP, and they reported that Tg80 is resected and binds Mre11 when flanking a DSB in the subtelomere. However, no 'Tg0' control is reported in this work, hence it is unknown how much Cdc13 or Mre11 would be detected by ChIP at that locus in absence of TG repeats. The authors further report that Tg80 gets resected, as measured by Southern blot and measurement of the relative enrichment of the 3' strand over the 5' strand within 70bp from the DSB site. This is not necessarily in contrast with my data, since I measured resection starting 300bp away from the DSB. Again in this experiment it would have been interesting to see the data in absence of TG repeats. When Tg80 was integrated at *MAT*, I detected some levels of ssDNA as well as Mre11 binding, but these amounts are not relevant when compared with a Tg0 construct.

It could also be that Tg80 behaves differently when located at a DSB in an internal position along the chromosome, given that subtelomeric chromatin far beyond the spread of SIR-mediated repression is unique in its nucleosomal modifications (Robyr et al. 2002). In addition, DSBs in this subtelomeric zone have been shown to have unique repair outcome (Taddei and Gasser 2004; Agmon et al. 2013). Therefore, the genomic location of the construct could be important. It is highly likely that a chromatin-based mechanism senses position and tailors the response accordingly. Perhaps the cell has developed ways to prevent maintenance of short TG tracts (of length comparable to a short telomere) in an internal position, because over generations these repeats could become unstable, either causing replication fork to stall, or sequestering telomeric factors away from the telomeres. An aspect of nuclear substructure, for example, the clustering of telomeres in foci, could favor a high local concentration of factors and influence end processing. In support of this hypothesis, clustering of telomeres in foci is promoted by the SIR proteins (in particular Sir3), and in a *sir4Δ* mutant I could detect an appreciable change in repair pathway choice.

### **Control of chromosome length by SMC proteins**

Another player in determining repair pathway choice could be the Structural Maintenance of Chromosome (SMC) proteins, which also sense DSBs and are involved in higher order chromatin folding. The characterization of survivors on galactose in TG-DSB-containing strains might provide insight into the effects of repeats on chromosome stability. I know that these survivors are stable at

least for a few generations. However, these cells have a chromosome shortened by 100kb and a *de novo* telomere. How is chromosome stability reorganized in light of the translocation?

Chromosomes stability and accurate segregation are safeguarded in the cell by SMC proteins. There are 3 SMC complexes: condensin (SMC1-3) responsible for chromosome assembly, cohesin (SMC2-4) that prevents early separation of chromatids in anaphase, and SMC5/6. They all share a conserved V-shaped structure, with two long arms, each of which has an ATP-binding head tail. SMC5/6 has been implicated in several processes: it is required for appropriate segregation and integrity of nucleolar DNA, and more in general of repetitive DNA (Torres-Rosell et al. 2005a; Torres-Rosell et al. 2005b). It has been involved also in replication termination. It associates to DSB in a Mre11-dependent manner and has been shown to promote the resolution of joint DNA molecules during recombination, both in mitosis and meiosis (Bermudez-Lopez et al. 2016; Bonner et al. 2016). SMC5/6 is necessary for movement of a persistent DSB to the nuclear periphery, thanks to its Mms21 component (E3 SUMO ligase) and its interaction with Slx5/8 STUbLs (Horigome et al. 2016). Movement of Tg80 to the periphery also requires SUMOylation (Siz2) and the STUbL Uls1, which recognizes polySUMO chains. While the requirement for Mms21 for Tg80 relocation was not tested, it is likely to be required for the initial monoSUMOylation event on the distal DSB side. However, the proximal side of Tg80, that is also the side whose relocation depends on Uls1, does not interact with Mps3: it would be interesting to test SMC5/6 role in relocation of the proximal side. It is possible that the SUMOylation target on that side is not a target of Mms21, because the SMC5/6 complex is recruited to a DSB through Mre11 (Lindroos et al. 2006), and TG repeats inhibit MRX binding. Alternatively or in addition, Uls1 might target protein(s) associated with repetitive DNA regions.

It is noteworthy that relocation of Tg80 to the NE is delayed due at least in part to telomerase elongation. A Ku80-Sir4 dependent pathway for telomerase recruitment was recently elucidated at telomeres (Chen et al. 2018): in G1 phase, Ku recognizes a bulged loop in TLC1 telomerase RNA moiety and interacts with Sir4. This complex facilitates accumulation of telomerase at DNA ends and can sustain basal telomerase activity in S phase also when the Cdc13-Est1 interaction on the ssDNA stretch is compromised. Uls1 was shown to interact with Sir4 C-terminal domain by biochemical assays (Zhang and Buchman 1997): this interaction was thought to be important for Uls1 interference with heterochromatin silencing when overexpressed. Since 80bp TG repeats seed telomerase elongation, it could be that the Uls1-Sir4 interaction has a role in the relocation dynamics that has not been explored. Indeed deletion of *SIR4*, like that of *ULS1*, alters repair pathway choice of Tg80, suggesting that Sir4 might be an important SUMOylation target with respect to repair. SUMOylation is known to interfere with NE interaction at Mps3 (Ferreira et al. 2011).

Notably, in absence of DNA damage the SMC5/6 complex does not require Mre11 to associate to DNA. In G2/M, SMC5/6 associates to chromosomes by binding cohesin (SMC1/3), while very few SMC5/6 molecules are detected along chromosomes in G1 (Jeppsson et al. 2014). The binding sites are mostly in intergenic regions that have a tendency for transcription-replication collisions. Moreover, SMC5/6 is not uniformly distributed: this is evident particularly on long chromosomes, where it concentrates around the centromere and is much less detectable towards the telomeres. The longer a chromosome arm, the more SMC5/6 accumulates in the centromeric region (Jeppsson et al. 2014). The reason for this distribution was not demonstrated but there are several indications that SMC5/6 helps relieving superhelical stress, which tends to be higher for long chromosomes. It has been difficult to demonstrate that SMC5/6 targets topological stress, because mutants have pleiotropic phenotypes, and their topological effect only becomes evident upon mutation of topoisomerases. Topological stress is one feature of both high transcription and replication: during replication, the passage of the fork separates the parental DNA strands causing the formation of supercoils ahead of the fork and sister chromatid intertwinings (SCI) behind. In yeast topoisomerases I and II (Top1 and Top2) resolve the supercoils, whereas SCIs are resolved by Top2. During transcription, supercoils are formed and resolved continuously. It was seen that in mutants of Top2 SMC5/6 accumulates along the chromosomes in a manner dependent on chromosome cohesion. This accumulation did not relate to the presence of DNA breaks, stalled replication forks or recombination (processes where SMC5/6 was shown to be involved), but was dependent on passage through S phase. This is coherent with the idea that SMC5/6 recognizes a structure normally resolved by Top2, but that persists after replication in absence of Top2. In fact, if Top2 is inactivated after replication in G2/M, the amount of SMC5/6 binding on chromosome arms does not increase (Jeppsson et al. 2014). Moreover, the modifications of two convergent natural gene promoters into high copy promoters is sufficient to induce a new SMC5/6 binding site (C. Sjoegren, personal communication). To demonstrate that SMC5/6 helps to resolve supercoils, the system of inducible translocation I discovered could become useful, because it would shorten the already short chromosome III and elongate chr VII. The TG-HO DSB could be placed at a site of high convergent transcription in the middle of a chromosome. This should induce SMC5/6 binding. Upon DSB induction, the translocation would cause the site to be located now at a telomeric region, where torsional stress is easily relieved by rotation of the chromosome arm. It would be interesting to observe a reorganization of SMC5/6 along the shortened chromosome arm, that would be in line with a topological function of SMC5/6.

This line of research is starting to be pursued by the Sjoegren lab in Stockholm. Since chromosome III is already small, to have a clearer phenotype they put the MNT2-HO-Tg80 construct in this

orientation (TG on the telomeric side of the break, opposite to the orientation I used) in the middle of another chromosome (XI), close to a site of high convergent transcription. Interestingly, they observe translocation also in this different chromosomal context. The translocation, however, is not onto chromosome VII but onto chromosome XIV. This result needs to be confirmed, and it is necessary to understand what kind of repair pathway the TG end (that is, this time, the translocating end) engages in. Importantly, this means that the inhibition of end joining observed in TG-flanked DSBs is not dependent on some specific feature of the *MAT* locus.

### **A possible role of transcription in nuclear organization of DNA damage**

One aspect that remains unexplored in the system we developed is the contribution of transcription and the role of RNA polymerase II (Pol II). An important role for transcripts in the DNA damage response is emerging in many organisms. In higher eukaryotes, these small RNAs are Dicer and Drosha dependent, and they were proposed to help recruitment of repair proteins to break sites, or to direct chromatin modification (Francia et al. 2012; Wei et al. 2012; Gao et al. 2014; Storici et al. 2014). *S. cerevisiae* lacks the RNAi machinery, yet small RNA species were detected and were proposed to participate actively in the repair process by acting as templates for homologous recombination reactions (Keskin et al. 2014). Furthermore, at telomeres TERRA, a long non-coding RNA transcribed from subtelomeric promoters, has major functions in telomere stability. Mammalian ALT cells overexpress TERRA: mounting evidence shows that increased TERRA transcription causes the formation of DNA:RNA hybrids and stimulates the binding of RPA. Persistent RPA binding stimulates the recombination with other telomeric sequences which constitutes the ALT mechanism of telomere maintenance (Arora et al. 2014; Arora and Azzalin 2015). Telomeres depleted of TRF2 are uncapped and tend to fuse by NHEJ. It was reported that the histone demethylase LSD1 increases its association with uncapped telomeres, even without significantly altering chromatin structure. The increased association of LSD1 with telomeres is instead dependent on Mre11: Lsd1 stimulates Mre11 nuclease activities and promotes the 3' G overhang processing that precedes chromosome fusions (Porro et al. 2014). Deprotected telomeres also overexpress TERRA, which bind LSD1 and are important to stabilize LSD1 interactions with the MRN complex. In *S. cerevisiae*, it was demonstrated that TERRA are overexpressed from a short telomere and a study used cytological live-cell assay to show that TERRA form a nuclear cluster with telomerase. The authors suggest that once the cell enters S phase, they guide telomerase to the telomere that needs to be elongated (Cusanelli et al. 2013). In absence of telomerase, TERRA molecules promote telomeric recombination of very short telomeres: there, the transcripts produced associate with their native locus in R-loops, but their

amount is not enough to recruit Rat1 and RNaseH, enzymes that normally cleave R-loops, hence in this condition TERRA promote DNA damage signaling and Rad51 recruitment(Graf et al. 2017).

The presence of damage-induced RNA species was reported that could affect the processing of ends: the presence of a few oligonucleotides of ssRNA with a 3'-OH terminus was shown to be a sufficient template for elongation by Pol II(Kadesch and Chamberlin 1982). In *S. pombe*, damage-induced RNAs (diRNAs) were identified at DSBs and reported to stabilize short ssDNA tracts, thereby inhibiting RPA binding(Ohle et al. 2016). In my system, transcription is occurring at the site of integration of TG repeats: the promoter of the *MAT* locus is about 1500bp away, and the one of *MAT $\alpha$ 1* is 350bp away. When a DSB occurs in an actively transcribed region, higher eukaryotes activate an ATM-dependent signaling pathway that shuts off transcription of the damaged region(Soutoglou et al. 2012). It has been shown instead that in *S. cerevisiae*, inhibition of transcription around the damaged locus also occurs, but is not Mec1/Tel1 dependent and is due to resection(Longhese et al. 2015). In the TG-HO system described in this thesis, given that the TG side of the break is not resected, transcriptional shutoff may not occur. It is possible that in such a situation the formation of R loops is favored, that is the reannealing of the nascent RNA strand to the native DNA sequence. R loops have been shown before to be associated with genomic instability and gross chromosomal rearrangements due to replication fork collapse(Al-Hadid and Yang 2016). It is not excluded that they act elsewhere as well. My system offers the opportunity to follow the effects of the stabilized transcription products on repair outcome at a single hard-to-repair break: to begin with, one could overexpress RNaseH or make use of the mutant *rnh1rnh201*, to see if and how DSB processing and repair pathway are affected by these RNA species. In fact, TERRA, R loops and diRNA are all substrates of RNaseH.

### **The role of end separation in DSB repair pathway choice**

Another question arising from my project is whether end separation is sufficient to promote ectopic recombination, or whether there is something intrinsic to the TG end that contributes to the translocation event on the opposite break end.

This question could be answered by the use of a strain with the same DSB at MAT and the MNT2 homology (without TG repeats), and with *rfa1-t11* mutation. This mutation maps to the OB fold in the N terminus of the Rfa1 subunit of RPA. It is essential for recruitment of MRX, but it does not affect resection, which makes it a great way to separate the function of these two events (resection and MRX binding) on repair. Seeber et al.(Seeber et al. 2016) demonstrated that Rfa1 promotes the function of MRX in holding break ends and sister chromatids together. They also show that this mutant has reduced repair efficiency in both HR and NHEJ tests. Nonetheless, with my system what

I would be scoring is not the absolute survival but rather the ratio NHEJ/translocation, that is, how end separation affects repair pathway choice, in absence of TG repeats (in the strain Tg0-HO-MNT2). This strain normally repairs only by end joining. If some of the galactose survivors in the *rfa1-t11* mutant would translocate, this would mean that an efficient recruitment of MRX is sufficient to affect repair pathway choice.

It is noteworthy that in T2(AG)3 strain, resection is as efficient as in a wt strain, but repair by NHEJ is only about 45%, versus the 5% of NHEJ in Tg80. This means that resection and repair pathway are not necessarily coupled. A further indication is the phenotype of *uls1Δ* and *sir4Δ* on Tg80: both of these mutants have almost no effect on the resection block on the TG side of the DSB, but increase 10-fold the frequency of NHEJ among galactose survivors. While resection is measured in a population of cells in a liquid culture, repair in my system always concerns a small percentage of the total population of cells plated. What my data suggest is that while the binding of Rap1 is most likely the key factor in rescuing the resection block of Tg80, other DSB factors not strictly dependent on Rap1 contribute to inhibiting end joining in this strain, or other factors Rap1-dependent are actively promoting GCRs. Whether this phenotype is an active promotion of GCRs or prevention of end joining could be figured out by quantifying the total amount of survivors on galactose for the two constructs, once the *MNT2* homology region downstream of the HO cut site has been removed: in this case NHEJ is going to be the only available pathway for repair, and if end joining is inhibited by some other factor that binds T2(AG)3, then the total amount of survivors in T2(AG)3-(no MNT2) should be decreased.

The phenotype of Tg80 *sir4Δ* is particularly interesting: at telomeres, Rap1 was proposed to inhibit end joining through three independent pathways, one dependent on Sir4, one on Rif2, and one on the central domain of Rap1 itself (Marcand et al. 2008). These pathways were shown to act also at an internal DSB flanked by 256 bp of telomeric repeats, but the mechanism is not known (Marcand et al. 2008). Moreover, at telomeres Sir4 and Uls1 were shown to prevent NHEJ (telomere fusions) in a synergistic manner, so it can be speculated that also in the described TG-HO system a double mutant *sir4Δuls1Δ* would have more NHEJ over HR repair (Lescasse et al. 2013). While 250bp of telomeric repeats can nucleate Sir4-mediated heterochromatin, 80bp are not enough to do so (Luo et al. 2002), yet I observe end joining inhibition also in Tg80, which is located in a transcribed locus (where Sir4 is not expected to bind), suggesting that Sir4 function in preventing end joining might be independent from its role in heterochromatin formation. Intriguingly, Sir4 was found to interact with several deubiquitylating enzymes, like Tom1 and Dia2 E3 ligases, Ubp10 and Ubp3 proteases. The significance of these interactions has been partially explored only in the context of heterochromatin



maintenance: for example, Dia2 was shown to promote silencing at telomeres and HM loci by keeping the amount of monoUb-H2B low. Ub-H2B is required for H3K4 and H3K79 methylation, that are markers of transcriptional activity and an obstacle for Sir4-mediated heterochromatin assembly. H3K79me is known to recruit Rad9 (the yeast homologue of 53BP1) that blocks resection and favors end joining(Wysocki et al. 2005). Moreover, Tom1 is known to be required for Dia2 ubiquitylation and degradation in G2 phase, while in S phase Dia2 is stabilized. Sir4 is also a target of Tom1. Since Sir4 is having such significant effect on repair of Tg80, despite the locus not being heterochromatic, it could be that Sir4 function at this DSB is to bring in ubiquitin ligases. A way to explore a possible role of Sir4 ubiquitylation would be to try complement Sir4 deletion with a Sir4-RKR mutant that is not ubiquitylated and quantify an effect of NHEJ repair. One could also get a comprehensive view of ubiquitylation with a mass-spec (SILAC) approach that compares ubiquitylation after a DSB +/- Tg repeats, exploiting the presence of lacO-repeats.

### **Relevant modifications to the TG-HO system**

TG-HO system offers the possibility to investigate the order of events at a persistent break in relation to the nuclear periphery. The relative movement of two homologous loci was studied previously in diploids(Rothstein and Rodney 2012). Now that we know how few telomeric repeats are able to affect break processing, we could tag the nonTG (translocating) side of the DSB, as well as the homologous donor on chr VII, and analyze several features: what is the timing required for the break and the donor site to come together? The rate of survival is very low compared to reported examples of ectopic recombination(Haber et al. 2016). One possible reason for this could be that the donor and acceptor sequences are located in different regions of the nuclear volume(Agmon et al. 2013), and contact frequency of donor and acceptor sequences is a major determinant of repair frequency(Haber et al. 2016). In addition, the donor (*MNT2*) is located in a subtelomeric region, hence embedded in heterochromatin at the nuclear periphery. This could make it less dynamic and decrease the chances of contact with the DSB during homology search(Batte et al. 2017). By visualization of the break and the donor site it would be possible to understand the dynamics of homology search for the two recombination partners and how they are affected by their chromosome location. Moreover, by adding a tag to the NPC one could examine how they move in relation to the NE. When do they relocate to nuclear pores and how long does the binding persist? Do the two ends meet at pores or beforehand?

Further insights on the effect of TG repeats on DSB repair could come from inserting the TG repeats on the opposite side relative to the HO, in a *MNT2-HO-TG80* setup: now, TGs would be on the

telomeric side of the break. A probable outcome of repair is illustrated in Figure 6. This system could be tuned to allow an unbiased screen for factors that promote NHEJ in presence of TG repeats. Upon DSB induction, the nonTG side will recombine with chromosome VII and likely be repaired by BIR, while the TG side of chromosome III will form an acentric chromosome with two telomeres. Since it harbors essential genes, this acentric chromosome will probably be maintained for several generations, but eventually it might be lost, causing cell death. As mentioned before, some preliminary data from the Sjogren lab indicate that in MNT2-HO-TG80 a translocation still takes place: it could be caused by a telomere-telomere fusion of the acentric chromosome with another chromosome, or by some microhomology region present within the 100kb. In any case, if this result will be confirmed, it will be important to establish the frequency of this translocation, as well as the rate of loss of the acentric chromosome. A rate of loss within a few hundreds of generations, together with a very low frequency of translocation, would allow to use the MNT2-HO-TG80 system for a mutagenic screen: random mutagenesis of the culture before cut induction with galactose, than plating on galactose, replicating plates (to allow time for loss of the acentric chromosome and consequent death of the corresponding colony), and screening the repair of survivors. Survivors repairing by end joining could then be characterized to find out which genes were hit by the mutagenesis. One positive control in this screen would be Uls1.

It must be said that this perspective is rather optimistic: essential genes will probably not be lost so easily, and cells with an acentric chromosome are able to survive for several generations (Dani and Zakian 1983). However, the system could be designed so that the gene recreated by recombination is not MNT2, but a toxic gene that becomes functional only upon BIR. This gene would allow for a positive selection of candidates whose loss favors end joining.

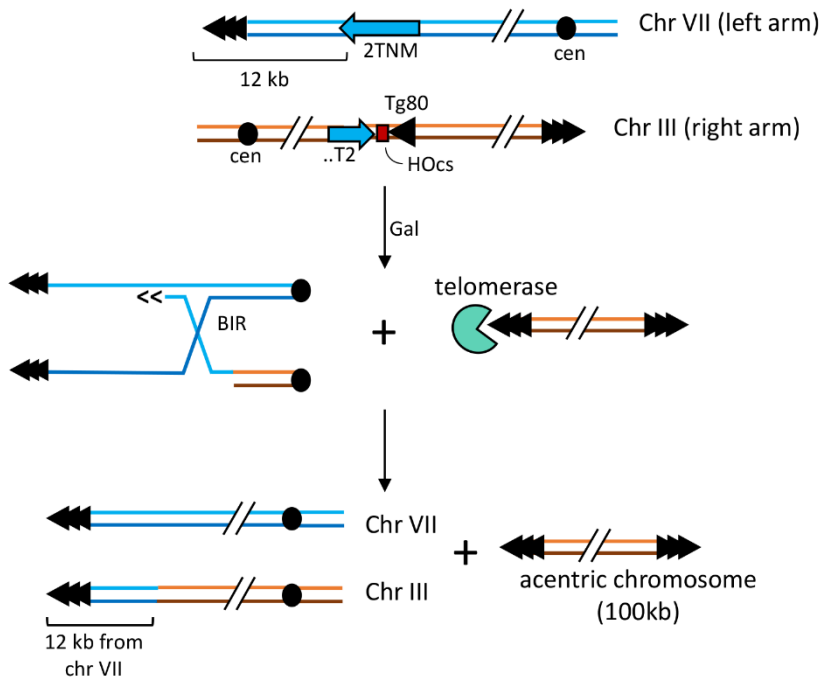


**Fig. 6. Outcome of repair when TG repeats are located on the telomeric side of the DSB.** 80 TG repeats will recruit telomerase and be elongated, causing the formation of an acentric chromosome. Because this chromosome has essential genes, it will be maintained for several generations. The other break end will likely invade MNT2 in the subtelomere of chromosome VII and induce BIR, with consequent duplication of the subtelomere of chromosome VII.

Many insights into the effect of TG repeats on repair would also come from other setups, with TG stretches flanked by a DSB, but a different homology region. In fact, all the non-NHEJ survivors I observed had a nonreciprocal translocation, and this way of repairing is possible because the loss of the subtelomere of chromosome VII is compatible with life. If the donor homology region was placed more centromere proximal, what would be the outcome of repair? There would likely be just very rare (NHEJ) survivors (5% of Tg80 survivors still repair by end joining), but in this condition repeats could also promote some kind of different GCR, or be extended creating genomic instability that can be followed over generations.

By inserting short repeats on both sides in the middle of a chromosome arm, it would be possible to investigate if it is the imbalance in the binding of MRX, rather than MRX itself, that determines repair pathway choice. If MRX binding is the key determinant for repair, the survivors would probably have elongated both ends, and 100kb of chromosome III will be maintained as a stable acentric chromosome for a few generations (Dani and Zakian 1983). But if it is rather the imbalance of MRX that prevents appropriate end joining in Tg80 construct, than in TG80-HO-TG80 the cell might compensate for the absence of MRX by upregulating end joining.

### A model system for the study of translocations

Another relevant point deriving from my work concerns the minimum homology required to see the translocation occur. This is relevant also for a possible application of this system to study translocations in mammalian cells. In fact, translocations are a hallmark of cancer development: they occur particularly frequently in genomic locations called Chromosome Fragile Sites (CFS) (Schwartz

et al. 2005), but the reasons are still largely mysterious. New generation sequencing data have allowed to correlate many features of CFS with translocation frequency, although it has been very difficult to establish causality (Hogenbirk et al. 2016) (so far, only an open chromatin structure is a solid predictive factor). One main reason has been the lack of a genetic system to study the aetiology of translocations. My study could provide a way to look at early molecular events at a DSB that is known to be prone to repair by translocation.

There are different kinds of translocation, and most of them in mammalian cells are mediated by alternative NHEJ, since HR is much less common in the mammalian nucleus. Whatever the mechanism, clearly the exposure of microhomology or repeated regions is a promoting factor. In particular, the translocation I isolated is a nonreciprocal translocation. Primary nonreciprocal translocations are quite rare, but characteristic of epithelial (Mitelman et al. 2007) and renal cancers (Ali et al. 2013). Moreover, the frequency of nonreciprocal translocations increases with cancer progression in most types of tumors. This study could therefore provide an excellent model system to get better insight into the mechanisms leading to this kind of rearrangements.

In conclusion, this thesis provides evidence that having as little as 80bp of TG repeats flanking a DSB has dramatic effects on its processing, its nuclear localization and the repair outcome. TG repeats block Mre11 binding and resection, causing break ends to come apart, thereby substantially favoring gross chromosomal rearrangements. Moreover, for the first time we can visualize by microscopy DSB separation without the use of mutants, and potentially also a complex chromosomal rearrangement. Much remains to be learned, and how the nuclear envelope, the cytoskeleton and genomic locations affect these events will be an exciting future research topic.

## References

- Agmon N, Liefshitz B, Zimmer C, Fabre E, Kupiec M. 2013. Effect of nuclear architecture on the efficiency of double-strand break repair. *Nature cell biology* **15**: 694-699.
- Al-Hadid Q, Yang Y. 2016. R-loop: an emerging regulator of chromatin dynamics. *Acta biochimica et biophysica Sinica* **48**: 623-631.
- Ali H, Daser A, Dear P, Wood H, Rabbitts P, Rabbitts T. 2013. Nonreciprocal chromosomal translocations in renal cancer involve multiple DSBs and NHEJ associated with breakpoint inversion but not necessarily with transcription. *Genes, chromosomes & cancer* **52**: 402-409.
- Amitai A, Seeber A, Gasser SM, Holcman D. 2017. Visualization of Chromatin Decompaction and Break Site Extrusion as Predicted by Statistical Polymer Modeling of Single-Locus Trajectories. *Cell reports* **18**: 1200-1214.
- Arora R, Azzalin CM. 2015. Telomere elongation chooses TERRA ALTERNATIVES. *RNA biology* **12**: 938-941.
- Arora R, Lee Y, Wischnewski H, Brun CM, Schwarz T, Azzalin CM. 2014. RNaseH1 regulates TERRA-telomeric DNA hybrids and telomere maintenance in ALT tumour cells. *Nature communications* **5**: 5220.
- Baarlink C, Grosse R. 2014. Formin' actin in the nucleus. *Nucleus (Austin, Tex)* **5**: 15-20.

- Batte A, Brocas C, Bordelet H, Hocher A, Ruault M, Adjiri A, Taddei A, Dubrana K. 2017. Recombination at subtelomeres is regulated by physical distance, double-strand break resection and chromatin status. *The EMBO journal*.
- Belin BJ, Lee T, Mullins RD. 2015. DNA damage induces nuclear actin filament assembly by Formin -2 and Spire-(1/2) that promotes efficient DNA repair. [corrected]. *Elife* **4**: e07735.
- Bermudez-Lopez M, Villoria MT, Esteras M, Jarmuz A, Torres-Rosell J, Clemente-Blanco A, Aragon L. 2016. Sgs1's roles in DNA end resection, HJ dissolution, and crossover suppression require a two-step SUMO regulation dependent on Smc5/6. *Genes & development* **30**: 1339-1356.
- Bonner JN, Choi K, Xue X, Torres NP, Szakal B, Wei L, Wan B, Arter M, Matos J, Sung P et al. 2016. Smc5/6 Mediated Sumoylation of the Sgs1-Top3-Rmi1 Complex Promotes Removal of Recombination Intermediates. *Cell reports* **16**: 368-378.
- Bukata L, Parker SL, D'Angelo MA. 2013. Nuclear pore complexes in the maintenance of genome integrity. *Current opinion in cell biology* **25**: 378-386.
- Bystricky K, Heun P, Gehlen L, Langowski J, Gasser SM. 2004. Long-range compaction and flexibility of interphase chromatin in budding yeast analyzed by high-resolution imaging techniques. *Proceedings of the National Academy of Sciences of the United States of America* **101**: 16495-16500.
- Bystricky K, Van Attikum H, Montiel MD, Dion V, Gehlen L, Gasser SM. 2008. Regulation of nuclear positioning and dynamics of the silent mating type loci by the yeast Ku70/Ku80 complex. *Molecular and cellular biology* **29**: 835-848.
- Chen CY, Chi YH, Mutalif RA, Starost MF, Myers TG, Anderson SA, Stewart CL, Jeang KT. 2012. Accumulation of the Inner Nuclear Envelope Protein Sun1 is Pathogenic in Progeric and Dystrophic Laminopathies. *Cell* **149**: 565-577.
- Chen H, Xue J, Churikov D, Hass EP, Shi S, Lemon LD, Luciano P, Bertuch AA, Zappulla DC, Geli V et al. 2018. Structural Insights into Yeast Telomerase Recruitment to Telomeres. *Cell* **172**: 331-343.e313.
- Chung DK, Chan JN, Strecker J, Zhang W, Ebrahimi-Ardebili S, Lu T, Abraham KJ, Durocher D, Mekhail K. 2015. Perinuclear tethers license telomeric DSBs for a broad kinesin- and NPC-dependent DNA repair process. *Nature communications* **6**: 7742.
- Churikov D, Charifi F, Eckert-Boulet N, Silva S, Simon MN, Lisby M, Geli V. 2016. SUMO-Dependent Relocalization of Eroded Telomeres to Nuclear Pore Complexes Controls Telomere Recombination. *Cell reports* **15**: 1242-1253.
- Conrad MN, Lee CY, Chao G, Shinohara M, Kosaka H, Shinohara A, Conchello JA, Dresser ME. 2008. Rapid telomere movement in meiotic prophase is promoted by NDJ1, MPS3, and CSM4 and is modulated by recombination. *Cell* **133**: 1175-1187.
- Cusanelli E, Romero CA, Chartrand P. 2013. Telomeric noncoding RNA TERRA is induced by telomere shortening to nucleate telomerase molecules at short telomeres. *Molecular cell* **51**: 780-791.
- Dani GM, Zakian VA. 1983. Mitotic and meiotic stability of linear plasmids in yeast. *Proceedings of the National Academy of Sciences of the United States of America* **80**: 3406-3410.
- Ferreira HC, Luke B, Schober H, Kalck V, Lingner J, Gasser SM. 2011. The PIAS homologue Siz2 regulates perinuclear telomere position and telomerase activity in budding yeast. *Nature cell biology* **13**: 867-874.
- Francia S, Michelini F, Saxena A, Tang D, de Hoon M, Anelli V, Mione M, Carninci P, d'Adda di Fagagna F. 2012. Site-specific DICER and DROSHA RNA products control the DNA-damage response. *Nature* **488**: 231-235.
- Gao M, Wei W, Li MM, Wu YS, Ba Z, Jin KX, Liao YQ, Adhikari S, Chong Z, Zhang T et al. 2014. Ago2 facilitates Rad51 recruitment and DNA double-strand break repair by homologous recombination. *Cell Res* **24**: 532-541.
- Geronimo CL, Zakian VA. 2016. Getting it done at the ends: Pif1 family DNA helicases and telomeres. *DNA repair* **44**: 151-158.
- Gilson E, Roberge M, Giraldo R, Rhodes D, Gasser SM. 1993. Distortion of the DNA double helix by RAP1 at silencers and multiple telomeric binding sites. *Journal of molecular biology* **231**: 293-310.
- Görlich MTB, Theis S, Christa K, Volker CC, Dirk. 2006. A selective block of nuclear actin export stabilizes the giant nuclei of. *Nature cell biology* **8**: 257.
- Graf M, Bonetti D, Lockhart A, Serhal K, Kellner V, Maicher A, Jolivet P, Teixeira MT, Luke B. 2017. Telomere Length Determines TERRA and R-Loop Regulation through the Cell Cycle. *Cell* **170**: 72-85.e14.
- Haber C-SL, Ruoxi WW, Hsiao-Han C, Daniel C, Mark RS, James E. 2016. Chromosome position determines the success of double-strand break repair.

- Hogenbirk MA, Heideman MR, de Rink I, Velds A, Kerkhoven RM, Wessels LFA, Jacobs H. 2016. Defining chromosomal translocation risks in cancer. in *Proceedings of the National Academy of Sciences of the United States of America*, pp. E3649-3656.
- Horigome C, Bustard DE, Marcomini I, Delgoushaie N, Tsai-Pflugfelder M, Cobb JA, Gasser SM. 2016. PolySUMOylation by Siz2 and Mms21 triggers relocation of DNA breaks to nuclear pores through the Slx5/Slx8 STUbL. *Genes & development* **30**: 931-945.
- Horigome C, Oma Y, Konishi T, Schmid R, Marcomini I, Hauer MH, Dion V, Harata M, Gasser SM. 2014. SWR1 and INO80 chromatin remodelers contribute to DNA double-strand break perinuclear anchorage site choice. *Molecular cell* **55**: 626-639.
- Jaspersen SL, Giddings TH, Jr., Winey M. 2002. Mps3p is a novel component of the yeast spindle pole body that interacts with the yeast centrin homologue Cdc31p. *The Journal of cell biology* **159**: 945-956.
- Jeppsson K, Carlborg KK, Nakato R, Berta DG, Lilienthal I, Kanno T, Lindqvist A, Brink MC, Dantuma NP, Katou Y et al. 2014. The chromosomal association of the Smc5/6 complex depends on cohesion and predicts the level of sister chromatid entanglement. *PLoS genetics* **10**: e1004680.
- Kadesch TR, Chamberlin MJ. 1982. Studies of in vitro transcription by calf thymus RNA polymerase II using a novel duplex DNA template. *The Journal of biological chemistry* **257**: 5286-5295.
- Kalendová A, Kalasová I, Yamazaki S, Uličná L, Harata M, Hozák P. 2014. Nuclear actin filaments recruit cofilin and actin-related protein 3, and their formation is connected with a mitotic block. *Histochem Cell Biol* **142**: 139-152.
- Keskin H, Shen Y, Huang F, Patel M, Yang T, Ashley K, Mazin AV, Storici F. 2014. Transcript-RNA-templated DNA recombination and repair. *Nature* **515**: 436-439.
- Khadaroo B, Teixeira MT, Luciano P, Eckert-Boulet N, Germann SM, Simon MN, Gallina I, Abdallah P, Gilson E, Geli V et al. 2009. The DNA damage response at eroded telomeres and tethering to the nuclear pore complex. *Nature cell biology* **11**: 980-987.
- Kim DI, Jensen SC, Roux KJ. 2016. Identifying Protein-Protein Associations at the Nuclear Envelope with BioID. *Methods in molecular biology (Clifton, NJ)* **1411**: 133-146.
- Konig P, Giraldo R, Chapman L, Rhodes D. 1996. The crystal structure of the DNA-binding domain of yeast RAP1 in complex with telomeric DNA. *Cell* **85**: 125-136.
- Korbel MS-W, Megumi O-S, Adrian MS, Balca RM, Jan O. 2017. Systematic Identification of Determinants for Single Strand Annealing Mediated Deletion Formation in *Saccharomyces cerevisiae*.
- Lapetina DL, Ptak C, Roesner UK, Wozniak RW. 2017. Yeast silencing factor Sir4 and a subset of nucleoporins form a complex distinct from nuclear pore complexes. *The Journal of cell biology*.
- Lawrimore J, Barry TM, Barry RM, York AC, Friedman B, Cook DM, Akialis K, Tyler J, Vasquez P, Yeh E et al. 2017. Microtubule dynamics drive enhanced chromatin motion and mobilize telomeres in response to DNA damage. *Molecular biology of the cell* **28**: 1701-1711.
- Lescasse R, Pobiega S, Callebaut I, Marcand S. 2013. End-joining inhibition at telomeres requires the translocase and polySUMO-dependent ubiquitin ligase Uls1. *The EMBO journal* **32**: 805-815.
- Li P, Jin H, Koch BA, Abblett RL, Han X, Yates JR, 3rd, Yu HG. 2017. Cleavage of the SUN-domain protein Mps3 at its N-terminus regulates centrosome disjunction in budding yeast meiosis. *PLoS genetics* **13**: e1006830.
- Lindroos HB, Strom L, Itoh T, Katou Y, Shirahige K, Sjogren C. 2006. Chromosomal association of the Smc5/6 complex reveals that it functions in differently regulated pathways. *Molecular cell* **22**: 755-767.
- Loeillet S, Palancade B, Cartron M, Thierry A, Richard GF, Dujon B, Doye V, Nicolas A. 2005. Genetic network interactions among replication, repair and nuclear pore deficiencies in yeast. *DNA repair* **4**: 459-468.
- Longhese NM, Michela C, Maxime W, Chiara Vittoria C, Marc D, Antonin M, Fabrizio d'Adda di F, Maria P. 2015. Resection is responsible for loss of transcription around a double-strand break in *Saccharomyces cerevisiae*.
- Lotterberger F, Karssemeijer RA, Dimitrova N, de Lange T. 2015. 53BP1 and the LINC complex promote microtubule-dependent DSB mobility and DNA repair. *Cell* **163**: 880-893.
- Luo K, Vega-Palas MA, Grunstein M. 2002. Rap1-Sir4 binding independent of other Sir, yKu, or histone interactions initiates the assembly of telomeric heterochromatin in yeast. *Genes & development* **16**: 1528-1539.
- Marcand S, Pardo B, Gratias A, Cahun S, Callebaut I. 2008. Multiple pathways inhibit NHEJ at telomeres. *Genes & development* **22**: 1153-1158.

- Marshall WF, Straight A, Marko JF, Swedlow J, Dernburg A, Belmont A, Murray AW, Agard DA, Sedat JW. 1998. Interphase chromosomes undergo constrained diffusional motion in living cells. *Current biology : CB* **7**: 930-939.
- McDonald D, Carrero G, Andrin C, de Vries G, Hendzel MJ. 2006. Nucleoplasmic beta-actin exists in a dynamic equilibrium between low-mobility polymeric species and rapidly diffusing populations. *The Journal of cell biology* **172**: 541-552.
- Mitelman F, Johansson B, Mertens F. 2007. The impact of translocations and gene fusions on cancer causation. *Nature reviews Cancer* **7**: 233-245.
- Miyamoto K, Gurdon JB. 2013. Transcriptional regulation and nuclear reprogramming: roles of nuclear actin and actin-binding proteins. *Cellular and molecular life sciences : CMLS* **70**: 3289-3302.
- Moore DM, Karlin J, Gonzalez-Barrera S, Mardiros A, Lisby M, Doughty A, Gilley J, Rothstein R, Friedberg EC, Fischhaber PL. 2009a. Rad10 exhibits lesion-dependent genetic requirements for recruitment to DNA double-strand breaks in *Saccharomyces cerevisiae*. *Nucleic acids research* **37**: 6429-6438.
- Moore DM, Karlin J, González-Barrera S, Mardiros A, Lisby M, Doughty A, Gilley J, Rothstein R, Friedberg EC, Fischhaber PL. 2009b. Rad10 exhibits lesion-dependent genetic requirements for recruitment to DNA double-strand breaks in *Saccharomyces cerevisiae*. *Nucleic acids research* **37**: 6429-6438.
- Nagai S, Dubrana K, Tsai-Pflugfelder M, Davidson MB, Roberts TM, Brown GW, Varela E, Hediger F, Gasser SM, Krogan NJ. 2008. Functional targeting of DNA damage to a nuclear pore-associated SUMO-dependent ubiquitin ligase. *Science (New York, NY)* **322**: 597-602.
- Ohle C, Tesorero R, Schermann G, Dobrev N, Sinning I, Fischer T. 2016. Transient RNA-DNA Hybrids Are Required for Efficient Double-Strand Break Repair. *Cell* **167**: 1001-1013.e1007.
- Oza P, Jaspersen SL, Miele A, Dekker J, Peterson CL. 2009. Mechanisms that regulate localization of a DNA double-strand break to the nuclear periphery. *Genes & development* **23**: 912-927.
- Peterson PO, Craig L. 2010. Opening the DNA repair toolbox: Localization of DNA double strand breaks to the nuclear periphery. <http://dxdoiorg/104161/cc9110317>.
- Porro A, Feuerhahn S, Lingner J. 2014. TERRA-reinforced association of LSD1 with MRE11 promotes processing of uncapped telomeres. *Cell reports* **6**: 765-776.
- Robyr D, Suka Y, Xenarios I, Kurdistani SK, Wang A, Suka N, Grunstein M. 2002. Microarray deacetylation maps determine genome-wide functions for yeast histone deacetylases. *Cell* **109**: 437-446.
- Rothstein JM-H, Rodney. 2012. Increased chromosome mobility facilitates homology search during recombination. *Nature cell biology* **14**: 510-517.
- Schober H, Ferreira H, Kalck V, Gehlen LR, Gasser SM. 2009. Yeast telomerase and the SUN domain protein Mps3 anchor telomeres and repress subtelomeric recombination. *Genes & development* **23**: 928-938.
- Schwartz M, Zlotorynski E, Kerem B. 2005. The molecular basis of common and rare fragile sites. *Cancer letters* **232**: 13-26.
- Seeber A, Hegnauer AM, Hustedt N, Deshpande I, Poli J, Eglinger J, Pasero P, Gut H, Shinohara M, Hopfner KP et al. 2016. RPA Mediates Recruitment of MRX to Forks and Double-Strand Breaks to Hold Sister Chromatids Together. *Molecular cell* **64**: 951-966.
- Soutoglou TP, Céline B, David C, Evi. 2012. DNAPKcs-dependent arrest of RNA polymerase II transcription in the presence of DNA breaks. *Nature structural & molecular biology* **19**: 276.
- Spichal M, Fabre E. 2017. The Emerging Role of the Cytoskeleton in Chromosome Dynamics. *Frontiers in genetics* **8**: 60.
- Stinus S, Paeschke K, Chang M. 2017. Telomerase regulation by the Pif1 helicase: a length-dependent effect? *Current genetics*.
- Storici HK, Ying S, Fei H, Mikir P, Taehwan Y, Katie A, Alexander VM, Francesca. 2014. Transcript-RNA-templated DNA recombination and repair. *Nature* **515**: 436-439.
- Strecker J, Stinus S, Caballero MP, Szilard RK, Chang M, Durocher D. 2017. A sharp Pif1-dependent threshold separates DNA double-strand breaks from critically short telomeres. *Elife* **6**.
- Taddei A, Gasser SM. 2004. Multiple pathways for telomere tethering: functional implications of subnuclear position for heterochromatin formation. *Biochimica et biophysica acta* **1677**: 120-128.
- Torres-Rosell J, Machin F, Aragon L. 2005a. Smc5-Smc6 complex preserves nucleolar integrity in *S. cerevisiae*. *Cell cycle (Georgetown, Tex)* **4**: 868-872.

- Torres-Rosell J, Machin F, Farmer S, Jarmuz A, Eydmann T, Dalgaard JZ, Aragon L. 2005b. SMC5 and SMC6 genes are required for the segregation of repetitive chromosome regions. *Nature cell biology* **7**: 412-419.
- Wang Y, Zhang X, Zhang H, Lu Y, Huang H, Dong X, Chen J, Dong J, Yang X, Hang H et al. 2012. Coiled-coil networking shapes cell molecular machinery. *Molecular biology of the cell* **23**: 3911-3922.
- Wei W, Ba Z, Gao M, Wu Y, Ma Y, Amiard S, White CI, Rendtlew Danielsen JM, Yang YG, Qi Y. 2012. A role for small RNAs in DNA double-strand break repair. *Cell* **149**: 101-112.
- Williams CC, Jan CH, Weissman JS. 2014. Targeting and plasticity of mitochondrial proteins revealed by proximity-specific ribosome profiling. *Science (New York, NY)* **346**: 748-751.
- Wysocki R, Javaheri A, Allard S, Sha F, Cote J, Kron SJ. 2005. Role of Dot1-dependent histone H3 methylation in G1 and S phase DNA damage checkpoint functions of Rad9. *Molecular and cellular biology* **25**: 8430-8443.
- Zhang Z, Buchman AR. 1997. Identification of a member of a DNA-dependent ATPase family that causes interference with silencing. *Molecular and cellular biology* **17**: 5461-5472.



# APPENDICES

## List of abbreviations

53BP1	p53 binding protein 1
A-EJ	Alternative End Joining
ALT	Alternative Lengthening of Telomeres
ATM	Ataxia-Telangectasia Mutated
ATR	Ataxia-Telangectasia and Rad3 related protein
CFS	Chromosome Fragile Site
CST	Cdc13-Stn1-Ten1 complex
DDR	DNA Damage Response
diRNA	Damage-induced RNA
DSB	Double Strand Break
dsDNA	Double-stranded DNA
Gal	Galactose
GCR	Gross Chromosomal Rearrangements
HR	Homologous Recombination
ITS	Internal Telomeric Sequences
LINC	Linker of Nucleoskeleton and Cytoskeleton
MRX(N)	Mre11-Rad50-Xrs2 (Nbs1 in mammals)
MSD	Mean Square Displacement
ncRNA	Non-coding RNA
NE	Nuclear Envelope
NER	Nucleotide Excision Repair
NHEJ	Non-homologous End Joining
NPC	Nuclear Pore Complex
PML	ProMyelocytic Leukemia
RPA	Replication Protein A
SCI	Sister Chromatids Intertwinings
SDSA	Synthesis Dependent Strand Annealing
SIR	Silent Information Regulators
SMC5/6	Structural Maintenance of Chromosomes
SPB	Spindle Pole Body
SSA	Single Strand Annealing
ssDNA	Single-stranded DNA
STUbL	SUMO-dependent Ubiquitin Ligase
SUMO	Small Ubiquitin-like Modifier
TRF (1/2)	Telomere Repeat-binding Factor
uSCR	Unequal Sister Chromatids Recombination



# Isabella Marcomini

Email: [isabella.marcomini2@gmail.com](mailto:isabella.marcomini2@gmail.com)

Address: Kastanienweg 11, 4052 Basel, Switzerland

Phone: +41 76 70 56 313

Date of birth: 15.12.1987

Nationality: Italian



I am a proactive and dedicated life science professional, eager to steer my career towards pharmaceutical business development. I enjoy setting up and managing complex projects, solving problems in an independent and focused manner, while making use of the expertise of a team: I like to motivate and coordinate other people to work together towards a goal. I like to set clear objectives and establish priorities. My peers describe me as enthusiastic, curious and results-oriented.

## Education

01.2012 – 06.2018     **PhD program “NCCR Frontiers in Genetics”**, joint program between University of Geneva and Friedrich Miescher Institute, Basel, Switzerland

- Title of thesis: “The effect of telomere-like repeats in processing of double strand breaks in *S. cerevisiae*” (*magna cum laude*). Advisor: Prof. Susan M. Gasser, Director of FMI, Basel
- Independent establishment of a model system for the study of chromosomal translocations in *S. cerevisiae*
- Development and application of diverse molecular biology techniques: real-time PCR, telomere PCR, chromatin IP, protein IP, RNA IP, western blot, protein purification, confocal microscopy, SMRT deep sequencing, DNA resection assay, several DNA repair assays, CHEF gels, yeast culture techniques and molecular cloning
- Coaching and mentoring of 2 starting PhD students
- Regular talks and poster presentations at international scientific conferences and internal institute seminars

10.2009 – 10.2011     **MSc Molecular Biosciences**, major in Molecular and Cellular Biology  
University of Heidelberg, Germany

10.2006 – 10.2009     **BSc Molecular Biology**  
University of Padua, Italy

## Research experience

04.2013 – 05.2016     management of a scientific facility for breeding of lizards (*Anolis carolinensis*) under direction of Dr. Janine Daum

Successful set up of reproduction conditions in captivity: baby lizard born in 08.2014

- 01.2012 – 03.2012     **PhD rotation** “The effects of targeting histone Htz1 to a DNA locus on chromatin dynamics”  
 Advisor: Prof. Susan M. Gasser, University of Basel
- 04.2012 – 06.2012     **PhD rotation** “Investigation of TOR2 interaction with RNA”  
 Advisor: Prof. Robbie J. Loewith, University of Geneva
- 07.2012 – 11.2012     **PhD rotation** “Rif1 N-terminus has a role in DNA replication”  
 Advisor: Prof. David Shore, University of Geneva
- 03.2010 – 07.2010     **MSc rotation** “SecA interaction with ribosome nascent chains in *E. Coli*”  
 Advisor: Prof. Bernd Bukau, University of Heidelberg
- 08.2010 – 11.2010     **MSc rotation** “A reporter cell line to detect antigenic variation in *T. brucei*”  
 Advisor: Dr. Luisa Figueiredo, Institute of Molecular Medicine (Lisbon, Portugal)

### **Conference presentations**

- 07.2017                    Gordon Research Conference: Biology of Aging (poster)  
 Les Diablerets, Switzerland
- 04.2017                    ABCAM conference on genome rearrangements and mutational signatures (poster)  
 Boston, USA
- 06.2016                    Genome stability and chromosome dynamics (poster)  
 Emmetten, Switzerland
- 05.2015                    Telomeric chromatin and telomere fragility, EMBO workshop (talk)  
 Singapore, Singapore
- 11.2014                    3R Meeting (poster)  
 Hakone, Japan
- 05.2014                    Telomeres, telomerase and disease, EMBO conference (poster)  
 Bruxelles, Belgium
- 03.2013                    DNA replication and recombination, Keystone Symposium (poster)  
 Banff, Canada
- 03.2012                    8<sup>th</sup> annual meeting NCCR Frontiers in Genetics (poster)  
 Saas Fee, Switzerland

### **Professional courses**

- “Introduction to project management principles and practices” online course by University of California, Irvine, 2018
- Antelope @ Novartis mentorship program, 2016
- Introduction to Project Management workshop, FMI, 2016
- “Introduction of Perfumery” online course by cosmetic scientist Karen Gilbert, 6 modules, 2017

### **Awards**

- Prize for best poster: EMBO conference on telomeres, telomerase and disease, Brussels, May 2014
- Travel grant by the Swiss Society for Molecular and Cellular Biosciences (SSMCB), August 2014

### **Languages**

Italian (mother tongue), English (professional level), German (professional level), French (basic)

## Memberships

Since 2015 Graduate Consulting Club, Basel

Since 2014 Swiss Society for Molecular and Cellular Biosciences (SSMCB)

## References

Prof. Susan M. Gasser	Dr. Kenji Shimada	Prof. Vincent Dion
Director of Friedrich Miescher Institute for Biomedical Research Basel, Switzerland	Project leader at Friedrich Miescher Institute for Biomedical Research Basel, Switzerland	Professor at Centre for Integrative Genomics Lausanne, Switzerland
+41 61 697 7255	+41 61 697 5583	+41 21 692 3901
susan.gasser@fmi.ch	kenji.shimada@fmi.ch	vincent.dion@unil.ch

## Publications

- **Marcomini I**, Shimada K, Delgosaie D, Yamamoto I, Seeber A, Cheblal A, Horigome C, Naumann U and Gasser SM. "Asymmetric processing of DNA ends at a double-strand break leads to unconstrained dynamics and ectopic translocation.", *Cell reports* 2018 Sept 4;24(10):2614-28
- Horigome C, Bustard DE, **Marcomini I**, Delgosaie N, Tsai-Pflugfelder M, Cobb JA, Gasser SM. "PolySUMOylation by Siz2 and Mms21 triggers relocation of DNA breaks to nuclear pores through the Slx5/Slx8 STUbL." *Genes & Dev.* 2016 Apr 15;30(8):931-45
- Huber D, Jamshad M, Hanmer R, Schibich D, Döring K, **Marcomini I**, Kramer G, Bukau B. "SecA Cotranslationally Interacts with Nascent Substrate Proteins In Vivo." *J Bacteriol.* 2016, 199(2)
- **Marcomini I**, Gasser SM "Nuclear organization in DNA end processing: telomeres vs double strand breaks." *DNA Repair (Amst)* 2015 Aug;32:134-40
- Horigome C, Oma Y, Konishi T, Schmid R, **Marcomini I**, Hauer MH, Dion V, Harata M, Gasser SM. "SWR1 and INO80 Chromatin Remodelers Contribute to DNA Double-Strand Break Perinuclear Anchorage Site Choice." *Mol. Cell.* 2014 Aug 21;55(4):626-39
- Lemmens L, Mattarocci S, **Marcomini I**, Shi T, Follonier C, Lopes M, Thomä N, Shore D. "Global control of DNA replication timing by the budding yeast telomere protein Rif1." *Epigenetics Chromatin*, 2013 Mar 18; 6(Suppl 1): P99

## Hobbies

- Violin (8<sup>th</sup> year violin diploma, conservatory of music "C. Pollini", Padova, Italy)
- Rock climbing (indoors and outdoors)
- Postcrossing (postcards exchange, [www.postcrossing.com](http://www.postcrossing.com))



## Acknowledgements

First and foremost I would like to thank my supervisor Susan Gasser for the guidance, the support and the freedom to perform this project in her lab. I am thankful to the NCCR Frontiers in genetics PhD program, that allowed me to gain precious knowledges and connections that proved very useful during my PhD. An important thanks goes to my committee members, Joachim Lingner, Jim Haber, Vincent Dion, Ulrich Rass: discussions have been always very productive and it has been a honor to have them as examiners. A particular thank to Vincent Dion, who supervised me during a rotation before my PhD and introduced me to the microscope and the field of DNA repair. I want to thank Chihiro, an ex postdoc in the lab, who started me on the break relocation project and taught me particularly the meditative aspects of spot clicking. Many thanks to Io Yamamoto, who worked with me for 2.5 months, and taught me a lot on cultural differences, the value of slowness, how to teach. I hope we will celebrate together in Japan. Thanks to the collaborators at NIBR for the deep sequencing, Ulrike Naumann and Edward Oakeley. A special thank to Monika Tsai, for the scientific contribution to my project but also for all the wise words and the empathy. Thanks to Vero, the lab angel, for sharing the bench and all associated equipment (the grass of the neighbor...). Thanks to Razel, for cleaning up behind me and always finding a spot to put my thousand plates. Thanks to Andrew Seeber, who helped me often at the microscope with neverending patience and was always full of useful tips, and to the FMI FAIM facility: Laurent Gelmant, Steven Bourke and Jan Eglinger for prompt response every time there was the slightest imaging issue. Thanks to Kenji Shimada, a mine of scientific resources and genetic tricks. To Daphne Cabianca, for the shared laughs and tears also outside the lab and the teaching of ChIP. Generally, I am extremely thankful to all the lab, it has been a pleasure to work with everybody in an extremely stimulating and friendly atmosphere. Thanks to David, the best flatmate I could get for sharing these intense years. Many thanks also to The Office: Ivana Murfuni, Gabriele Fontana, Benoit Falquet, Michi Hauer, for scientific discussions and coffee gigs. Thanks to all the friends who dragged me out of the lab when I needed it. Finally, a big thank to my parents for always supporting me.